# Material and Thermal Transport in Vertical Granular Flows.

Thesis by

Venkata V.R. Natarajan.

In Partial Fulfillment of the Requirements

for the Degree of

Doctor of Philosophy

California Institute of Technology

Pasadena, California

1997

(Submitted 1st October, 1996)

# Acknowledgements

I would like to express my sincere gratitude to Professor Melany Hunt for all her faith, encouragement and support during the course of the last five years. I consider myself extremely fortunate to have had the opportunity to work with such an understanding adviser. I would also like to express my deepest appreciation to Professors Allan Acosta and Rolf Sabersky for having served as mentors at some very definitive moments during my stay at Caltech. It was a privilege to interact with them.

I would like to thank Professor John Brady for the interest he displayed in my work. His inputs and suggestions certainly improved the content of my thesis. I'm also grateful to Professors Christopher Brennen and Fred Raichlen for having taken the time to scrutinize my thesis and for serving on my committee. I owe an immense debt of gratitude to all the professors who taught the courses I took at Caltech.

Erik Taylor and Craig Tibbetts provided invaluable inputs during different stages of my dissertation and I would like to express my sincerest appreciation to them both. Furthermore, I would like to thank Roberto Zenit, Lakshman Benedict, Simone Francis, Rajesh Kedia and Carl Wassgren for their timely help during the course of my thesis work. Rodney Rojas and John van Deusen proved to be very considerate and reassuring during some lonely and tedious times in the laboratory. I would like to thank them both for their support.

I do not have the appropriate words in my vocabulory to describe my gratitude to Sudipto Sur and Kamran Mohseni for being pillars of great support during some personally very trying times during the last year of my stay at Caltech. It is only during times of duress that we recognize our true friends, for only they have the courage to stand by us in our battles against the forces of adversity. Hence, I would

like to dedicate this thesis to all those people, both family and friends, who stood by me during those troubled times, gave me the courage to overcome personal loss, and the faith to walk that last mile home.

# Abstract

The term "granular material flow" is applied in the literature to particulate flows such as the flow of coal down an inclined chute, the discharge of grains from a hopper or the motion of debris in a landslide. In these flows, the material has an overall bulk motion; however, individual particles may collide, roll or slide against each other, and may interact with the bounding surfaces. Hence, the individual particle motions are composed of a mean velocity component and a fluctuating, or random, velocity component. An analogy is drawn between this random motion and the random motion of molecules. As a result, much of the theoretical analysis of these flows has developed from concepts derived from dense-gas kinetic theory. Although this random velocity component is a key property in analytical studies, there have been few attempts to measure its magnitude in experimental studies. In the current work, measurements were made of two components of the average and fluctuating velocities in the flow of granular material in a vertical chute for flows with different particle and boundary properties. The fluctuation velocities were highly anisotropic, with the streamwise components being 2 to 2.5 times the magnitude of the transverse components. Increasing the surface roughness of the particles reduced the fluctuation velocities significantly.

Another area of considerable industrial interest is particle mixing in monodisperse and polydisperse particle flows. Because of the random component of particle motion, the particles can exhibit a diffusive motion similar to that found in gases and liquids. In the second part of this work, local self diffusion coefficients were measured in the granular flow using image processing techniques to track individual particles. The influence of flow shear rates and fluctuation velocities on the self diffusion coefficients

was investigated. The self-diffusion coeffecients were found to increase with the shear rate and the fluctuation velocity, with the coefficients in the streamwise direction being an order-of-magnitude higher than those for the transverse direction. The surface roughness of the particles led to a decrease in the self-diffusion coefficients.

The effect of shearing on the convective heat transfer from a heater immersed in a granular flow was investigated experimentally. Comparisons were made with previous experiments and with results obtained for unsheared plug flows. The results indicated that the medium density close to the wall played a critical role in determining the overall heat transfer.

Finally, theoretical solutions, based on a combination of the dense-gas kinetic theory and an empirical friction model, were generated to study and compare experimental and theoretical results for velocity profiles and heat transfer characteristics in vertical, fully developed granular flows. The results indicated good agreement between theoretical and experimentally measured mean velocity proflies but the fluctuation velocity magnitudes were usually underpredicted by the theoretical solutions. There was qualitative agreement between experimental and theoretical results for convective heat transfer.

# Contents

# List of Figures

# List of Tables

# Nomenclature

| | |
|---|---|
| A | dimensionless channel half-width |
| Ba | Bagnold Number |
| Bi | Biot Number |
| $\mathbf{C}$ | particle fluctuation velocity (Kinetic Theory) [m/s] |
| C | magnitude of particle fluctuation velocity (Kinetic Theory) [m/s] |
| $\mathbf{c}$ | local particle velocity (Kinetic Theory) [m/s] |
| $c_{air}$ | specific heat of air [Ws/kg °C] |
| $c_p$ | specific heat of particle [Ws/kg °C] |
| $\mathrm{D}_{ij}$ | self-diffusion coefficient tensor [$m^2/s$] |
| $D$ | self-diffusion coefficient for isotropic diffusion (Einstein relation) [$m^2/s$] |
| $D_{xx}$ | coefficient of self-diffusion in streamwise direction [$m^2/s$] |
| $D_{yy}$ | coefficient of self-diffusion in transverse direction [$m^2/s$] |
| $D1_i$ | dimensionless self-diffusion coefficient in direction 'i' |
| $D2_i$ | dimensionless self-diffusion coefficient in direction 'i' |
| $D2$ | dimensionless trace of 2-D self-diffusion tensor |
| $e_p$ | particle-particle coefficient of restitution |
| $e_w$ | particle-wall coefficient of restitution |
| $\mathbf{F}$ | specific body force [$N/m^3$] |
| $Fr$ | coefficient in expression for frictional normal stress |
| $f^{(0)}$ | Maxwellian velocity distribution function (Kinetic Theory) |
| $f^{(1)}$ | single particle velocity distribution function (Kinetic Theory) |
| $f^{(2)}$ | pair distribution function (Kinetic Theory) |
| $g$ | acceleration due to gravity [$m/s^2$] |

$g_0$ radial distribution function

$h$ mean heat transfer coefficient [W/m$^2$°C]

$h_{pf}$ heat transfer coefficient between particle and surrounding fluid [W/m$^2$°C]

$h_{wp}$ wall-particle heat transfer coefficient [W/m$^2$°C]

$h_\iota$ local heat transfer coefficient at location '$\iota$' [W/m$^2$°C]

$\mathbf{I}$ identity matrix

$\mathbf{k}$ unit vector directed from center of particle 1 to center of particle 2 (Kinetic Theory)

$k_c$ thermal conductivity of assembly at critical density [W/m°C]

$k_e$ effective thermal conductivity at mean solid fraction [W/m°C]

$k_g$ thermal conductivity of interstitial gas [W/m°C]

$k_{kt}$ streaming thermal conductivity (Hsiau & Hunt 1993b) [W/m°C]

$k_{mc}$ effective molecular conductivity (Einstein & Gelperin 1971) [W/m°C]

$k_p$ thermal conductivity of particle [W/m°C]

$k_s$ thermal conductivity of solid material [W/m°C]

$k_{tol}$ total thermal conductivity $k_{mc} + k_{kt}$ [W/m°C]

$l$ modified mean free path of interstitial fluid molecules [m]

$l_p$ characteristic particle length [m]

$N_f$ frictional normal stress [N/m$^2$]

Nu$^*$ modified Nusselt number (Sullivan & Sabersky 1975)

Nu$^*_{eff}$ effective modified Nusselt number (Ahn 1989)

$\mathbf{n}$ unit normal vector directed from the wall into the flow

$n$ exponent in expression for frictional normal stress

$\mathbf{P}$ total pressure tensor [N/m$^2$]

P$_f$ contribution to pressure tensor from frictional interactions [N/m$^2$]

P$_{kt}$ contribution to pressure tensor from collisional and streaming interactions (Kinetic Theory) [N/m$^2$]

$p$ exponent in expression for frictional normal stress

$\mathrm{Pe}^*$ modified Peclet number (Sullivan & Sabersky 1975)

$\mathrm{Pe}^*_{eff}$ effective modified Peclet number (Ahn 1989)

$q_h$ diffusive heat flux [W/m$^2$]

$q_w$ wall heat flux [W/m$^2$]

$\mathbf{R}$ diffusive displacement in Einstein relation [m]

$R_{Lij}$ scaled correlation of instantaneous fluctuation velocity

$\mathbf{r}$ particle location (Kinetic Theory) [m]

$\mathbf{S}$ deviatoric part of the rate of deformation tensor [s$^{-1}$]

$S_f$ frictional shear stress [N/m$^2$]

$\mathbf{T}$ granular temperature (Kinetic Theory) [m$^2$/s$^2$]

$\mathbf{T}^*$ dimensionless granular temperature

$T$ thermodynamic temperature [ °C]

$T_{bulk}$ temperature of bulk material [ °C]

$T_{Lij}$ Lagrangian time scale [s]

$T_{w-\iota}$ wall temperature at location $\iota$ [ °C]

$T_{wp-\iota}$ local temperature of particle adhered to wall at location $\iota$ [ °C]

$\mathrm{T}_{\sigma/2}$ granular temperature at a distance of half a particle diameter from the wall [m$^2$/s$^2$]

$t$ time [s]

$\mathbf{u}$ mean velocity (Kinetic Theory) [m/s]

$\mathrm{u}_{sl}$ slip velocity [m/s]

$u'_i$ fluctuation velocity in direction 'i' [m/s]

$u_x$ mean streamwise velocity [m/s]

$u_{x-\sigma/2}$ mean streamwise velocity at a distance of half a particle diameter from the wall [m]

$u^*_x$ dimensionless mean streamwise velocity

| | |
|---|---|
| $u'_x$ | streamwise fluctuation velocity [m/s] |
| $u_y$ | mean transverse velocity [m/s] |
| $u'_y$ | transverse fluctuation velocity [m/s] |
| $W$ | channel half-width [m] |
| X | dimensionless streamwise coordinate |
| Y | dimensionless transverse coordinate |
| $\alpha_c$ | thermal diffusivity of assembly at critical density [$m^2/s$] |
| $\alpha_e$ | effective thermal diffusivity at mean solid fraction [$m^2/s$] |
| $\Gamma$ | flux of fluctuating energy (Kinetic Theory) [$kg/s^3$] |
| $\gamma$ | specific fluctuation energy dissipation (Kinetic Theory) [$kg/ms^3$] |
| $\gamma_s$ | shear rate [$s^{-1}$] |
| $\Delta x_i$ | self-diffusive displacement in direction 'i' [m] |
| $\Delta x$ | self-diffusive displacement in streamwise direction [m] |
| $\Delta y$ | self-diffusive displacement in transverse direction [m] |
| $\delta$ | wall-particle coefficient of friction |
| $\delta_{bl}$ | thickness of thermal boundary layer [m] |
| $\delta_{eff}$ | effective roughness of surfaces [m] |
| $\iota$ | location of thermocouple on heater wall |
| $\Lambda$ | function of solid fraction in Bagnold Number |
| $\mu_f$ | dynamic viscosity of interstitial fluid in Bagnold Number [kg/ms] |
| $\nu$ | solid fraction |
| $\nu_{ave}$ | average solid fraction |
| $\nu_{min}$ | minimum solid fraction for frictional interactions |
| $\nu_0$ | close-packed solid fraction |
| $\nu^*$ | maximum shearable solid fraction for a particle assembly |
| $\nu_{\sigma/2}$ | solid fraction at a distance of half a particle diameter from the wall |
| $\rho$ | bulk density of material [$kg/m^3$] |

| | |
|---|---|
| $\rho_{air}$ | density of air [kg/m$^3$] |
| $\rho_p$ | particle density [kg/m$^3$] |
| $\sigma$ | particle diameter [m] |
| $\Phi$ | perturbation function in single particle velocity distribution function (Kinetic Theory) |
| $\phi$ | internal angle of friction |
| $\phi_A$ | surface coverage factor |
| $\phi'$ | specularity coefficient (Kinetic Theory) |
| $\chi$ | thermal resistance of interstitial fluid layer |
| $\Psi$ | local particle property (Kinetic Theory) |

# Chapter 1 Introduction

The term "granular material" refers to any assembly of a large number of discrete solid particles dispersed in a fluid. The flow of coal down an inclined chute, the discharge of grains from a hopper or the motion of debris in a landslide are all examples of granular material flows. Such flows are of significant relevance in a number of chemical, pharmaceutical, fertilizer and food processing industries, where many processes involve the handling of material in granular or powdered form. Some typical examples encountered in industry are the dehydration of grain prior to storage, the handling and conveying of foodstuff prior to packaging, and the calcination of limestone. Numerous industrial applications in the cosmetics, chemical, pharmaceutical and detergent manufacture industries also involve the mixing of different materials in granular form. Furthermore, many of the above mentioned industrial applications also include processes involving heat transfer either to or from the granular materials. Most industrial design and development of equipment to handle, store, transport, mix or heat granular materials is based mainly on empirical approaches. However, over the last couple of decades, significant research efforts have been directed at obtaining a better theoretical and experimental understanding of the rheological, heat transfer and mixing characteristics of such flows.

A typical granular flow consists of the solid granular component dispersed in an interstitial fluid, usually air. Bagnold (1954) identified three broad regimes of granular flow behavior based on the relative contribution of the interstitial fluid towards the overall dynamics of the flow. These regimes were distinguished by a dimensionless

quantity, the "Bagnold number" $Ba$,

$$Ba = \Lambda^{\frac{1}{2}} \rho_p \sigma^2 \left( \frac{du_x}{dy} \right) / \mu_f, \tag{1.1}$$

where $\sigma$ is the diameter, $\Lambda$ is a function of the solid fraction, $\rho_p$ is the particle density, $du_x/dy$ is the shear rate and $\mu_f$ is the dynamic viscosity of the interstitial fluid. The Bagnold number is equivalent to the Reynolds number in that it is a ratio of the inertial forces to the viscous forces in the granular flow. For values of $Ba < 40$, the flow is characterized as being "macroviscous", with the viscosity of the interstitial fluid playing a dominant role in determining the dynamics of the flow. Values of $Ba > 450$ characterized a "grain-inertia" regime, where the dynamics of the flow are determined primarily by particle-particle interactions and the interstitial fluid plays a negligible role. However, as discussed later, in detail, the interstitial fluid always plays a crucial role in determining the convective heat transfer characteristics of such flows, irrespective of the flow regime.

## 1.1 Research Developments in Granular Flows

### 1.1.1 Constitutive Relations

Over the past two decades, significant efforts have been made to describe the flows of granular materials in terms of concepts borrowed from dense-gas kinetic theory (Chapman & Cowling 1971). While a granular flow has an overall bulk motion, the individual particles making up the material may collide, roll or slide against each other, and may interact with the bounding surfaces. Hence, the individual particle motions are composed of a mean component and a fluctuating, or random component. An analogy is drawn between this random motion and the random motion of molecules in a dense gas. Ogawa (1978) used the term "granular temperature" to quantify the random motions of particles about the mean velocity. The granular temperature is

defined as the average of the sum of the squares of the three fluctuating velocity components. Since the granular temperature is a measure of the specific random kinetic energy of the flow, it replaces the thermodynamic temperature in the dense-gas kinetic theory based analysis of rapid granular flows. However, significant differences exist between the interactions amongst gas molecules in a dense gas and particles in a granular flow. Unlike the collisions between molecules, the collisions between granular particles are inelastic and always involve a dissipation of the random kinetic energy. Hence, in order to sustain the flow, it is necessary to supply fluctuation energy to the system, either through shear work or through vibration. Otherwise, in the absence of any fluctuation energy source, the granular materials would ultimately clump into a single mass (McNamara & Young 1992). These analogies between dense gases and granular flows are expected to be valid in the "rapid granular flow" regime, (Campbell 1990) characterised by high shear rates and low to moderately high solid fractions in the flows.

As in the case of dense gases, the transport phenomena in the rapid granular flow regime are determined by two mechanisms. The first is the streaming, or kinetic, mode which accounts for the transport of particle properties as the particles move freely across void spaces in the flows. The second mechanism is the collisional mode, which accounts for transfer of momentum during collisional interactions between particles. The kinetic mode is dominant at low solid fractions because the particles can "stream" over longer distances. The collisional mode dominates at higher solid fractions as the increased proximity of particles increases the frequency of collisions.

Savage & Jeffrey (1981) and Jenkins & Savage (1983) were responsible for the initial development of constitutive models for granular flows based on dense-gas kinetic theory. They derived integral forms for the stress and fluctuation energy flux due to the collisional interactions between the particles. Lun et al. (1984) used elements of the Chapman-Enskog dense-gas kinetic theory ( Chapman & Cowling 1971)

to develop the kinetic theory for granular flows of slightly inelastic particles. Both collisional and streaming modes of transport were included, enabling the theory to be extended to dilute systems as well. Furthermore, Lun et al. (1984) acknowledged the fact that the presence of gradients in the velocity, density and granular temperature profiles in a rapid granular flow meant that the system was not in a equilibrium state and hence could not be described by a Maxwellian velocity distribution function. They were successful in incorporating a first order correction for the velocity distribution function, though it entailed an assumption of collisional isotropy.

Jenkins & Richman (1985) extended the kinetic theory treatment to treat inelastic particles using Grad's method of moments. Farrell et al. (1986) extended the kinetic theory model to investigate simple shear flows of binary mixtures of smooth, inelastic, spherical particles, considering only the collisional mode of property transport. Lun & Savage (1987) extended the theory of Lun et al. (1984) to flows of rough, inelastic and spherical particles by introducing a roughness coefficient to account for the effects of surface friction in collisions between particles. The presence of particle surface friction led to particle rotational velocity fluctuations; the presence of rotary inertia usually reduced stresses within the flow field. This study only considered the collisional mode of property transfer. Lun (1991) extended the last study by considering the streaming contribution to the transport phenomena as well. Jenkins & Richman (1988) introduced an anisotropic Maxwellian velocity distribution function into their kinetic theory analysis of the plane simple shear of smooth inelastic circular disks in order to study the anisotropy of the second moments. Richman & Oyediran (1992) incorporated the effects of grain size reduction, due to collisions, within a typical kinetic theory model. All the above mentioned works are limited by the extreme complexity involved in extending their results to general flow situations with non-uniform shear fields. Goldshtein & Shapiro (1995) also modified the Chapman-Enskog theory to derive the Euler-like hydrodynamic equations for a system of moving spheres

of constant roughness and elasticity, considering only the collisional motion. Their solution form is appropriate for the description of rapid shearless motions of granular materials, especially in vibrofluidized regimes.

The constitutive models based on dense-gas kinetic theory are more appropriate for the rapid granular flow regime, where particle interactions are characterized by short-durational collisional contacts. Such flows are usually driven by very high rates of deformation. There also exists a wealth of literature dealing with the behavior of granular materials subjected to slow deformation; i.e. in the "quasi-static" regime. Particle interactions in the quasi-static regime are predominantly long-duration and involve significant relative sliding or rolling. Historically, attempts at modeling flow behavior in this regime have drawn extensively from results derived in the area of soil mechanics and plasticity. Examples of work in this area include Goodman & Cowin (1971), Savage (1979), De Josselin de Jong (1971) and Mandl & Fernandez-Luque (1970). None of these models account for motion at the microscopic scale of individual particles.

A large number of granular flows of practical interest fall in a transitional regime where both long-duration frictional and short-duration collisional or translational interactions play significant roles. Johnson & Jackson (1987) proposed constitutive relations for such flow regimes by assuming the total stress to be a simple sum of the frictional and collisional-translational contributions. They used the relations derived by Lun et al. (1984) to determine the collisional-translational contributions, and assumed a simple plane-shear Coulombic yield criterion to describe the frictional interactions. Johnson et al. (1990) and Anderson & Jackson (1992) used this model to investigate flows in inclined chutes and attempted to make comparisons with experimental observations. This theory is described in detail in section 2.1.2.

### 1.1.2 Experimental Studies

Experimental work in the area of granular materials is still limited, and confined to simple geometries. Some notable examples of such work in vertical chutes or channels include Takahashi & Yanai (1973), Savage (1979), Nedderman & Laohakul (1980), Hsiau & Hunt (1993a) and Tuzun et al. (1982). Studies on inclined chutes include those of Johnson et al. (1990), Savage (1979), Augestein & Hogg (1978), Drake (1991), Patton (1985) and Ahn (1989). Studies in shear cells include those of Savage & Sayed (1984), Hanes & Inman (1985) and Wang & Campbell (1992). The inability to make accurate measurements of velocity, granular temperature or fluctuation velocities, and solid fractions have severely limited the opportunities availiable for experimentation in the field of granular flows. Ahn, Brennen & Sabersky (1991) and Hsiau & Hunt (1993a) measured mean and fluctuation velocities in the streamwise direction using fiber-optic probes. Drake (1991) measured both fluctuation velocity components in a two-dimensional, high-shear-rate low-density flow down an inclined chute one particle thick, using high speed photographic techniques. The latter work also presented evidence that the fluctuation velocities were anisotropic. Recent experimental efforts have focussed on making measurements of density within the bulk of the flowing material. Techniques considered include Magnetic Resonance Imaging (Nakagawa et al. 1993) and gamma-ray tomography (Hosseiniashrafi & Tuzun 1993). Such intrusive techniques usually restrict the nature of materials that may be used during the course of the experiments. All the kinetic theory models require precise values for the physical properties of individual particles like the coefficients of restitution and friction. Foerster et al. (1994) and Mullier et al. (1991) made measurements of single particle coefficients of restitution and friction respectively.

### 1.1.3 Computer Simulations

Given the inherent limitations in performing reliable and exhaustive experiments, significant attention has been devoted in recent years towards the simulation of granular flows in a variety of geometries and flow situations. Typically, such simulations are based on models derived from Molecular Dynamics. A large number of particles (usually disks or spheres) are placed in a desired geometry and assigned initial random values of translational and rotational velocities. The particles are allowed to collide with each other and sufficient time is allowed to elapse in order to achieve a steady state. Subsequently, it is possible to calculate the mean and fluctutational velocities, the density profiles as well as the values of the components of the stress tensor. The advantage of such simulations lies primarily in the fact that they enable one to maintain significant control over a large number of physical and geometrical parameters like coefficients of friction and restitution, particle sizes, domain dimensions etc. It would be extremely tedious to perform actual experiments over such a wide range of parameters. Apart from being used to validate the constitutive models based on kinetic theory, such simulations have been used in recent years to examine flows in situations for which no reliable theoretical analyses have been attempted on any reasonable scale, e.g. in vibrated beds or in transitional flows in vertical hopper-bin configurations. Notable examples of work in the area of such simulations are Campbell & Brennen (1985), Walton & Braun (1986), Louge (1994), Walton (1992), Wassgren (1997) and Langston et al. (1994).

### 1.1.4 Boundary Conditions

Most theoretical analyses of granular flows are also hindered by the complexity of conditions to be assumed at boundaries, either at the bounding walls or between two distinct phases within a flow. Unlike Newtonian flows, no-slip conditions are rarely

encountered in most practical granular flows. Invariably, slip is present at the walls. The extent of slip depends on a variety of factors like particle and wall coefficients of restitution and friction, and the nature and size of asperities at the wall. The existence of slip, coupled with shearing of the flow at the wall, generates shear work which may be converted into fluctutating kinetic energy of the individual particles. This energy is usually dissipated into pure heat either by inelastic collisions or due to frictional interactions between particles. However, collisional or frictional interactions between particles and the bounding walls may also dissipate the random kinetic energy. Consequently, the bounding walls may serve as sources or sinks of fluctuating energy. As a result, the general flow field of a granular flow cannot be solved independantly of the conditions at the boundaries. Jenkins & Richman (1986) used kinetic theory arguments and a Maxwellian fluctuation velocity distribution to balance momentum and energy generation, flux and dissipation between flows of smooth, nearly elastic, circular disks and a bumpy boundary. However, apart from the limitations imposed by the assumption of a Maxwellian fluctuation velocity distribution, this work suffered from the additional drawback that the statistical averaging procedure involved the expansion of the fluctuation velocity distribution about a location not accessible to the center of any particle within the flow. Consequently, the location where the boundary conditions applied did not coincide with the location of the physical boundary encountered by particles adjacent to the boundary. Richman (1988) rectified this defect and extended the work to study flows of identical, smooth, nearly elastic spheres using a modified, more elaborate fluctuation velocity distribution function. Later, Richman & Marciniec (1990) continued the work to derive boundary conditions for granular flows at bumpy boundaries. Jenkins (1992) employed Coulombic friction, and both tangential and normal restitution to study boundary conditions for rapid granular flows with flat, frictional walls. Johnson & Jackson (1987) included frictional effects to derive equations for momentum and fluctuation energy balance at the walls

for the case of plane shear flows. These boundary conditions are discussed in detail in section 2.2.

In many instances, phase boundaries are encountered within the granular flows. Typical examples include funnel flows in hoppers, and some flows in vertical chutes, where a low-density flow regime may exist adjacent to a high-density, nearly-packed solid plug regime. Jenkins & Askari (1991) tried to model this flow by considering a momentum and energy balance at the interface between the two flows. They assumed the "solid" phase to be composed of highly agitated particles exchanging momentum and energy through collisions, but with no mean bulk motion. The low density flowing regime was modeled using standard kinetic theory arguments. Yi & Campbell (1992) asserted that it was unrealistic to assume such a sharp transition from a rapid flow regime to a solid state and that any transition from fluid-like rapid flow behavior to a solid-like behavior would be through an intermediate quasi-static state. Such a quasi-static state is characterized by long-duration contacts between particles unlike the binary collisions assumed in kinetic theory.

### 1.1.5 Mixing and Segregation

Another area of considerable research and industrial interest is particle mixing and segregation in monodisperse and polydisperse flows. Numerous applications in the chemical, pharmaceutical and food industries require the homogenization of mixtures of components that may vary in size, density, shape and surface properties. However, such property differences often promote segregation of the components, especially if the mixture is sheared or subjected to vibration. Scott & Bridgewater (1976), Tuzun & Arteaga (1992), Arteaga & Tuzun (1990), Dolgunin & Ukolov (1995), Ristow (1994), Baumann et al. (1994), Hill & Kakalios (1994), Zik et al. (1994), Peciar et al. (1994), Savage & Lun (1988), Johanson (1978) and Stephens & Bridgewater (1978) are some of the researchers to have studied problems of percolation and segregation

in polydisperse mixtures in a variety of different geometries. Williams (1976), Savage (1987), Poux et al. (1991) and Savage (1993) have reviewed developments in the area of mixing and segregation.

The existence of random components of particle velocities in granular flows leads to the possibility of the existence of diffusive particle motion, in monodisperse flows, analogous to that found in gases and liquids. Studies based on kinetic theories by Savage & Dai (1993) and by Hsiau & Hunt (1993b) define a granular self-diffusion coefficient that is proportional to the square root of the granular temperature and the particle diameter and is analogous to the corresponding coefficient for gaseous self-diffusion (Chapman & Cowling 1971). Studies based on kinetic theory show a strong dependence of the granular temperature on shear rates, and therefore the self-diffusion coefficients are expected to be functions of shear rates as well.

Several experimental studies have sought to investigate this relation between shear rates and self-diffusion coefficients. Hwang & Hogg (1980) examined the dependence of the transverse diffusion coefficients on the shear rate for flows in an inclined chute. Scott & Bridgewater (1976) studied the diffusive process in a simple shear cell subjected to reciprocating strains. Their results were later corrected by Bridgewater (1980) by appropriately accounting for Taylor dispersion effects. Buggisch & Loffelmann (1989) investigated the effect of shear on diffusion in an assembly of polydisperse vertical cylindrical rods in a Couette apparatus. Zik & Stavens (1991) conducted experiments on a vertically vibrated layer of grains, and measured diffusive displacements in the transverse direction. A similar vibratory experiment was also performed by Hunt et al. (1994). This experiment demonstrated that, for thin beds, the particle mixing in the direction of vibration was diffusive and could be modelled using the diffusion coefficient as defined by Savage & Dai (1993) and Hsiau & Hunt (1993b). All these experiments indicated that granular mixing could be modeled as a simple self-diffusive process. However, none of these experiments made actual measurements

of the fluctuation velocities. Savage & Dai (1993), Campbell (1993a) and Dai (1993) conducted computer simulations based on molecular dynamics models to examine self-diffusion in simple unbounded shear flows. Dai (1993) considered the effect of particle surface roughness. Hsiau & Hunt (1993a) studied the evolution of the mixing layer at the center in a vertical channel flow. They examined the influence of different wall conditions, chute widths and particle diameters on the diffusive process and measured the streamwise mean and fluctuation velocity profiles using fiber-optic probes. However, they did not make any measurements of the transverse fluctuation velocities. Furthermore, their diffusion studies were confined to the central uniform flow regime, and hence relationships between the shear rates and the diffusion coefficients could not be examined. They also did not examine diffusion in the streamwise direction.

In the areas of highly viscous suspensions, several studies, such as Eckstein et al. (1977) and Leighton & Acrivos (1987a), investigated the effect of the shear rate on the self diffusion coefficients. Both of these experiments used a Couette device to study the diffusion of a single tracer particle in the direction transverse to the direction of mean motion. Bossis & Brady (1987) investigated the self diffusive behavior of sheared concentrated suspensions using Stokesian Dynamics simulations. In addition, there have been investigations into the effect of an inhomogenous shear field on the net migration of particles in suspensions (Nott & Brady 1994, Leighton & Acrivos 1987b, Jenkins & McTigue 1990).

### 1.1.6 Heat Transfer in Granular Flows

While the flow characteristics of granular media have been the subject of intensive investigation in recent years, studies of heat transfer in such media, both experimental and theoretical, have been relatively few in number even though convective heat transfer to solid-gas flows is encountered in numerous process applications. While the

effects of the interstitial fluid are neglected while studying the dynamical behavior of most granular flows, it plays a vital role in the heat transfer process. Sun & Chen (1988) showed that in most cases, the heat transfer due to conduction at particle-particle and particle-wall contacts contributes negligibly to the overall heat tranfer process unless the particles have very high conductivities and are placed in a vacuum. Hence, the dominant mode of heat transfer is through heat exchange between the particles and the interstitial fluid. Furthermore, in the case of spherical particles, the local solid fraction immediately adjacent to a wall is always zero, and all heat transfer from a heated wall is through the interstitial fluid. Schlunder (1982) reviewed some of the earlier work in the area. Sullivan & Sabersky (1975) investigated the convective heat transfer from a flat plate immersed in a flowing granular medium in a vertical hopper-bin arrangement. They attempted to model the behavior of the fluid layer immediately adjacent to the heated surface in terms of a contact resistance that was directly proportional to the "effective" thickness of the interstitial fluid layer adjacent to the wall and inversely proportional to the diameter of spherical particles in the granular medium. It was expected that the contact resistance should have the same numerical value for geometrically similar arragements of particles adjacent to the wall. Conversely, any changes in the boundary conditions or particle sizes and shapes would alter the value of the contact resistance. Sullivan & Sabersky found good agreement between their measurements and their theoretical model. However, most of their experiments were performed in the plug flow regime with negligible variations in flow densities adjacent to the heated plate.

Spelt et al. (1982) extended Sullivan & Sabersky's work to investigate heat transfer to flows in an inclined chute at much higher velocities. They observed good agreement between their data and Sullivan & Sabersky's (1975) theoretical model for slow high-density flows, but found that beyond a certain flow speed, for a given material and depth of flow, the Nusselt number decreased with increasing Peclet numbers (or de-

creasing particle residence times adjacent to the wall). Patton et al. (1986) and Ahn (1989) also examined heat transfer in the inclined chute geometry and determined that at low flow velocities, the Nusselt number increased as particle residence times adjacent to the walls decreased, but beyond a certain point, any further decrease in particle residence times adjacent to the wall reduced the heat transfer coefficients. However, in the last two cited works, a measured average value of flow density was used to calculate the average flow velocity and hence all data for a particular material collapsed onto a single curve, unlike the results of Spelt et al. (1982). In the latter work, the static density of the bulk material was used to determine the flow velocity and hence a separate curve was obtained for each depth of flow. Patton (1985) derived a model based on the Reynolds analogy to extend Sullivan & Sabersky's work to flows with varying solid fraction. However, this model assumed that heat transfer within the bulk (away from the wall) was dominated by particle mixing. Ahn (1989) used finite different methods to develop numerical solutions for the convective heat transfer problem. He assumed the flow to be of uniform velocity but with a density gradient adjacent to the wall. This density gradient was determined from the value of the mean solid fraction and was approximated by a cubic profile.

All the studies cited above, with the exception of Sullivan & Sabersky (1975), recognized that the density of the flow close to the heated surface played a crucial role in determining the heat transfer characteristics of the granular flow. Gelperin & Einstein (1971) showed that for a solid-gas bulk material, the conductivity due to molecular conduction decreased significantly with a decrease in solid fraction. The conclusions reached from the studies cited above were that at high densities and low flow rates, there was little change in the density of granular material close to the wall; as a result, the value of the contact resistance at the wall remained reasonably constant. However, at higher flow rates, due to shearing-induced dilation of the flow close to the wall, there was a progressive increase in thermal resistance adjacent to

the wall. When coupled with lower bulk densities, there was a progressive decrease in heat transfer with a decrease in particle residence times adjacent to the wall.

In contrast, Wang & Campbell (1992) and Hunt & Hsiau (1993b) showed, that for low-density, highly-sheared flows, the thermal conductivity may actually increase with shear rate, because at low densities, the highly agitated particles could stream across longer distances leading to an enhancement of thermal mixing. Wang & Campbell (1992) performed their experiments in an annular shear cell. Hsiau & Hunt (1993b) used kinetic theory arguments to arrive at a streaming thermal conductivity value that was directly proportional to the square root of the granular temperature and varied inversely with the solid fraction of the material. Hence, it seems that for sheared flows, there may be two factors operating in opposition to one another as densities are reduced close to the wall. While the molecular conductivity goes down with increasing dilation, there is a possibility of an increase in the streaming contribution to the overall conductivity.

While few efforts in the area of granular flows have considered density effects close to the wall, Kubie & Broughton (1975) attempted to include the effects of void fraction variations close to the heat-transfer surface in their model describing heat transfer to gas fluidized beds. Kubie (1985) also tried to relate the contact resistance at the wall to the statistical variation of thermal properties in the vicinity of the heat-transfer surface. An earlier work, Botteril & Desai (1972) also identified particle packing density and mobility near the heated surface as being important factors governing heat transfer to a fluidized or packed bed.

## 1.2 Overview of Thesis

The analytical background for most of the work in this thesis is discussed in Chapter 2. Sections 2.1 and 2.2 describe the kinetic theory of Lun et al. (1984) along with

the modifications of Johnson & Jackson (1987) incorporating some frictional features. The governing equations and the boundary conditions are discussed in detail, especially in the context of the vertical channel flows studied in this work. Section 2.3 gives an overview of the theoretical background describing diffusion phenomena, especially in monodisperse systems. The appropriate equations describing heat-transfer in granular flows are presented in section 2.4.

Experimental apparatus and procedures for determining velocity profiles and self-diffusion coefficients for granular flows in vertical chutes are described in Chapter 3. The image-processing methods used to identify and track particles are discussed in detail in section 3.1. Data pertaining to the velocity profiles is presented in section 3.2 while the results for the self-diffusion experiments are presented in section 3.3.

Chapter 4 describes the heat-transfer experiments in detail. The apparatus and procedure are discussed in section 4.1 while the experimental data and results are discussed in section 4.2.

Chapter 5 examines the numerical solutions of the momentum and energy equations discussed in Chapter 2 and attempts to compare the results with experimentally obtained data. The effects of particle properties like size and coefficient of restitution are considered, along with the effects of the boundary on both momentum and heat transfer. Comparisons are also made between theoretical and experimental values of the self-diffusion coefficients.

Chapter 6 summarises the work performed for this thesis and identifies its conclusions and limitations.

# Chapter 2 Analytical Background

## 2.1 Constitutive Equations

As stressed in the introduction, most of the theoretical developments in the area of granular flows over the last two decades have centered around the use of concepts based on dense-gas kinetic theory. The work of Lun et al. (1984) forms the basis of most of the discussions pertaining to kinetic theory in this work. However, the theory of Lun et al. restricts all particle interactions to take the form of instantaneous binary collisions and does not account for any frictional contacts between particles. Such a description is better suited for granular flow regimes that involve rapid deformation and have relatively low flow densities. When deformation rates are low, particles are much closer together and inter-particle contacts are sustained for long durations and the dynamics are more of a frictional nature. Most real granular flows, and flows investigated during the course of experiments in this work, are somewhat intermediate in nature and display features of both frictional and collisional interactions. As noticed in the current set of experiments, granular flows often exhibit phase boundaries between high-density low-deformation and low-density high-deformation regimes. Johnson & Jackson (1987) proposed constitutive relations and boundary conditions for the intermediate case that assumed stresses to be a simple sum of the contributions from the two extreme sources. They assumed the collisional-translational contributions to be of the form prescribed by Lun et al. (1984). The frictional contributions were based on a Coulombic, empirical, macroscopic model. This development is described in the latter part of this section.

### 2.1.1 Kinetic Theory Contributions

In order to model the random motion of particles in a manner consistent with dense gas kinetic thery, it is essential to assume a single particle velocity distribution funciton analogous to the Maxwellian distribution assumed for gas molecules. However, granular flows are not equilibrium flows and particle motions are not self-sustaining; unlike the case for gas molecules, particle collisions are inelastic and there is a continuous dissipation of energy. The existence of such a dissipative mechanism leads to the presence of gradients in velocity, density and granular temperature within the flow and hence the single particle motions can longer be described by a Maxwellian distribution. Lun et al. assumed their single particle velocity distribution to be of the form:

$$f^{(1)} = f^{(0)}(1 + \Phi), \tag{2.1}$$

where $\Phi$ is a perturbation function such that $\Phi \ll 1$, and $f^{(0)}(\mathbf{r},\mathbf{c};t)$ is the Maxwellian velocity distribution function:

$$f^{(0)}(\mathbf{r},\mathbf{c};t) = \frac{n}{(2\pi\mathbf{T})^{\frac{3}{2}}}\exp\left(-\frac{C^2}{2\mathbf{T}}\right). \tag{2.2}$$

In the above equation, $\mathbf{r}$ and $\mathbf{c}$ are the particle's location and local velocity respectively while $t$ is the time and $n$ is the local particle number density. $C$ is the magnitude of the fluctuation velocity $\mathbf{C}$ and $\mathbf{T}$ is the granular temperature. The fluctuation velocity is the local velocity deviation from the mean velocity $\mathbf{u}$ where $\mathbf{u} =< \mathbf{c} >$ and $\mathbf{C} = \mathbf{c} - \mathbf{u}$. The granular temperature is a measure of the specific kinetic energy of the particles and is given by $\mathbf{T} =< C^2 > /3$, where the symbol $< >$ represents an ensemble averaged quantity. For any local particle property $\Psi$, the ensemble average is determined by averaging $\Psi$ over the entire velocity space:

$$< \Psi >= \frac{1}{n}\int \Psi f^{(1)}(\mathbf{r},\mathbf{c};t)d\mathbf{c}. \tag{2.3}$$

Details regarding the derivation of the perturbation function can be found in Lun

et al. (1984). In the limit of perfectly elastic particles, the perturbation function of Lun et al. is identical to that of Chapman & Cowling (1971).

In order to perform the collision integrals to evaluate the flux of material properties, it is essential to determine a pair distribution function, $f^2(\mathbf{r}_1, \mathbf{c}_1, \mathbf{r}_2, \mathbf{c}_2; t)$. The probability of finding a pair of particles in the volume elements $\delta\mathbf{r}_1$, $\delta\mathbf{r}_2$ centered about $\mathbf{r}_1$ and $\mathbf{r}_2$ and having velocities within the ranges $\mathbf{c}_1$ and $\mathbf{c}_1 + \delta\mathbf{c}_1$, and $\mathbf{c}_2$ and $\mathbf{c}_2 + \delta\mathbf{c}_2$ is $f^{(2)}(\mathbf{r}_1, \mathbf{c}_1, \mathbf{r}_2, \mathbf{c}_2; t)\delta\mathbf{r}_1\delta\mathbf{r}_2\delta\mathbf{c}_1\delta\mathbf{c}_2$. Lun et al. used the Enskog assumption for dense gases to define the pair distribution function as:

$$f^2(\mathbf{r}_1, \mathbf{c}_1, \mathbf{r}_2, \mathbf{c}_2; t) = g_0(\nu) f^{(1)}(\mathbf{r} - \sigma\mathbf{k}, \mathbf{c}_1; t) f^{(1)}(\mathbf{r}, \mathbf{c}_2; t), \tag{2.4}$$

which assumes that the probability of finding a pair of particles at a certain location is determined from the product of the single particle distribution functions and the radial distribution function $g_0(\nu)$, evaluated when the particles are in contact. Here, $\sigma$ is the particle diameter and $\mathbf{k}$ is the unit vector directed from the center of particle 1 to the center of particle 2. Throughout this work, the form of the radial distribution function used is the one suggested for sheared flows by Lun & Savage (1987):

$$g_0(\nu) = (1 - \nu/\nu^*)^{-2.5\nu^*}. \tag{2.5}$$

Here $\nu^*$ is the maximum shearable solid fraction for the particle assembly. It must be noted that the radial distribution function defined above is based on the assumption of collisional isotropy which requires an isotropic distribution of collision angles between the two colliding spheres.

Following the derivation procedures of Lun et al. (1984), the following hydrodynamic equations are obtained:

$$\frac{d\rho}{dt} = -\rho\nabla \cdot \mathbf{u}, \tag{2.6}$$

$$\rho\frac{d\mathbf{u}}{dt} = \rho\mathbf{F} - \nabla \cdot \mathbf{P}, \tag{2.7}$$

$$\frac{3}{2}\rho\frac{d\mathbf{T}}{dt} = -\mathbf{P}_{kt} : \nabla\mathbf{u} - \nabla\cdot\mathbf{\Gamma} - \gamma, \tag{2.8}$$

where $\rho$ is the bulk flow density and is equal to the product of the particle density $\rho_p$ and the solid fraction $\nu$. In the above equations, $\mathbf{P}$ is the total pressure tensor, $\mathbf{P}_{kt}$ is the contribution to the stress tensor from the collisional and translational components, $\mathbf{F}$ the specific body force, $\mathbf{\Gamma}$ the fluctuating energy flux and $\gamma$ is the specific energy dissipated due to particle collisions. As explained in Lun et al. both $\mathbf{P}_{kt}$ and $\mathbf{\Gamma}$ are composed of both the streaming and collisional components of momentum and energy transfer respectively.

Using the appropriate form of the perturbation function $\Phi$, Lun et. al. obtained the following expression for the stress tensor $\mathbf{P}_{kt}$, the fluctuating energy flux $\mathbf{\Gamma}$ and the specific energy dissipation $\gamma$.

$$\mathbf{P}_{kt} = \left[\rho_p g_1(\nu, e_p)\mathbf{T} - \rho_p\sigma\frac{8}{3\sqrt{\pi}}\eta\nu^2 g_0\mathbf{T}^{\frac{1}{2}}\nabla\cdot\mathbf{u}\right]\mathbf{I} - 2\rho_p\sigma g_2(\nu, e_p)\mathbf{T}^{\frac{1}{2}}\mathbf{S}, \tag{2.9}$$

$$\mathbf{\Gamma} = -\rho_\mathbf{p}\sigma\left[g_3(\nu, e_\mathbf{p})\mathbf{T}^{\frac{1}{2}}\nabla\mathbf{T} + g_4(\nu, e_\mathbf{p})\mathbf{T}^{\frac{3}{2}}\nabla\nu\right], \tag{2.10}$$

$$\gamma = \frac{\rho_p}{\sigma}g_5(\nu, e_p)\mathbf{T}^{\frac{3}{2}}, \tag{2.11}$$

where $\mathbf{I}$ is the identity matrix and $\mathbf{S}$ is the deviatoric part of the rate of deformation tensor, and is given by:

$$\mathbf{S} = \frac{1}{2}(u_{n,p} + u_{p,n}) - \frac{1}{3}u_{l,l}\delta_{n,p}, \qquad l, n, p = x, y, z, \tag{2.12}$$

and $\eta = \frac{1}{2}(1 + e_p)$.

The coefficients $g_1$, $g_2$, $g_3$, $g_4$ and $g_5$ are expressed as:

$$g_1(\nu, e_p) = \nu + 4\eta\nu^2 g_0, \tag{2.13}$$

$$g_2(\nu, e_p) = \frac{5\sqrt{\pi}}{96}\left\{\frac{1}{\eta(2-\eta)g_0} + \frac{8}{5}\frac{3\eta-1}{2-\eta}\nu + \frac{64}{25}\eta(\frac{3\eta-2}{2-\eta} + \frac{12}{\pi})\nu^2 g_0\right\}, \tag{2.14}$$

$$\begin{aligned} g_3(\nu, e_p) &= \frac{25\sqrt{\pi}}{16\eta(41-33\eta)}\left\{\frac{1}{g_0} + \frac{12}{5}\eta[1+\eta(4\eta-3)]\nu\right. \\ &+ \left.\frac{16}{25}\eta^2[9\eta(4\eta-3) + \frac{4}{\pi}(41-33\eta)]\nu^2 g_0\right\}, \end{aligned} \tag{2.15}$$

$$g_4(\nu, e_p) = \frac{15\sqrt{\pi}}{4}\frac{(2\eta-1)(\eta-1)}{41-33\eta}\left(\frac{1}{\nu g_0} + \frac{12}{5}\eta\right)\frac{d}{d\nu}(\nu^2 g_0), \tag{2.16}$$

$$g_5(\nu, e_p) = \frac{48}{\sqrt{\pi}}\eta(1-\eta)\nu^2 g_0. \tag{2.17}$$

### 2.1.2 Frictional Contributions

Unlike the micro-structural analysis inherent in the kinetic theory developments discussed above, constitutive models for the frictional behavior of granular materials are primarily based on empiricism. Schoefield & Wroth (1968) and Roscoe (1970) developed upon the "critical-state" theory that postulated the existence of a collection of yield surfaces in the principal-stress space, one for each value of the bulk density of the granular material. The constitutive relations required the principal axes of stress and rate of deformation to be aligned, with the major principal rate-of-deformation axis parallel to the minor (compressive) principal stress axis. A proper choice of geometry for the yield surfaces described the dilation accompanying the deformation of granular materials and also predicted the Coulombic proportionality between shear and normal stresses in plane shearing. However, the requirement of alignment of the principal stress and rate of deformation axes was not very realistic. Yet other theories (de Jong 1971) do not require such an alignment. Jackson (1983) has reviewed these theories in detail.

All the flows examined in this thesis involved the fully-developed plane shearing of a granular material. Under such circumstances, the granular material is in a critical state and the shear stress is directly proportional to the normal stress, with the normal stress being related to the density of the flow. Furthermore, in plane shearing of fully-developed flows, the principal axes of stress are inclined at $\pm\frac{1}{4}\pi$ to the direction of flow. Also, in the critical state, the ratio of the major to the minor pricipal stress is given by $(1+\sin\phi)/(1-\sin\phi)$ where $\phi$ is defined as the internal angle of friction. Under these conditions, the frictional shear stress, $S_f$, and the frictional normal stress, $N_f$, are related by the expression:

$$S_f = N_f \sin\phi. \tag{2.18}$$

Experimental observations show that the frictional normal stress increases rapidly with bulk density and diverges as the close-packed bulk density $\nu_0$ is approached. Johnson, Jackson & Nott (1990) used such experimental observations as their basis in proposing the following simple algebraic expression to describe the frictional normal stress in a granular flow undergoing plane shear.

$$\begin{aligned} N_f &= Fr\frac{(\nu-\nu_{min})^p}{(\nu_0-\nu)^n} \qquad \nu > \nu_{min} \\ &= 0 \qquad\qquad\qquad\qquad \nu < \nu_{min}, \end{aligned} \tag{2.19}$$

where $Fr$, $n$ and $p$ are constants. It is assumed that at solid fractions below $\nu_{min}$, particles are no longer in long-durational contact and hence, all frictional contributions to the stress go to zero. Johnson & Jackson (1987) and Johnson, Jackson & Nott (1990) assumed that the total stress is a simple sum of the contributions from the kinetic theory and frictional analyses at any rate of flow deformation. These assumptions have been made in the numerical portion of this thesis as well.

## 2.2 Boundary Conditions

As with the bulk material, the interactions between the flow particles and the wall may be collisional or frictional in nature. Jenkins & Richman (1986) and Richman (1988) used kinetic theory arguments to balance momentum and energy transfer between the flow material and the bounding surface. Their model did not include the effect of frictional interactions at the wall and also required a very specific description of the geometric structure of the wall. Johnson & Jackson (1987) derived boundary conditions for granular flows using arguments similar to those of Hui et al. (1984), and also included frictional interactions. In the limiting case of purely collisional interactions between the wall and the flow particles, their conditions reduced to a form similar to that of Richman (1988). However, because their conditions did not invoke any explicit description of the boundary geometry, certain experimentally determined parameters have to be incorporated into their conditions. The boundary conditions derived by Johnson & Jackson (1987) have been used in this work.

Equating the stress exerted by the flow on the boundary with the limit of the stress in the flowing material on approaching the boundary results in the following condition on the slip velocity,

$$\frac{\mathbf{u_{sl}} \cdot (\mathrm{P_f} + \mathrm{P_{kt}}) \cdot \mathbf{n}}{|\mathbf{u_{sl}}|} + \frac{\phi' \sqrt{3} \pi \rho_p \nu \mathbf{T}^{\frac{1}{2}} |\mathbf{u_{sl}}| g_0(\nu)}{6\nu^*} + N_f \tan\delta = 0. \qquad (2.20)$$

The slip velocity, $\mathbf{u_{sl}} = \mathbf{u} - \mathbf{u_{wall}}$, is the relative velocity between the particles in contact with the wall and the wall itself. The unit normal vector directed inwards from the wall into the flow is designated as $\mathbf{n}$. The first term in Equation (2.20) above is the limit of the stress in the flow approaching the wall. The second term represents the stress acting on the boundary due to particle-wall collisions. The "specularity coefficient" $\phi'$ is defined as the average fraction of the relative tangential momentum transferred during a collision between the particle and the boundary. It serves as a measure of the roughness of the bounding surface and ranges from zero for perfectly

specular collisions to unity for perfectly diffuse collisions. The third term in Equation (2.20) represents the frictional stress on the bounding wall and $\delta$ is the angle of friction between the wall and the flowing material.

A boundary condition on the fluctuating energy is obtained from an energy balance on a slice of vanishingly small thickness of material enclosing an element of the solid boundary and is given by:

$$-\mathbf{n}\cdot\mathbf{\Gamma} = \frac{\pi\rho_p\nu(1-{e_w}^2)\sqrt{3}\mathbf{T}^{\frac{3}{2}}g_0(\nu)}{\nu^*} - \frac{\phi'\sqrt{3}\pi\rho_p\nu\mathbf{T}^{\frac{1}{2}}|\mathbf{u_{sl}}|^2 g_0(\nu)}{6\nu^*}. \tag{2.21}$$

While the first term on the right hand side of Equation (2.21) represents the dissipation of fluctuation energy due to inelastic particle-wall collisions, the second term represents the production of fluctuation energy at the boundary due to shear work. The left hand side of Equation (2.21) represents the net fluctuation energy flux into the bulk. It is important to note that implicit in Equation (2.21) is the assumption that all shear work due to collisional stresses is converted into random fluctuation energy. It is also assumed in this work that all shear work due to frictional stresses is converted into internal thermal energy of the bulk material.

## 2.3 Self-Diffusion

Self diffusion refers to the motion (displacement) of particles in a monodisperse system, which cannot be accounted for by the mean motion of the material. An example of self-diffusive motion, in a uniform flow, is depicted in Figure 2.1. It arises as a consequence of the existence of the random fluctuation velocity components. Savage & Dai (1993) and Campbell (1993a) have considered the diffusive behavior of granular systems in a manner analogous to the diffusive behavior of suspended particles undergoing Brownian motion in a liquid (Einstein 1956). Under these circumstances, were a system to be simply diffusive, the diffusive displacements or the mean-square particle displacement due to the random velocity components can be related to the

coefficient of self-diffusion $D$ by the kinematic expression:

$$\lim_{t\to\infty} < |\mathbf{R}|^2 >= 6Dt, \tag{2.22}$$

where $\mathbf{R}$ is the diffusive displacement and $t$ is the time. In the case of a granular flow, the fluctuation velocities may be anisotropic. Under such circumstances, it is more appropriate to define a diffusion coefficient tensor $\mathbf{D}_{ij}$ as

$$\lim_{t\to\infty} < \Delta x_i \Delta x_j >= 2\mathbf{D}_{ij}t, \tag{2.23}$$

where $\Delta x_i$ is the diffusive displacement in direction '$i$'. It must be noted, that for very short timescales, the root-mean-square diffusive displacements vary linearly with time (Campbell 1993a).

The self diffusion coefficients can also be determined in a statistical manner, without tracking the particles explicitly (Taylor 1922, Batchelor 1949), based on techniques developed to investigate diffusion in stationary homogeneous turbulence. For large $t$, it is found that:

$$\lim_{t\to\infty} < \Delta x_i \Delta x_j >= \sqrt{< u'_i{}^2 >< u'_j{}^2 >}\, T_{Lij}t, \tag{2.24}$$

where the instantaneous magnitude of the fluctuating velocity component is given by $u'_i$ and the Lagrangian time scale $T_{Lij}$ is defined as:

$$T_{Lij} = \int_{-\infty}^{\infty} R_{Lij}(\xi)d\xi, \tag{2.25}$$

with $R_{Lij}$, a scaled correlation of the instantaneous fluctuating particles, given by:

$$R_{Lij}(\xi) = \frac{< u'_i(t)u'_j(t+\xi) >}{\sqrt{< u'_i{}^2 >}\sqrt{< u'_j{}^2 >}}. \tag{2.26}$$

The assumption that the flow is statistically stationary implies that $R_{Lij}$ is independent of $t$. From Equations (2.23) and (2.24-2.26), it is seen that:

$$\mathbf{D}_{ij} = (\sqrt{< u'_i{}^2 >}\sqrt{< u'_j{}^2 >}\, T_{Lij})/2. \tag{2.27}$$

Hsiau & Hunt (1993b) and Savage & Dai (1993) used kinetic theory arguments to arrive independently at the following expression for the self-diffusion coefficient:

$$\mathbf{D}_{ii} = \frac{\sigma(\pi \mathbf{T})^{\frac{1}{2}}}{8(1+e_p)\nu g_0(\nu)}. \tag{2.28}$$

In the case of perfectly elastic particles, Equation (2.28) reduces to the classical Chapman-Enskog expression.

Each of the above representations of the self-diffusion tensor is based on the assumption that the fluctuation velocity field is homogeneous and stationary. Equation (2.28) has the added assumption that the fluctuation velocity field is isotropic. The applicability of Equation (2.23) for the determination of the diffusion tensor in simple shear flows is convenient since for a simple unbounded granular shear flow, with a uniform shear rate, the generation of granular temperature through shear work is balanced by its dissipation through collisions. Therefore, even if the mean velocity field is inhomogeneous, the fluctuation velocity field is homogeneous and the granular temperature is only a property of the strain rate and the material. However, such a uniform fluctuation field is rarely encountered in experiments where the boundaries serve as sources or sinks for the random kinetic energy. The presence of boundaries leads to gradients in the fluctuation velocity field. A phenomenon that arises because of the mean velocity gradient is "Taylor dispersion" (Taylor 1953, 1954). Transverse fluctuations cause a particle to be displaced transverse to the direction of mean motion to a position where the mean velocity is different from that at its initial position. This velocity difference manifests itself as an apparent diffusive displacement of the particle as depicted in Figure 2.2. Hence, it is essential to separate the total diffusive behavior in the direction of mean motion into its "Taylor diffusive" and "random diffusive" components with the latter contribution arising out of the particle fluctuation velocity in the streamwise direction.

## 2.4 Heat Transfer

Sullivan & Sabersky (1975) studied the problem of convective heat transfer from a flat plate to a flowing granular medium. On the basis of their observations and experimental results, they proposed an approximate analytical model that attempted to account for the particulate nature of the material, and arrived at the following semi-empirical relation:

$$\mathrm{Nu}^* = \frac{1}{(\chi + \frac{1}{2}\sqrt{\frac{\pi}{\mathrm{Pe}^*}})}, \tag{2.29}$$

where

$$\mathrm{Nu}^* = \frac{\mathrm{h}\sigma}{k_{\mathrm{g}}}, \tag{2.30}$$

and

$$\mathrm{Pe}^* = (\frac{\mathrm{UL}}{\alpha_{\mathrm{c}}})(\frac{\sigma}{\mathrm{L}})^2(\frac{k_{\mathrm{c}}}{k_{\mathrm{g}}})^2. \tag{2.31}$$

Appendix I explains the derivation of Equation (2.29) in greater detail. The expression in Equation (2.29) was derived for a uniform plug flow, at a velocity U past a heated plate of length L. The thermal conductivity and the diffusivity of the bulk material, at critical density, are given by $k_c$ and $\alpha_c$ respectively while $k_g$ is the conductivity of the interstitial fluid. In essence, this model considered the flow regime to be composed of two distinct regions: the bulk flow material, considered as a continuum with uniform density (the critical density) and velocity, and an interstitial fluid layer seperating the heated wall from the granular material continuum. The interstitial fluid layer was assumed to have a thermal resistance $\chi$, which may be defined as $\chi^{-1} = \frac{h_{wp}\sigma}{k_g}$ where $h_{wp}$ is the wall-particle heat transfer coefficient (or the thermal conductance between particles and the wall). The thermal conductance is expected to be a strong function of the local geometric arrangement of particles as this would significantly influence the "effective" thickness of the interstitial fluid layer. As a consequence, $\chi$ would depend on factors like the particle shape and the wall surface roughness. Schlunder (1982) developed the following expression for $h_{wp}$, obtained by

integrating the local conduction flux across the gas-filled gap between a sphere and a plane at point contact.

$$h_{wp} = \phi_A \frac{4k_g}{\sigma} \left[ (1 + \frac{2l + 2\delta_{eff}}{\sigma}) ln(1 + \frac{\sigma}{2l + 2\delta}) - 1 \right], \tag{2.32}$$

where $\phi_A$ is a surface coverage factor, $l$ is the modified mean free path of interstitial fluid molecules and $\delta$ is the effective roughness of the surfaces. From Equation (2.32), it is evident that the thermal conductance $h_{wp}$ is inversely proportional to the particle diameter, which implies that the total heat transfer coefficient increases with a decrease in particle diameter. This result is consistent with the observation that for smaller particle diameters, for the same solid fraction, the effective thickness of the interstitial fluid layer adjacent to the wall is lower. Another factor of importance is that the surface coverage factor, $\phi_A$, defined as the area on the wall projected by particles per unit wall area, is a function of the solid fraction adjacent to the wall. The effective thickness of the interstitial fluid layer also increases for low density flows where particles immediately adjacent to the walls may not always be in constant contact with the wall. Consequently, $\chi$ has a strong dependance on the density of the flow, adjacent to the wall and is not expected to be a constant (as assumed by Sullivan & Sabersky) for flows where the density close to the wall varies significantly with the velocity or strain rate.

While the expression in Equation (2.29) agreed well with the experimental results of Sullivan & Sabersky (1975), Spelt et al. (1982), Patton et al. (1986) and Ahn (1989) for very low velocity, high density flows, experimental data deviated significantly from the theoretical predictions at higher velocities. As the velocities increased, the value of $Nu^*$ initially increased with the value of $Pe^*$ to a maximum, and decreased with further increase in velocity. As identified in all these studies, the reason for this discrepancy lay in the fact that at high densities and low flow rates, the density of the granular material remained close to its critical density. However, at higher flow

rates, the flow adjacent to the wall dilated significantly and densities were much lower than the critical densities. This lead to an increase in the effective thickness of the interstitial fluid layer and increased the value of the thermal contact resistance $\chi$. Furthermore, as evident in the following expression for the bulk conductivity of a solid-gas bulk material, proposed by Gelperin & Einstein (1971), the conductivity due to molecular conduction decreases significantly with a decrease in solid fraction. They defined the effective conductivity of the bulk material $k_{mc}$ as:

$$\frac{k_{mc}}{k_g} = 1 + \frac{\nu(1 - \frac{k_g}{k_s})}{\frac{k_g}{k_s} + 0.28(1-\nu)^{0.63(\frac{k_g}{k_s})^{-0.18}}} \tag{2.33}$$

where $k_g$ and $k_s$ are the conductivities of the gas and the solid material respectively.

Hsiau & Hunt (1993b) used arguments based on the dense-gas kinetic theory model, assuming that the only mode of heat transfer was the streaming mode. Heat transfer during the collisional interactions amongst the particles was assumed to be negligible. Apart from the assumptions inherent in the kinetic theory analysis, the Biot number ($\mathrm{Bi} = \frac{h_{pf} l_p}{k_p}$) was assumed to be less than 0.1 to allow a lumped mass analysis for the particles. Here, $h$ is the heat transfer coefficient between particle and the surrounding fluid, while $k_p$ and $l_p$ are the particle's conductivity and characteristic length respectively. Under these assumptions, they arrived at the following expression for the effective conductivity $k_{kt}$:

$$k_{kt} = \frac{\rho c_p \sigma (\frac{\mathbf{T}}{\pi})^{\frac{1}{2}}}{9\nu g_0(\nu)}, \tag{2.34}$$

where $c_p$ is the specific heat capacity of a particle and $\rho$ is the mixture density, also expressible as $\nu\rho_p$. Equation (2.34) implies that a decrease in the solid fraction would allow particles to stream across larger distances, thereby enhancing the effective conductivity. The similarity of the form of Equations (2.28) and (2.34) for the self-diffusion coefficient and the effective conductivity leads to the conclusion that enhanced particle mixing enhances the effective streaming conductivity of the flowing

material. This trend was corraborated, albeit qualitatively, by Wang & Campbell (1992) during the course of their experiments in an annular shear cell.

A comparison of Equations (2.33) and (2.34) suggests that for low-density, highly sheared flows, the two mechanisms may be operating in opposition to one another. A decrease in density reduces the bulk molecular conductivity, but may simultaneously enhance the streaming conductivity.

An attempt was made in the numerical portion of this thesis to identify the relative effects of the two mechanisms and their influence on the overall convective heat transfer, by solving the following internal energy equation over the flow field.

$$\rho c_p \frac{DT}{Dt} = -\nabla \cdot q_h - \mathbf{P}_f : \nabla \mathbf{u} + \gamma, \tag{2.35}$$

where $T$ refers to the thermodynamic temperature, $\mathbf{P}_f$ is the frictional stress tensor, and $\gamma$ is the contribution due to the inelastic dissipation of random kinetic energy into pure thermal energy. The relation $\nu\rho_p c_p + (1-\nu)\rho_{air} c_{air} \approx \rho c_p$ was applied in the above equation. Also, as evident from the second term in the right side of Equation (2.35), it is assumed that all work done against frictional stresses is converted into heat, and not into random kinetic energy. Furthermore, the diffusive flux term in Equation (2.35) may be written as:

$$\nabla \cdot q_h = -\nabla \cdot (k_{tot} \nabla T), \tag{2.36}$$

where $k_{tot}$ is defined as the simple sum of the thermal conductivity contributions due to molecular conductivity, $k_{mc}$ and the streaming or kinetic conductivity, $k_{kt}$, arising out of the kinetic theory analysis.

The analytical background provided in this chapter forms the basis for the numerical investigations described in Chapter 5.

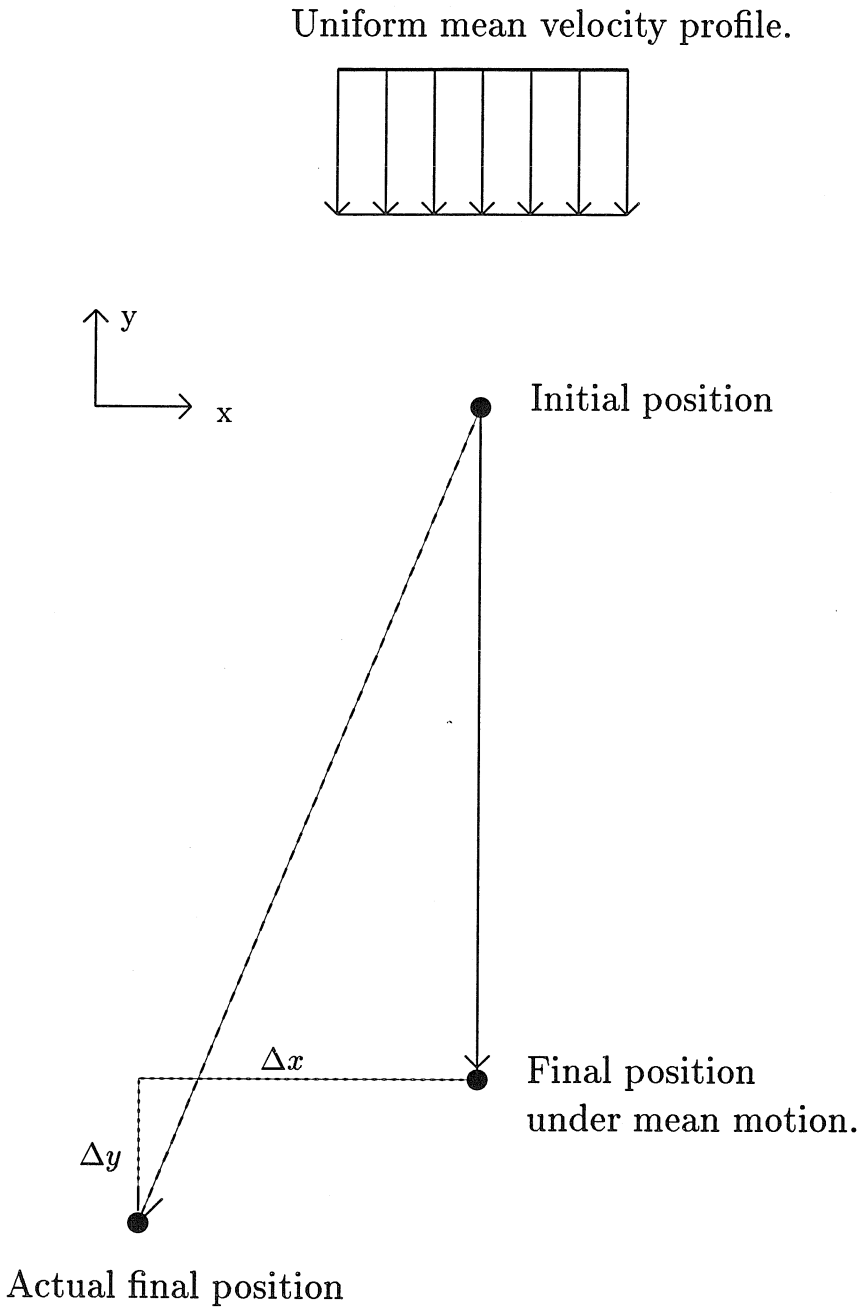


Figure 2.1: An example of self-diffusive motion in a uniform flow. $\Delta x$ and $\Delta y$ are diffusive displacements.

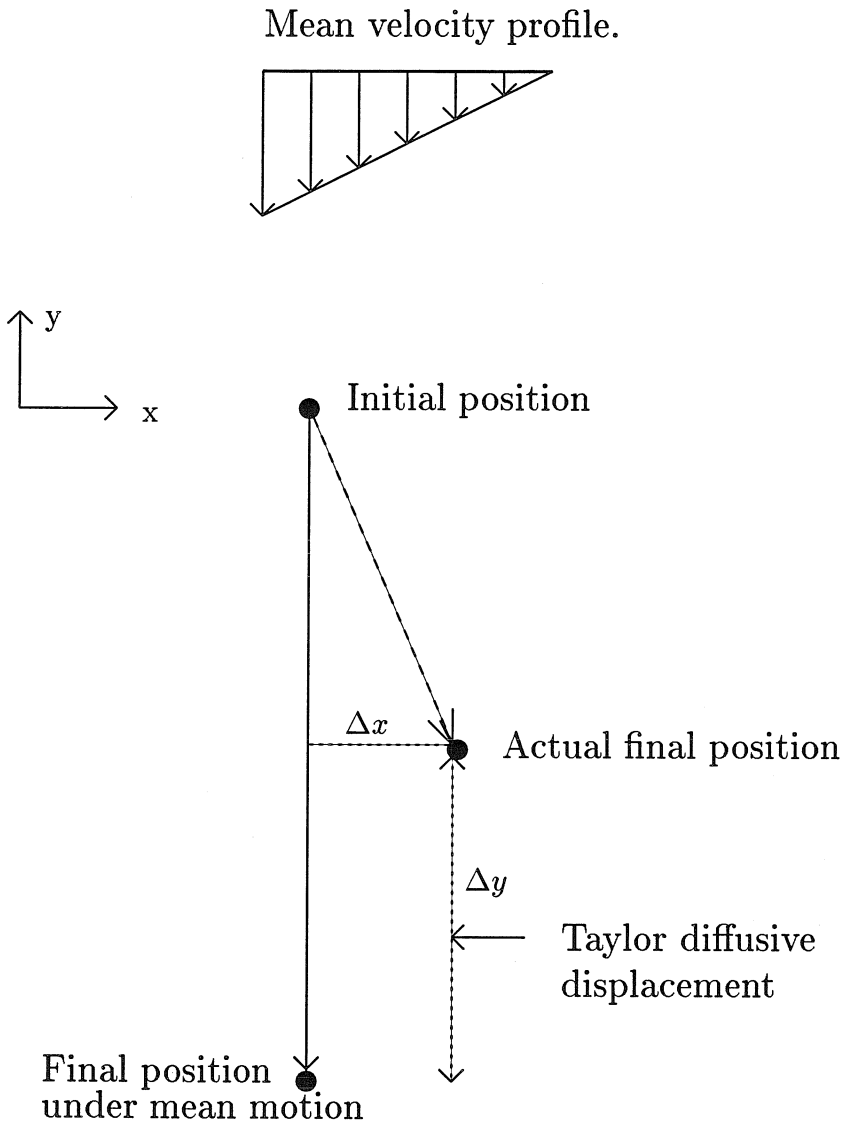


Figure 2.2: An example of Taylor-diffusion in a sheared flow without any random diffusion component in the y-direction. $\Delta x$ and $\Delta y$ are diffusive displacements.

# Chapter 3 Experimental Studies of Velocity Profiles and Self-Diffusion Coefficients

## 3.1 Apparatus and Procedures

All the experiments described and discussed in this work were performed in a vertical chute apparatus. The first set of experiments, to measure mean and fluctuating velocity profiles and self-diffusion coefficients, were performed in a vertical chute 100 cm high and 2.18 cm deep. The schematic of the vertical chute facility is shown in Figure 3.1. The whole structure was made of alder wood. The chute was designed in a manner that made it possible to dismantle the test section easily, and different side walls could be inserted, depending upon the desired boundary conditions. It was also possible to vary the width of the test section. Unless specified, all the velocity and self-diffusion results presented in this chapter are for a test section width of 5 cm. Polished tempered-glass plates were used for the front and back surfaces to minimize friction at these surfaces and to create a two-dimensional flow. An upper hopper fed the particles into the test section. A flow control valve with a variable exit width was used to control the material flow rate. The material flow rate was measured by collecting the material exiting the test section over a specified period of time and weighing the sample. The chute was dismantled and cleaned after every three runs in order to minimize the effects of dirt and static charge. The nominal diameter of the particles used in all the experiments was 3 mm. As shown in Hsiau & Hunt (1993a),

the surface conditions at the sidewalls have a significant influence on the velocity and fluctuation velocity profiles. For comparison of velocity profiles, two different sidewall conditions were used: polished glass, and walls roughened by adhering 3 mm diameter glass spheres to the surface in a regular, close-packed, hexagonal pattern.

The technique used to measure velocities was based on the work of Taylor & Hunt (1993) and incorporated the use of imaging methods. In all the experimental runs, the flow was seeded with a small proportion of black tracer particles (2% by weight). After filling the channel and the hopper with the flow material, the exit valve was opened in order to initiate the flow. Simultaneously, the front section of the flow was filmed and recorded on video tape using a commercial video recorder. The video recorder used was a JVC "Videomovie", high resolution CCD device with S-VHS-C capabilities. In order to subsequently process the video tapes, the camera was connected to a frame-grabber board (Silicon Video Mux, 1-Meg) mounted in a personal computer. The frame-grabber has the ability to "capture" sequences of image frames at a specified frame rate and to store them, in digitized form, in an on-board memory buffer. The length of each image sequence stored was limited by the available capacity of memory on the frame-grabber board buffer. Once an image sequence had been captured by the frame-grabber, it was transferred from the board's buffer to the memory on the host personal computer so that the on-board buffer could be freed to capture the next sequence of images. This process was repeated until an appropriate number of image sequences had been digitized and stored, for the particular flow being investigated.

The stored digitized images contained pixel values on a grey scale of 0 to 255 (8 bit), with 0 representing black and 255 white. Each of the stored image frames was then processed to remove any shadows, and to enhance the contrast between the black tracer particles and the non-tracer background. Figure 3.2 depicts typical examples of a pair of raw and processed images. Then each tracer particle in the first image in a sequence was identified, along with its centroid. Subsequently the shift

in a tracer particle's position between two consecutive images was determined using an autocorrelation process (Taylor & Hunt 1993). In this autocorrelation process, a small window was drawn, in the first image, around the identified tracer particle. This window was then overlaid on the next image, but was shifted in order to account for the particle motion between the two images. The corresponding pixel values for the window, and the underlying portion of the second image were multiplied, and the resultant values summed over all pixel locations to obtain an autocorrelation value appropriate to the amount of shift applied. This process was repeated for a range of anticipated particle displacements. The shift producing the maximum autocorrelation value was assumed to represent the actual displacement of the particle. As a check, the displacement of a particle between two successive images could be calculated from the positions of its centroid in those images. The frames were acquired from the video tape at the rate of 30 frames per second (f.p.s). The velocity was then calculated from the displacement and the time step. This measurement technique involved the averaging of velocities over a finite length of the chute which varied from 2 to 2.5 cm. The flow section was divided into bins of equal width, in the transverse direction. In all the velocity profiles shown, the velocity and position were obtained by averaging over the velocities and positions of all the tracer particles detected within a particular bin. In all the results presented here, unless indicated, the bin width was 1.5 mm or half a particle diameter.

In all cases, the $x$-direction was the direction of mean flow, while the $y$-direction was transverse to the flow. All transverse measurements were made with reference to the axis of symmetry. For each velocity (and fluctuation velocity) profile shown, 60 sequences of images were examined, each sequence containing 108-182 images. As a result, each data point in the velocity profile was based on an average of 250-450 velocity measurements. As both the vertical and horizontal displacements could be measured, it was possible to compute the ensemble-averaged streamwise velocity

$u_x(y)$ and the ensemble-averaged transverse velocity $u_y(y)$. The latter in all cases was very close to zero, as is expected in this flow where the mean direction of motion is vertical. If there were "N" data points in a particular bin "b", then $u_x(y) =< V >$ and $u_y(y) =< U >$ where $V$ and $U$ were the streamwise and transverse components of the measured velocity data points in that bin. The coordinate $y$ representative of bin "b" was equal to the average of the transverse coordinate positions of all the data points in that bin. The ensemble-averaged streamwise fluctuation velocities were computed as $u'_x(y) = < (V - < V >)^2 >^{\frac{1}{2}}$ and the ensemble-averaged transverse fluctuation velocities as $u'_y(y) = < U^2 >^{\frac{1}{2}}$. Errors in the fluctuation velocities were less than 4% for the streamwise components and 7% for the transverse components. These errors resulted primarily from the uncertainty in determining the centroid of the particles.

To make the diffusion measurements, specific tracer particles were tracked for reasonable durations so that the diffusive displacements could be computed as a function of time. Equation (2.23) was used in order to evaluate the diffusion coefficients. For each particle, its position in each frame of a sequence of images was identified and stored. In this way, the displacement-time histories for a significant number of tracer particles were accumulated. For each shear rate condition, at least 40 sequences of images, each consisting of 182 images were examined to extract the tracer trajectory data. The number of particle histories used in the diffusion calculations varied from 250 to 700. Frames were grabbed from the video tape at the rate of 30 f.p.s., the same rate as for the velocity measurements. All the experiments were performed using spherical glass beads with an average diameter of 3 mm and a density of 2500 kg/m$^3$. Three different types of beads were used: clear well-rounded high quality beads with a standard deviation of 2.13% of the mean particle diameter (Type A); glass beads dyed white with an acrylic dye to alter the surface frictional properties (Type B); and clear low-quality glass beads with a diametric standard deviation of 3.34% (Type C). The dyed beads had a standard deviation of 2.88% of the mean

particle diameter. The average static angle of repose was 28° for particles of Type A, 31.5° for particles of Type B and 28.5° for those of type C.

In order to examine diffusive behavior, three flows with the roughened sidewalls were examined for each particle type. Table 3.1 lists this set of experiments, including the mean speed of each flow. Though the front and back surfaces were cleaned and polished, some frictional interaction was expected at these walls. Also, the presence of the front and back glass walls was likely to induce a "layered" flow structure parallel to the front wall. Liu, Kalos & Chester (1974) performed Monte Carlo simulations for a "classical hard sphere" system in a vertical channel and observed that layering occurred parallel to the channel walls, with the density at the walls being higher than that in the bulk. A schematic of such a layering phenomenon is depicted in Figure 3.3. Louge (1994) observed similar density oscillations in a rapid granular flow simulation using a periodic Couette geometry that was bounded by a flat frictional wall at the bottom. In the current experiments, any shear at the front and back walls was likely to dilate the flow at those surfaces. Furthermore, the plane of shearing was perpendicular to the front wall (unlike the configuration examined by Louge 1994) and density variations caused by the presence of the front and back walls were likely to be affected by the shear-induced dilation of the bulk. Hence, it was difficult to assess the net effect of the front and back surfaces on the flow velocity and the diffusion coefficients. However, for the particles of Type A, it was possible to observe the movement of tracer particles within the bed and to estimate the effect of the glass walls on the average velocities. The measurements indicated that the velocity within the bed was slightly higher than at the wall. The difference increased with flow rate and was about 4% for the smallest valve opening and 8-9% for the largest valve opening. This difference led to large values of the solid fractions, which were calculated using average velocities measured at the surface. Calculated values for the average solid fraction varied from 0.55 to 0.7. While it was visually obvious in the case

of the roughened sidewalls that the solid fraction increased from the edges towards the center of the flow, no efforts were made to actually measure the density profile since the variations would be within the uncertainty of the measurement techniques.

## 3.2 Velocity Profiles: Observations and Discussion

A significant portion of this thesis deals with the determination of average and fluctuation velocity profiles for both the streamwise and transverse directions using the imaging methods described previously. In all references in this work, the term "streamwise" refers to the direction of mean motion in the chute, while the term "transverse" refers to the direction normal to the direction of mean motion of the flow. Also, in this work, the term "rough" wall refers to the wall condition created by sticking 3 mm particles on the wall surface in a regular hexagonal closed pack. In all the flows examined, the flows were fully developed and steady over the section of interest. The flows were usually fully developed within a distance of ten particle diameters from the top of the chute. As the flow was symmetric about the central axis, only the right-hand profile is displayed in all the figures. All the velocity profiles, unless otherwise specified, were measured by averaging over a length of 2 to 2.5 cm, at a mean distance of 130 particle diameters from the top of the chute.

The mean and fluctuation velocity profiles for the particles of Type A, with the rough walls condition are shown in Figures 3.4-3.6. In each case, it can be inferred from the streamwise velocity profile that the flow essentially consists of a central core with a uniform velocity distribution, bounded by sheared zones, about five to six particle diameters thick, adjacent to the walls. Slip velocities are about 20 to 27% of the centerline velocities. The shape of the velocity profiles, and the extent of the shear zones, remains constant with an increase in mean flow rate, over the range of flow rates investigated. This phenomenon is observed in Figure 3.14 which depicts

the streamwise velocity profiles for the particles of Type A, with the local velocities normalized by the average velocity of the flow. Figures 3.7-3.9 depict the mean and fluctuation velocity profiles for particles of Type B, while similar measurements for particles of Type C are shown in figures 3.10-3.12. The horizontal flow velocities were close to zero for all the flows. Figure 3.13 depicts the horizontal velocity measurements for the experiments with particles of Type A. The shapes of the velocity profiles were similar for all three particle types.

Figure 3.15 indicates a typical example of the ensemble-averaged local velocities measured at three axial stations along the flow. This set of data is for experiment 3. As can be seen, both the mean and the fluctuation velocity profiles are consistent for all three stations. Figure 3.16 shows velocity profiles for the same flow as Figure 3.15, except that the measurements are made over three distinct averaging intervals that were two minutes apart. All the profiles are consistent, indicating that both mean and fluctuating velocities are steady. Similar behavior was noticed for all the flows investigated. Figure 3.17 shows velocity profiles, measured over three different averaging periods for the flow in experiment 4. The steadiness of the flow is apparent from the consistency of all three velocity profiles.

The effect of wall conditions on the velocity profiles is shown in figure 3.18. Both the cases have identical exit valve widths of 1.3 cm. For the polished glass sidewalls, the shear layer is only 1 particle diameter thick, and a plug flow occurs across most of the flow section. The velocity at the wall, in this case, is only about 4% less than the velocity in the bulk. In contrast, for the roughened walls, the shear layer is about five to six particle diameters thick. Also, the fluctuation velocity values are higher in the case of the rough walls than in the case of the smooth glass walls. For the roughened walls, shear work at the wall is converted into the random kinetic energy of the individual particles, which is conducted into the bulk. Furthermore, visual observations indicate that for the roughened sidewalls, there is a definite decrease in

solid fraction from the center towards the walls. However, for the smooth sidewalls, the absence of any shear across most of the flow leads to a nearly uniform solid fraction across the section. In the latter case, the material seems to approach a close-packed condition. Under such circumstances, there is little room for the particles to move relative to each other: a condition that is reflected in the low fluctuation velocity values. Hsiau & Hunt (1993a) showed that there was negligible transverse diffusion across the central axis for the smooth wall condition. Similar observations were also made in the self-diffusion experiments in this work, and are detailed in subsequent sections.

An important feature is the marked anisotropy of the fluctuation velocities, with the component in the direction of mean motion being significantly higher than the transverse component. This feature manifests itself during the diffusion process as well. It was noticed that for particles of Types A and C, the vertical fluctuation velocities scaled reasonably well with the local mean streamwise flow velocity, as shown in Figure 3.19. However, such scaling was not evident for the dyed particles of Type B. For all particle types, the horizontal fluctuation velocities scaled well with the local streamwise velocity in the plug and low shear regimes, but scaled poorly in the sheared regimes adjacent to the wall. Figure 3.20 shows this feature. The reasons for such scaling are not clear, given the lack of knowledge of the appropriate constitutive relations that govern this particular flow situation.

The invariance of the streamwise fluctuation velocity with position leads to the possibility of there being a coherent fluctuating motion of the entire flow regime, as opposed to fluctuating motions of individual particles. While visual observations, and particle displacement-time analyses, did not detect such motion for the range of mean flow rates examined for this work, such a coherent "chugging" motion was visually observed for higher flow rates. There is a possibility that such a periodic motion might have existed for the experimental cases presented. The ability to account for such

motions was curtailed by the limitations of the experimental techniques. Hence, it is possible that the validity of the measurements of the streamwise fluctuation velocities might be compromised by the existence of coherent fluctuation velocity components. The magnitude of this discrepancy is likely to increase with the flow rate.

Also, for all cases with the rough walls, the transverse fluctuation velocity increases from a minimum (non-zero) value at the center to a maximum close to the wall. However, particles in the layer immediately adjacent to the wall have a lower fluctuation velocity than those centered approximately one particle diameter away from the wall. Friction between the particle surface and the wall may impart a significant rotational velocity to the particles closest to the wall. Subsequent collisions of these particles with particles further away from the wall may convert much of this rotational energy into translational energy, which manifests itself as an increase in the translational fluctuational velocity. However, a similar variation in the streamwise fluctuation velocities is not evident; variations across the channel are significantly less. Note that the rotational components of the fluctuation velocity could not be measured.

The mean velocity profiles and visual observations suggest that the flows show a smooth transition from a uniform-velocity highly dense central region, to a relatively less-dense sheared regime close to the walls. From visual observations, it is evident that particles in the central region interact exclusively through semi-permanent sliding contacts at very high densities. The long-term frictional contacts are evident in the outer shear layer as well, though in the latter regime, collisional interactions also occur. However, the binary collision hypothesis, central to the development of constitutive relations based on dense-gas kinetic theory, does not appear to be applicable here.

Almost all the theoretical analyses of flow in vertical channels predict a central plug regime under certain conditions, along with a sheared regime along the walls.

Hui & Haff (1986) have used relations developed by Haff (1983) for kinetic grain flow at very high concentrations to generate solutions for such flows. While their treatment was based on a binary-collision hypothesis, and did not include the effects of friction, their results for the mean velocity profiles and the "thermal" velocity profiles have some qualitative similarities with the measured profiles. Further comparison of the measured data with analytical results is deferred until Chapter 5 where the numerical solutions are discussed in detail. One important factor is that the analytic treatments for this geometry are based on the "continuum hypothesis", which requires that changes in flow properties occur over length scales that are large relative to the particle scale. However, as is evident from the mean velocity profiles within the shear layer, significant changes in the mean velocity occur over distances of half a particle diameter.

Figure 3.21(a) compares the velocity profiles for particle types A and B. The results presented are for experiments 2 and 5. For all the exit openings, it was observed that the corresponding mean flow speed was higher for the dyed particles than for the clear particles. The reason for this phenomenon is not clear, although it might be due to the fact that friction reduces relative particle motion, causing the particles to clump together, thereby increasing the flow density. Figure 3.21(b) and Figure 3.21(c) compare the fluctuation velocity profiles for the same cases as Figure 3.21(a). The dyed particles have lower fluctuation velocities across most of the bulk, indicating a significant damping of the translational fluctuation velocities due to friction.

Normalized fluctuation velocity distributions were calculated from the velocity data accumulated from each data point. Figure 3.22 compares the normalized transverse fluctuation velocity distributions, at three representative transverse locations, for the rough and smooth wall conditions with an exit valve width of 1.3 cm. In these figures, $f(U)$ represents the fraction of the total number of velocity observations for each data point that were equal to the velocity $U$. A similar comparison between the

streamwise fluctuation velocity distributions is displayed in Figure 3.23. The distributions for the condition of the rough wall approximate a Maxwellian distribution while those for the smooth glass wall conditions deviated substantially.

## 3.3 Self-Diffusion: Observations and Discussion

As reviewed in section 2.3, Equation (2.23) was used to evaluate the self diffusion coefficients in this work. As stated earlier, Equation (2.23) carries the assumption that the fluctuation velocity field is homogeneous and stationary within the region where the diffusion coefficient is being evaluated. However, as discussed in the previous section, the presence of boundaries leads to gradients in the fluctuation velocity field.

In order to make realistic comparisons between the shear rates, fluctuation velocities and diffusion coefficients, the flow section in each experiment was divided into three regimes, as depicted in Figure 3.24. These were the central high-density uniform-flow regime, the moderate-shear regime close to the walls, and the intermediate low-shear regime connecting these two regimes. The latter regime is referred to as the "low-shear transition regime" in subsequent discussions. Within each regime, the streamwise and transverse fluctuation velocities were relatively uniform with standard deviations for the streamwise fluctuation velocities around 5-7% of the mean value. The standard deviations for the transverse fluctuations were the highest in the moderate-shear regime, being about 9-12% of the mean value. The deviations of the transverse fluctuations were much lower in the two inner regimes. The present work approximates each of the three regimes as a simple shear flow. Each of the sheared regimes was 2-2.5 particle diameters wide. As the averages indicated in Equation (2.23) were carried out over ensembles of particles that were tracked at different times and initial positions in the flow, the flows were assumed to be homogeneous and steady within each regime of interest. Figures 3.15 and 3.16 indicate that these

are reasonable assumptions. When tracking particles in the moderate-shear regime, particles within a distance of 1.5 diameters from the wall were not considered in order to avoid particles that bounce off the walls and any three dimensionality effects at the corners.

As discussed in the previous chapter, the presence of a shear field augments self-diffusion in the direction of mean motion, due to "Taylor Diffusion" effects. It is necessary to separate the net diffusive displacement in the direction of mean motion into its two components: one due to the random fluctuation velocity and the other due to the gradient in mean velocity. To determine the diffusion coefficient due to the random fluctuations at the end of each time step, it was necessary to subtract from a particle's total diffusive displacement, the displacement contribution due to mean velocity difference during that time step, which was done by referring to the mean velocity profile. The remaining component is referred to as the "random" diffusion component in subsequent sections.

The diffusion coefficient based on kinetic theory arguments indicates that the diffusion increases with an increase in granular temperature and with the diameter of the particles. Furthermore, as $\nu g_0(\nu)$ is an increasing function of the solid fraction, diffusion decreases with an increase in the solid fraction. Although kinetic theory arguments may not be appropriate at high solid fractions, the diffusion coefficients at high solid fractions are expected to have a similar dependence on the fluctuation velocities, the particle diameter and the solid fraction, as long as a rigid close-packed state is not reached. Therefore, a non-dimensional parameter$D1_i$:

$$D1_i = \frac{D_{ii}}{\sigma u'_i}, \tag{3.1}$$

is defined to examine the dependance of the diffusion coefficient on the fluctuation velocity $u'_i$ and the particle diameter. However, it is impossible in this work to quantify the density dependence because the actual density profiles were not measured.

Another non-dimensional parameter used by Bridgewater (1980), Campbell (1993a) and Savage & Dai (1993) is $D2_i$:

$$D2_i = \frac{D_{ii}}{\sigma^2 \gamma_s}, \tag{3.2}$$

where $\gamma_s$ is the shear rate.

In the case of simple uniform-shear flows, at moderate solid fractions, the granular temperature depends only on the material properties and the shear rate; hence $D1$ or $D2$ could be used interchangeably. In this work, both coefficients were considered since the functional dependence of the fluctuation velocities on the shear rates is not known.

Figure 3.25 shows the variation of $< \Delta y \Delta y >$ with time for experiment 1. The mean-square transverse displacements increase linearly with time in each of the three regimes. Diffusive displacements are the highest in the moderate shear regime, significantly less in the low-shear transition regime and least, but non-zero, in the central uniform-flow regime. This trend is consistent in all the flows examined. Figures 3.26-3.33 show the measurements for the rest of the flows. Figure 3.34 depicts the same data as Figure 3.27, but with error bars included. The error bars in the figures reflect the uncertainty in determining the centroid of a particle. The uncertainty in the slope of the best fit line ranged from 3% to 8.8%.

The variation of $D_{yy}$ with shear rate for all three particle types is depicted in Figure 3.35. For all particle types, diffusion coefficients are much higher in the moderate-shear regime than in the low-shear transition regime. However, diffusion is observed to be a much more sensitive function of shear rate in the transition regime than in the moderate-shear regime. Also, for comparable shear rates, the particles of Type B (dyed) have lower values of $D_{yy}$ than those for Type A. The simulations by Dai (1993) showed a significant reduction in the coefficients of diffusion for rough particles. However, results for solid fractions of more than 0.5 were not presented.

The variation of $D_{yy}$ with transverse fluctuation velocity for particles of Type A is shown in Figure 3.36(a). Again, diffusion increases more rapidly with an increase in fluctuation velocity in the uniform and low-shear regimes than in the moderate-shear regime. Qualitatively similar results are observed in Figure 3.36(b) for the case of particles of Type B.

Savage & Dai (1993) have plotted $D2$ as a function of the solid fraction. Although the solid fraction profiles could not be determined in these experiments, $D1_i$ and $D2_i$ have been plotted against the mean transverse position of each shear regime in a flow. As noted earlier, the solid fraction decreases and $D_{yy}$ increases near the walls. Figure 3.37 depicts the values of $D1_y$ for the particles of types A and B. For particles of Type A, the values of $D1_y$ are very close to each other for each of the three regimes for experiments 2 and 3. However, the values for the case of experiment 1 (the smallest exit width) deviate from this behavior. As noted earlier, $D1_y$ does not account for the solid fraction. While measurements were not made, it was visually observed that the solid fraction decreased from the center towards the walls in all the sheared flows. Such a density variation does explain the increase in $D1_y$ with transverse position in the case of the two wider exit openings in Figure 3.37. The reason for the deviation of the values for the case of the smallest exit width is not clear. If examined in terms of a density distribution, the results suggest that in the latter case, there is greater relative dilation in the moderate-shear layer, and relatively greater compaction of the two inner layers, in comparison to the other two exit conditions. Figure 3.37 also shows the value of $D1_y$ for the case of the particles of Type B. For the sheared regimes of experiments 5 and 6, the values are quite consistent, though significant deviation occurs in the uniform regime. The values of $D1_y$ are consistently lower, in the sheared regimes, for the case of the particles of Type B, indicating a significant reduction in diffusive behavior due to the presence of friction.

The values of $D2_y$ for the case of particles of all three types are presented in Table

3.2. The values for the center of the channel are not given since the shear rate here is zero and $D2_y$ cannot be defined. As in the case of $D1_y$, the values of $D2_y$ are almost equal for the case of the sheared zones for experiments 2 and 3. Again, results for the case of the smallest exit opening deviate from the others.

Note that $D2_y$ is 0.053 for the low-shear regimes in experiments 2 and 3. This value is close to the value of 0.057 reported by Bridgewater (1980), based on the work of Scott & Bridgewater (1976) who performed their experiments in a shear cell over shear rates in the range of 0.16 $s^{-1}$ to 0.62 $s^{-1}$, which is lower than but comparable to the strain rates in the low-shear transition regimes of the current set of experiments. In addition, Savage & Dai (1993) reported that their simulations results were in good agreement with Bridgewater's (1980) results, for a solid fraction of 0.5. They do not mention the range of strain rates examined. Measurements made from the figures of Campbell (1993a) indicate the value for $D2_y$ to be about 0.025, for a solid fraction of 0.5. Again, the range of strain rates examined is not indicated. Also, Bridgewater (1980) reported that diffusion in their experiment was isotropic when corrected for Taylor dispersion. As subsequent discussions show, isotropy is not observed in the current set of experiments.

The variation of $< \Delta x \Delta x >$ with time is shown in Figure 3.38, for experiment 1; similar results are observed for the other experiments and are shown in Figures 3.39-3.46. The figures display curves for the total diffusion, as well as for the "random diffusion" component. As expected, Taylor dispersion contributions are largest for the moderate-shear regime, much lower for the low shear transition regime, and non-existent in the central uniform regime, where all diffusion is due to random velocity fluctuations. It must be noted that, for extensive Taylor diffusion to occur, gradients in the mean streamwise velocity profile must be accompanied by transverse fluctuation velocities adequate enough for the particles to move across the streamwise velocity gradient. As in the case of transverse diffusion, the random diffusive displacements

are the highest in the moderate-shear regime, lower in the transition low-shear regime and least in the center. This trend is true of all the flows investigated, though relative magnitudes vary. The variation of the streamwise mean-square random displacements with time is linear for all the regimes. The uncertainty in the slope of the best fit lines was between 6% and 13%. The curves for total diffusion could not be fitted consistently by a single power law and were not examined further.

Figure 3.47 depicts the variation of $D1_x$ with transverse position for the case of particles of types A and B. As for $D1_y$, $D1_x$ increases from the center towards the moderate-shear regime. The same arguments, based on the variation of solid fraction, may be extended in this case as well. However, the values of $D1_x$ for Type A are close to each other, within each regime, in all three shear regimes for all the flow rates, unlike the results shown in Figure 3.37. The results for particles of Type B are similar to those for the particles of Type A, though not as consistent amongst the three different flow rates. The values of $D2_x$ for the sheared regimes are listed in Table 3.2. In comparison to $D2_y$, these values show greater deviation from each other within each sheared regime, especially for the low-shear transition regime. However, the overall trends are similar. Also, the corresponding values are lower for the particles of Type B, indicating a reduction in streamwise diffusion due to friction.

Profiles for $< \Delta y \Delta x >$ are shown in Figure 3.48 for experiment 3. The values are extremely small and within the error limits of the measuring technique. This result was characteristic of all the cases considered.

Figure 3.49 shows the values of $D1$, the trace of the diffusion tensor normalized by the root-mean-square fluctuation velocity. The measured values are reasonably consistent for all the regimes for the case of the particles of Type A. In the case of the particles of Type B, the results for the two larger exit width conditions are consistent for all three regimes, but values for the narrowest exit condition diverge for the low-shear and uniform-flow regimes. The values of the trace of the diffusion

tensor normalized by the strain rate, $D2$, are listed in table 2.

Figures 3.49 and 3.47 are notably similar since the values of $D_{xx}$ are almost an order-of-magnitude higher than $D_{yy}$ for all the regimes examined. This similarity is reflected in the values of $D2_x$ and $D2$ in Table 3.2. The anisotropy in the diffusion coefficient arises as a result of the anisotropy in the fluctuation velocities. While a direct comparison of the measured diffusion coefficients with those predicted by the arguments based on kinetic theory (Equation 2.28) is inhibited by the inability to measure solid fractions in the flows, it is useful to make some comparisons using reasonable estimates for the solid fraction and the coefficient of restitution. The form of the radial distribution function, $g_0(\nu)$, used is defined in Equation (2.5), with the maximum shearable solid fraction $\nu^*$ equal to 0.64. Using values of 0.9 for the coefficient of restitution and 0.5 for the solid fraction, $D_{ii}/\sigma \mathbf{T}^{1/2}$ (from Equation 2.28) is equal to 0.022 and reduces to 0.0075 for a solid fraction of 0.56. In comparison, in the moderate-shear regime in Experiment 3, $D1_y$ is equal to 0.035. However, if the transverse diffusion coefficient $D_{yy}$ is normalized by the root-mean-square fluctuation velocity, a value of 0.019 is obtained. Both of these values are close to the value for $D1_y$ (of the same order of magnitude) for an assumed solid fraction of 0.5. However if the trace of the diffusion tensor is normalized by the root-mean-square velocity (see Figure 3.49), a value of 0.22 is obtained. Using the condition of isotropy, which is assumed in deriving Equation (2.28), the kinetic theory value is 0.044 for a solid fraction of 0.5 and reduces sharply at higher solid fractions. The cause of the discrepancy may lie in the assumptions of isotropy in Equation (2.28). The use of an isotropic radial distribution function to describe the wall-bounded sheared flows of the type encountered in the current experiments may not be appropriate. Furthermore, as previously noted, the current experiments do not belong to the rapid granular flow regime that is well represented by theory based on the kinetic theory of dense gases. Hence, while the measured diffusion coefficients conform to the trends predicted by

the kinetic theory, it is apparent from the discussion above that the expression for diffusion coefficients derived from kinetic theory, (Equation 2.28), cannot be used to make quantitative predictions for the high-density flows examined here.

The marked anisotropy of the diffusive behavior of the flows considered contrasts with the results of Scott & Bridgewater (1976), as examined by Bridgewater (1980). In those experiments, the particles were 18.6 mm in diameter and the strain rates were lower than those considered in the present work. Furthermore, while both Savage & Dai (1993) and Campbell (1993a) report that their simulations indicate somewhat larger diffusion in the streamwise direction, the differences are not as large as those observed in this work. More importantly, even when the diffusion coefficients are normalised by the appropriate fluctuation velocities (Figures 3.37, 3.48), the difference between the non-dimensionalized parameters continues to be substantial. Campbell (1993a) has suggested that the diffusional anisotropy is enhanced because the shear motion may introduce an internal structure that permits greater freedom of motion in preferred directions. Also, even though their streamwise fluctuation velocities are comparable in magnitude, the diffusion coefficients $D_{xx}$ are much lower in the uniform flow regime than in the low-shear transition regime. Obviously, the solid fraction plays a very important role here.

Strongly anisotropic diffusion coefficients have been observed in systems other than those considered in this work. Ladd (1992) reported that his dynamical simulations of sedimenting spheres in a suspension revealed that the value of the diffusion coefficient in the direction of sedimentation was more than an order of magnitude higher than the diffusion coefficient in the transverse direction. Solid fractions in the range of 0.05 to 0.5 were considered and the anisotropy was seen to increase with a decrease in the solid fraction.

The coefficients of diffusion usually increase with the mean flow velocity in the uniform flow regime. This observation seems consistent with the fact that the fluctua-

tion velocity components scale reasonably well with the local mean velocity. Hwang & Hogg (1980) reported that their measurements for transverse diffusion in an inclined chute were comparable with a model in which the diffusion coefficient was composed of two parts: one proportional to the shear rate and the other a constant indicative of the "intrinsic" random fluctuations of the particles. However, they did not indicate any relation between this intrinsic component and the mean flow velocity. Their measured transverse diffusion coefficients were of the same order as those measured in the current experiments in the moderate-shear regimes.

In order to examine the influence of boundary conditions on the diffusional behavior, diffusion measurements were made for the flow with smooth sidewalls whose velocity profiles are shown in Figure 3.18. By fitting straight lines to the results, values of 0.020 and 0.0017 were obtained for $D_{xx}$ and $D_{yy}$ in the regimes close to the wall. These results were an order of magnitude lower than the typical corresponding values for the sheared flows. Furthermore, the magnitude of the diffusive displacements were of the order of the error associated with the measuring technique. High flow densities, combined with much lower fluctuation velocities severely inhibit diffusion. However, as the results of Hsiau (1993), and the diffusion results for the central uniform regime in the current set of experiments show, in the case of sheared flows, tangible diffusion occurs in the unsheared regions. There seems to be a mechanism of conduction of fluctuation velocities into the central regimes from the walls, which, combined with a less packed structure, supports diffusion in the unsheared regimes for the shear flow situation.

| Expt no. | Particle type | Exit width (cm) | Mean speed (cm $s^{-1}$) | Flow rate (kg $s^{-1}$) |
|---|---|---|---|---|
| 1 | A | 1.0 | 5.8 | 0.091 |
| 2 | A | 1.3 | 9.5 | 0.163 |
| 3 | A | 1.5 | 12.2 | 0.233 |
| 4 | B | 1.0 | 6.7 | 0.100 |
| 5 | B | 1.3 | 10.5 | 0.175 |
| 6 | B | 1.5 | 13.9 | 0.256 |
| 7 | C | 1.0 | 6.4 | 0.098 |
| 8 | C | 1.3 | 8.8 | 0.154 |
| 9 | C | 1.5 | 11.4 | 0.217 |

Table 3.1: List of experiments.

| | $D2_y$ | | $D2_x$ | | $D2$ | |
|---|---|---|---|---|---|---|
| Expt | LS | MS | LS | MS | LS | MS |
| 1 | 0.039 | 0.033 | 0.511 | 0.181 | 0.549 | 0.212 |
| 2 | 0.053 | 0.019 | 0.420 | 0.162 | 0.472 | 0.181 |
| 3 | 0.053 | 0.018 | 0.603 | 0.194 | 0.655 | 0.212 |
| 4 | 0.024 | 0.027 | 0.231 | 0.173 | 0.255 | 0.200 |
| 5 | 0.020 | 0.017 | 0.310 | 0.127 | 0.335 | 0.143 |
| 6 | 0.020 | 0.015 | 0.359 | 0.136 | 0.383 | 0.150 |
| 7 | 0.050 | 0.025 | 0.571 | 0.160 | 0.621 | 0.185 |
| 8 | 0.047 | 0.019 | 0.554 | 0.171 | 0.602 | 0.190 |
| 9 | 0.052 | 0.015 | 0.660 | 0.160 | 0.712 | 0.176 |

Table 3.2: Values of $D2_i$: LS, low shear; MS, moderate shear

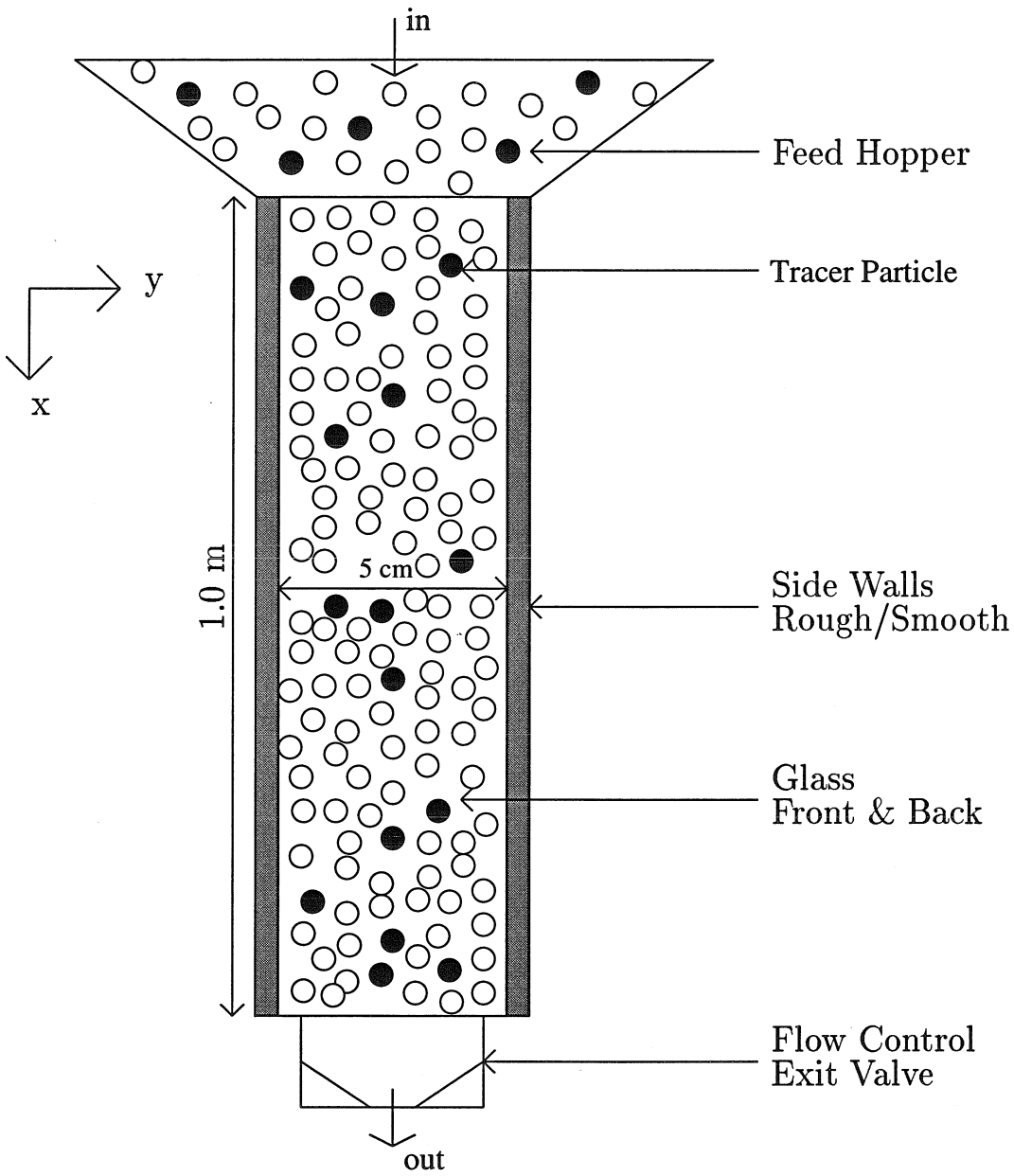


Figure 3.1: Schematic of the vertical channel facility.

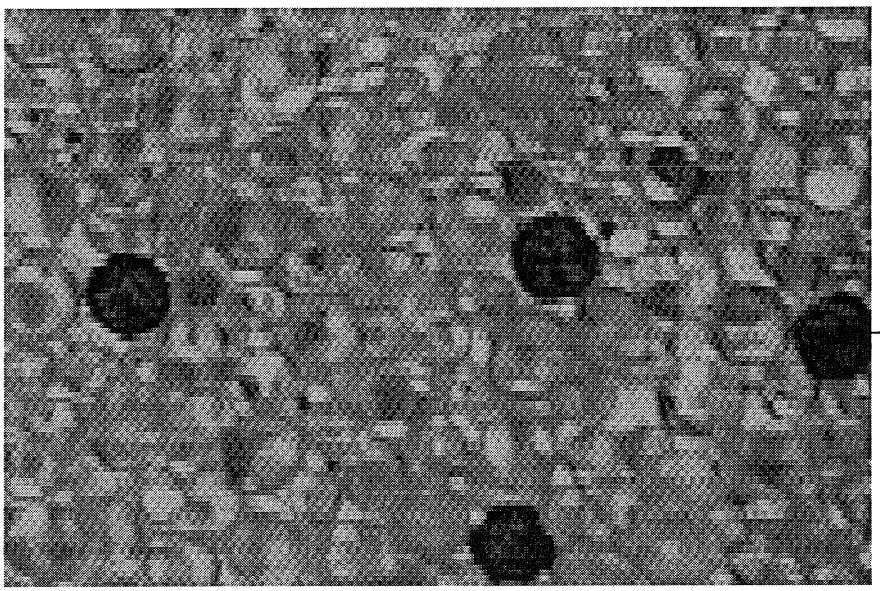


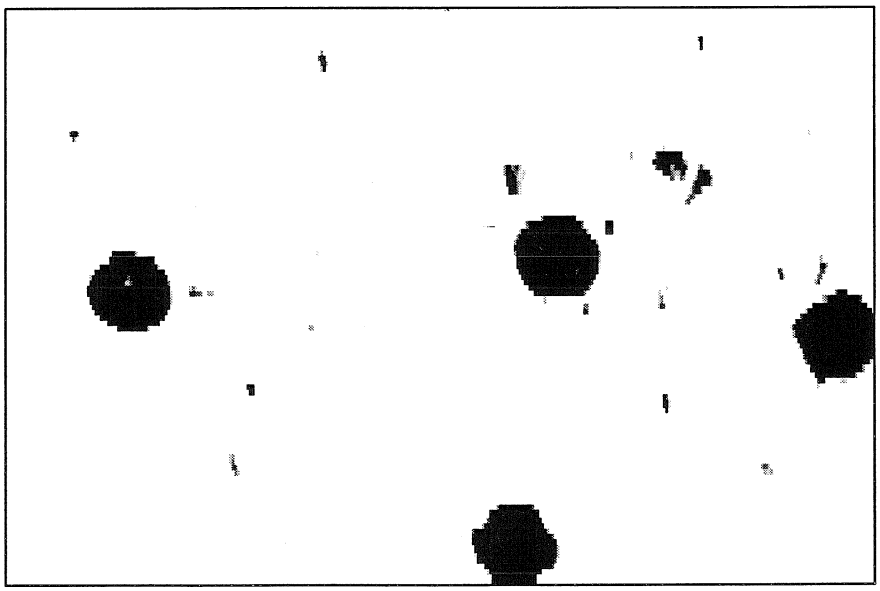


Figure 3.2: A typical example of a (a) raw image frame and (b) a processed image frame used to determine velocity and diffusion profiles.

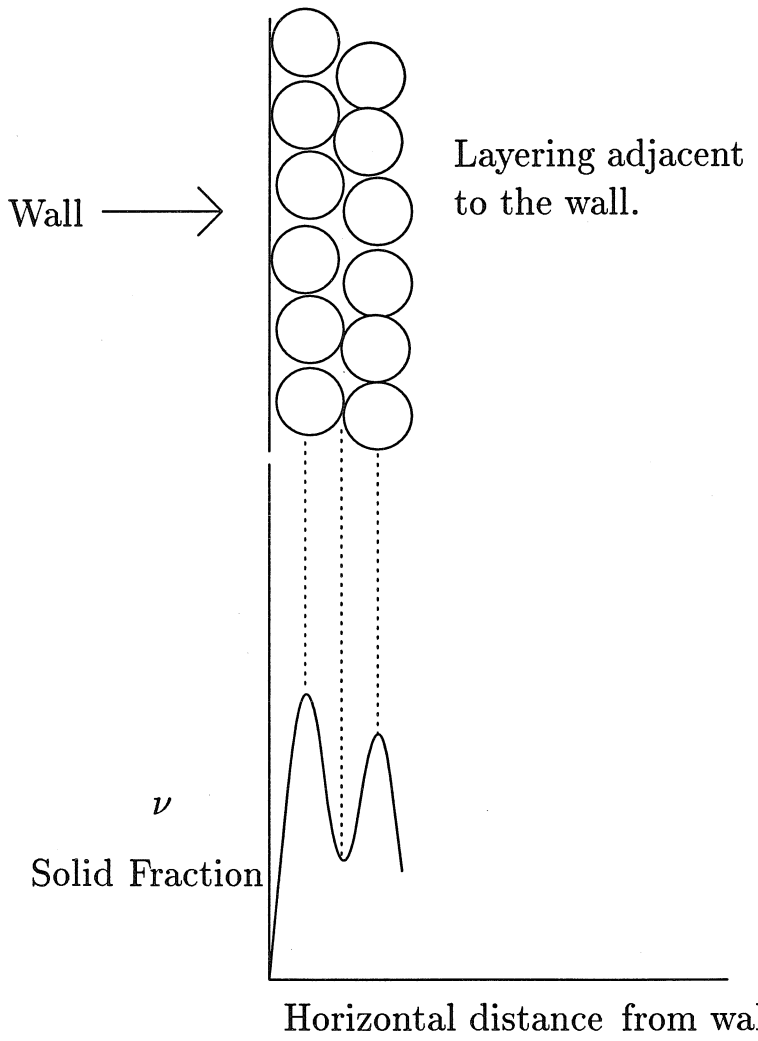


Figure 3.3: Schematic of the layering phenomenon that occurs adjacent to walls in dense granular flows.

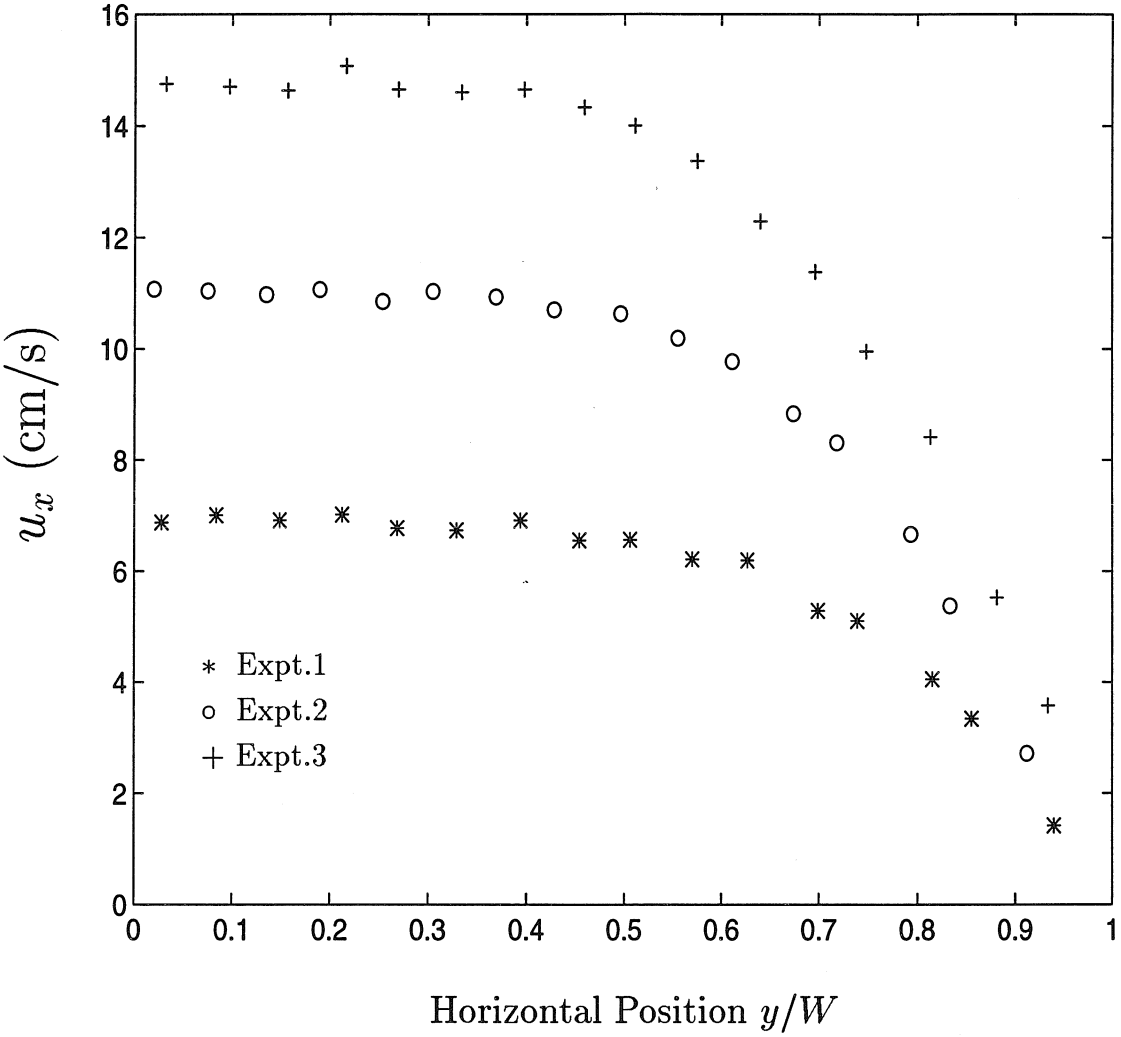


Figure 3.4: The mean streamwise velocity profiles for particles of Type A. W=2.5 cm.

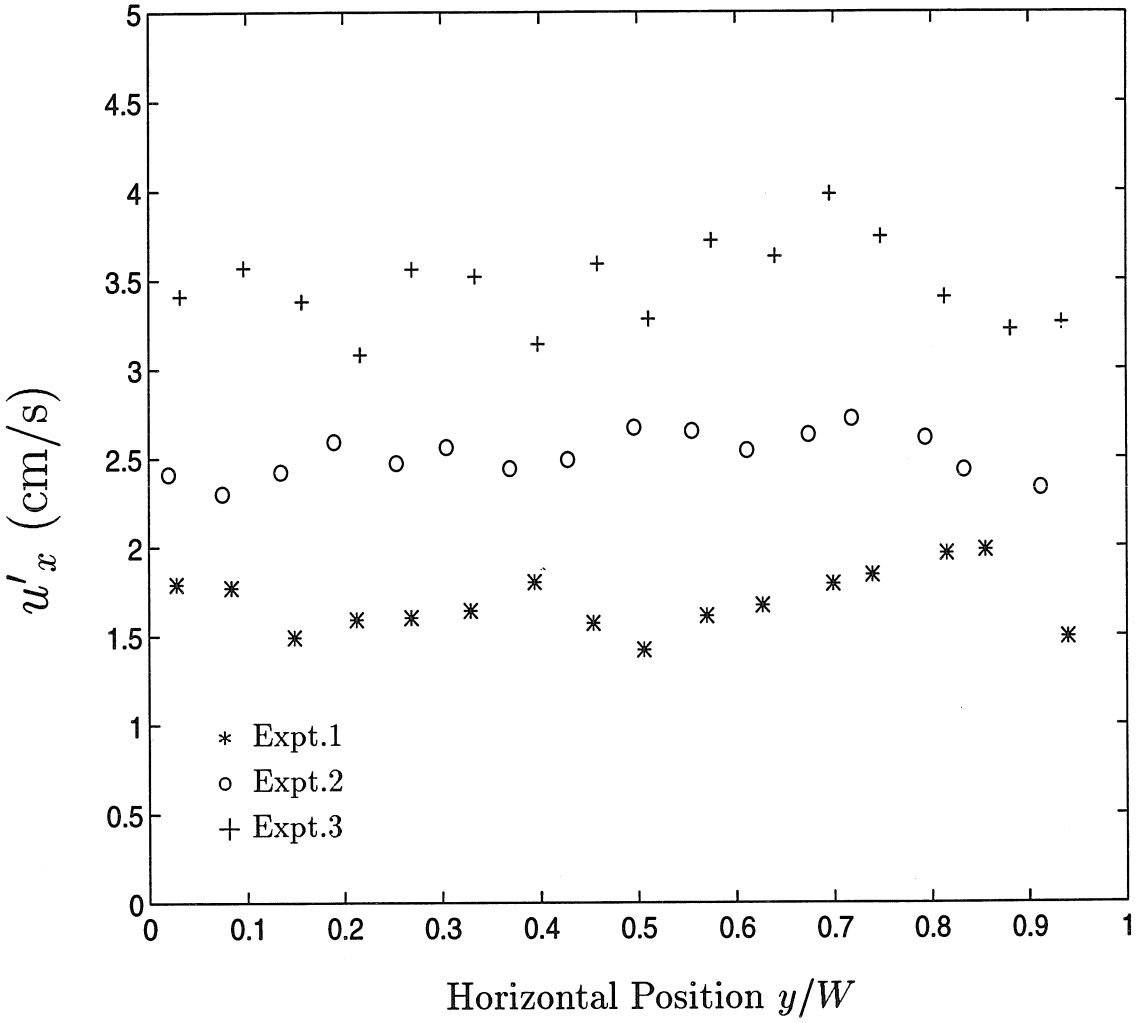


Figure 3.5: The streamwise fluctuation velocity profiles for particles of Type A. W=2.5 cm.

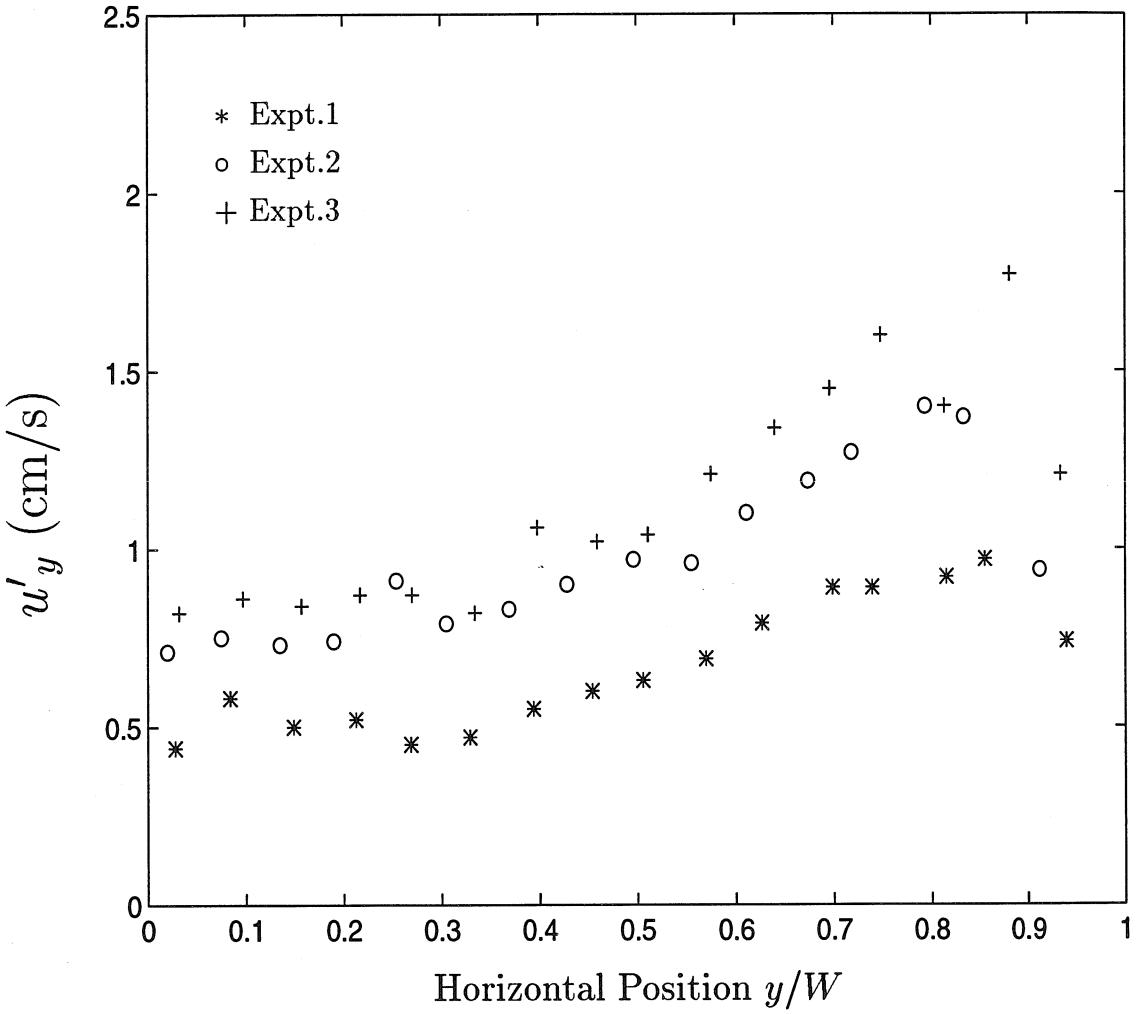


Figure 3.6: The transverse fluctuation velocity profiles for particles of Type A. W=2.5 cm.

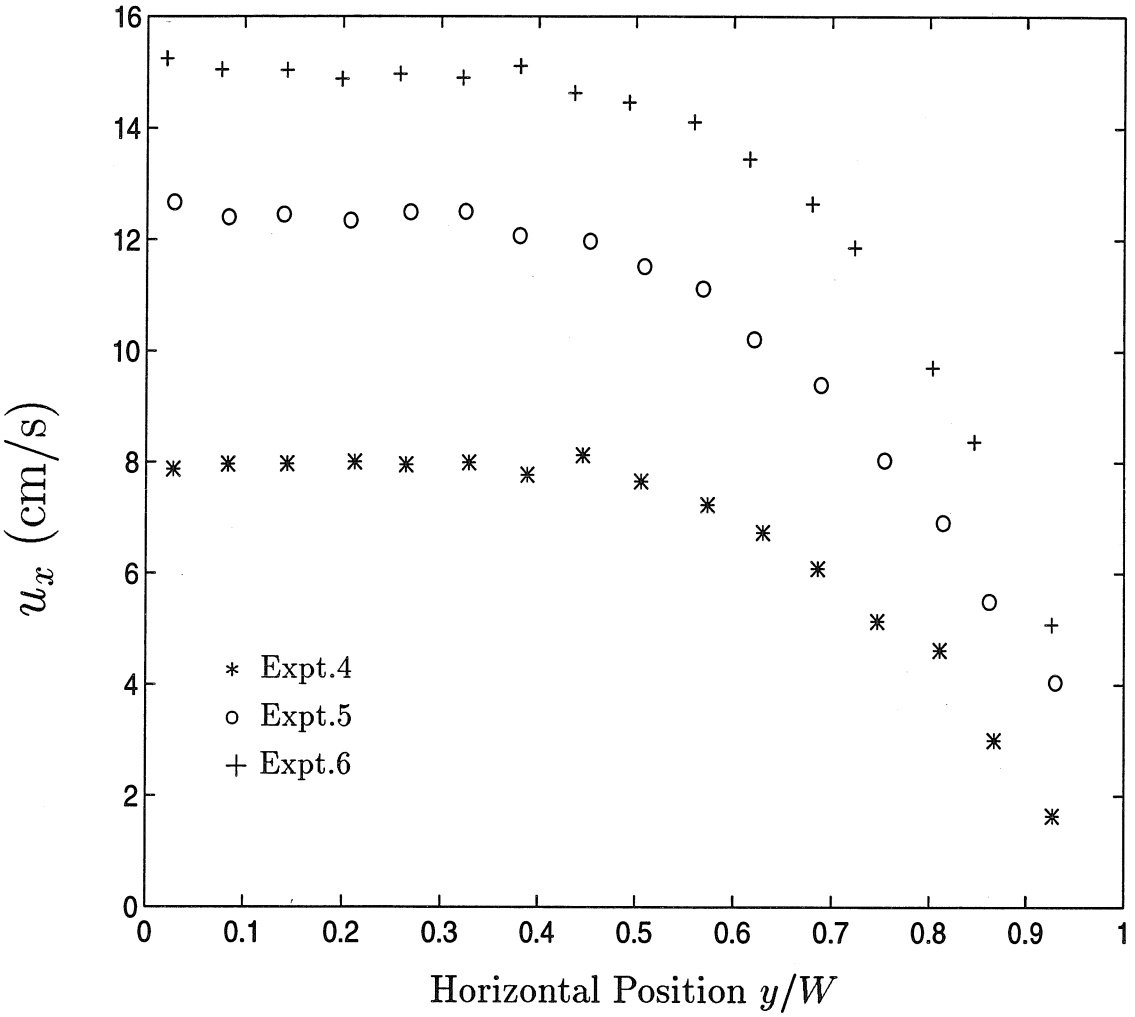


Figure 3.7: The mean streamwise velocity profiles for particles of Type B. W=2.5 cm.

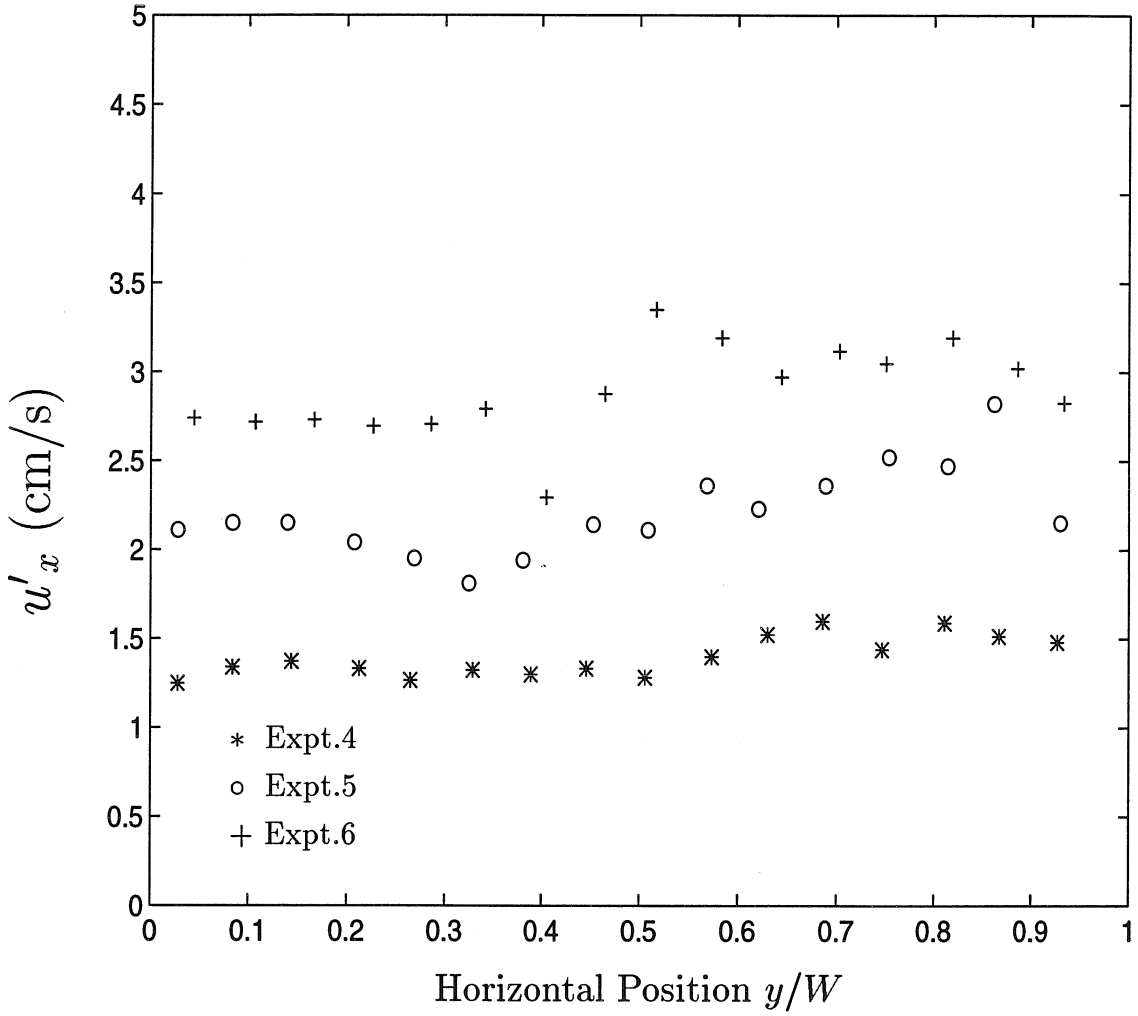


Figure 3.8: The streamwise fluctuation velocity profiles for particles of Type B. W=2.5 cm.

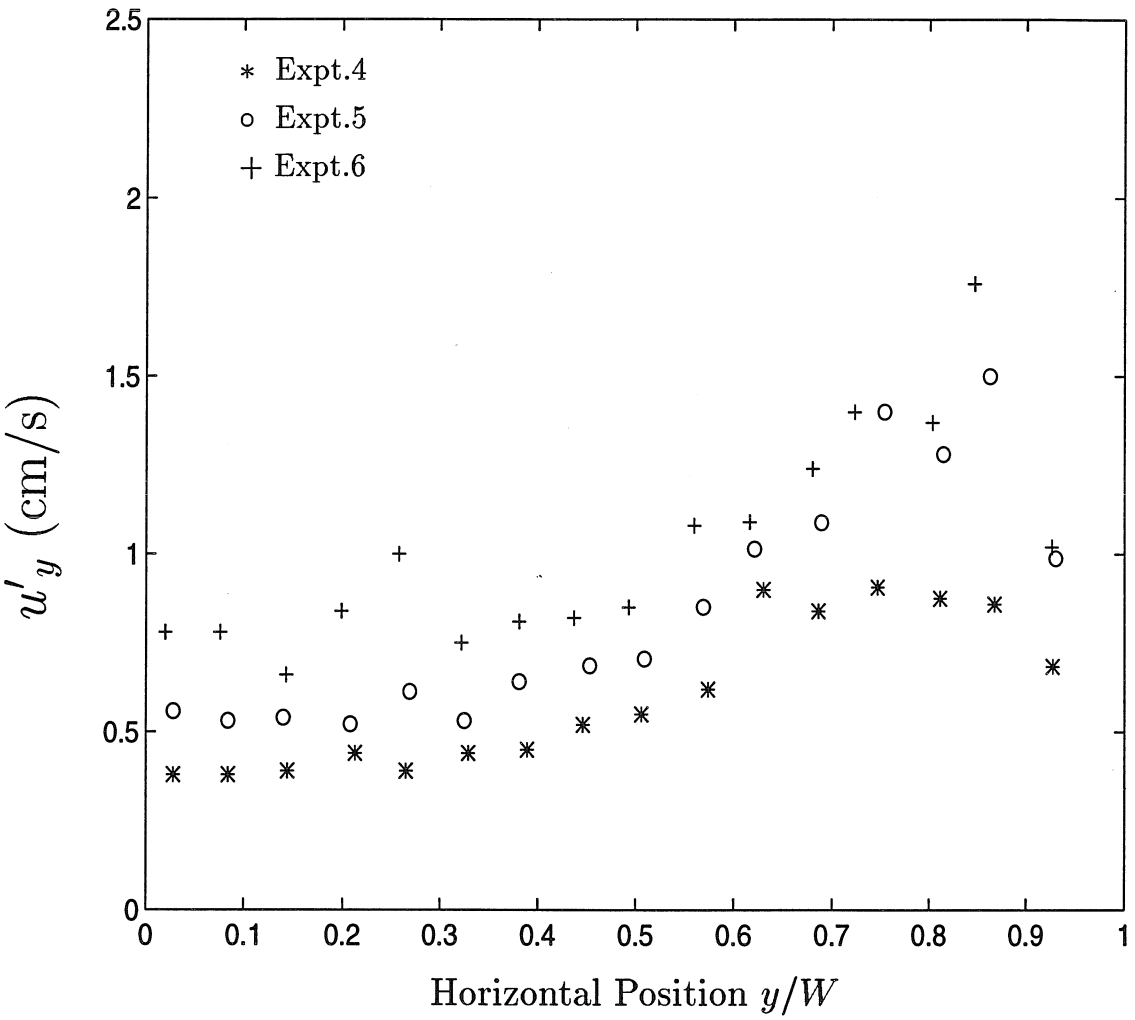


Figure 3.9: The transverse fluctuation velocity profiles for particles of Type B. W=2.5 cm.

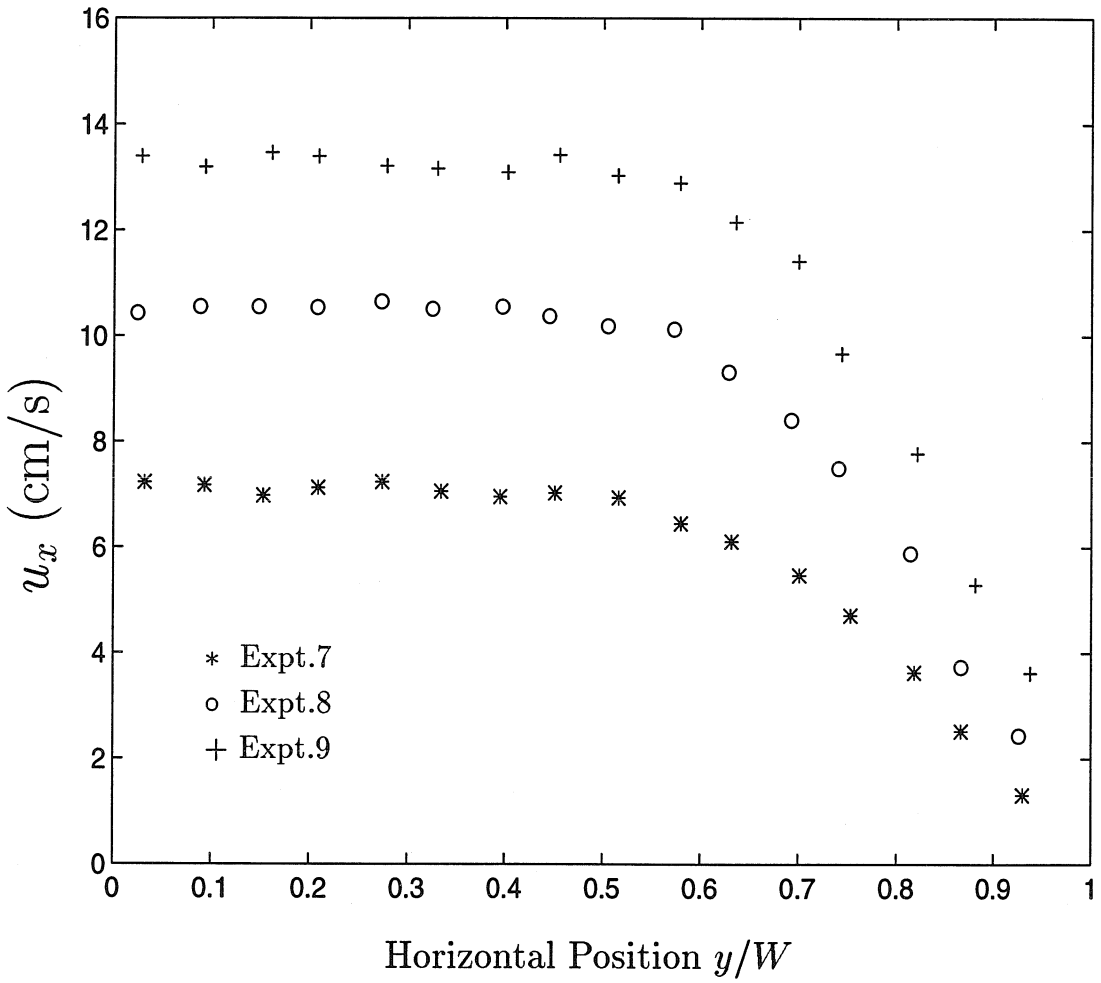


Figure 3.10: The mean streamwise velocity profiles for particles of Type C. W=2.5 cm.

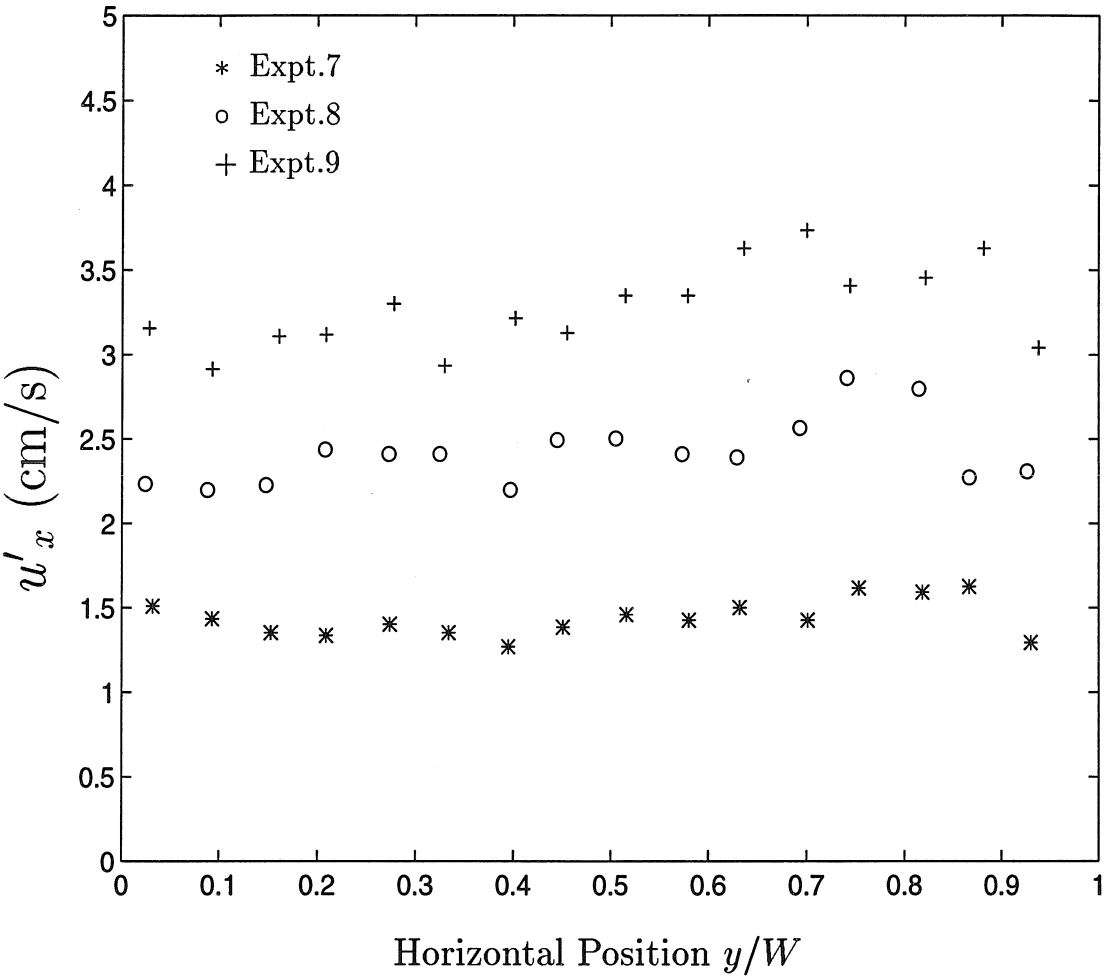


Figure 3.11: The streamwise fluctuation velocity profiles for particles of Type C. W=2.5 cm.

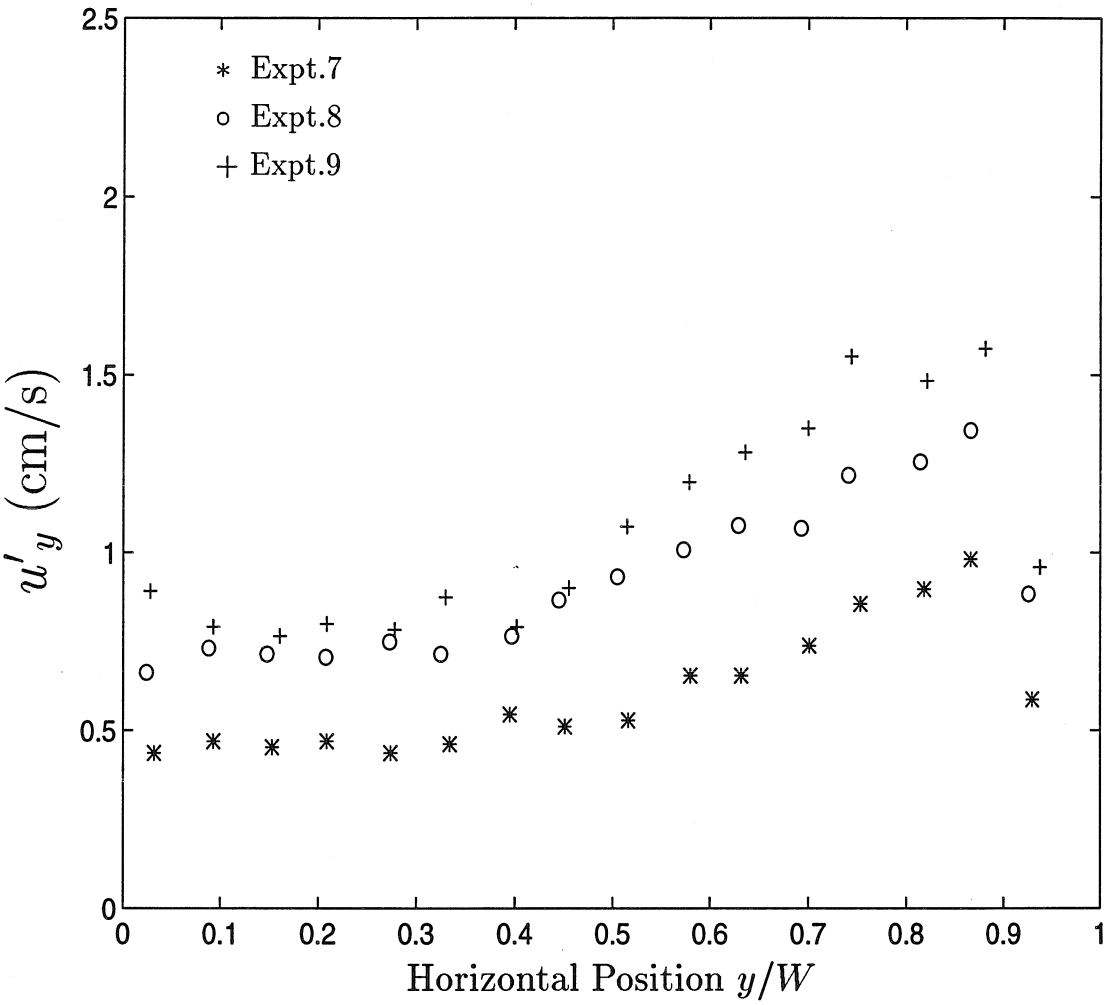


Figure 3.12: The transverse fluctuation velocity profiles for particles of Type C. W=2.5 cm.

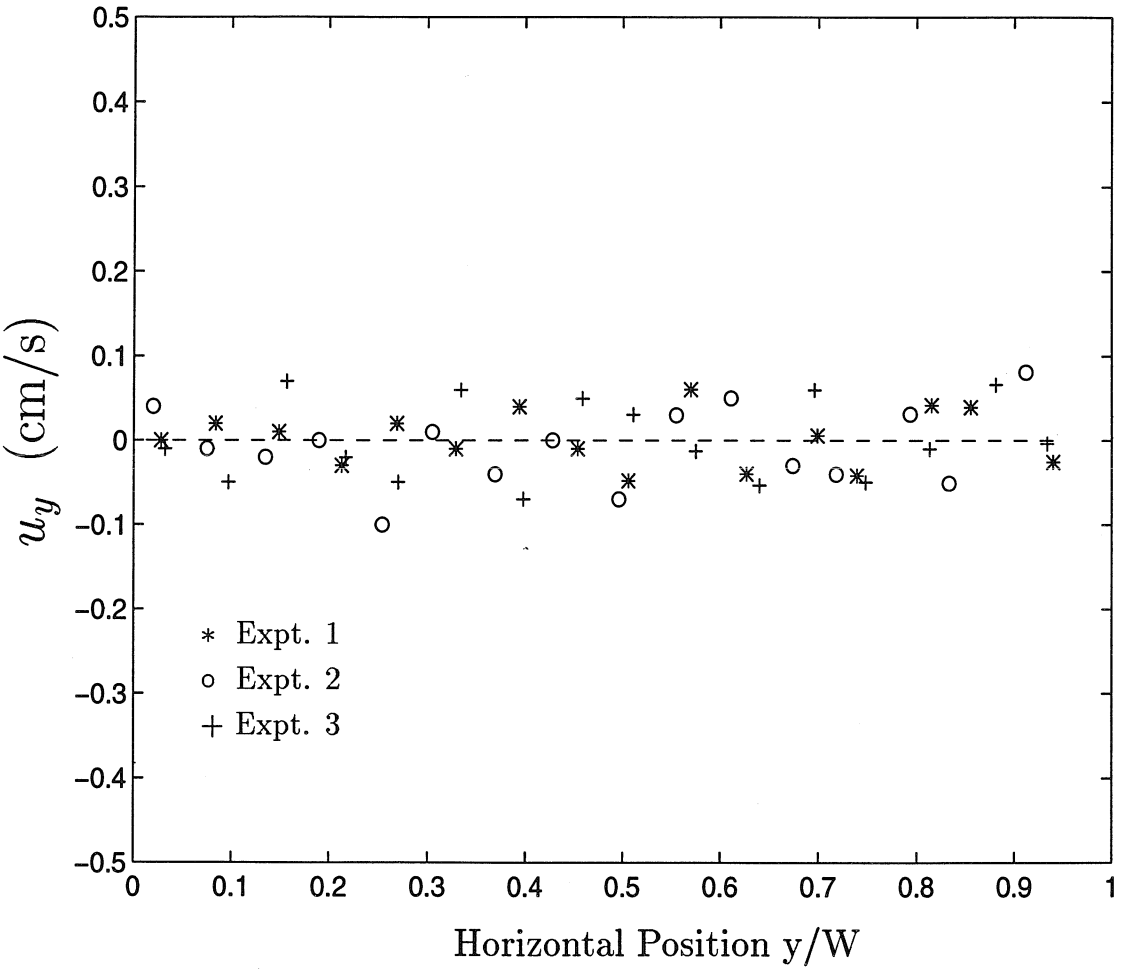


Figure 3.13: The transverse mean velocity profiles for particles of Type A. W=2.5 cm.

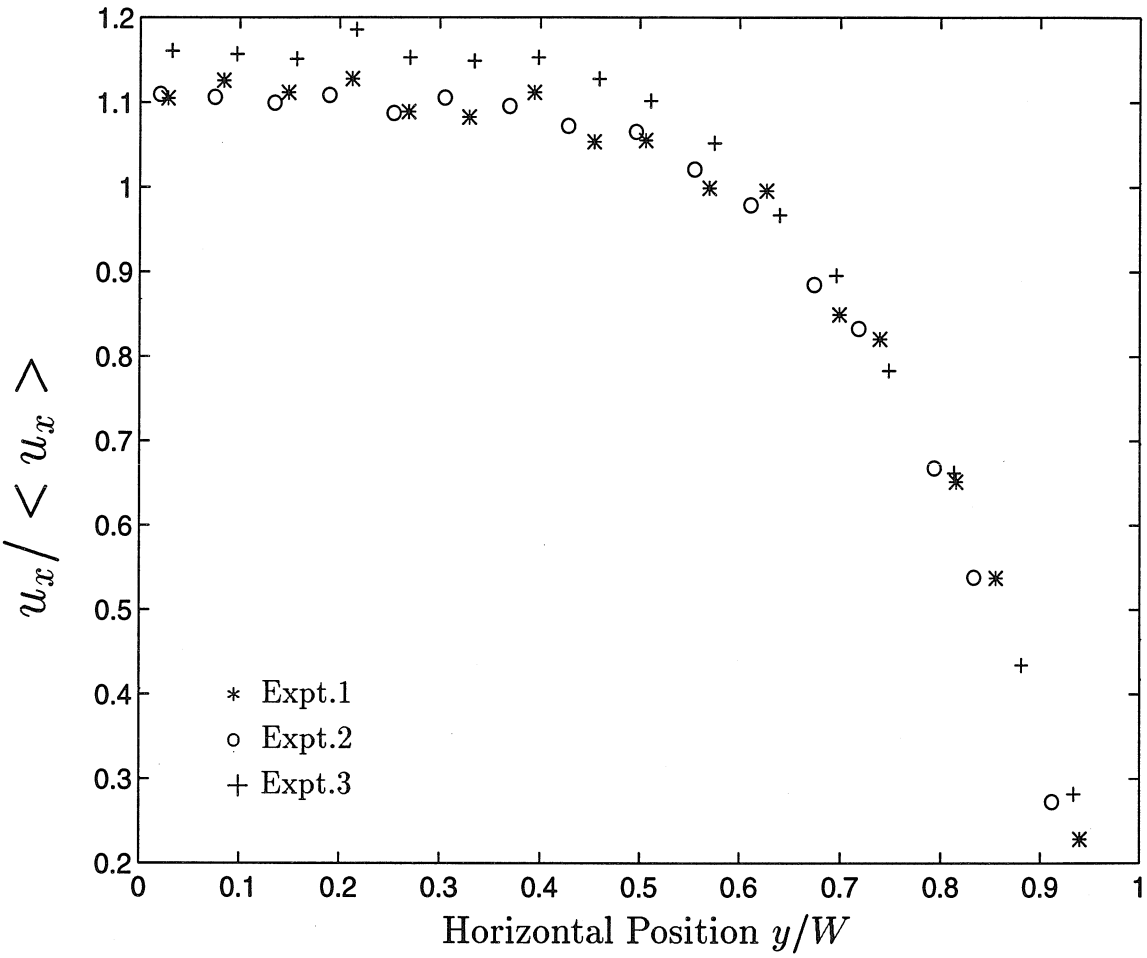


Figure 3.14: The normalized mean streamwise velocity profiles for particles of Type A. W=2.5 cm.

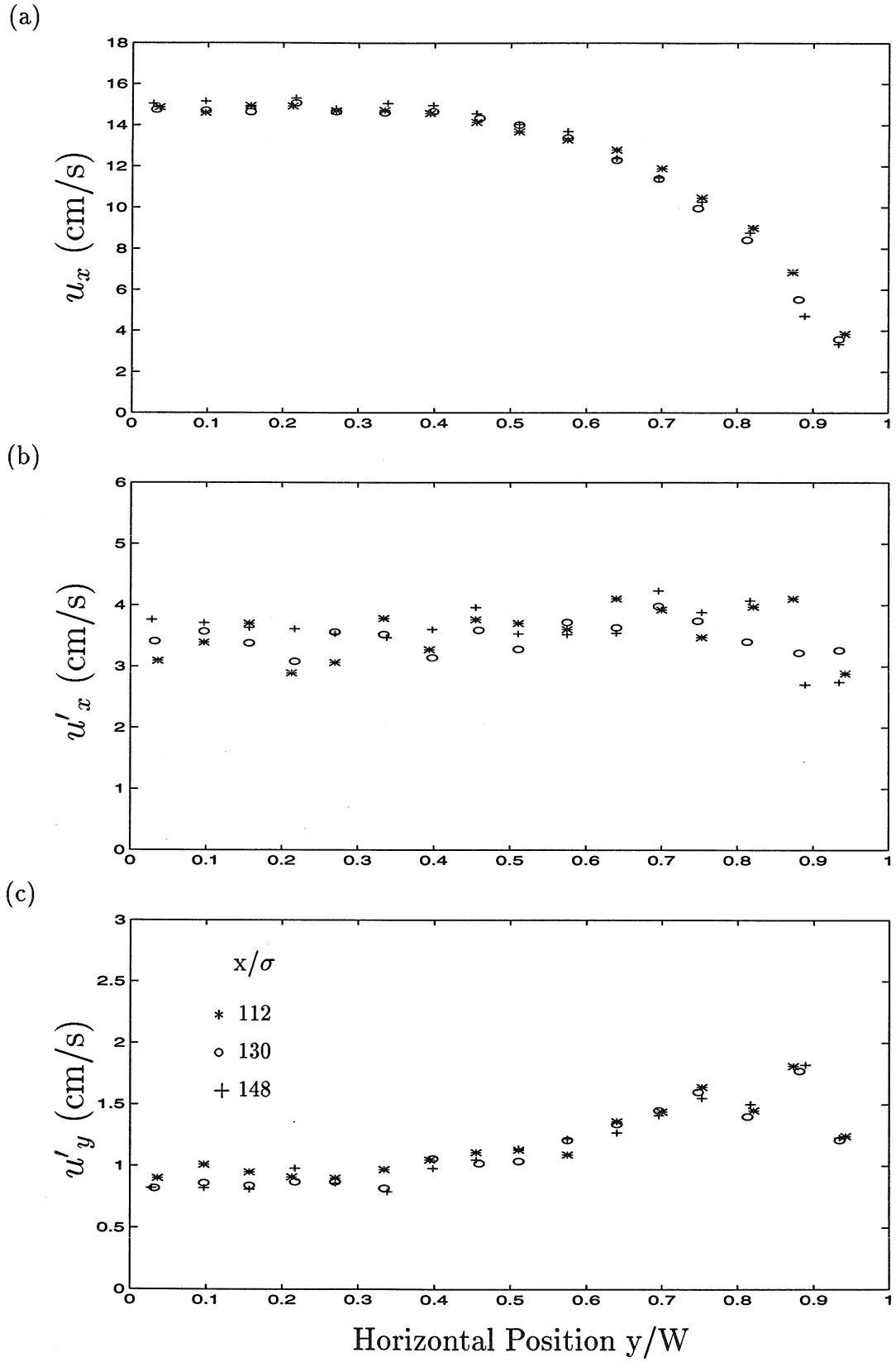


Figure 3.15: (a) The mean streamwise, (b) streamwise fluctuation and (c) transverse fluctuation velocity profiles at three axial positions for Expt. 3. W=2.5 cm.

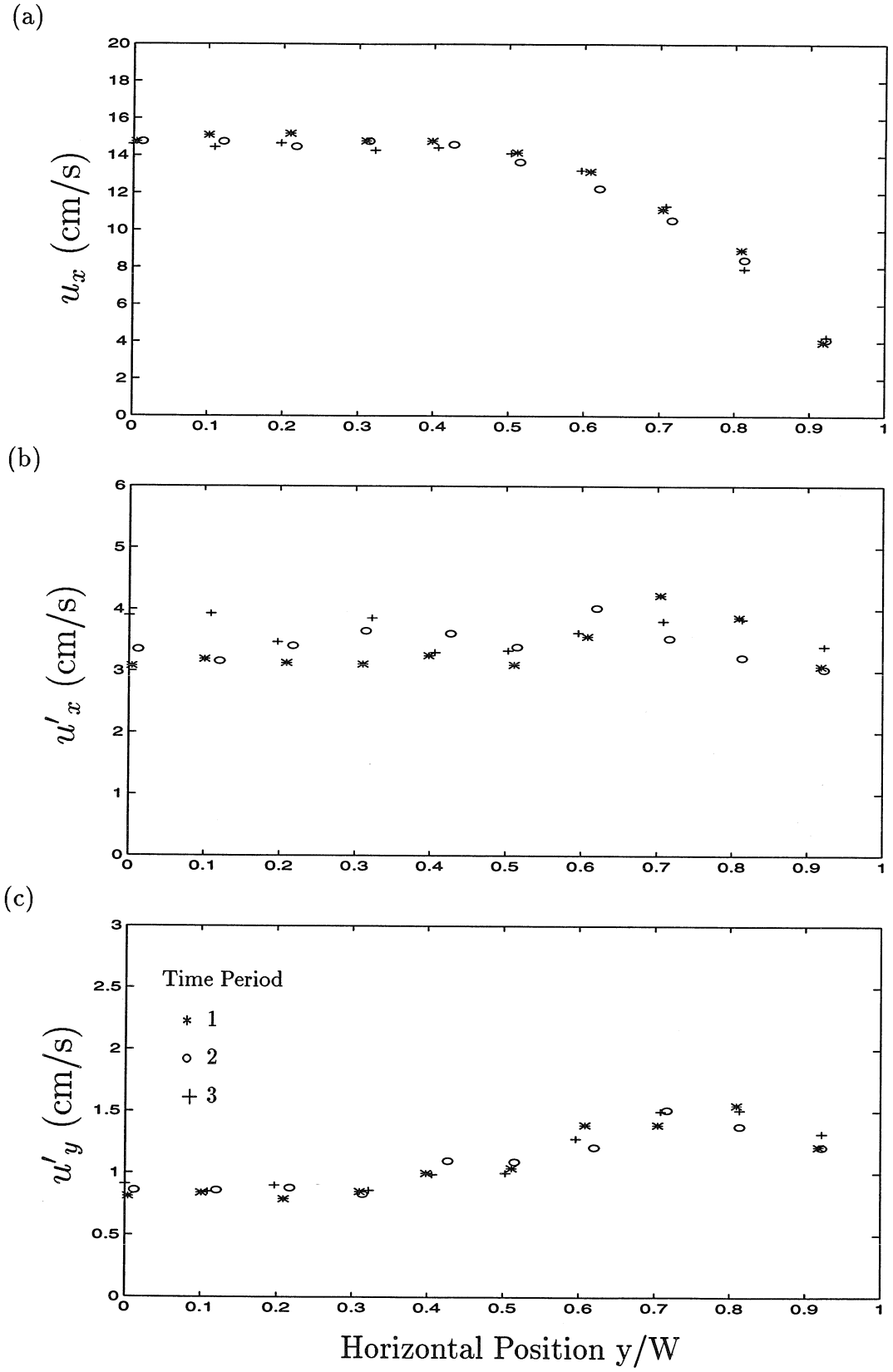


Figure 3.16: (a) The mean streamwise, (b) streamwise fluctuation and (c) transverse fluctuation velocity profiles for three distinct time periods in Expt. 3. W=2.5 cm.

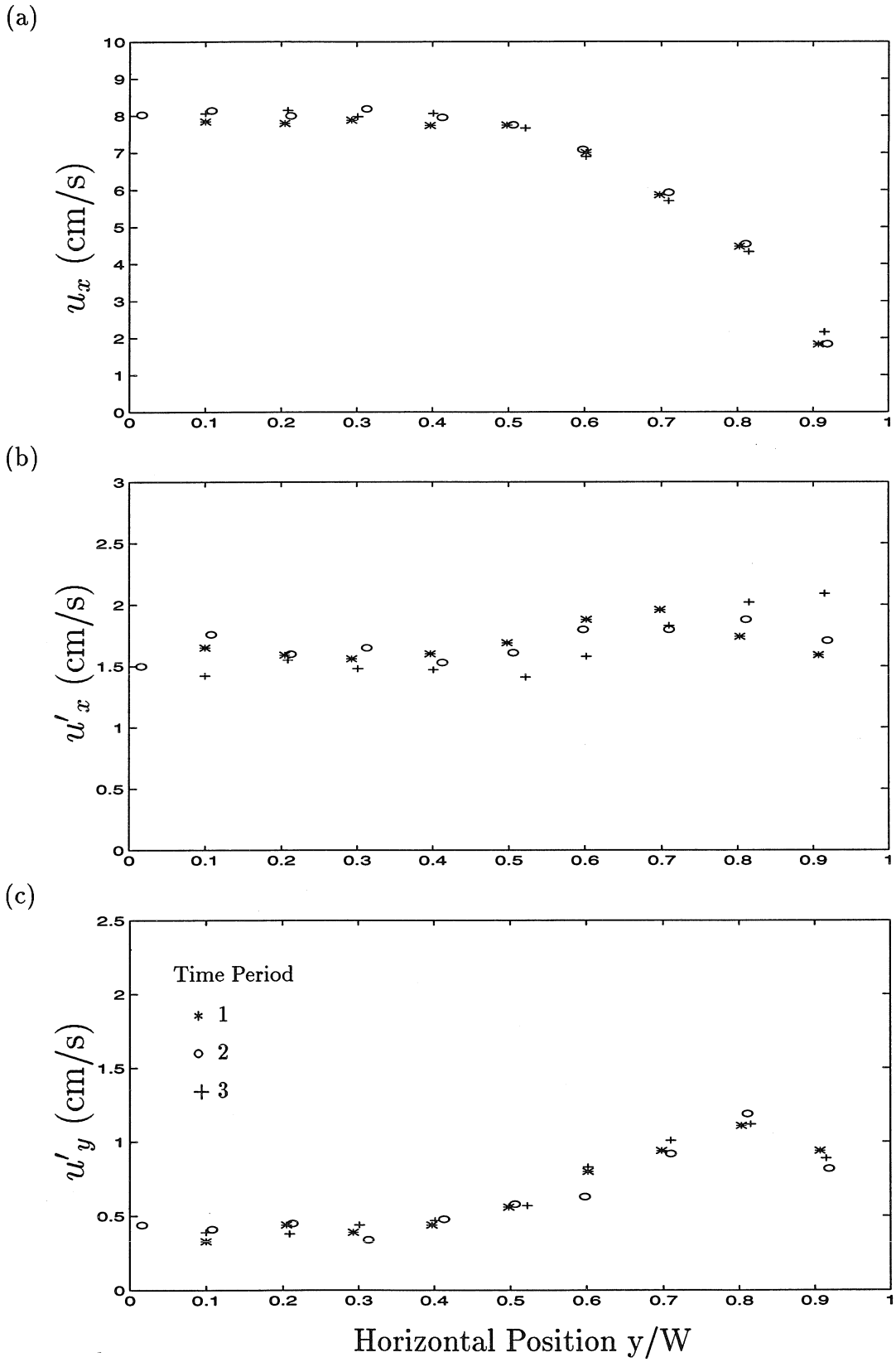


Figure 3.17: (a) The mean streamwise, (b) streamwise fluctuation and (c) transverse fluctuation velocity profiles for three distinct time periods in Expt. 4. W=2.5 cm.

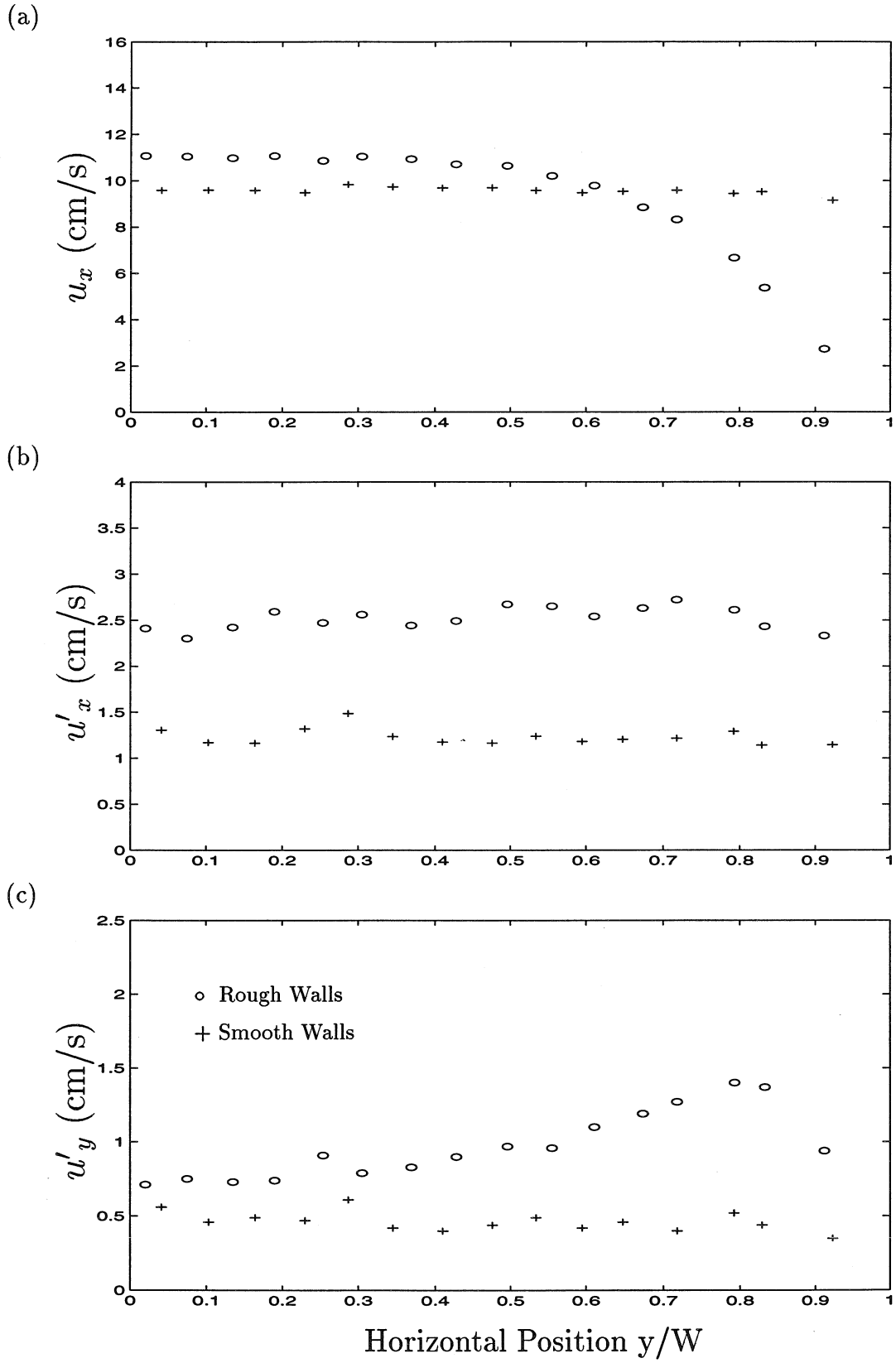


Figure 3.18: (a) The mean streamwise, (b) streamwise fluctuation and (c) transverse fluctuation velocity profiles for smooth glass and rough walls. Exit valve width=1.3 cm. W=2.5 cm.

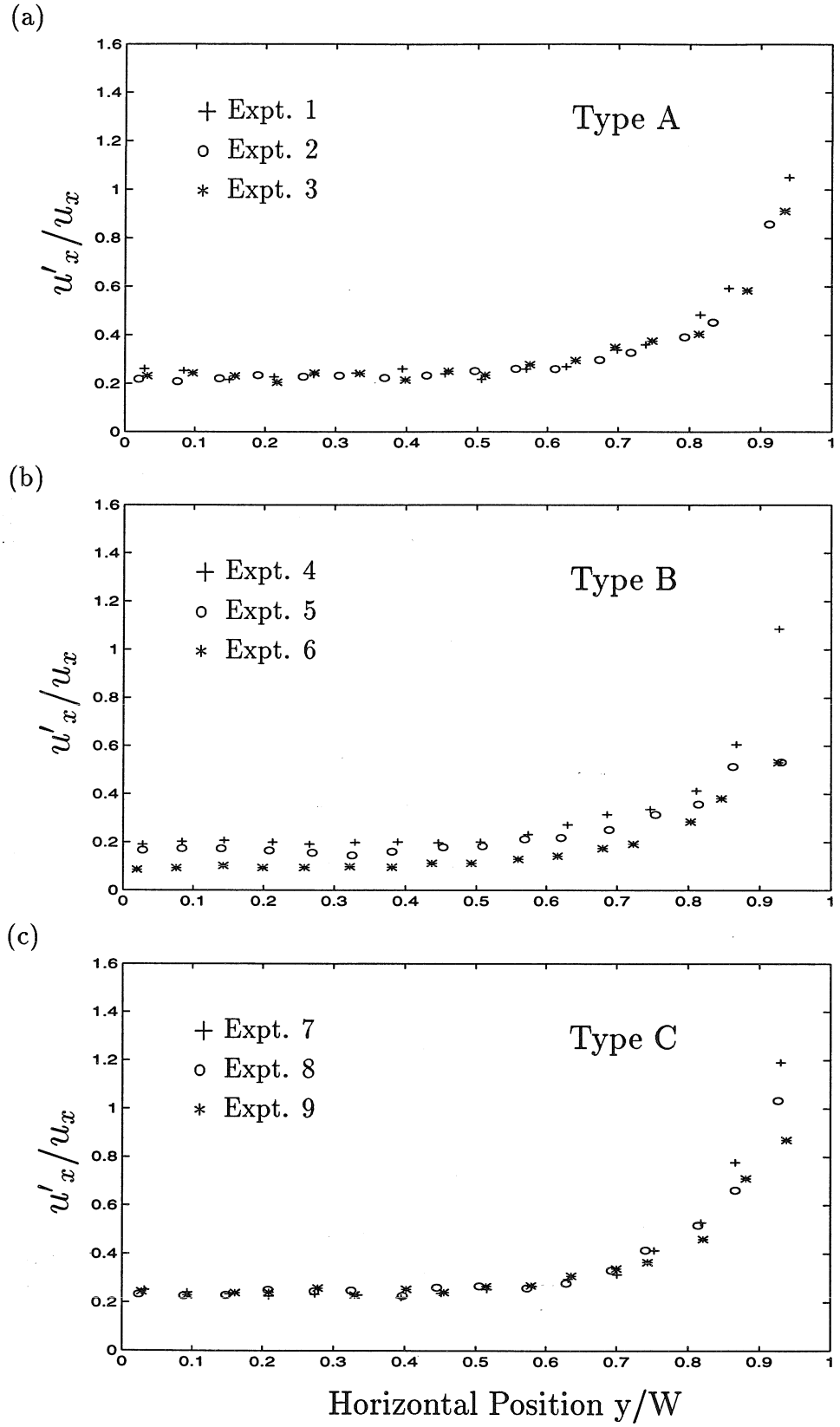


Figure 3.19: The normalized streamwise fluctuation velocities for particles of (a) Type A, (b) Type B and (c) Type C. W=2.5 cm.

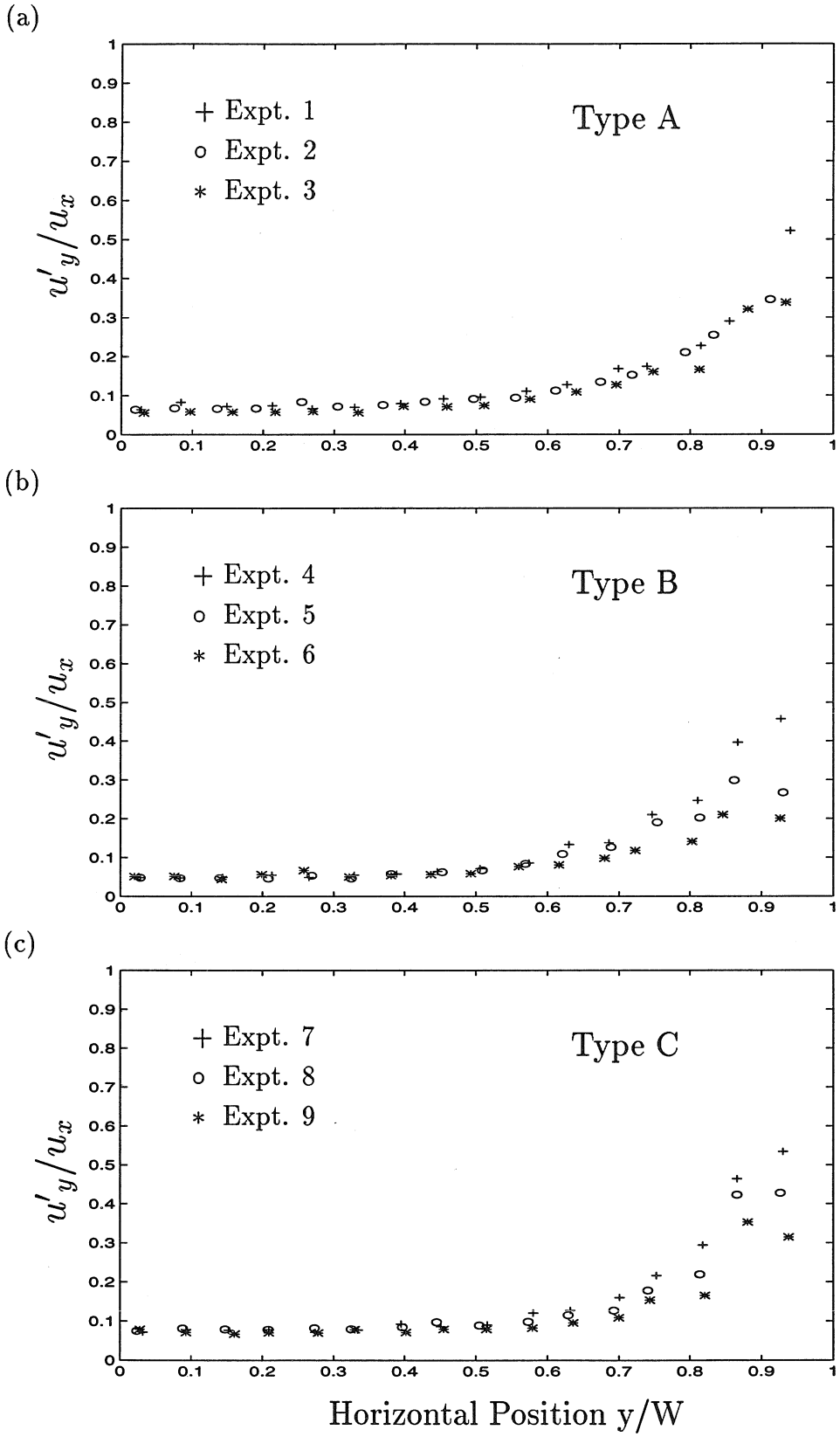


Figure 3.20: The normalized transverse fluctuation velocities for particles of (a) Type A, (b) Type B and (c) Type C. W=2.5 cm.

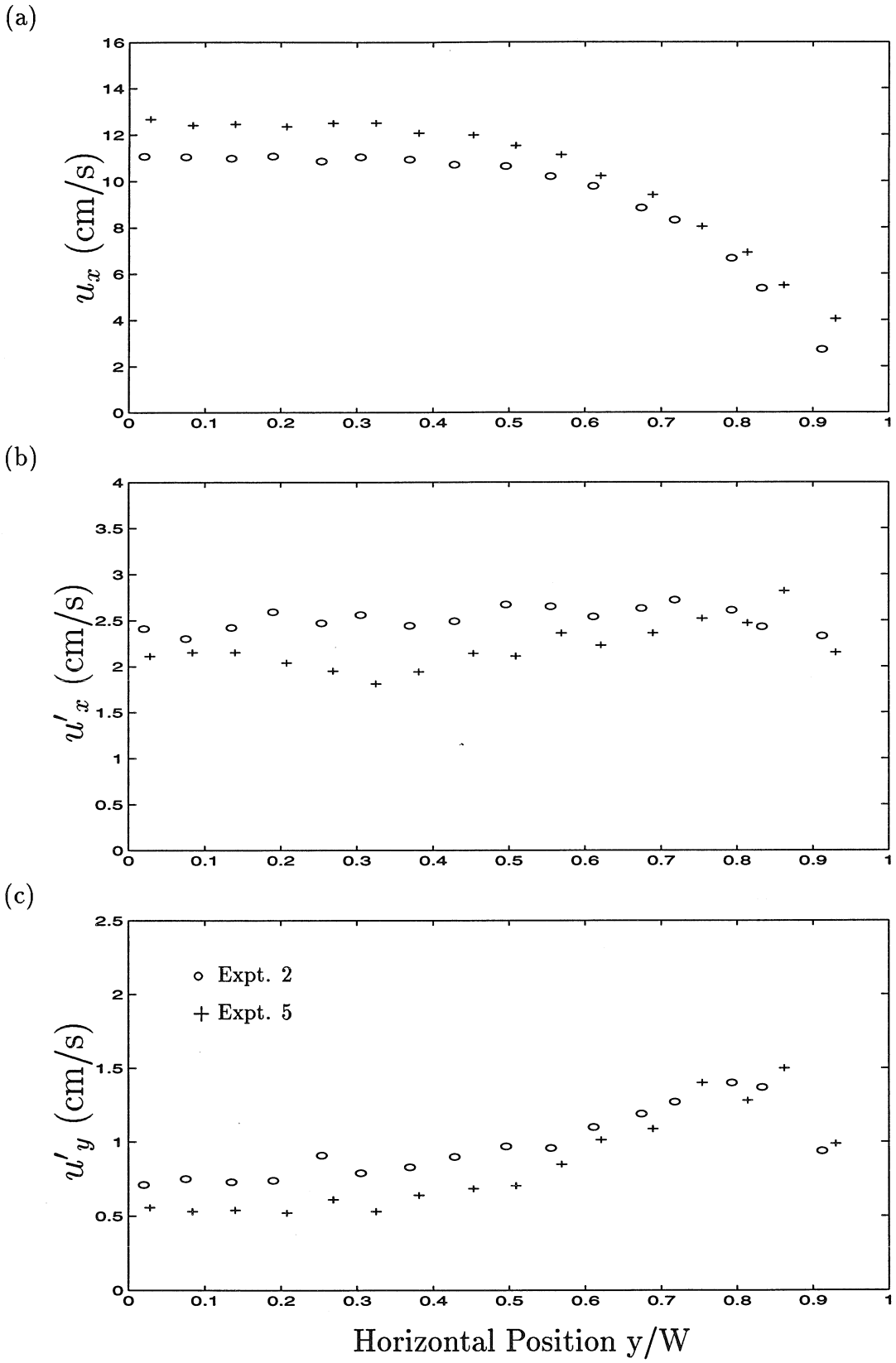


Figure 3.21: (a) The mean streamwise, (b) streamwise fluctuation and (c) transverse fluctuation velocity profiles for Expts 2 (Type A particles) and 5 (Type B). W=2.5 cm.

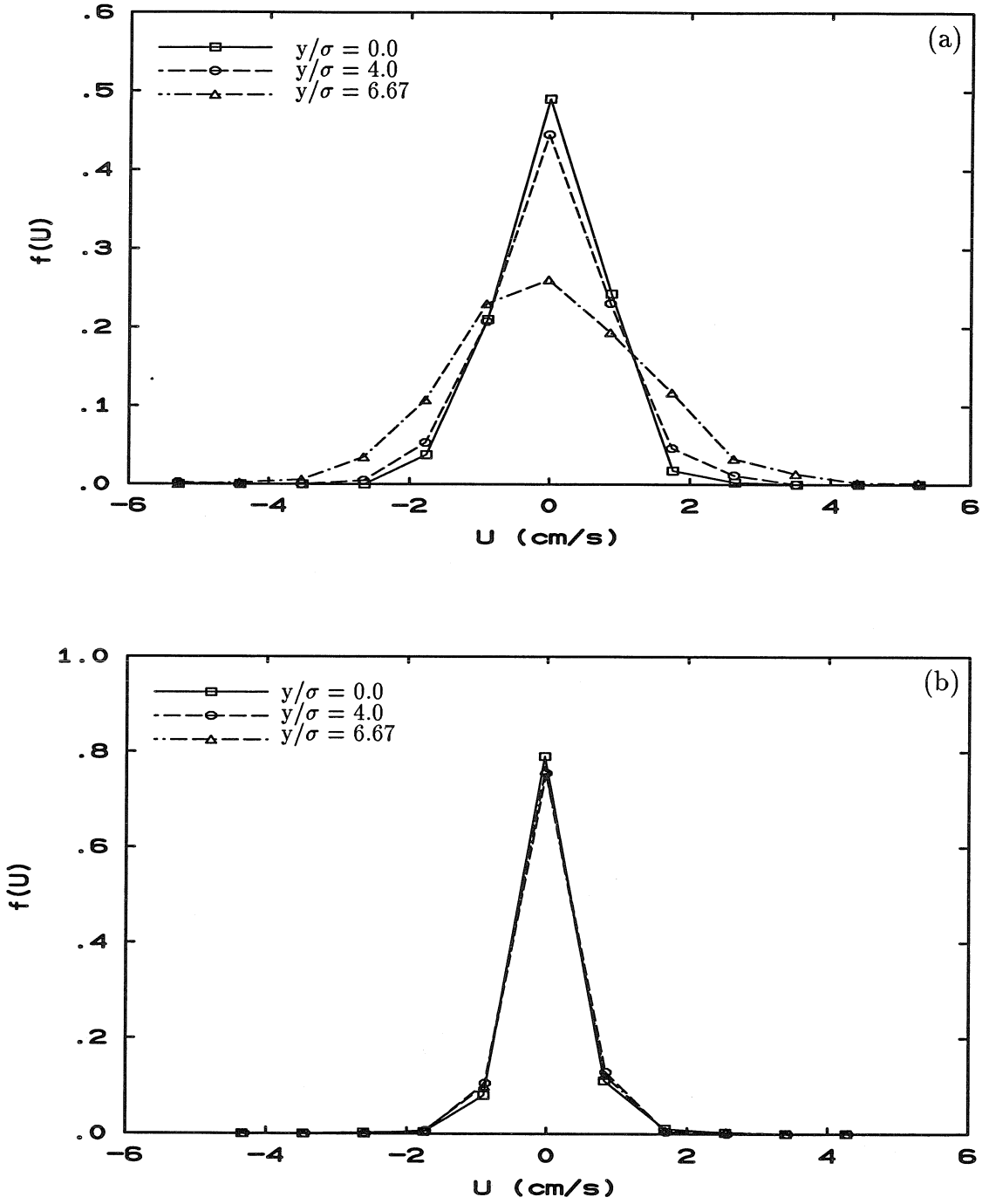


Figure 3.22: Distribution of transverse fluctuation velocities for (a) rough and (b) smooth walls. In these figures U represents the transverse fluctuation velocity and f(U) the fraction of the total number of velocity observations for each data point that were equal to the fluctuation velocity U. Exit valve width = 1.3 cm.

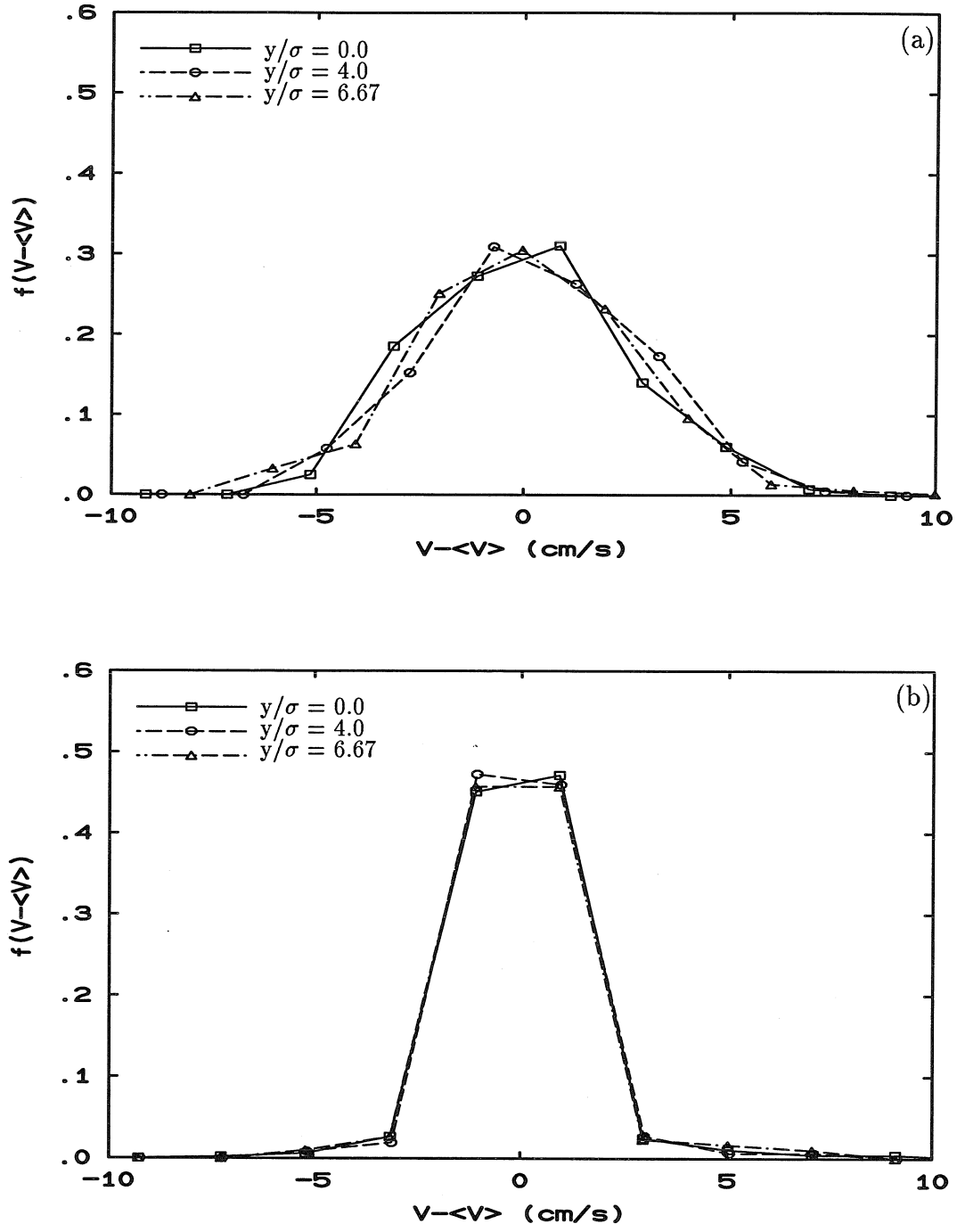


Figure 3.23: Distribution of streamwise fluctuation velocities for (a) rough and (b) smooth walls. In these figures V-<V> represents the transverse fluctuation velocity and f(V-<V>) the fraction of the total number of velocity observations for each data point that were equal to the fluctuation velocity V-<V>. Exit valve width = 1.3 cm.

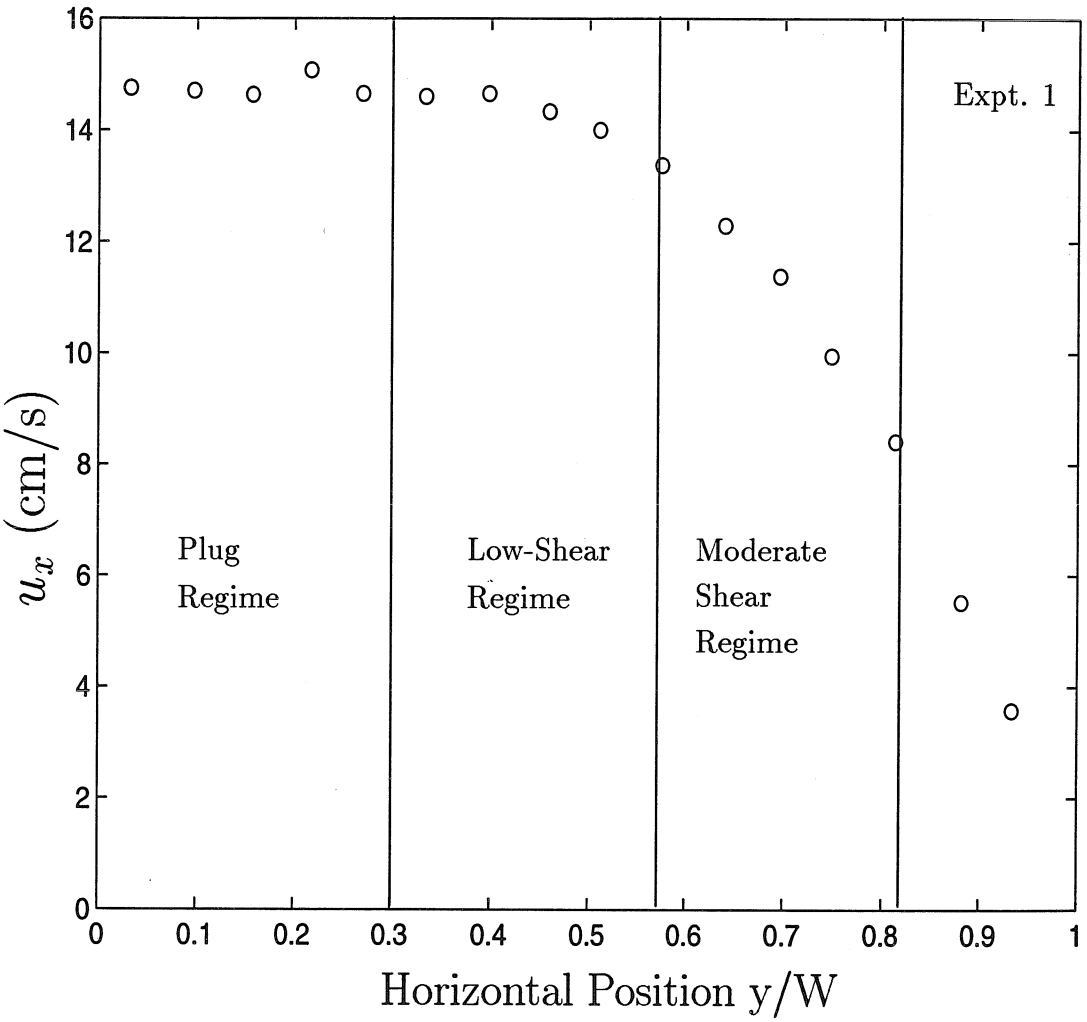


Figure 3.24: Typical partitioning of the flow into three shear regimes in order to calculate self-diffusion coefficients.

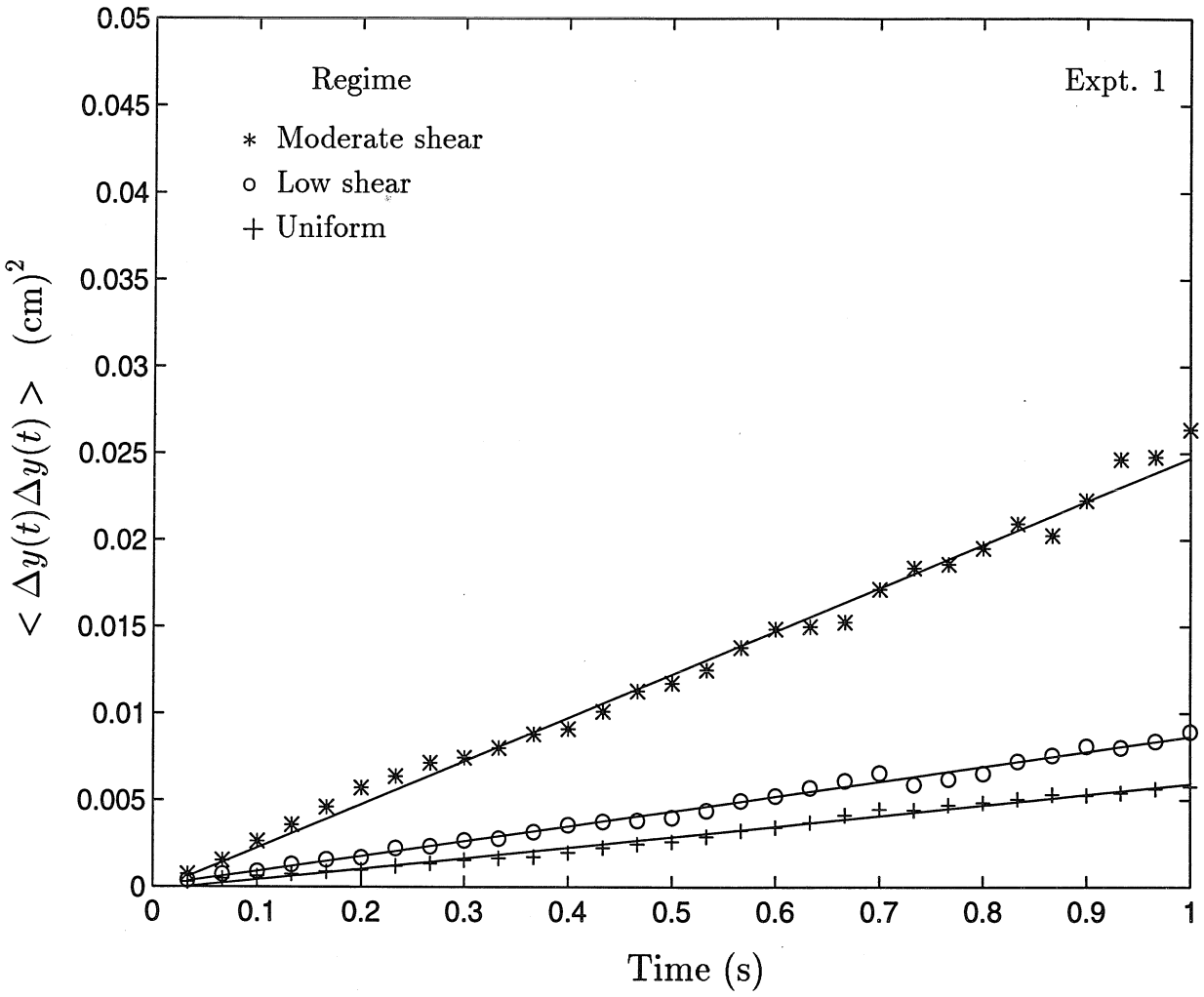


Figure 3.25: Variation of mean-square transverse diffusive displacement with time. Expt. 1.

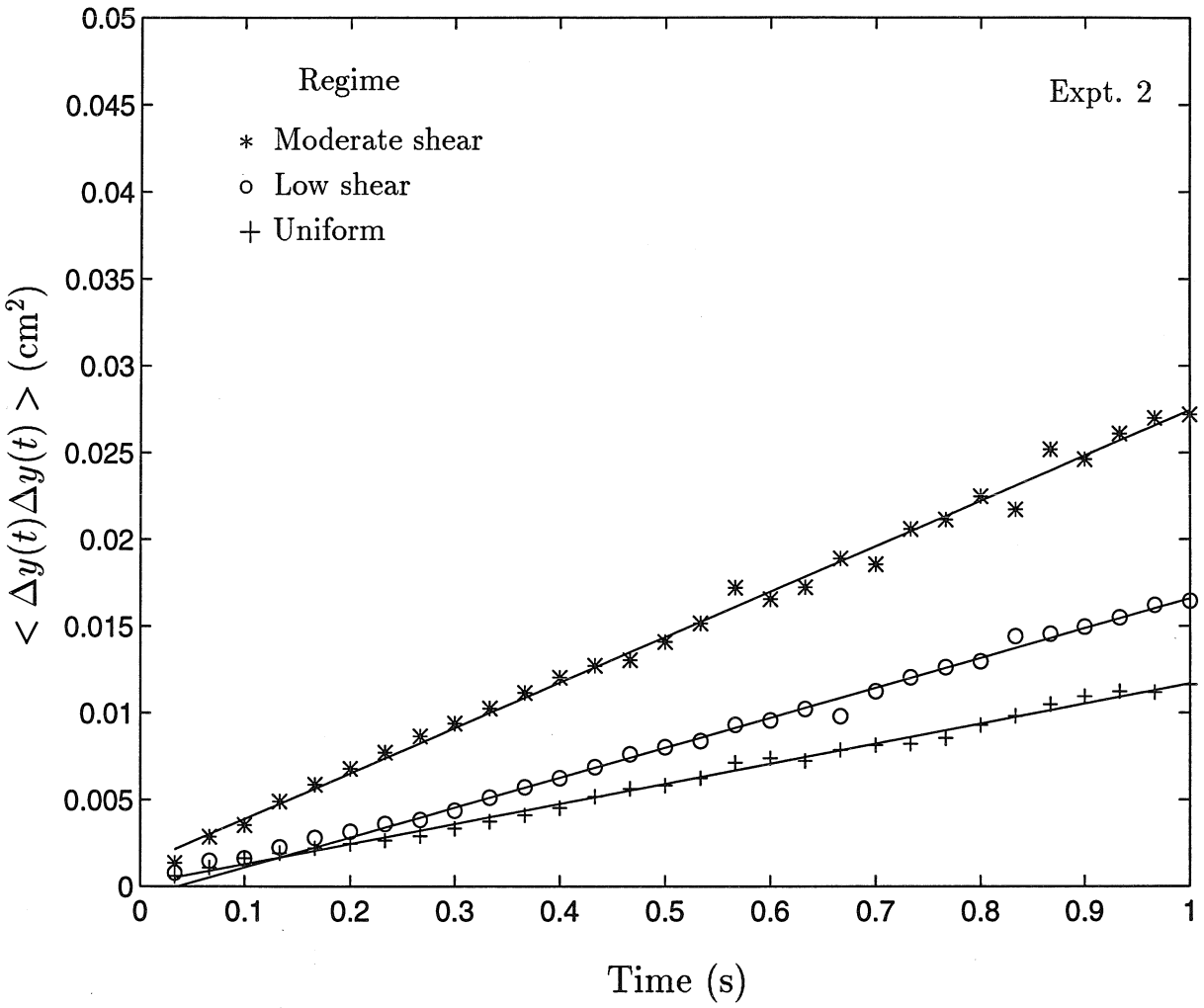


Figure 3.26: Variation of mean-square transverse diffusive displacement with time. Expt. 2.

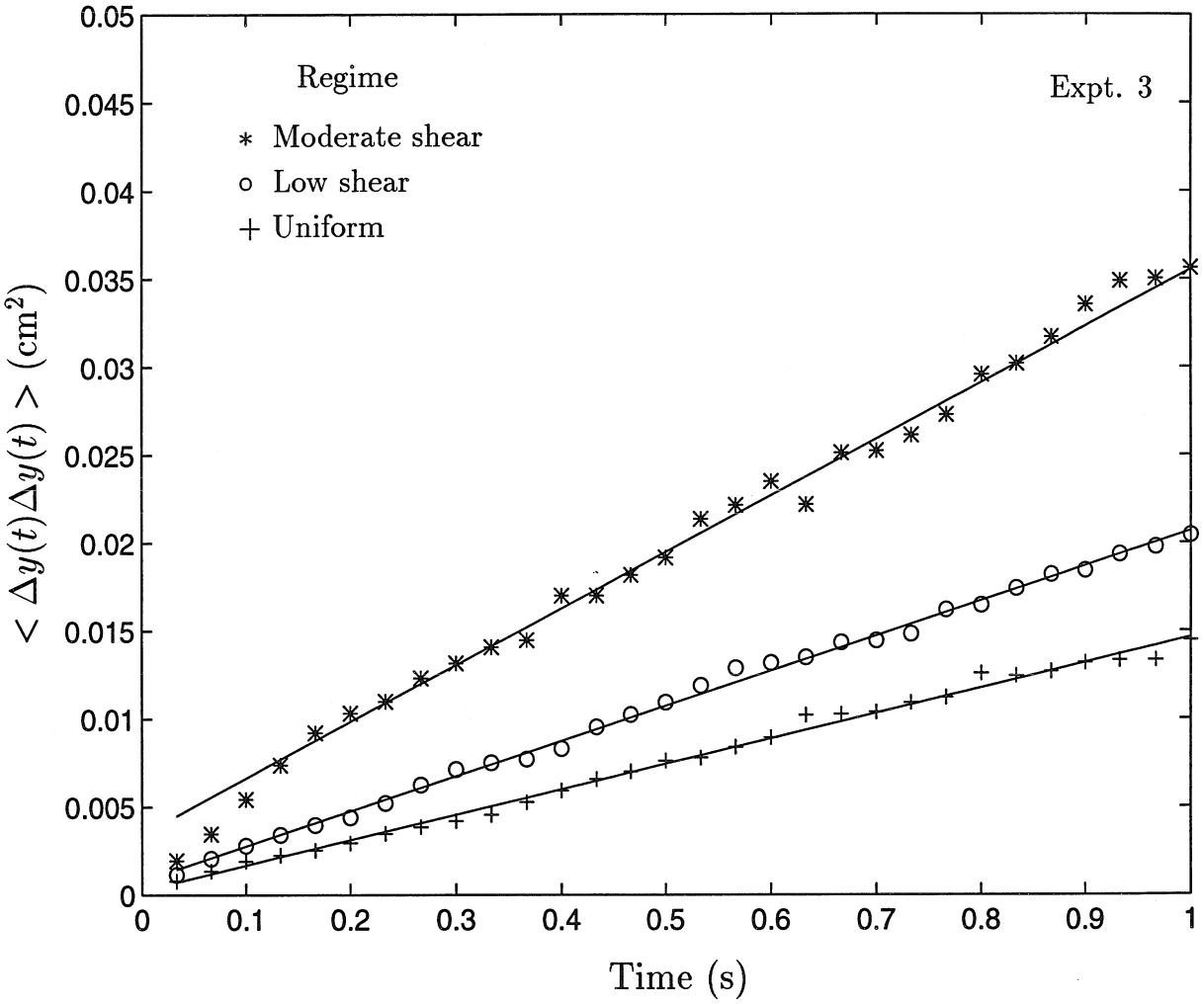


Figure 3.27: Variation of mean-square transverse diffusive displacement with time. Expt. 3.

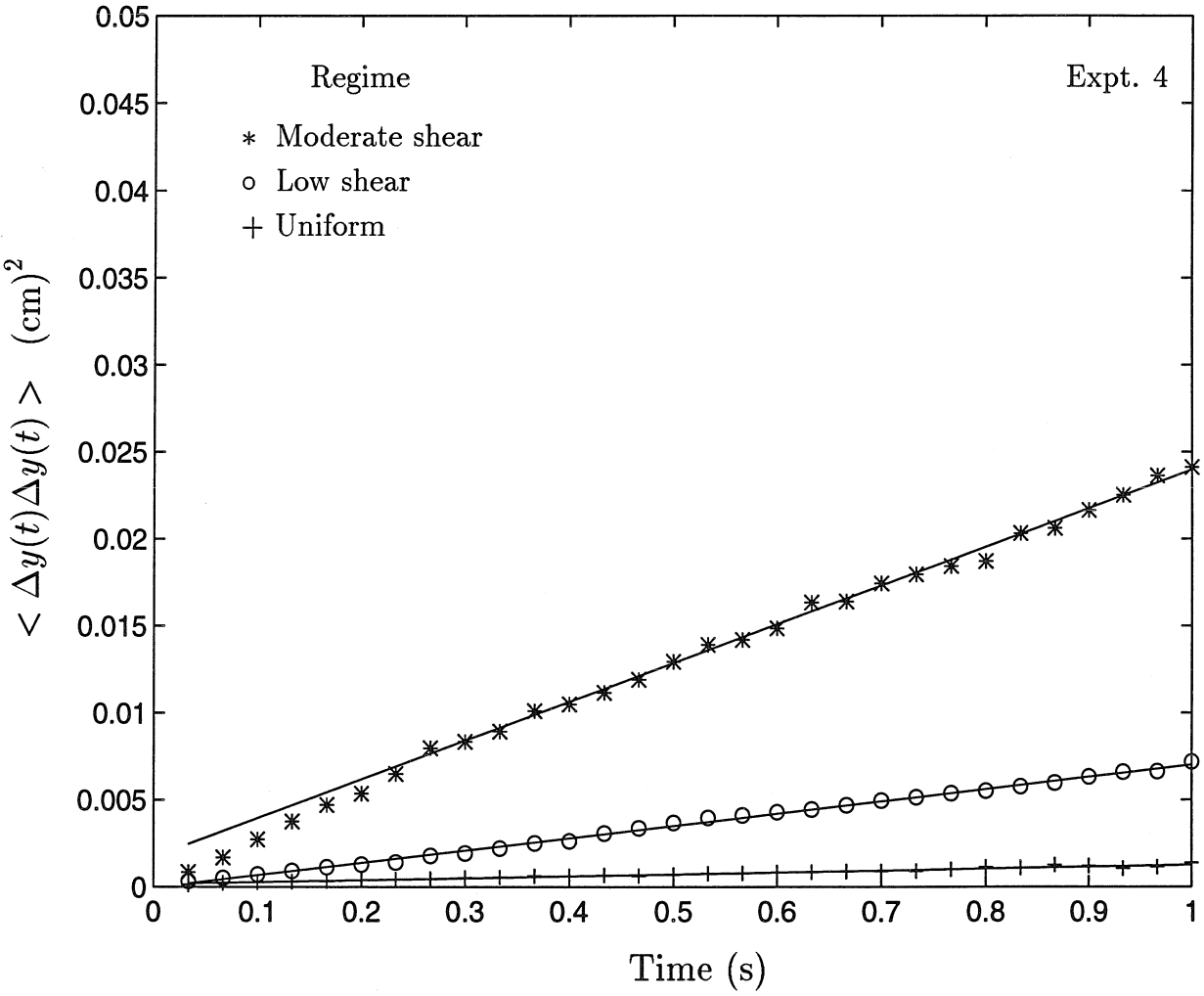


Figure 3.28: Variation of mean-square transverse diffusive displacement with time. Expt. 4.

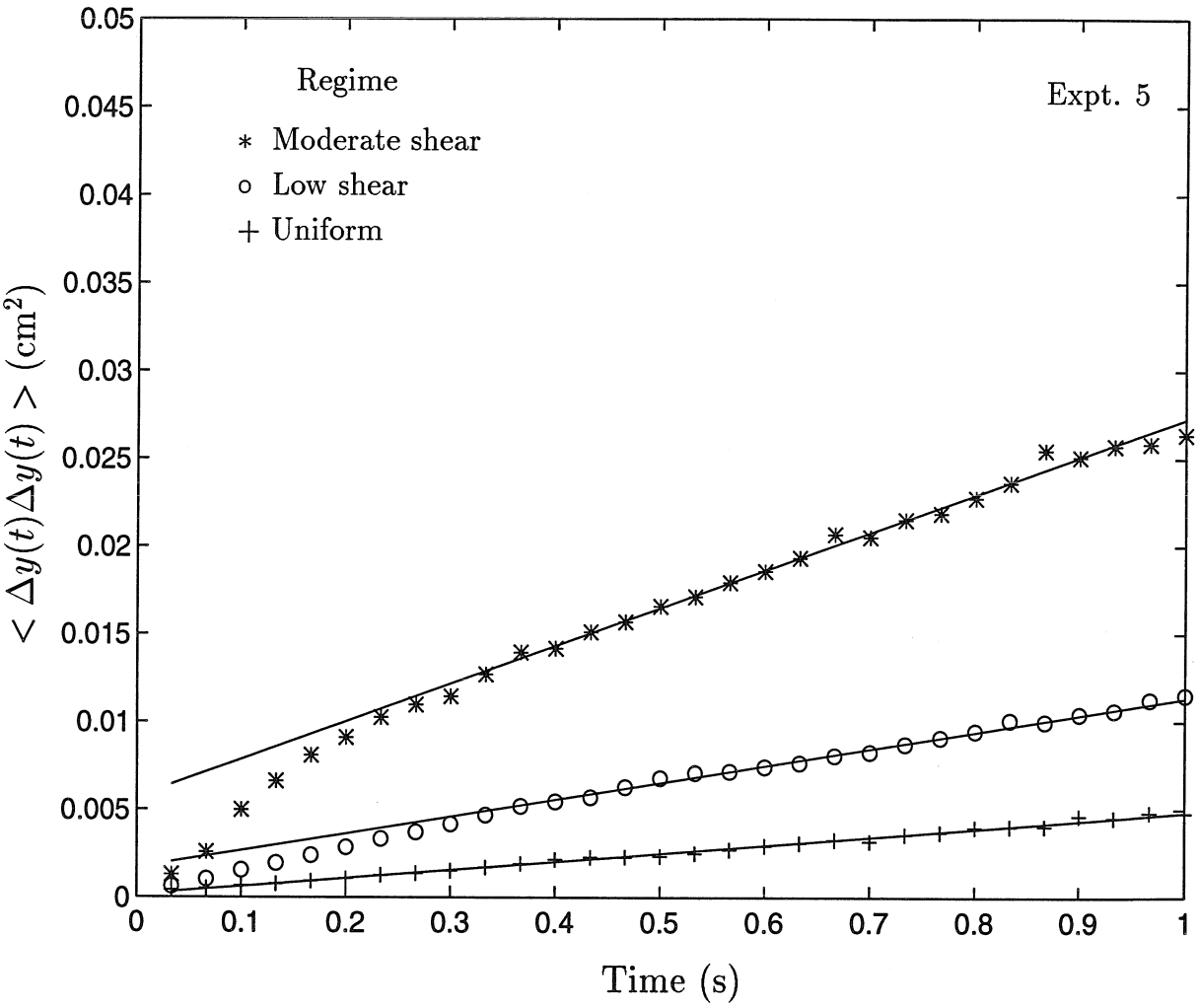


Figure 3.29: Variation of mean-square transverse diffusive displacement with time. Expt. 5.

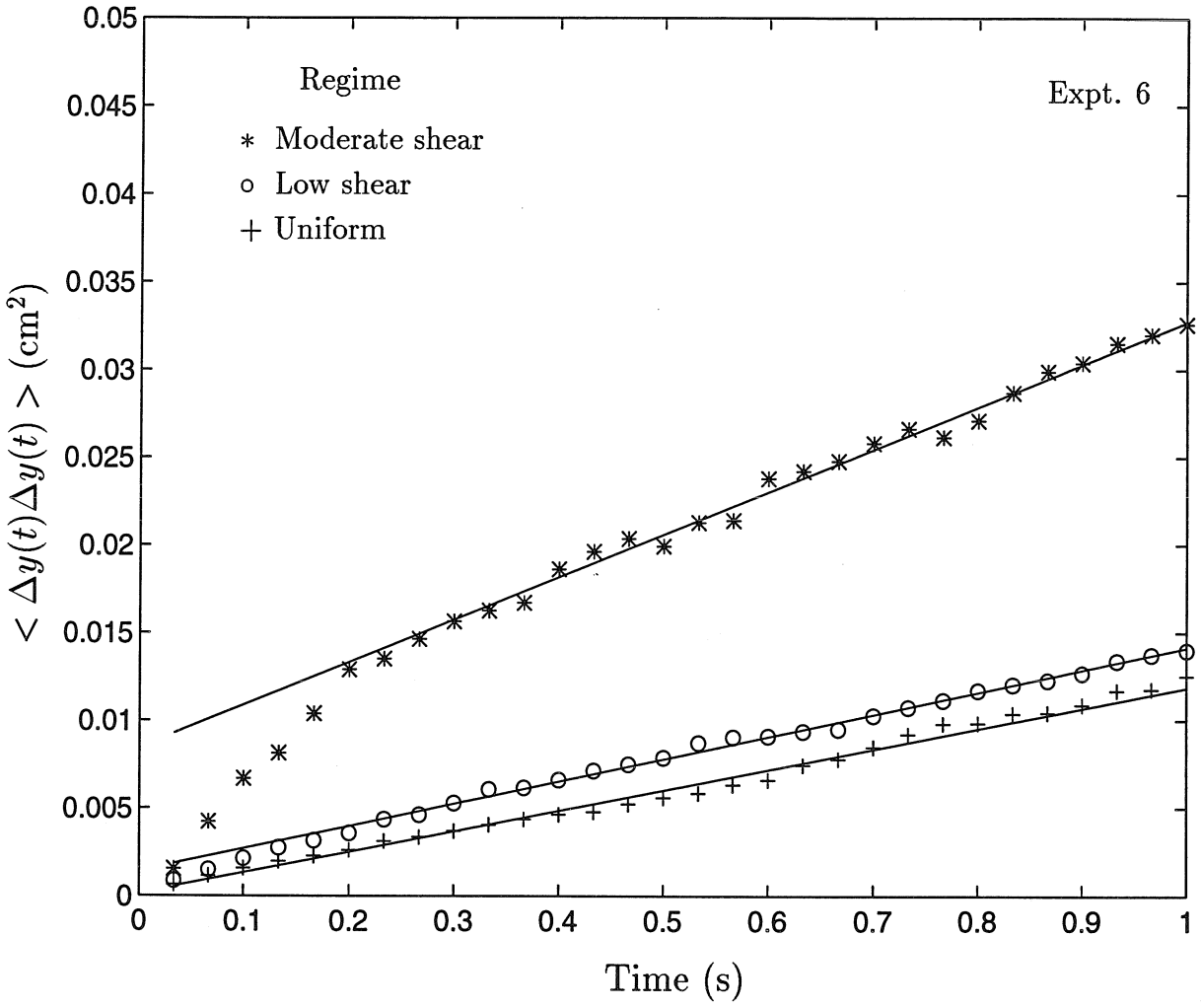


Figure 3.30: Variation of mean-square transverse diffusive displacement with time. Expt. 6.

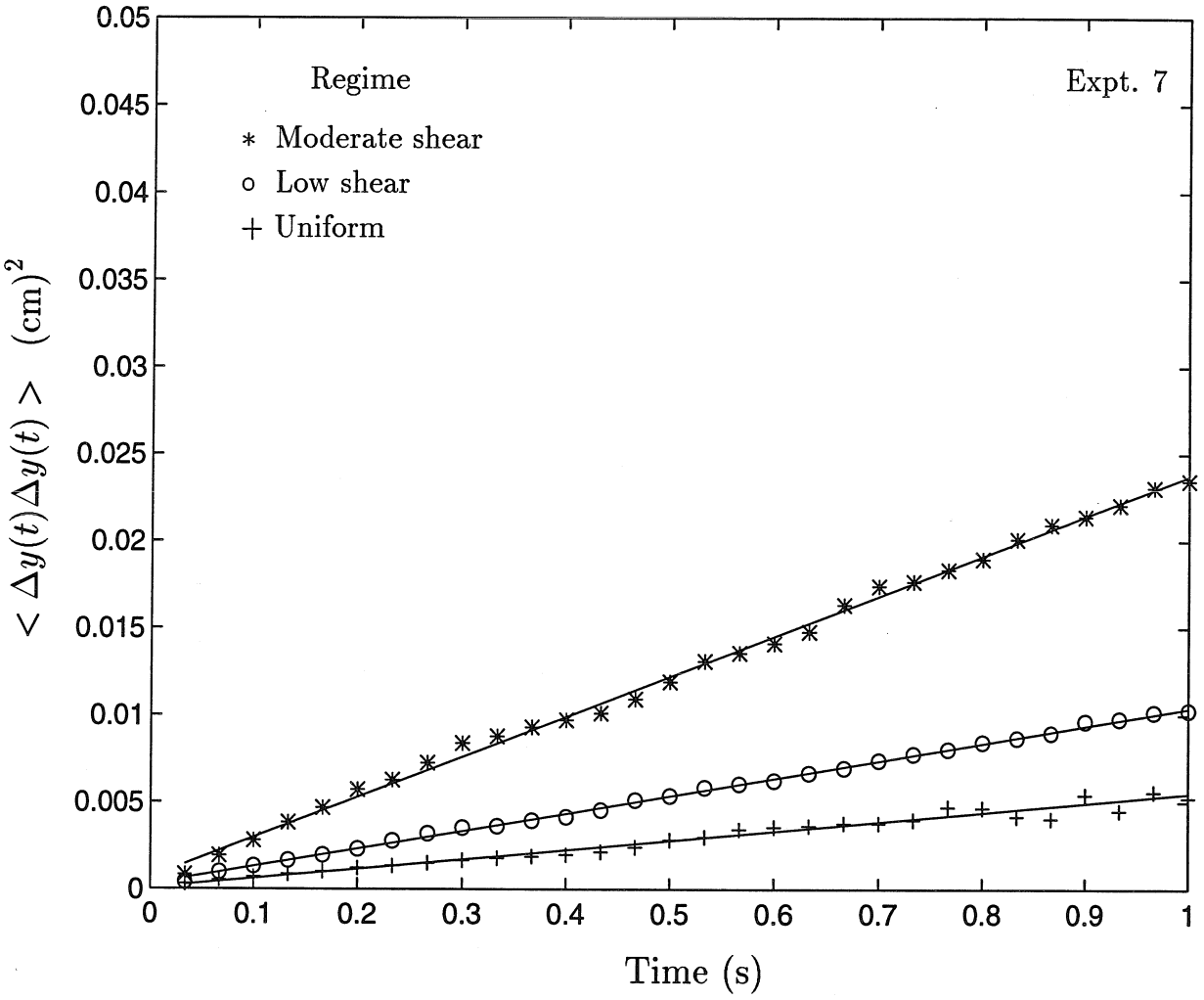


Figure 3.31: Variation of mean-square transverse diffusive displacement with time. Expt. 7.

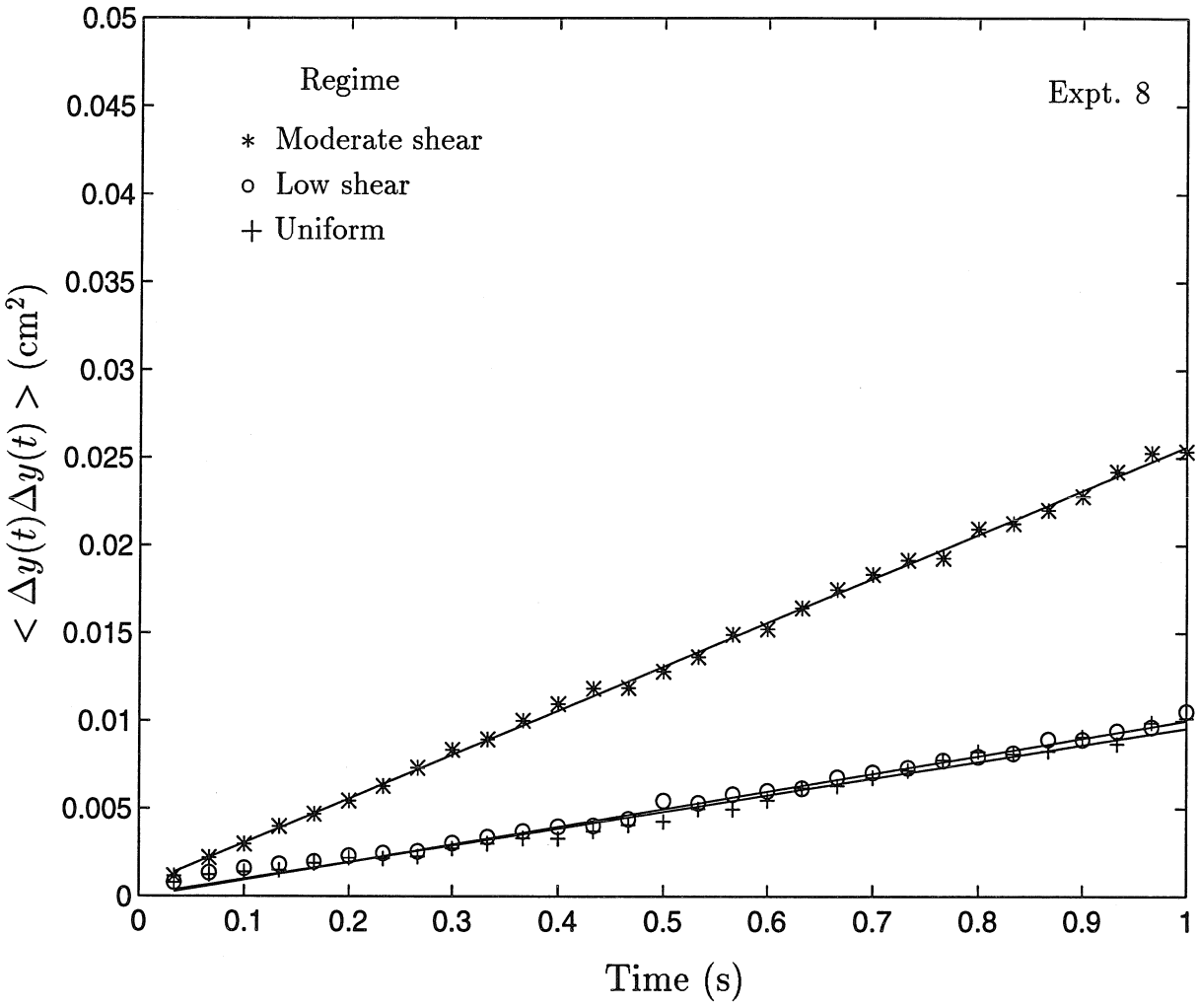


Figure 3.32: Variation of mean-square transverse diffusive displacement with time. Expt. 8.

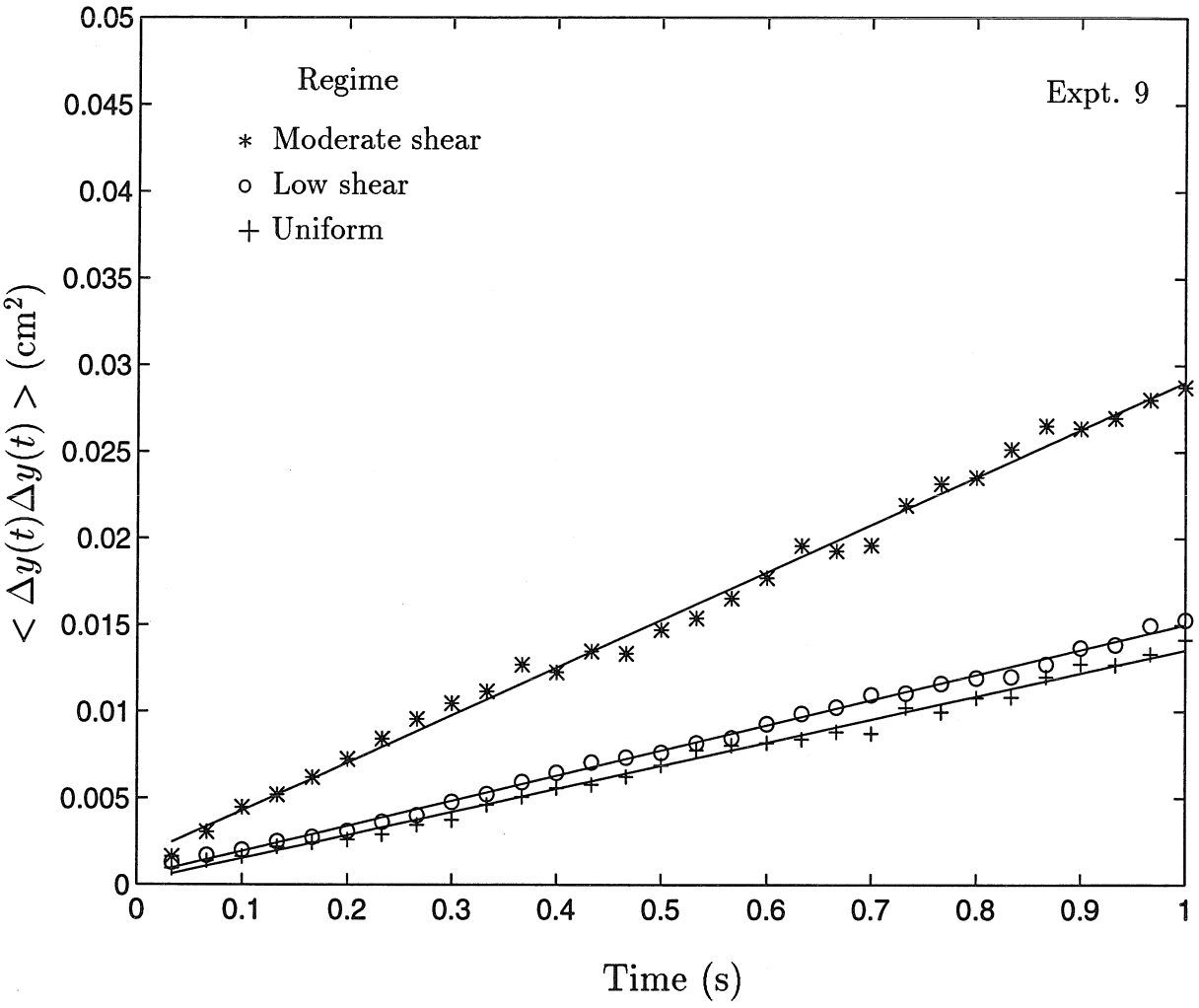


Figure 3.33: Variation of mean-square transverse diffusive displacement with time. Expt. 9.

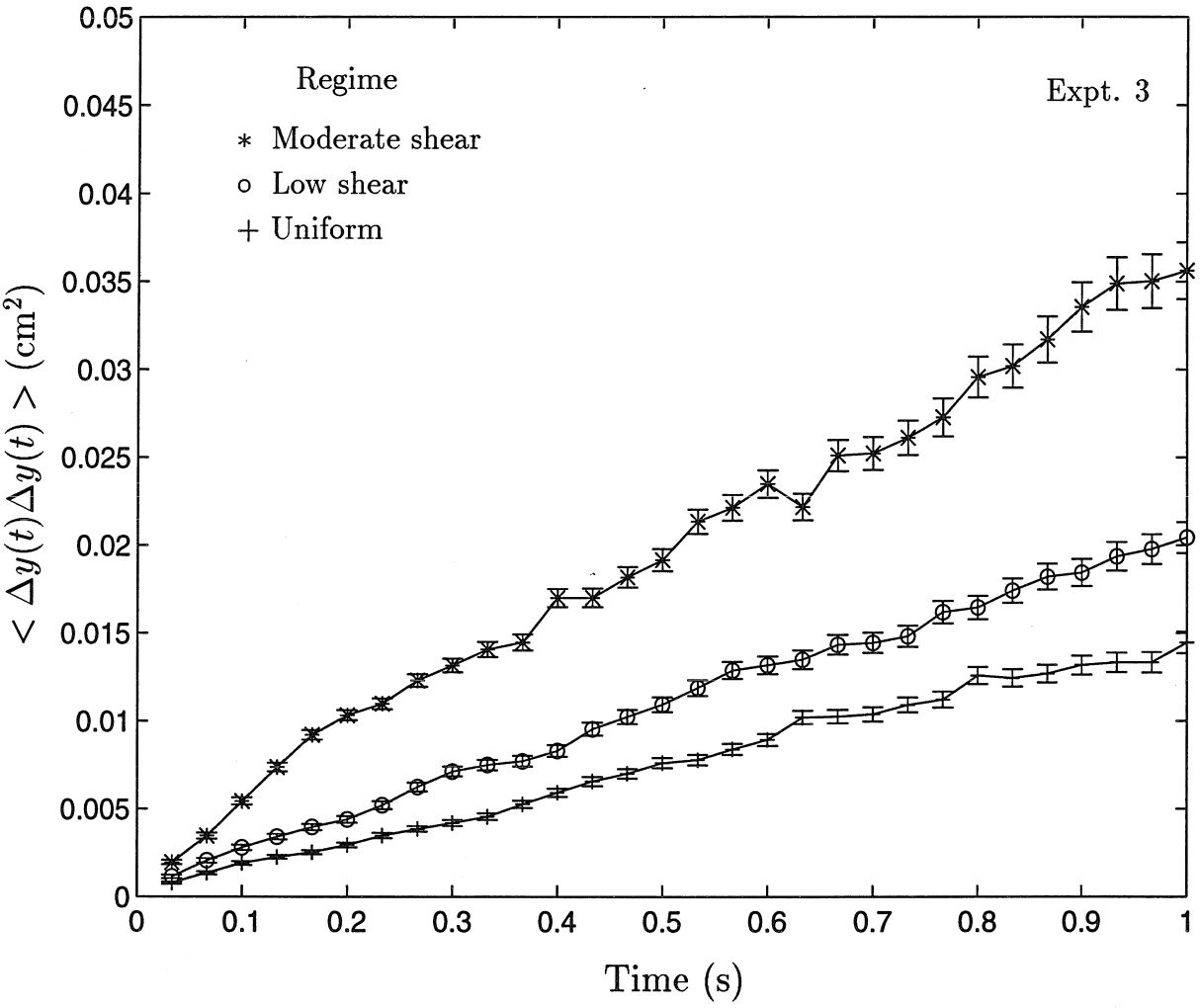


Figure 3.34: Variation of mean-square transverse diffusive displacement with time. Expt. 3. Extent of error bars.

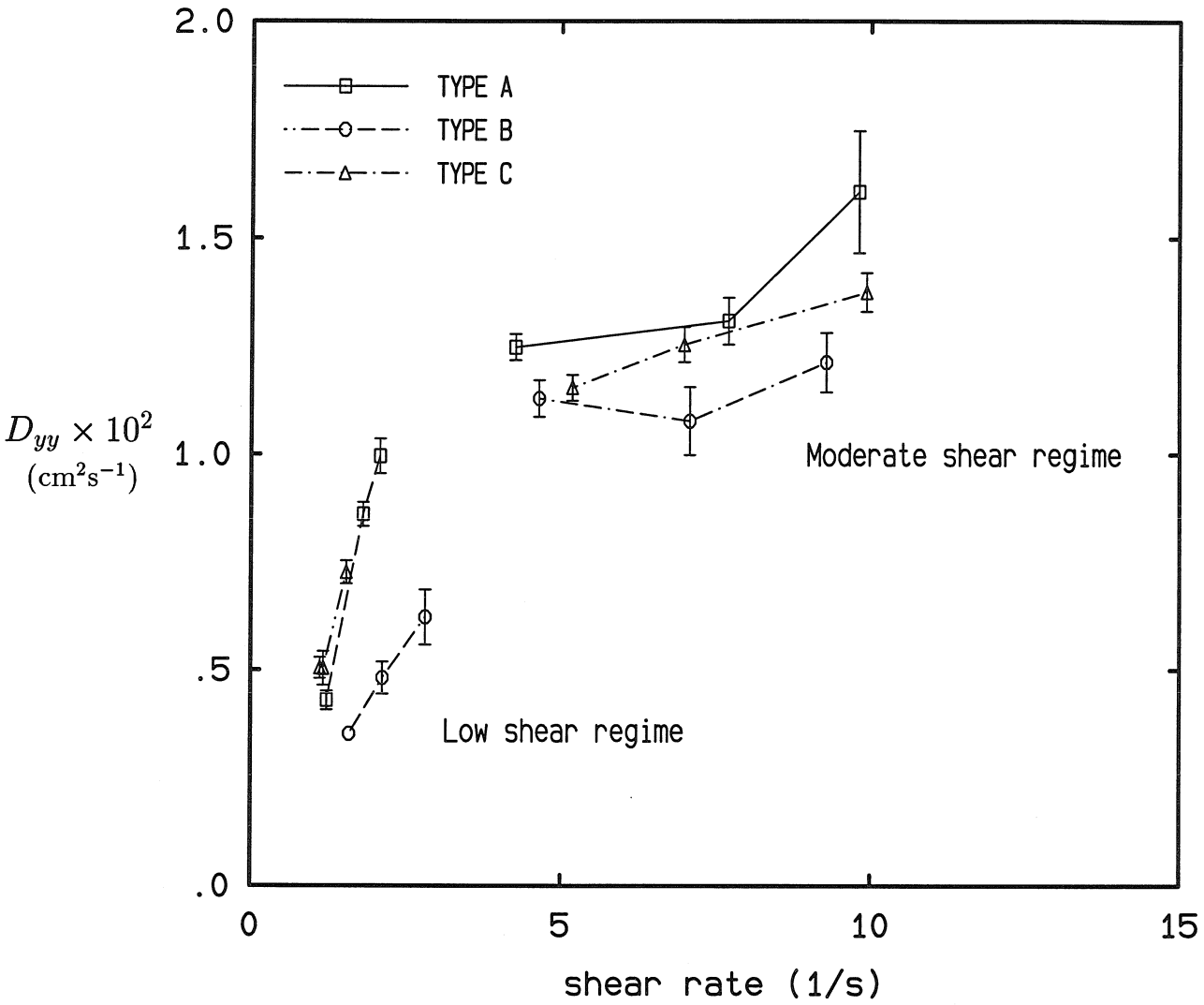


Figure 3.35: Variation of the coefficient of transverse diffusion $D_{yy}$ with shear rate for Expts 1-9.

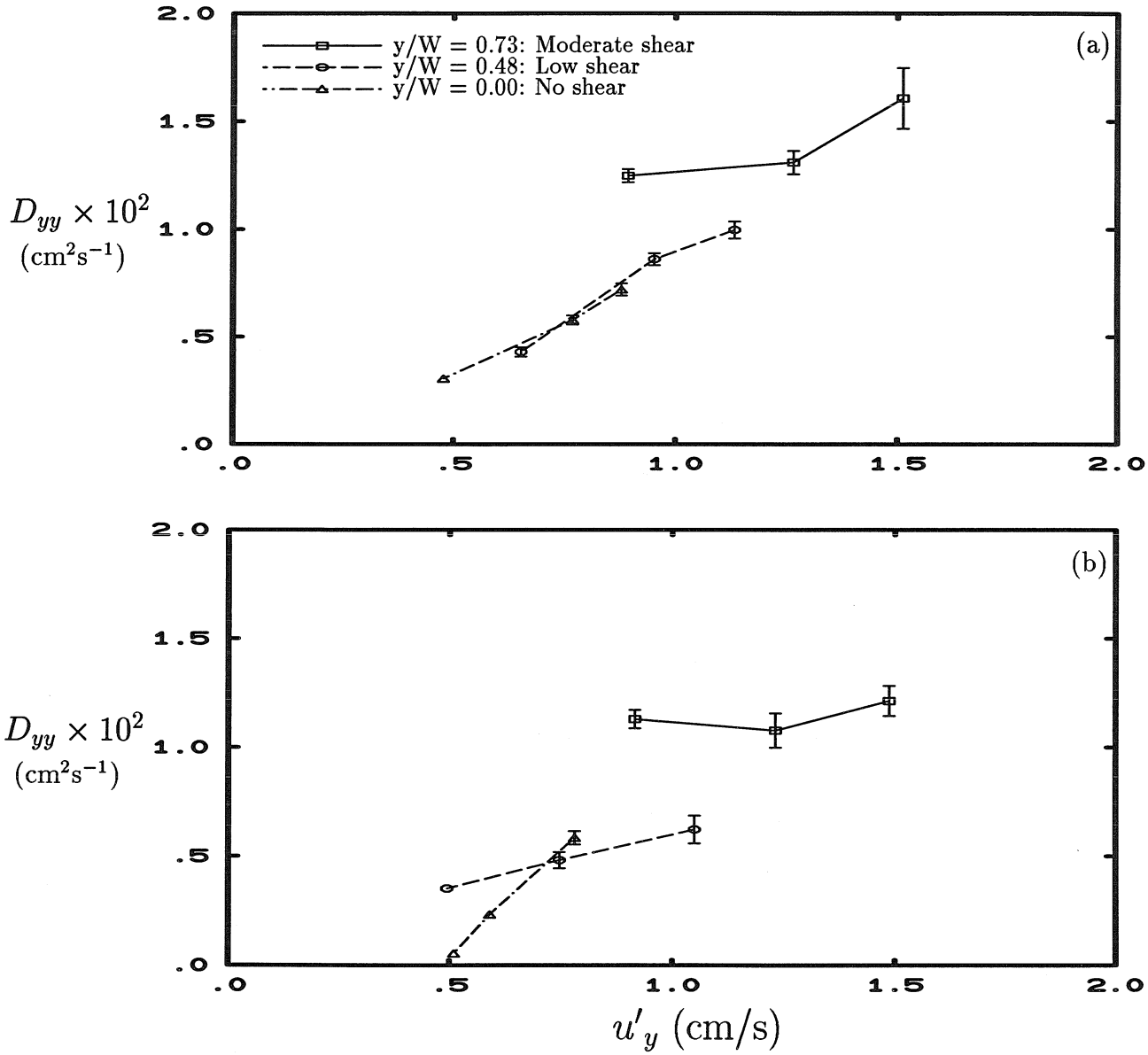


Figure 3.36: Variation of the coefficient of transverse diffusion $D_{yy}$ with transverse fluctuation velocity for particle types (a) A and (b) B.

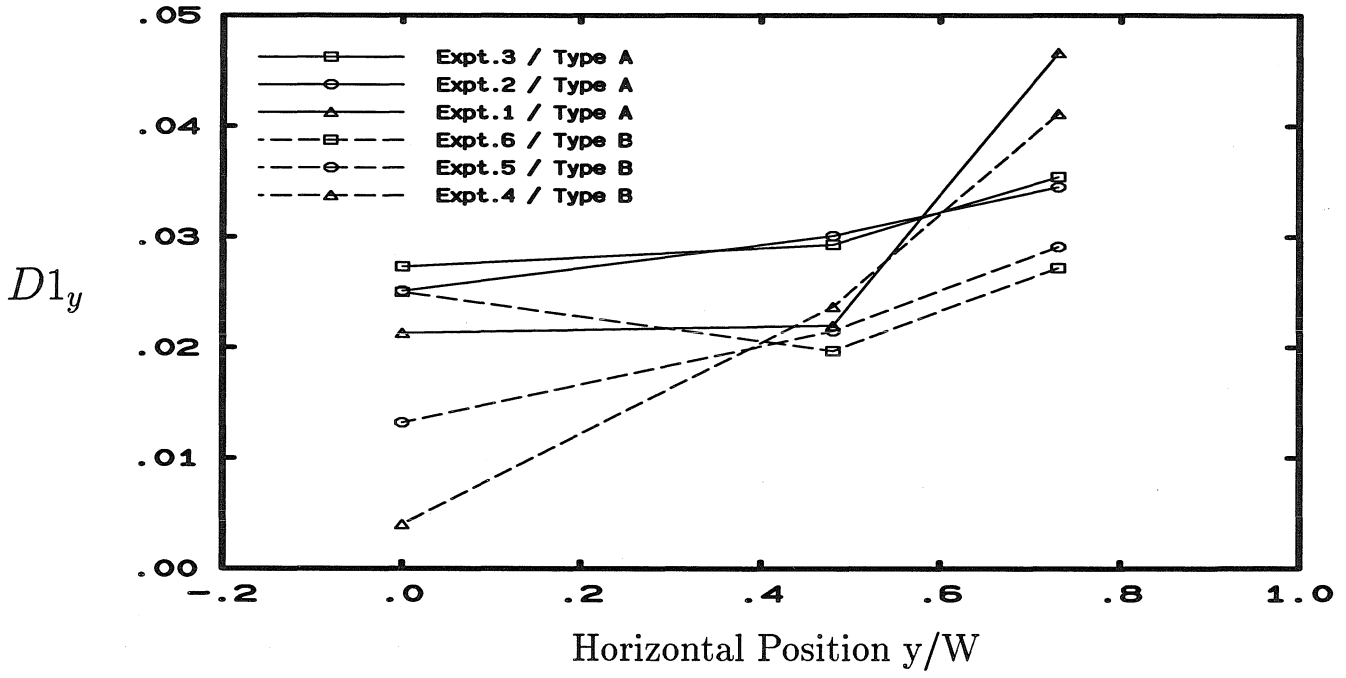


Figure 3.37: Variation of $D1_y$ with position (or shear regime) for particle types A and B. W=2.5 cm.

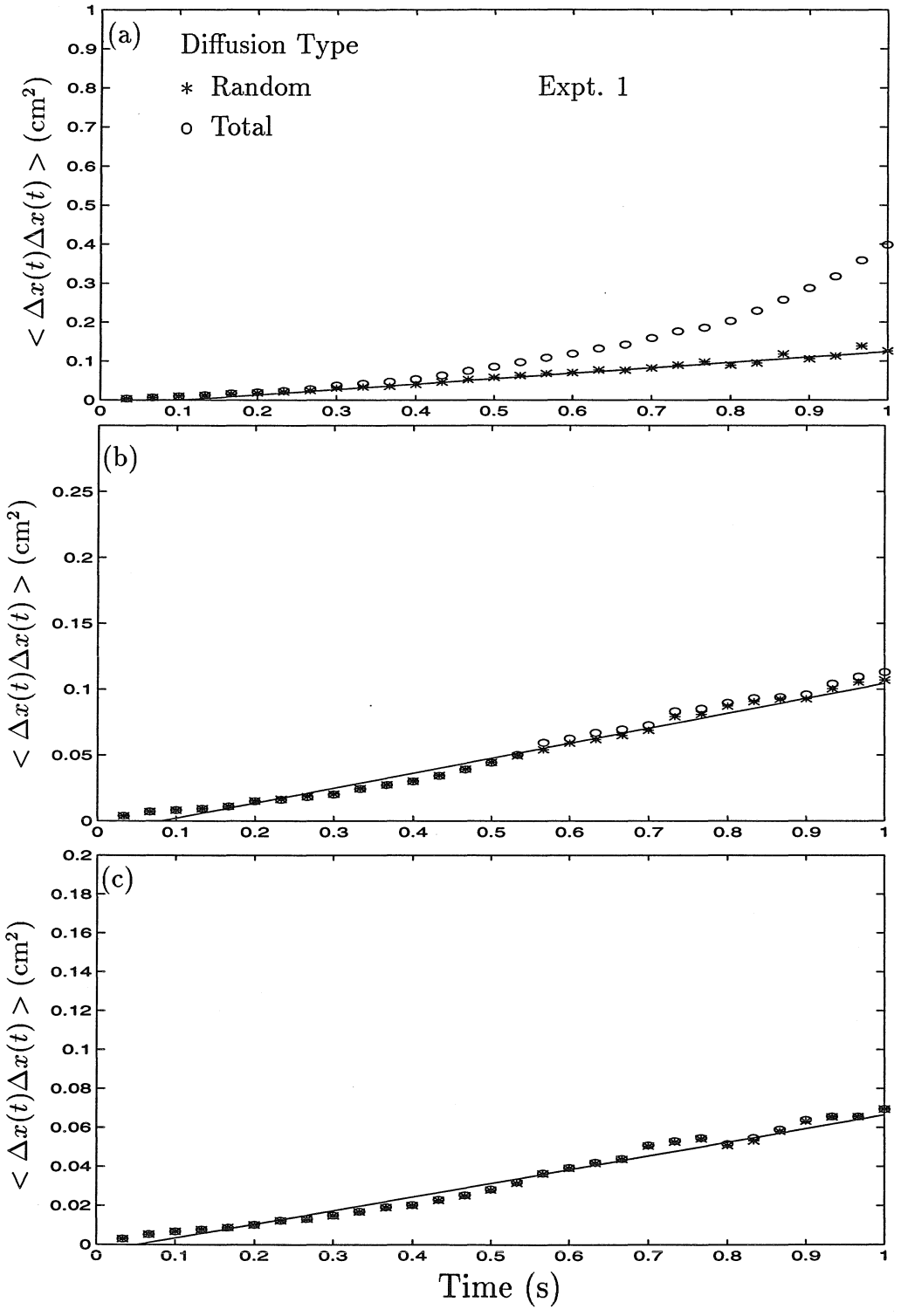


Figure 3.38: Variation of mean-square streamwise diffusive displacement with time for the (a) moderate-shear, (b) low-shear and (c) uniform regimes in Expt. 1.

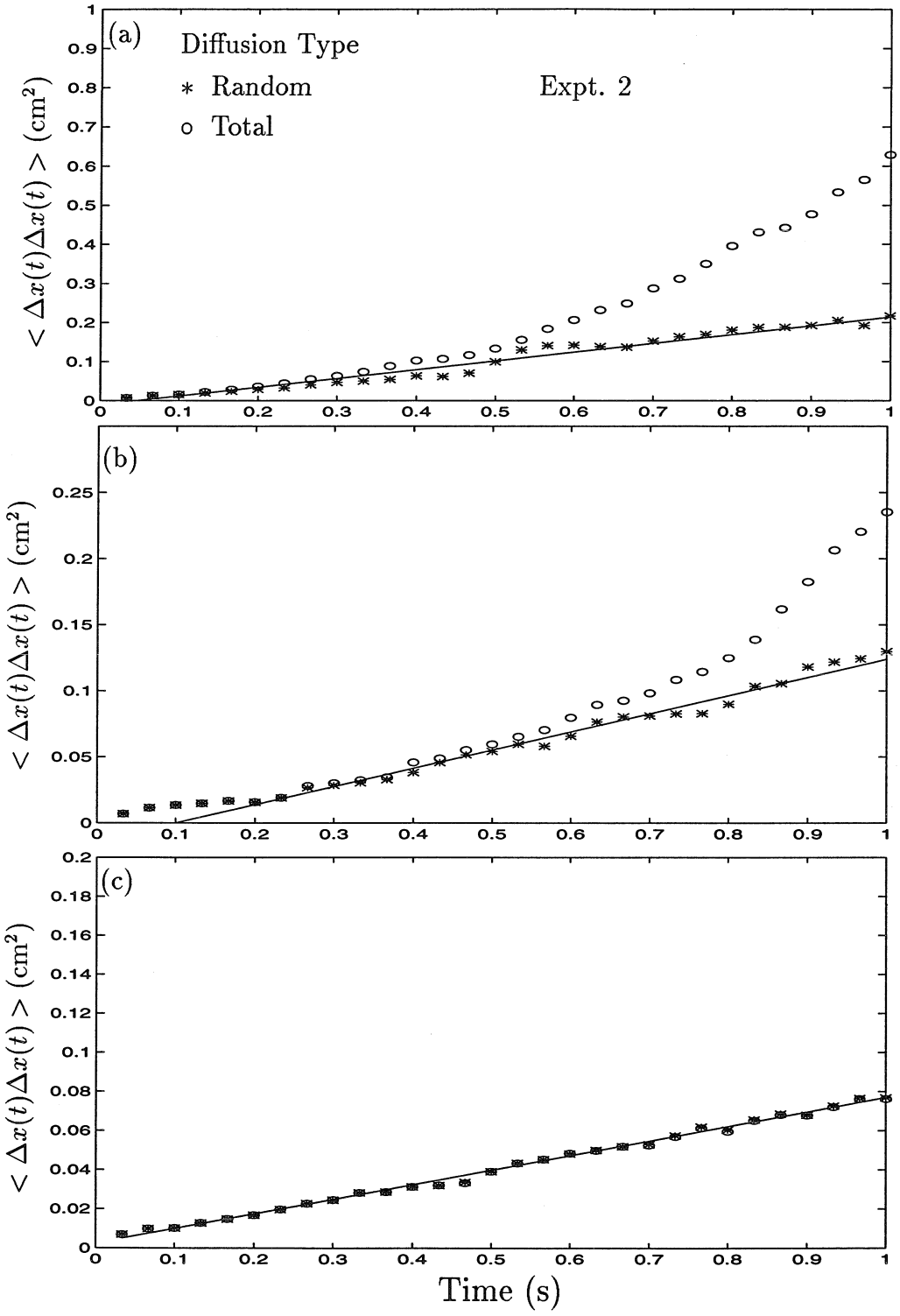


Figure 3.39: Variation of mean-square streamwise diffusive displacement with time for the (a) moderate-shear, (b) low-shear and (c) uniform regimes in Expt. 2.

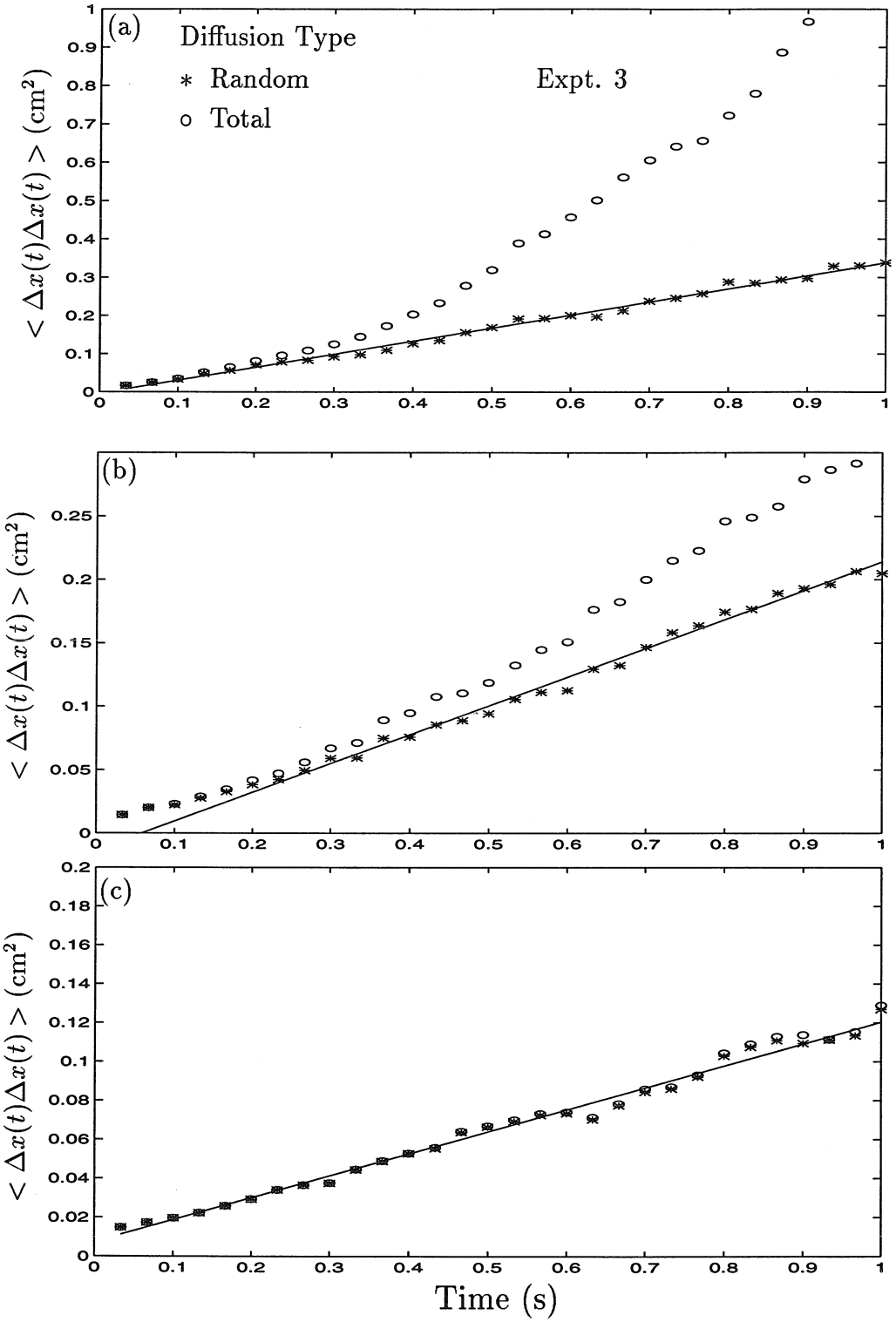


Figure 3.40: Variation of mean-square streamwise diffusive displacement with time for the (a) moderate-shear, (b) low-shear and (c) uniform regimes in Expt. 3.

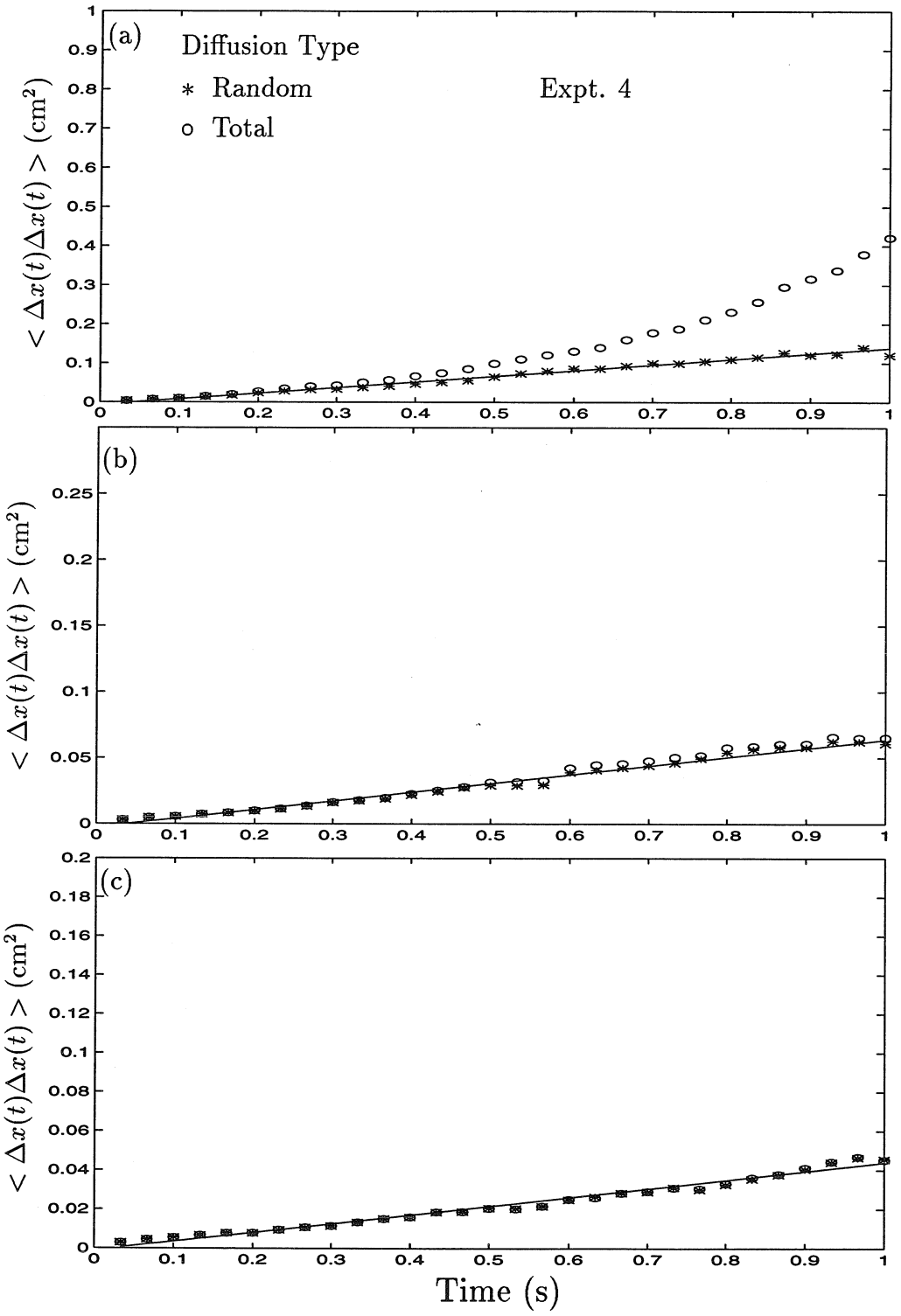


Figure 3.41: Variation of mean-square streamwise diffusive displacement with time for the (a) moderate-shear, (b) low-shear and (c) uniform regimes in Expt. 4.

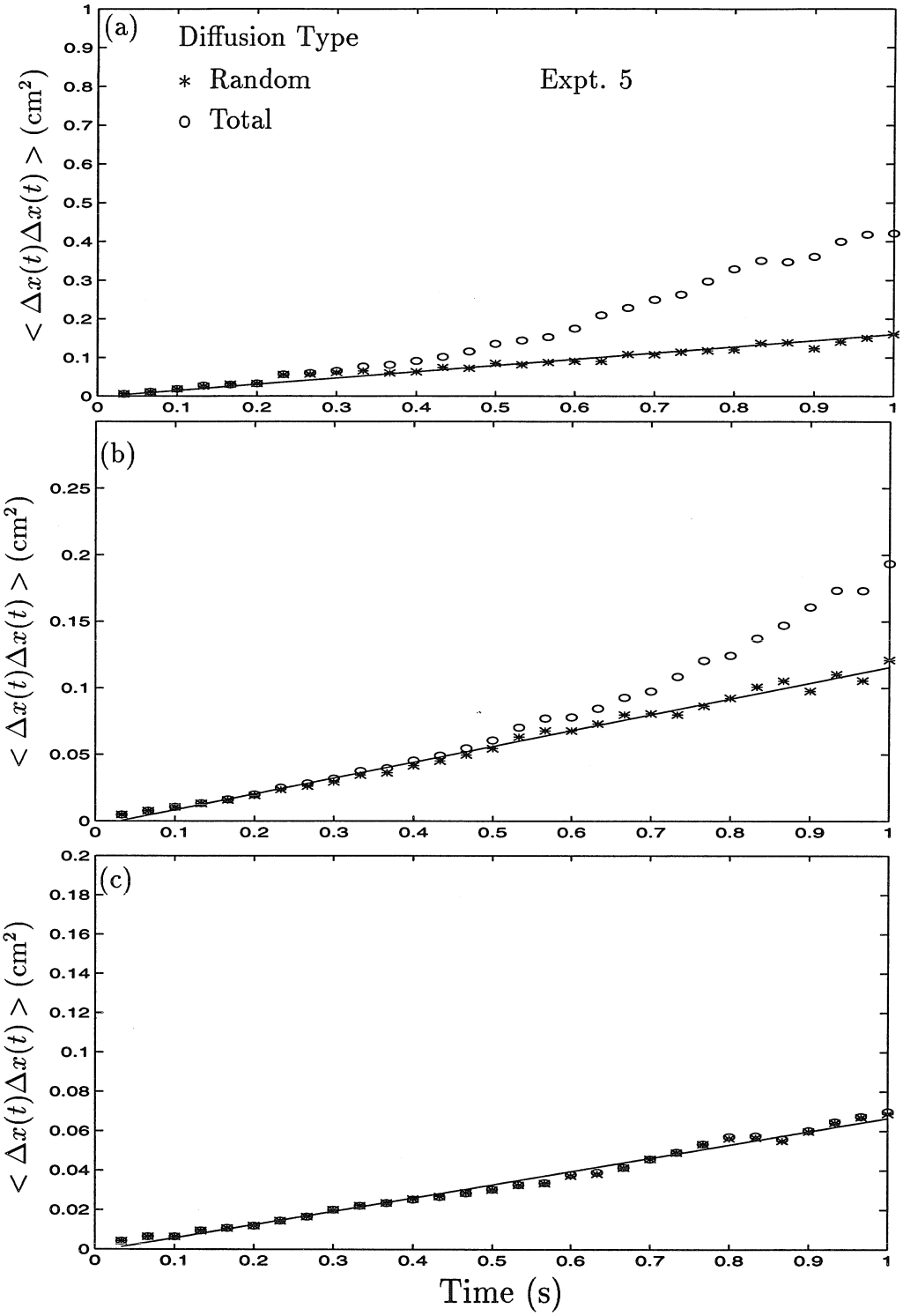


Figure 3.42: Variation of mean-square streamwise diffusive displacement with time for the (a) moderate-shear, (b) low-shear and (c) uniform regimes in Expt. 5.

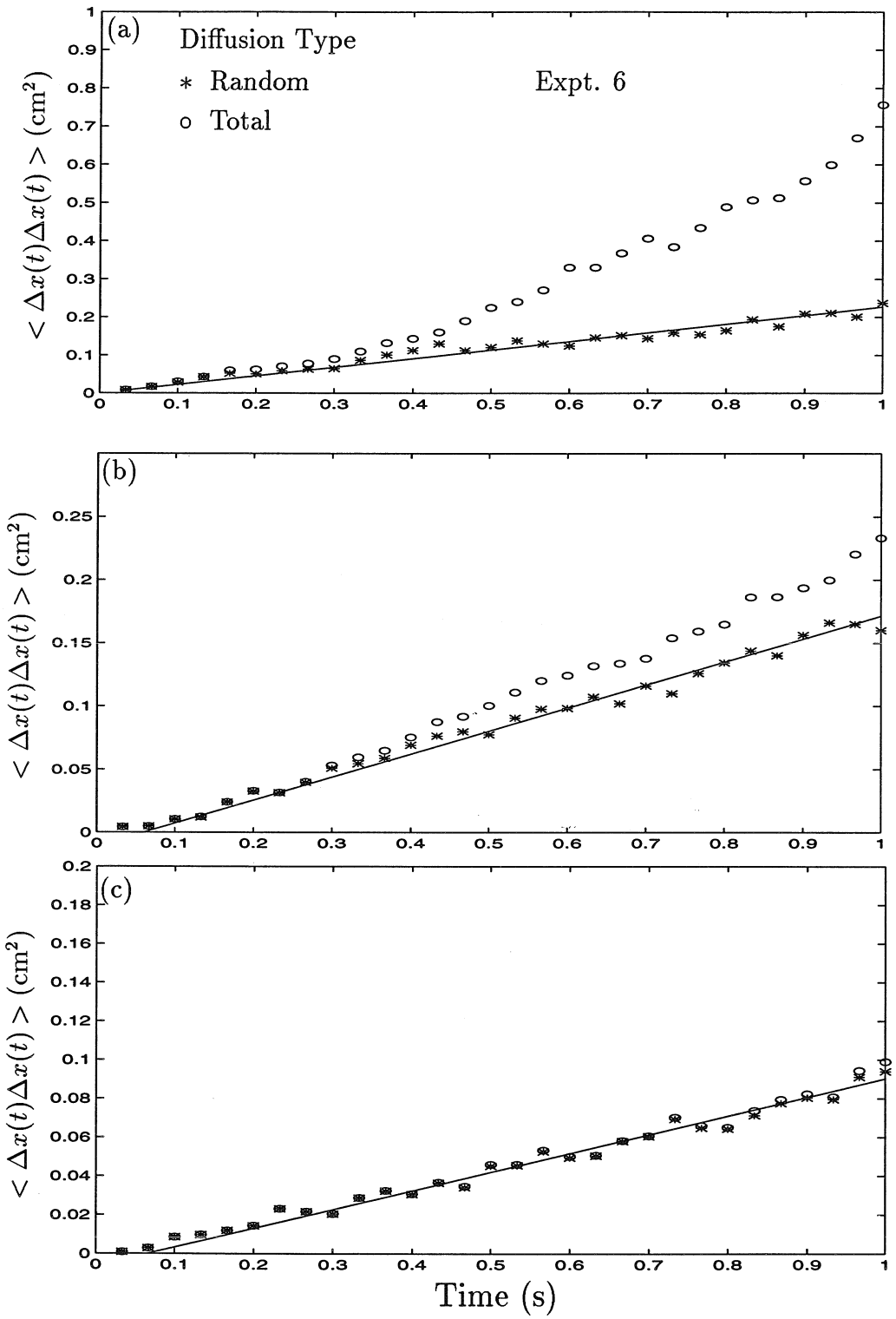


Figure 3.43: Variation of mean-square streamwise diffusive displacement with time for the (a) moderate-shear, (b) low-shear and (c) uniform regimes in Expt. 6.

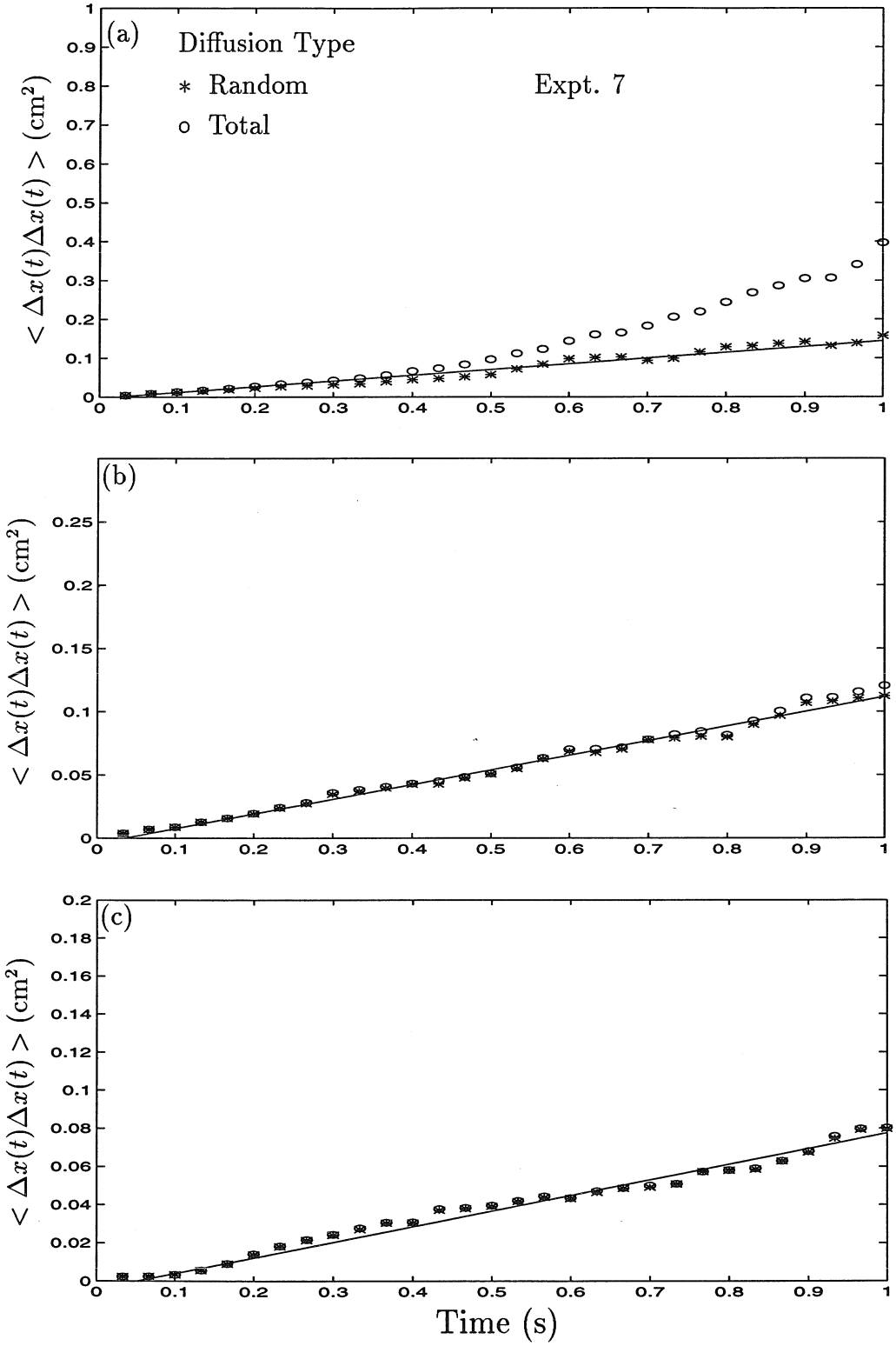


Figure 3.44: Variation of mean-square streamwise diffusive displacement with time for the (a) moderate-shear, (b) low-shear and (c) uniform regimes in Expt. 7.

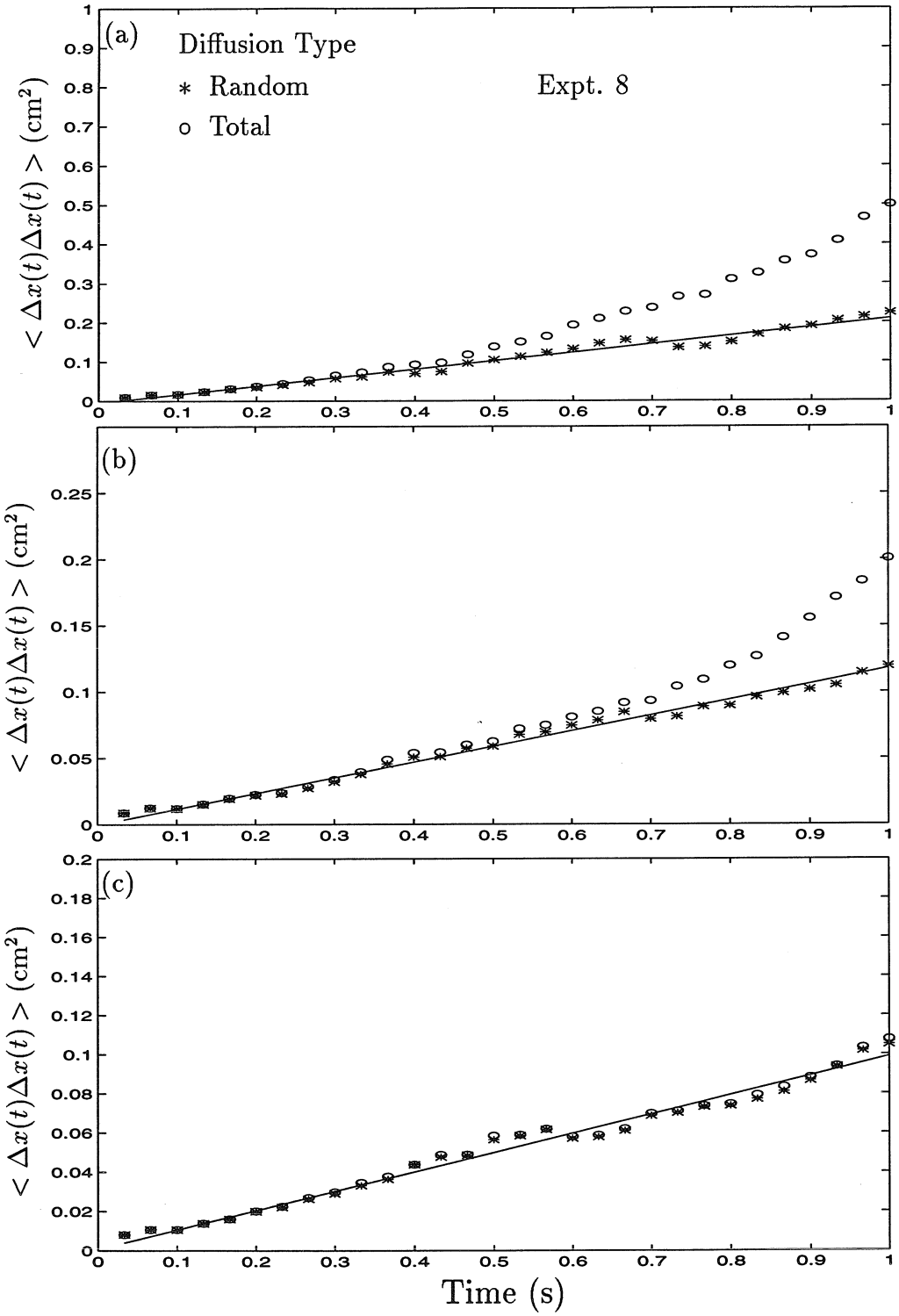


Figure 3.45: Variation of mean-square streamwise diffusive displacement with time for the (a) moderate-shear, (b) low-shear and (c) uniform regimes in Expt. 8.

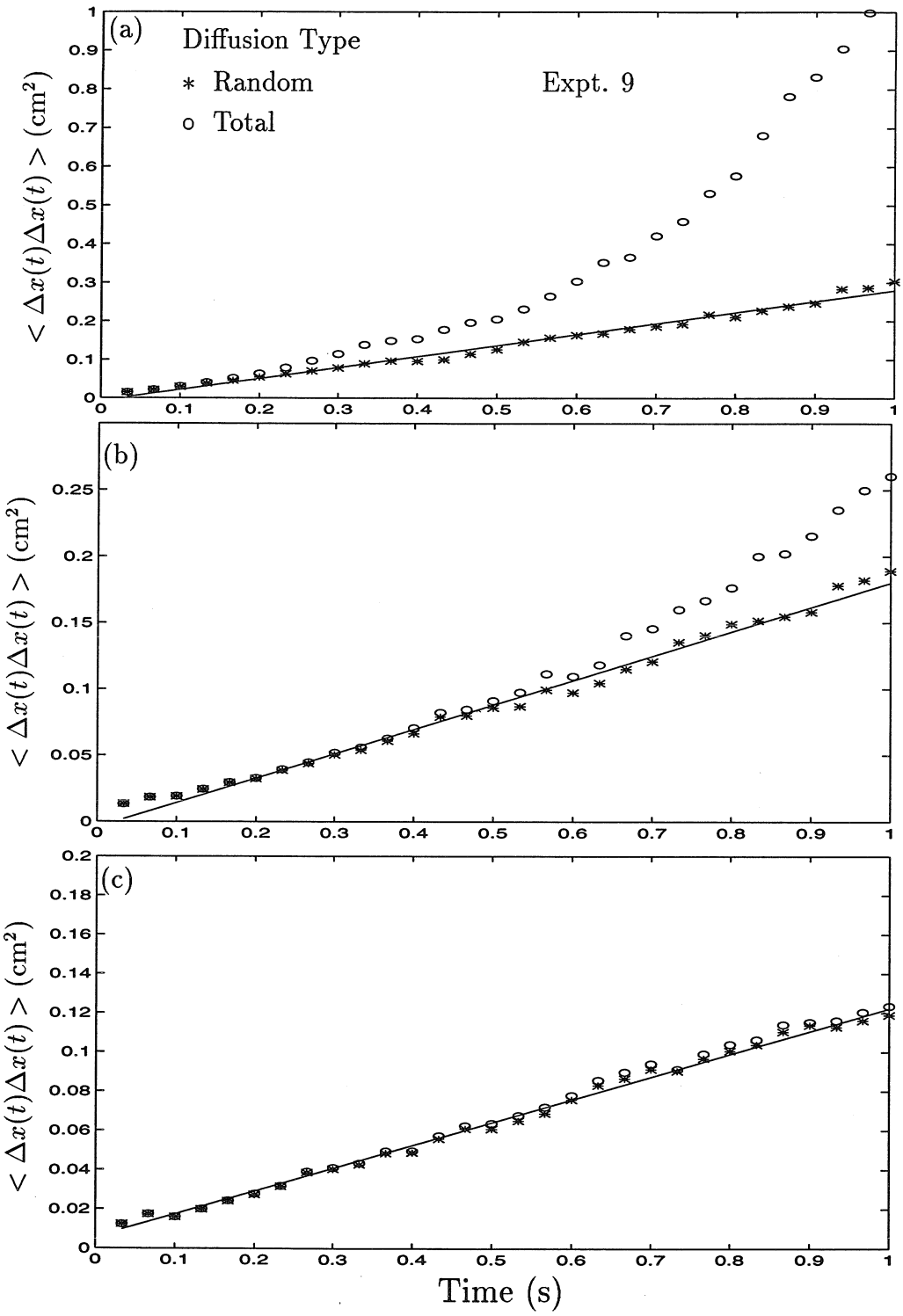


Figure 3.46: Variation of mean-square streamwise diffusive displacement with time for the (a) moderate-shear, (b) low-shear and (c) uniform regimes in Expt. 9.

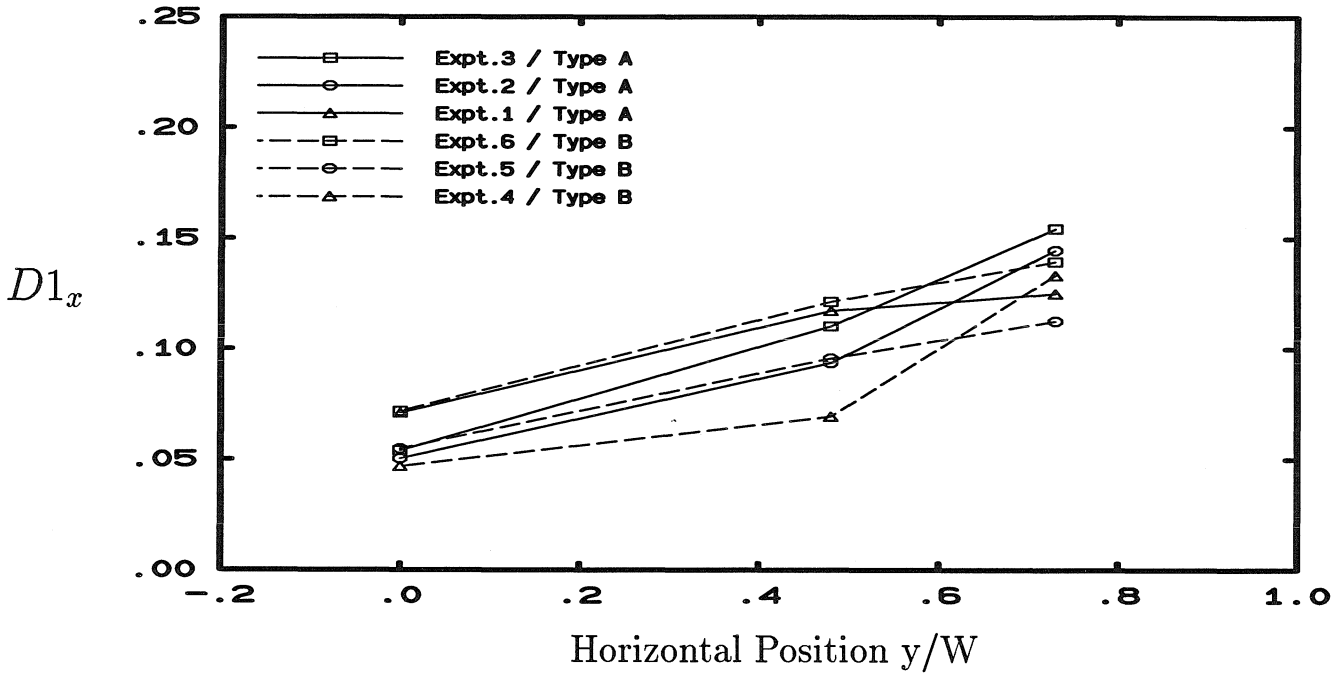


Figure 3.47: Variation of $D1_x$ with position (or shear regime) for particle types A and B. W=2.5 cm.

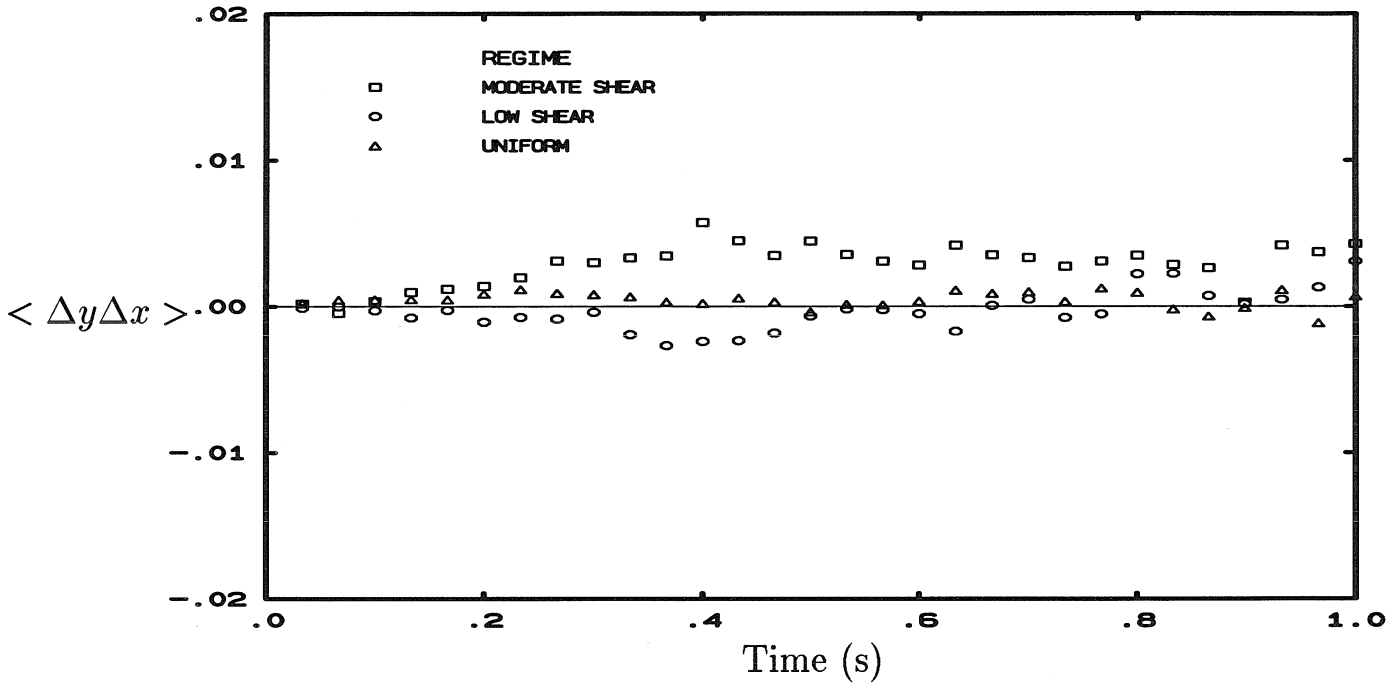


Figure 3.48: Variation of $< \Delta y \Delta x >$ with time for Expt. 3.

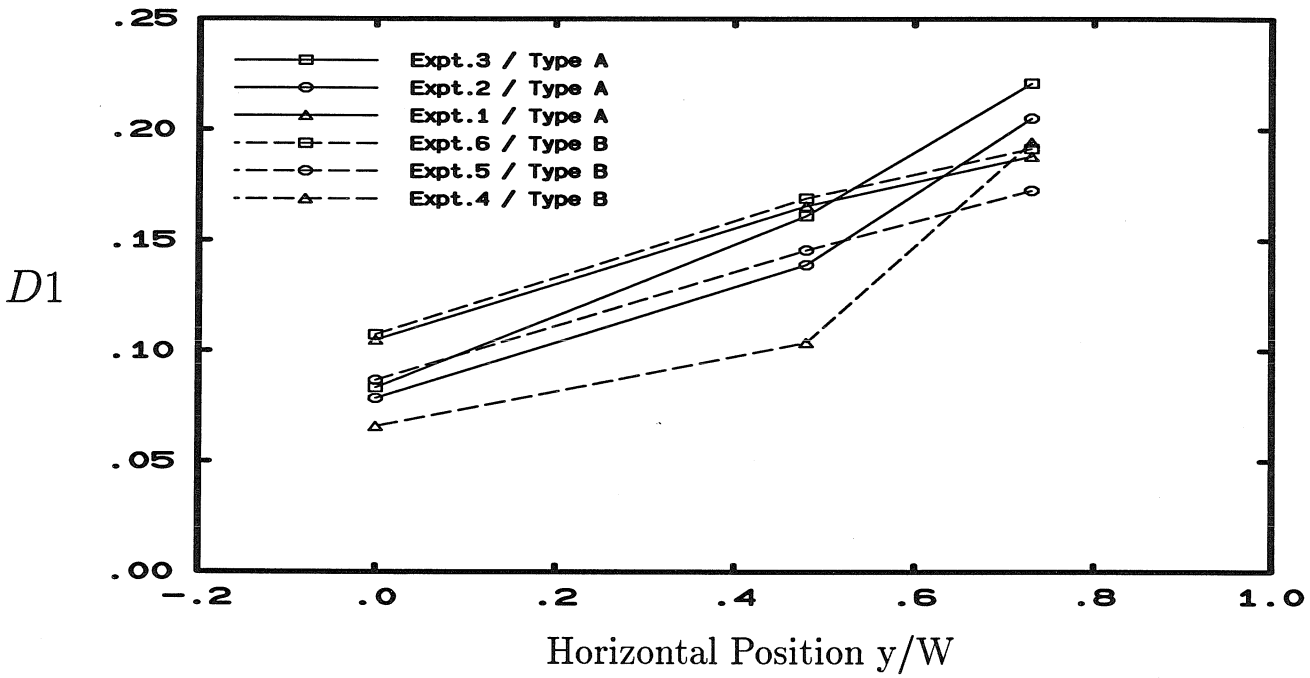


Figure 3.49: Variation of D1 with position (or shear regime) for particle types A and B. W=2.5 cm.

# Chapter 4 Experimental Study of Heat Transfer in Granular Flows in a Vertical Channel

## 4.1 Apparatus and Procedures

The aim of the current set of experiments was to extend the investigation of heat transfer in granular materials to sheared flows. The experiments of Sullivan & Sabersky (1975), Spelt et al. (1982), Patton et al. (1986) and Ahn (1989) were performed with relatively short heating sections, which may not have allowed any significant development of the thermal boundary layer. The longest of these test sections, that of Ahn (1989) was only 50.66 particle diameters long, for the case of particles of 3 mm diameter that were studied in this work.The current set of experiments sought to remove this shortcoming by using a significantly longer heating section. The current set of experiments were performed in the vertical channel facility shown in Figure 4.1. The channel was 130 cm high and 3 cm deep. A heating plate 100 cm long was mounted at the center of the flow section, effectively splitting the channel into two identical sections, each 7 cm wide. The upper hopper was fed by a conveyor. The conveyor was 6 m long from flange to flange and was designed to operate at an inclination of 75°. It was capable of conveying coarse sand at a maximum flow rate of 70 tons per hour. The conveyor consisted of a belt with integrally moulded rubber buckets. The belt was driven by a 10 HP three phase motor. The upper hopper was capable of holding 50 lbs of material. A flow control valve with a variable exit

width was used to control the material flow rate. Polished tempered glass plates, 0.32 cm thick, were used for the front and back surfaces to minimize friction, and to create a two-dimensional flow. At each surface, two such glass plates were used, one on either side of the heating plate's edge, to keep the heating plate in position. In order to minimize heat loss from the heating plate to the glass walls, lucite lugs, 0.16 cm thick and 0.48 cm long, were attached to the glass walls, thereby creating an effective air gap of 0.16 cm thickness between the glass wall and the heating plate. Side walls with smooth polished aluminium plates were used to generate unsheared, almost uniformly dense plug flows. The sheared flows were created by using sidewalls with 3 mm spherical glass particles glued in a regular hexagonal close-packed pattern. The chute was dismantled and cleaned after every three runs to minimize the effect of dirt and static charge. The glass particles used for the experiments had a nominal diameter of 3 mm and a density of 2500 $kg/m^3$.

The heating plate consisted of a strip heater, 122 cm long, and 2.54 cm wide, embedded between two aluminium plates, each 1.6 mm thick. The strip heater was a commercially available "Omegalux" flexible silicone rubber fibreglass insulated device with an etched foil heating element. It had a total wattage of 240W at a watt density of $3875W/m^2$, and a maximum operating temperature of 232 °C, well above the temperatures encountered in these experiments. The heater was attached to the aluminium plates using a commercially available "Omegabond 101", high conductivity epoxy paste in order to ensure a very high quality of thermal contact. To minimize heat losses from the top and bottom of the heater, lucite inserts were place at either end of the heating plate, separated from the heated section by an air gap 4.8 mm wide. This design reduced heat losses to under ten percent for most flows, though for some cases, these losses were as high as fifteen percent. The power of the heater strip was controlled by a 120V A.C. variable autotransformer.

By careful adjustment of the exit valve, two identical granular flows were created,

one on either side of the central heating plate. One flow was designated as the "experimental" flow and the other as the "guard" flow. Five heat flux sensors, spaced 20.33 cm apart, were mounted on the experimental side and three such sensors were mounted on the guard side. These sensors measured the actual value of the heat flux into the flows, thereby reducing the effort required to account for various losses. The heat flux sensors used were commercially available "RdF Micro-Foil Heat Flow Sensors" and had a length of 3.5 cm, a width of 2.85 cm, and were less than 0.5 mm thick. Each heat flux sensor had a sensitivity of 3.513 microvolts/($W/m^2$) and a thermal resistance of 0.0038°F/($W/m^2$). The heat flux sensors were attached to the surface using the "Omegabond" high conductivity paste. The heat flux sensor voltages were read off a digital multimeter. The heat flux sensors were tested for reliability and accuracy by running a series of natural convection experiments, for different values of the autotransformer settings. Comparisons between the power values calculated from the input voltage and those read directly off the heat flux sensors revealed discrepancies that were usually less than 2-2.5 %. The variation in the readings of the individual heat flux sensors were less than 2%.This exercise also enabled the testing of the sensors over a range of surface temperatures and no significant change in reliability of performance was detected.

However, when the experiments were run with the glass particles, it was noticed that while the maximum variations amongst the readings of the first four heat flux sensors, on the experimental side, were under 6 percent, the last heat flux sensor reading was up to 11 percent lower than the average for the first four heat flux sensors. It was conjectured that increased heat losses were occurring from the lowest section of the heating plate into the flow. Part of the reason for this discrepancy also lay in the increased thickness of the heating strip at the bottom, because of the presence of wires leading to the power supply. This was corraborated by lower temperature readings in the last 20% of the heating plate. Hence, the first 82.16 cm of the flow

were designated as the test section and all heat transfer measurements were based on temperature and heat flux measurements made within this section. Calculations also revealed that theoretical heat losses across the 4.8 mm wide air gap between the heating plate and the lucite inserts were a negligible fraction of the heat flow across the heat flux sensors, into the flowing material.

Eighteen K-type thermocouples, of size 36 guage, were embedded on the experimental side of the heating plate to measure the wall temperature. They were placed in small receptacles dug on the aluminium surface, and bonded to the surface using a commercially available, very high conductivity "Omegatherm 201" silicone paste. Six similar thermocouples were mounted on the guard side. Figure 4.2 shows the positions of the thermocouples on the heater plate. The thermocouples were connected to a pair of insulated rotary switches, and the temperatures were read off with a pair of hand held thermometers. The thermocouple readings showed that temperature gradients in the heating plate, transverse to the flow direction, were very low (less than 0.5 °C), indicating a negligible heat loss from the edges of the heated plate. In all the experiments, the glass walls were insulated with styrofoam padding. Insulation tape and insulation wool were used to further reduce losses from the edges of the heating plate.

For each experiment, before proceeding to the heat transfer portion, the flows were filmed in a manner identical to the procedures already described in the previous chapter. The tapes were subsequently processed using the image processing techniques in order to measure the velocity profiles. After the filming, the experiment was insulated so that the heat transfer measurements could be made. In each experiment, the exit valve was first set to the desired width and then the conveyor was switched on. Temperatures were read off periodically from two "control" thermocouples to determine when the system had reached a steady state. A steady state was assumed to be reached when temperatures did not vary by more than $\pm 0.2$°C over

a period of 20 minutes. The experiments took up to two hours to reach a steady state. Once the steady state had been achieved, the readings of all the thermocouples and heat flux sensors were noted, along with the inlet temperature, $T_{bulk}$, of the bulk material. Assuming the local heat transfer coefficient at location $\iota$ to be given by $h_\iota = q_w/(T_{w-\iota} - T_{bulk})$, the average heat transfer coefficient, $h$, was then calculated using the relation:

$$h = \frac{\Sigma h_\iota}{N} \tag{4.1}$$

where $q_w$ was the heat flux at the wall and $T_{w-\iota}$ was the wall temperature at location $\iota$. $N$ was the number of locations where temperatures were measured. The exit mass flow rate was measured at regular intervals, to ensure that there were no blockages within the flow loop.

## 4.2 Observations and Discussion

The first set of experiments were performed with the smooth aluminum side wall conditions in order to examine the convective heat transfer to plug flows. The aim of this set of experiments was to extend the experimental studies of Sullivan & Sabersky (1975) to higher flow velocities and to investigate the effect, if any, of the longer heated test section. It must be noted that the experiments of Sullivan & Sabersky were limited to flow velocities in the range of 0.5-5 cm/s, considerably lower than the velocities achieved in the current set of experiments. Also, Spelt et al. (1982), Patton et al. (1986) and Ahn (1989) all performed their experiments in inclined chutes which had a smooth bottom surface. While these experiments investigated flow velocities that were higher than the velocities in this work, the similarity of the geometry at the heating surface made the comparison of experimental results, a profitable exercise.

In order to examine the effect of input power on the heat losses within the system, the first five experiments (in increasing order of the flow velocity) were each performed

at four different values of input power. The autotransformer was set at 80%, 85%, 90% and 95% of the maximum voltage value. Figure 4.3 shows the results of these experiments. It can be seen that the heat transfer coefficients were essentially constant over this range. All subsequent experiments were repeated twice or thrice, and the data points represent the average of these results. The difference between the average wall temperature and the bulk temperature ranged from 17 °C to 30 °C for each of these experiments.

Figure 4.4 shows the variation of the average heat transfer coefficient with the bulk flow velocity. It is seen that the heat transfer coefficient initially increases with the increase in velocity, but reaches a maximum. Beyond the maximum, for further increase in the flow velocity, the heat transfer coefficient decreases initially, and then remains essentially constant. Figure 4.5 compares the observations of the current experiments, with the experimental and semi-empirical (Equation 2.29) results of the similar set of experiments performed by Sullivan & Sabersky (1975). At low Peclet numbers ($Pe^* < 600$), there is good agreement between the current experimental observations and the semi-empirical prediction. A value of 0.09 for $\chi$ was found to fit the plug flow for the current experiments remarkably well in the low Peclet number regime. This value is extremely close to the value of 0.085 that Sullivan & Sabersky used to fit their data, noting the fact that the two experiments were performed in essentially identical geometries. Ahn (1989) found in his experiments in an inclined chute that in the low Peclet number regime, $\chi = 0.025$ described the data most appropriately. He attributed this difference in the value of $\chi$ to differences in the geometry of the two experimental setups. In an inclined chute, gravitational compaction of the particles reduces the effective width of the air gap between the heated wall and the flow. In contrast, in a vertical channel, there is no such compaction, as there is no component of gravity in a direction normal to the wall. Hence, the effective wall-flow air gap is likely to be thicker for a vertical channel flow as particles moving away

from the wall are not forced back by gravity. The latter case therefore leads to an increased value for $\chi$, which is a measure of the thermal resistance due to the air layer adjacent to the heated plate.

A comparison between the results of Patton (1985), Ahn (1989) and those of the current set of experiments are presented in Figure 4.6, for the case of particles of 3 mm diameter. While all profiles show the presence of a maximum, there are important differences as well. The first important factor is that the average heat transfer coefficients, for comparable Peclet numbers, are much higher in the case of Ahn (1989). Also, the maximum occurs at $Pe^* \approx 4000$ (Equation 2.31) in the case of Ahn's experiments, while in the current experiments its value is close to 600. Note that there are significant differences in the values of the measured average heat transfer coefficients as measured by Patton (1985) and Ahn (1989) inspite of the fact that both experiments were performed in essentially identical geometries with heating sections of comparable length. Significantly, Patton's results show the heat transfer coefficient to be almost constant over a significant range of $Pe^*$, similar to the observations in our experiments. Such a behavior is not observed in Ahn's results. The reason for the higher heat transfer coefficients in Ahn's and Patton's experiments may lie in the fact that flows in an inclined chute are likely to be much more dense close to the walls, due to gravitational compaction, than flows in a vertical chute. Therefore, bulk conductivities closer to the wall are likely to be higher in the case of flows in an inclined chute, for comparable flow velocities.

As discussed in Chapter 2, the existence of a maximum, and the subsequent decrease in $Nu^*$ (Equation 2.30) with increasing flow velocity, was explained in terms of the near-wall dilation of the flow that occurs at higher flow rates. It is expected that, due to the influence of gravitational compaction, much higher velocities would be needed in an inclined chute to achieve the density values at which the heat transfer coefficient begins to decrease. This, coupled with the much shorter length of the test

section, may explain the much higher values of Pe*, at which the maximum occurs, in the case of Patton (1985) and Ahn's (1989) data.

Ahn (1989) sought to improve upon Sullivan & Sabersky's model by proposing two new parameters, an effective Nusselt number, $Nu^*_{eff}$, and an effective Peclet number, $Pe^*_{eff}$ defined as follows:

$$Nu^*_{eff} = Nu^* \frac{k_c}{k_e} = \frac{k_c}{k_e} \frac{h\sigma}{k_g}, \tag{4.2}$$

$$Pe^*_{eff} = Pe^* \frac{\alpha_c}{\alpha_e} \left( \frac{k_e}{k_c} \right)^2 = \left( \frac{UL}{\alpha_e} \right) \left( \frac{\sigma}{L} \right)^2 \left( \frac{k_e}{k_g} \right)^2 \tag{4.3}$$

where $k_e$ and $\alpha_e$ are the effective thermal conductivity and diffusivity of granular materials at a given mean solid fraction. The value of $k_e$ is obtained from Equation (2.33) with $k_e = k_{mc}$. Ahn (1989) found that using the above expressions in Sullivan & Sabersky's relation (Equation 2.29) resulted in very good agreement between his data and the semi-empirical relation. While the latter treatment is an improvement over the previous theory in that it makes an attempt to account for the variations in density with flow rate, it still suffers from the shortcoming that the effective parameters are based on the mean flow solid fraction and not the solid fraction at the wall. The values of Nu* in Ahn's experiments indicate that in most cases the thermal boundary layer is less than a particle diameter in thickness. Under these circumstances, the solid fraction at the wall is of primary importance, and in all but the most dilute of flows, its value is significantly less than the mean solid fraction. Consequently, no effort was made in this work to present the data in terms of the parameters in Equations (4.2) and (4.3). Furthermore, measurements of the mean solid fractions for the flows in the current set of experiments did not show significant variations with the flow rates. However, it must be reiterated, that visual observations did indicate reasonable dilation of the flow close to the walls, at higher flow velocities, even in the case of smooth aluminium walls.

The second set of heat transfer experiments were performed with a "rough" side-wall condition, that was achieved by gluing 3 mm spherical particles (identical to those used for the flows) onto the wall and heating plate surfaces. The aim of this set of experiments was to shear the flow adjacent to the heated surface so that the influence of shear-induced dilation on the convective heat transfer coefficient could be investigated. Another objective was to investigate any augmentation in the heat transfer coefficient due to the "streaming" conductivity component, as discussed in Chapter 2.

Figure 3.18 shows the effect of wall conditions on the velocity profiles. As has already been discussed in Chapter 3, streamwise flow velocities at the wall, for the rough wall condition, are much lower than for the smooth wall condition, for the same mean flow rate of material. Furthermore, at the wall, the fluctuation velocities are much higher for the flow with the rough boundaries.

In the set of experiments with rough walls, it was necessary to calculate the temperature of the layer of particles glued to the wall, as the thermocouples measured only the temperature at the heater surface, and not the temperature at the flow/wall particle interface. This was done by evaluating the expression for the wall-particle heat transfer coefficient, $h_{wp}$, in Equation (2.32). A value of $2.7 \times 10^{-7}$ m was assumed for $l$ (Martin 1984), along with a value of 0.85 for the surface coverage factor $\phi_A$ (Schlunder 1982). Neglecting any effects of radiation, and assuming the value of the net surface roughness, $\delta$, to be zero, a value of 224.67 W/m$^2$°C was obtained for $h_{wp}$. The local temperature of the layer of particles glued to the wall was then obtained from the expression:

$$q_w = h_{wp}(\mathrm{T_{w-\iota}} - \mathrm{T_{wp-\iota}}), \tag{4.4}$$

where $\mathrm{T_{w-\iota}}$ is the local wall temperature at location $\iota$ and $\mathrm{T_{wp-\iota}}$ is the local temperature of the wall particle layer at the same location. The value of $(\mathrm{T_{w-\iota}} - \mathrm{T_{wp-\iota}})$ was usually between 6 °C and 8.5 °C.

Figure 4.7 shows the variation of the heat transfer coefficients with flow velocities adjacent to the wall, for the second set of experiments. For the sake of comparison, the results of the first set of experiments are also depicted on the same graph. The same data is presented in terms of a $Nu^*$ versus $Pe^*$ graph, together with the theoretical Sullivan-Sabersky curve (Equation 2.29) in Figure 4.8. Figure 4.9 is identical to Figure 4.8 but with error bars included to account for the uncertainties in the measurements of the heat flux sensors. A value of $\chi = 0.114$ was found to fit the data for the sheared flows up to the maximum value of $Nu^*$.

Before comparing the results for the sheared flows with those for the plug flows, note that $Pe^*$ is based on physical properties evaluated at the critical value of the solid fraction. While this retains reasonable validity in the context of plug flows, at least for low flow velocities, in the case of sheared flows, even at very low velocities, the flow adjacent to the wall is influenced quite noticeably by the wall particles as reflected in the higher fluctuation velocities adjacent to the walls. Under such circumstances, the near-wall solid fraction is not close to the critical value, even for sheared flows at low velocities. A more appropriate Peclet number would be one based on properties evaluated at the solid fraction adjacent to the wall.

Figure 4.10 depicts the results of the two sets of experiments, for slip velocities up to 10 cm/s. In the case of sheared flows, the heat transfer coefficient initially increases with an increase in flow velocity adjacent to the wall and ultimately reaches a constant value, for the regime of flows examined. It was not possible to investigate flows at higher flow rates, because the flows became quite unsteady and began to "surge" significantly. At low values of the flow velocity (below 4 cm/s), the heat transfer coefficients for the sheared flows are higher than those for the plug flows. (In order to highlight this effect, the Sullivan-Sabersky curve is plotted in h-U coordinates with a $\chi$ value of 0.085 in Figure 4.10.) Such a result is significant in the light of the fact that the solid fraction, adjacent to the wall, for the sheared flows is less than

that for the plug flows. However, at velocities greater than 4 cm/s, the trend reverses and the heat transfer coefficients for the plug flows are higher.

As discussed earlier, it was anticipated that in a sheared flow, while the bulk molecular conductivity ($k_{mc}$) would decrease as a result of shear induced dilation, the "streaming" conductivity ($k_{kt}$ for the kinetic-theory model) would increase due to the increased mobility of the particles. Furthermore, particle agitation close to the walls could probably enhance heat transfer by enhancing thermal mixing within the boundary layer. Using the approximation $\mathrm{Nu}^* \approx \sigma/\delta_{bl}$ (where $\delta_{bl}$ is the boundary layer thickness), it is seen that the thickness of the thermal boundary layer is comparable for the two flows. Under such circumstances, particle induced mixing within the boundary layer becomes more significant. From the comparisons in the previous paragraph, it appears that for the sheared flows at low values of flow slip velocities, the particle agitation close to the walls compensates for the low solid fractions due to shear-induced dilation, leading to higher values for the heat transfer coefficients. However, on increased shearing, the decrease in the solid fraction close to the walls outweighs the enhancement in thermal conductivity due to particle agitation and mixing. For higher values of $\mathrm{Nu}^*$, $\delta_{bl}/\sigma$ becomes small and the effects of particle agitation are reduced. Hence, at higher velocities (and shear rates), the plug flows have higher heat transfer coefficients than the sheared flows.

It is difficult to explain the eventual constant value of the average heat transfer coefficient for both sets of experiments. This result is in contrast to the results of Spelt et al. (1982), Patton et al. (1986) and Ahn (1989). Each of them saw a rapid decline in the heat transfer coefficients beyond the maximum value. One explanation would be that a balance between the two conflicting conductivity mechanisms is reached. However, a stronger likelihood is that the range over which the heat transfer coefficients remain constant is extremely small (due to the limitations of the experiment) and that for higher flow velocities, the profiles would show a decline.

Another possible explanation is provided by Figure 3.35 where it is seen that the rate of change of the diffusion coefficient $D_{yy}$ with the shear rate is lower in the moderate shear regime, as compared to the low shear regime. On the basis of this observation, it may be argued that the rate of change of solid fraction with density is higher at low shear rates than at moderate shear rates. Hence, noting from the results presented in Chapter 3 that the shear rates adjacent to the wall increase with the mean flow rate, it may be conjectured that at higher flow rates, the solid fraction adjacent to the wall remains essentially unchanged in such flows, at least over the range of flow rates investigated.

Figure 4.11 depicts the variation of the local heat transfer coefficient with vertical position, for the first five experiments for both the plug flow and shear flow situations. The autotransformer was set at 90% for each of these experiments. All the profiles show a continuous decrease of the local heat transfer coefficient with the vertical position, consistent with the thickening of the boundary layer.

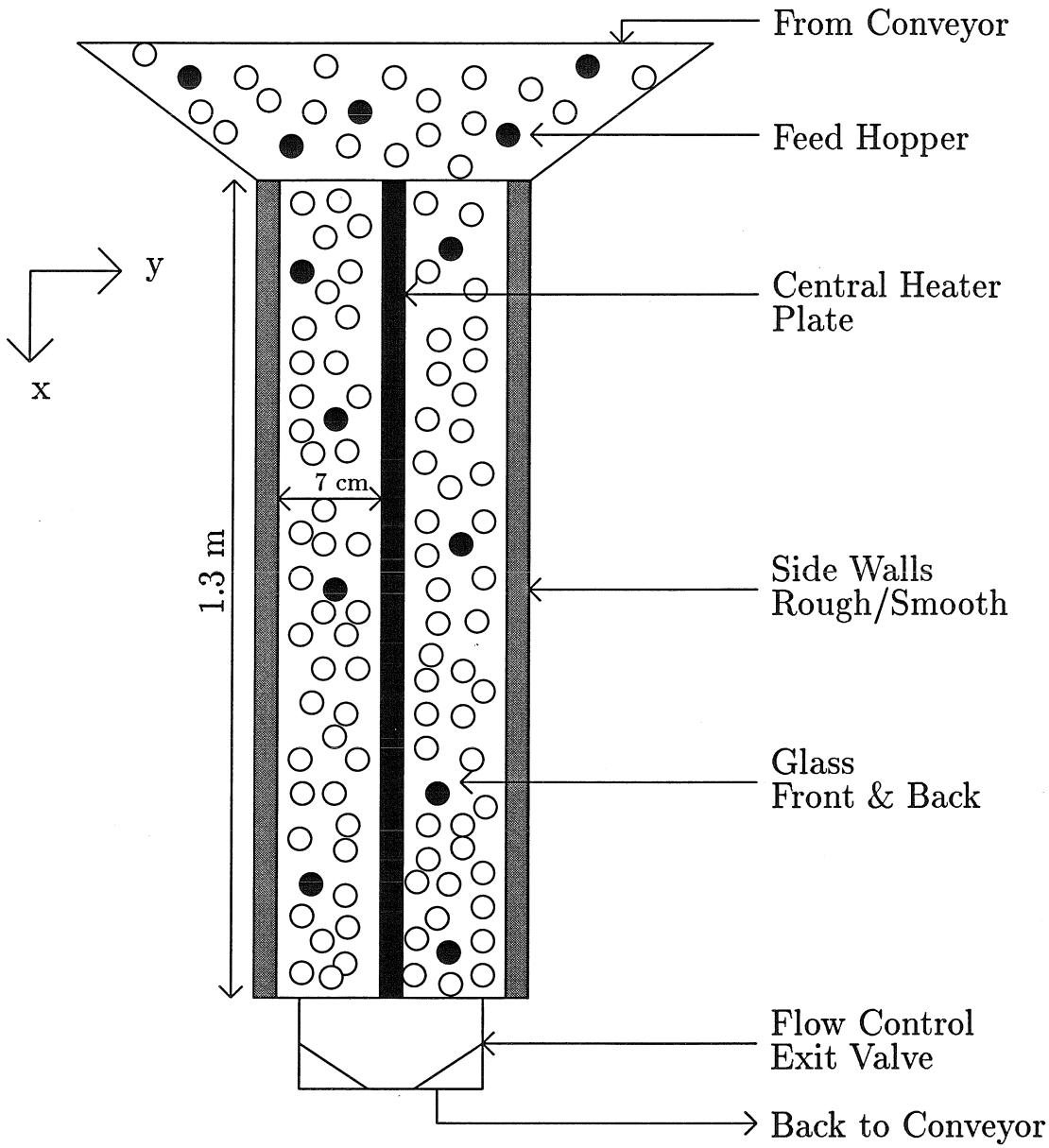


Figure 4.1: Schematic of the vertical channel facility for the heat transfer experiments. Note that the figure is not to scale.

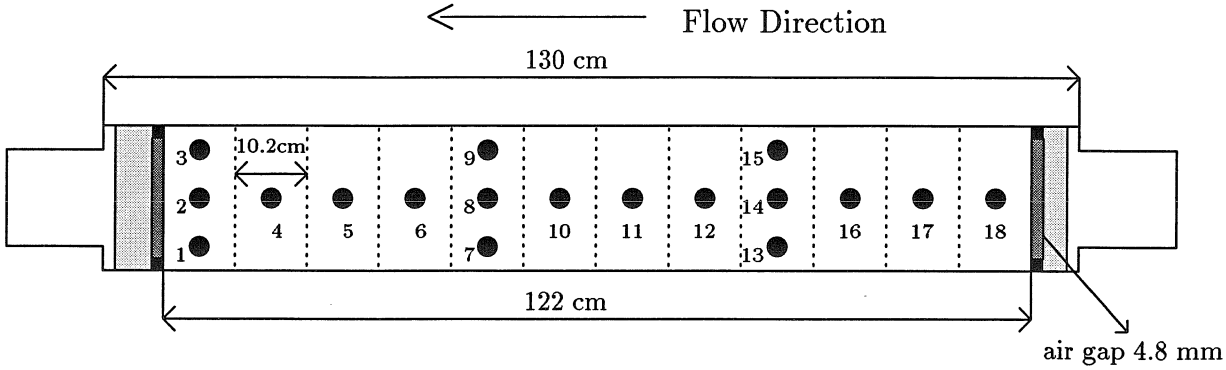


(a) Location of thermocouples on experimental side of central heating plate.

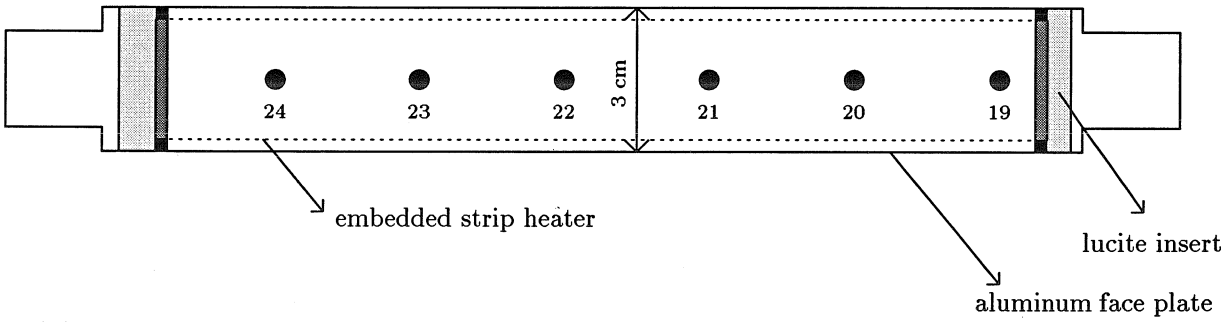


(b) Location of thermocouples on guard side of central heating plate.

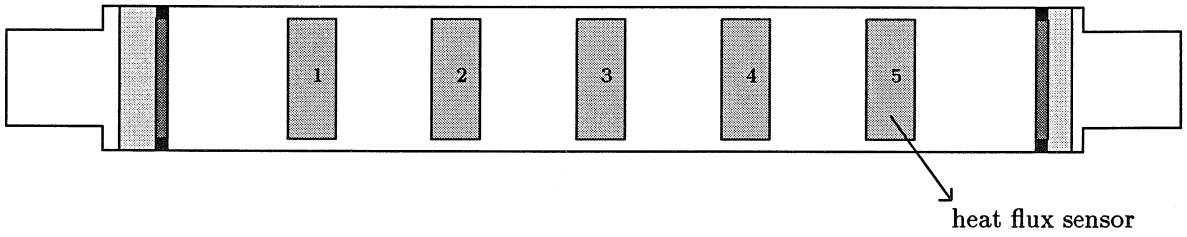


(c) Location of heat flux sensors on experimental side of central heating plate.

Figure 4.2: Schematic of the central heating plate. Note that the figures are not to scale.

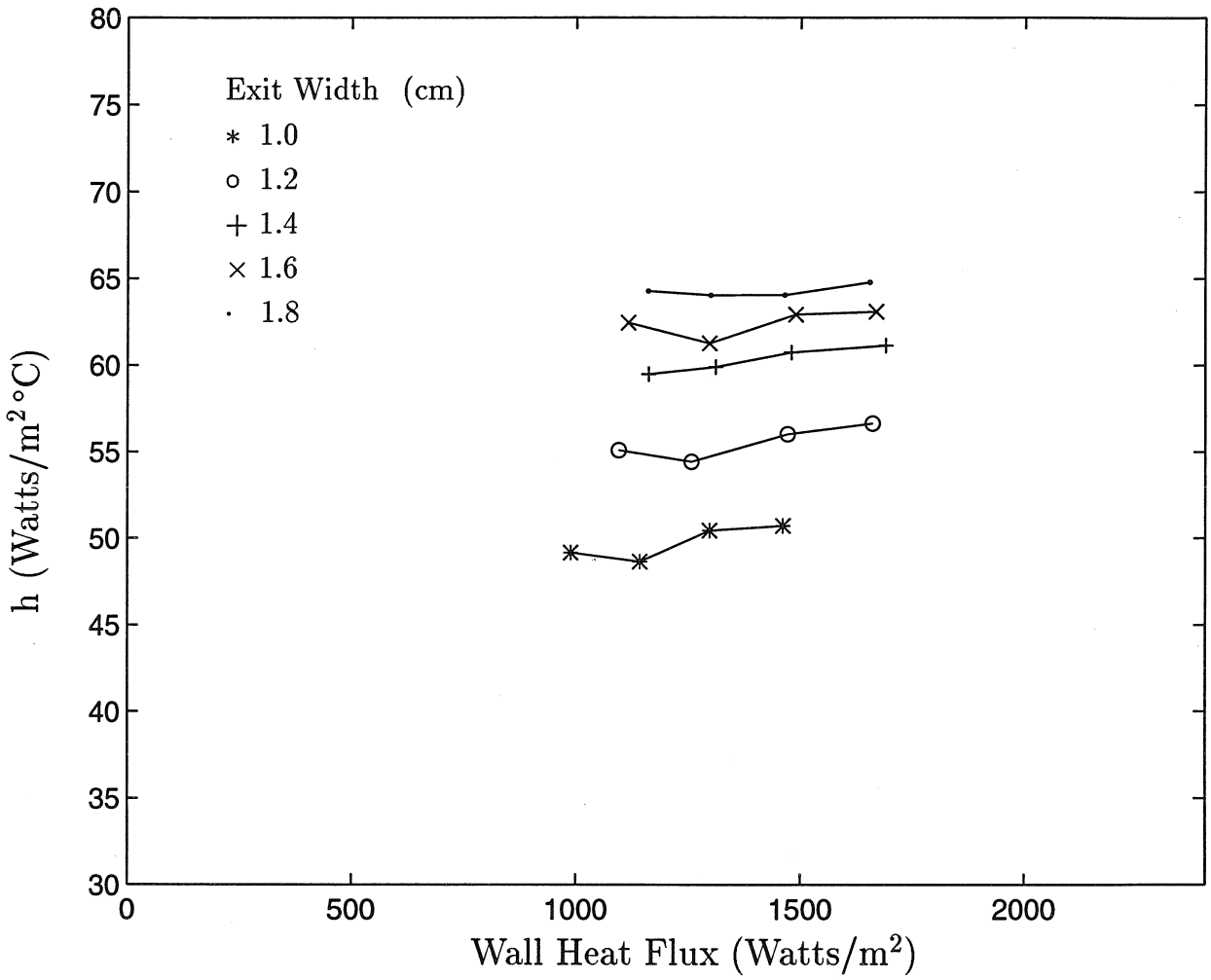


Figure 4.3: Variation of the measured heat transfer coefficient with the wall heat flux for the first five experiments with plug flow.

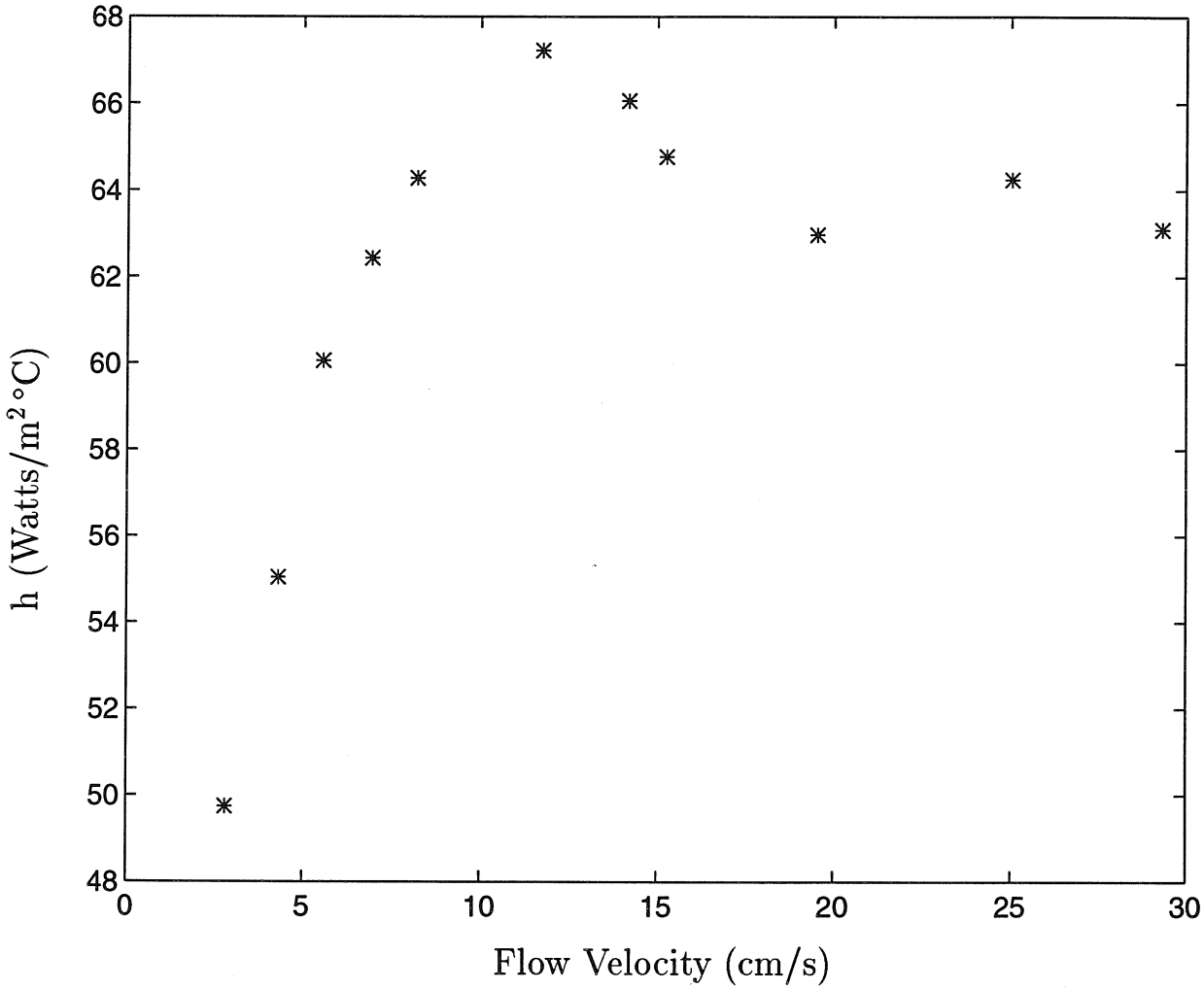


Figure 4.4: Variation of the measured heat transfer coefficient with flow velocity for the experiments with plug flow.

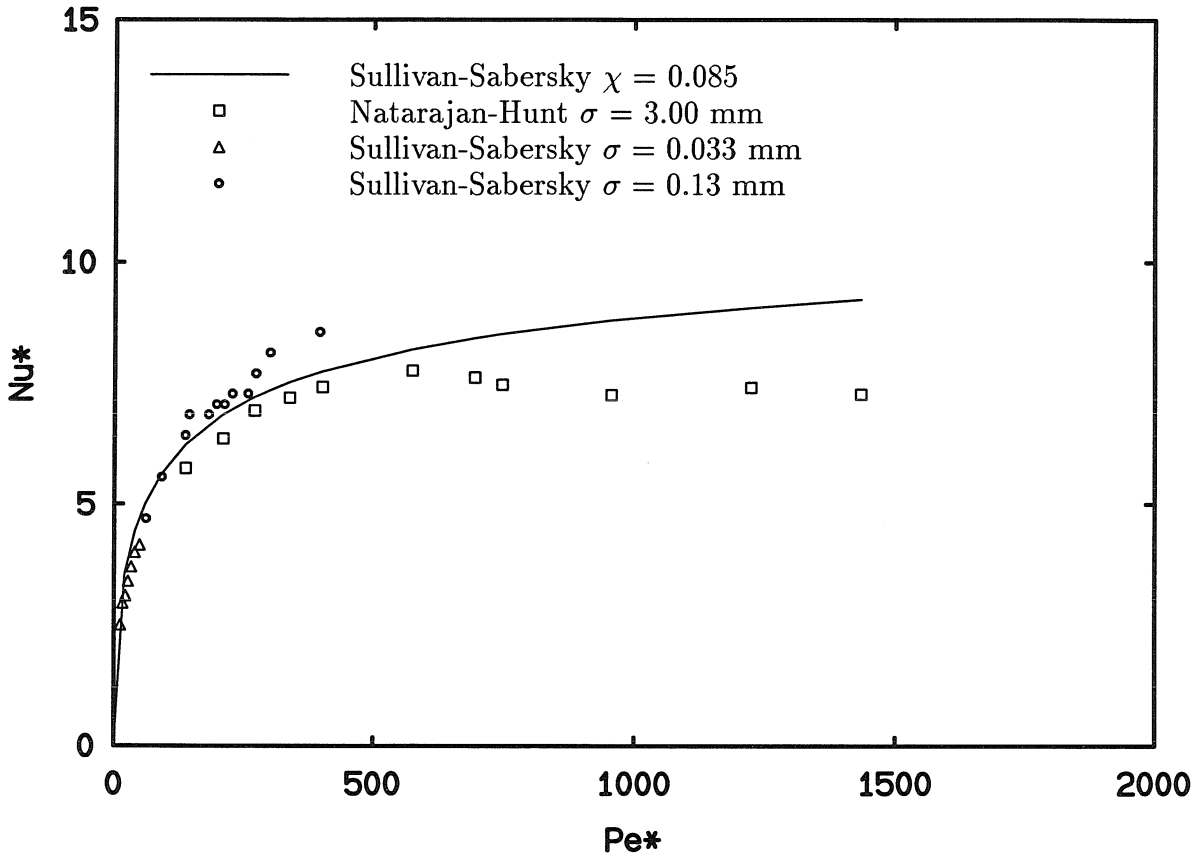


Figure 4.5: A comparison of the plug flow results of the current set of experiments with some of the experimental and theoretical results of Sullivan & Sabersky (1975).

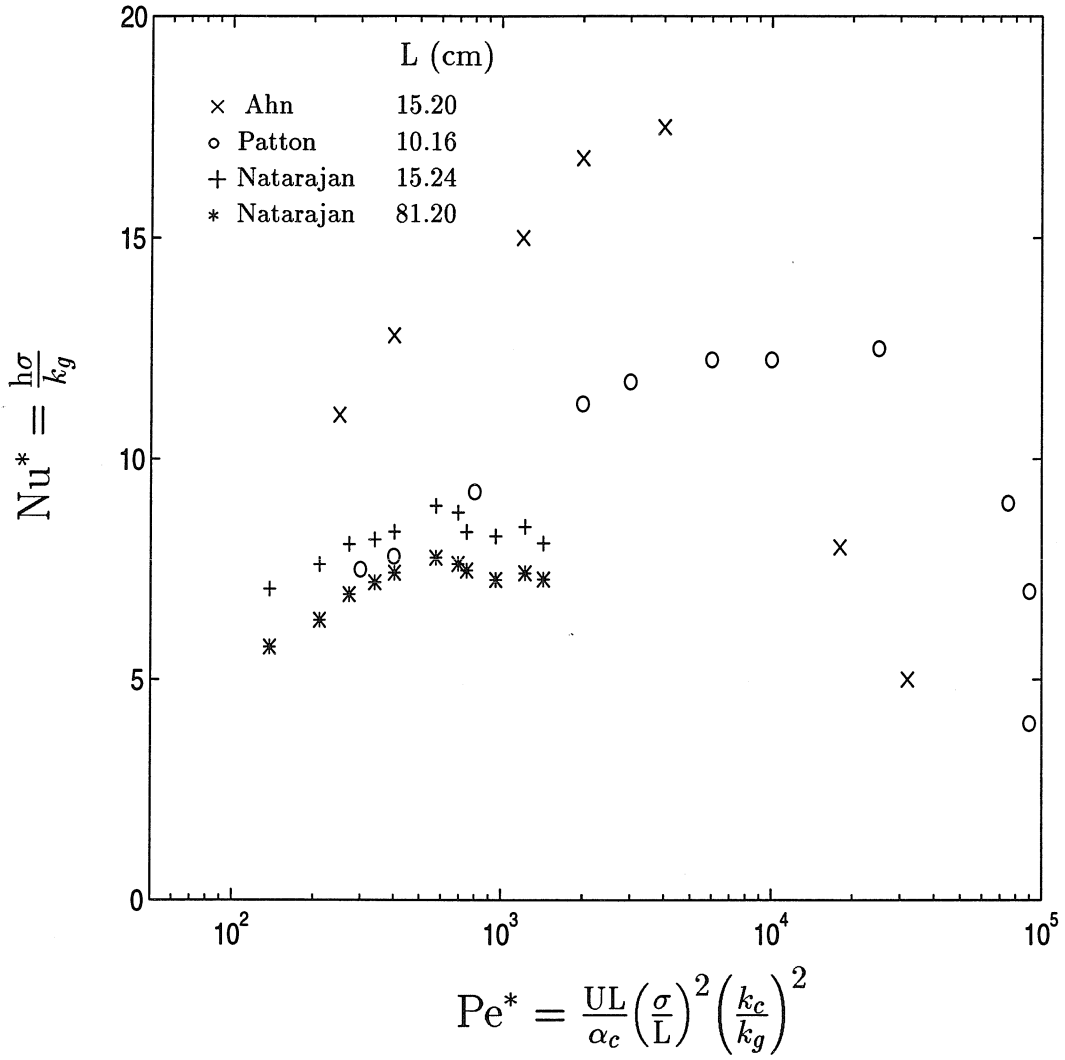


Figure 4.6: Variation of $Nu^*$ with $Pe^*$. Comparison of the plug flow results of the current set of experiments with the experimental results of Patton (1985) and Ahn (1989).

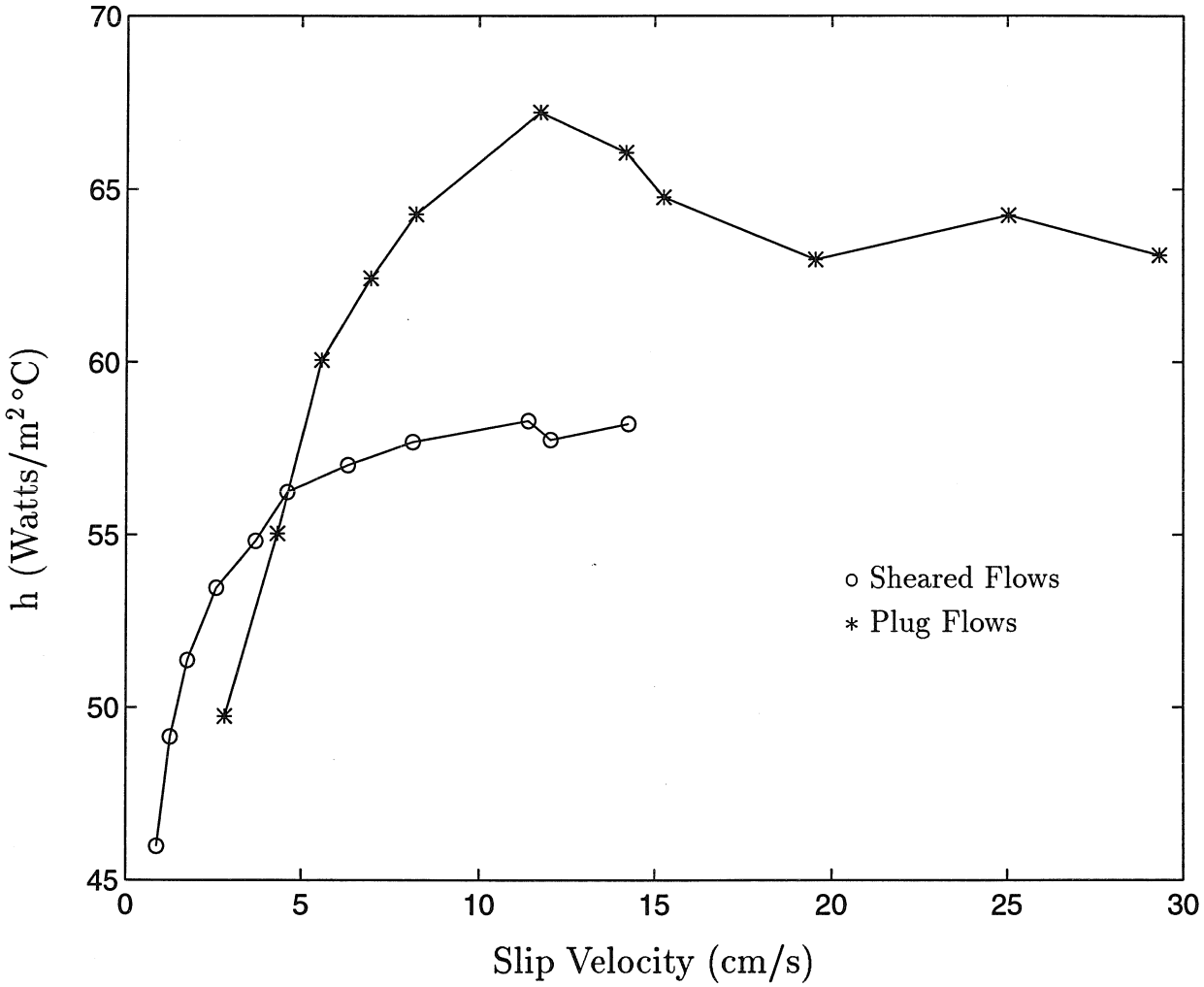


Figure 4.7: A comparison of the variation of the measured heat transfer coefficient with the flow slip velocity for the shear flow and plug flow experiments.

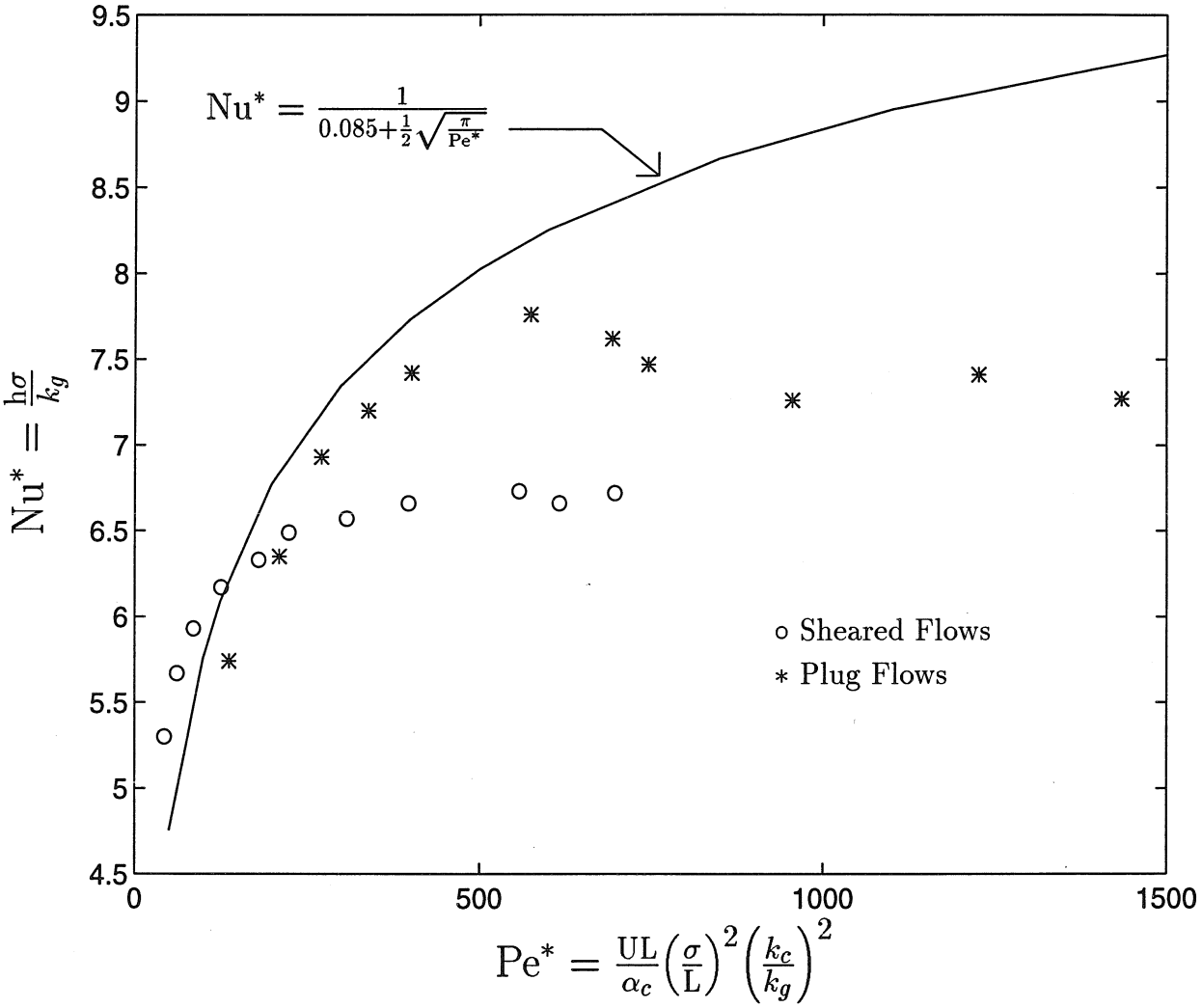


Figure 4.8: A comparison of the variation of Nu* with Pe* for the shear flow and plug flow experiments. Also shown is the semi-empirical result of Sullivan & Sabersky (1975).

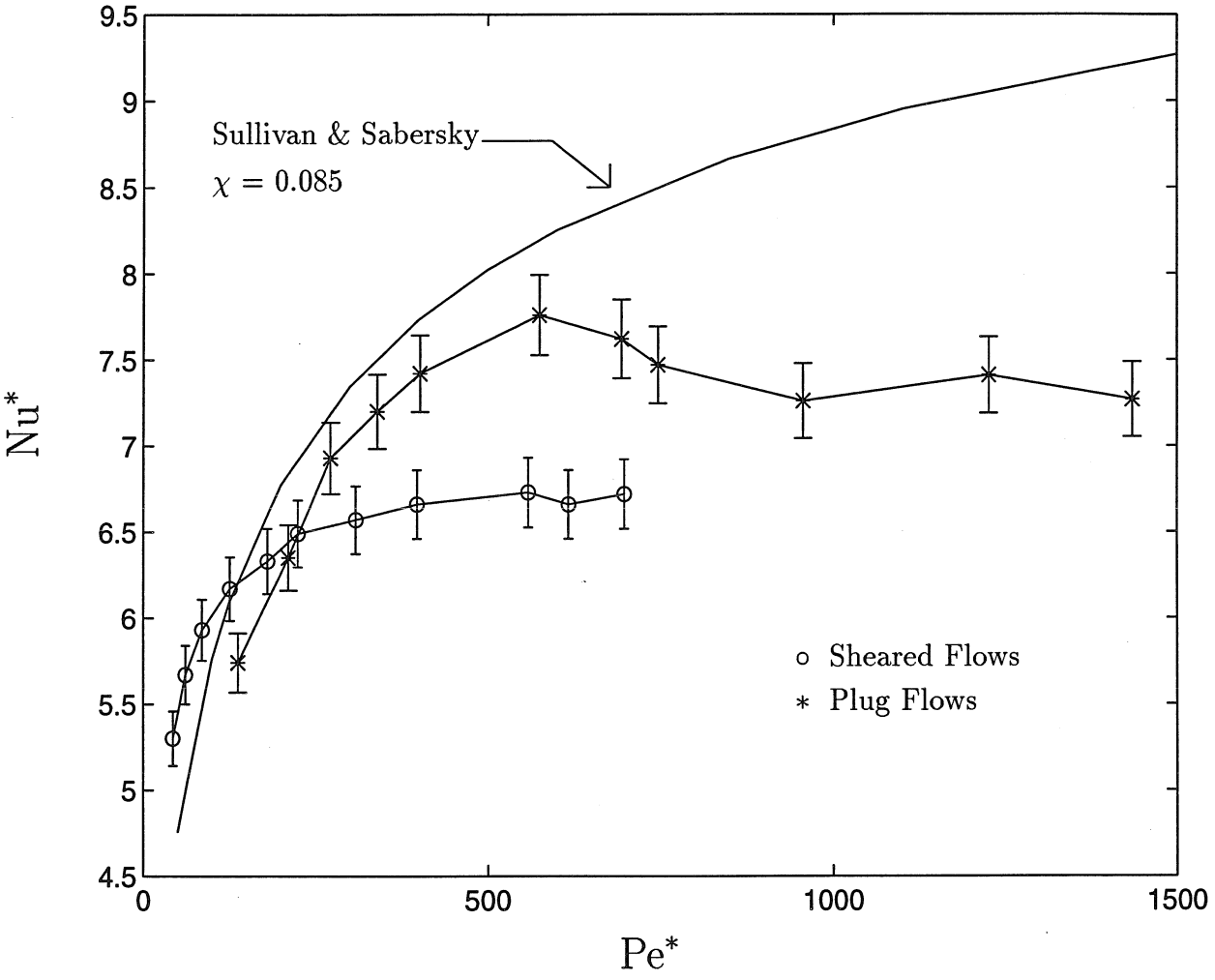


Figure 4.9: A comparison of the variation of Nu* with Pe* for the shear flow and plug flow experiments along with error bars. Also shown is the semi-empirical result of Sullivan & Sabersky (1975).

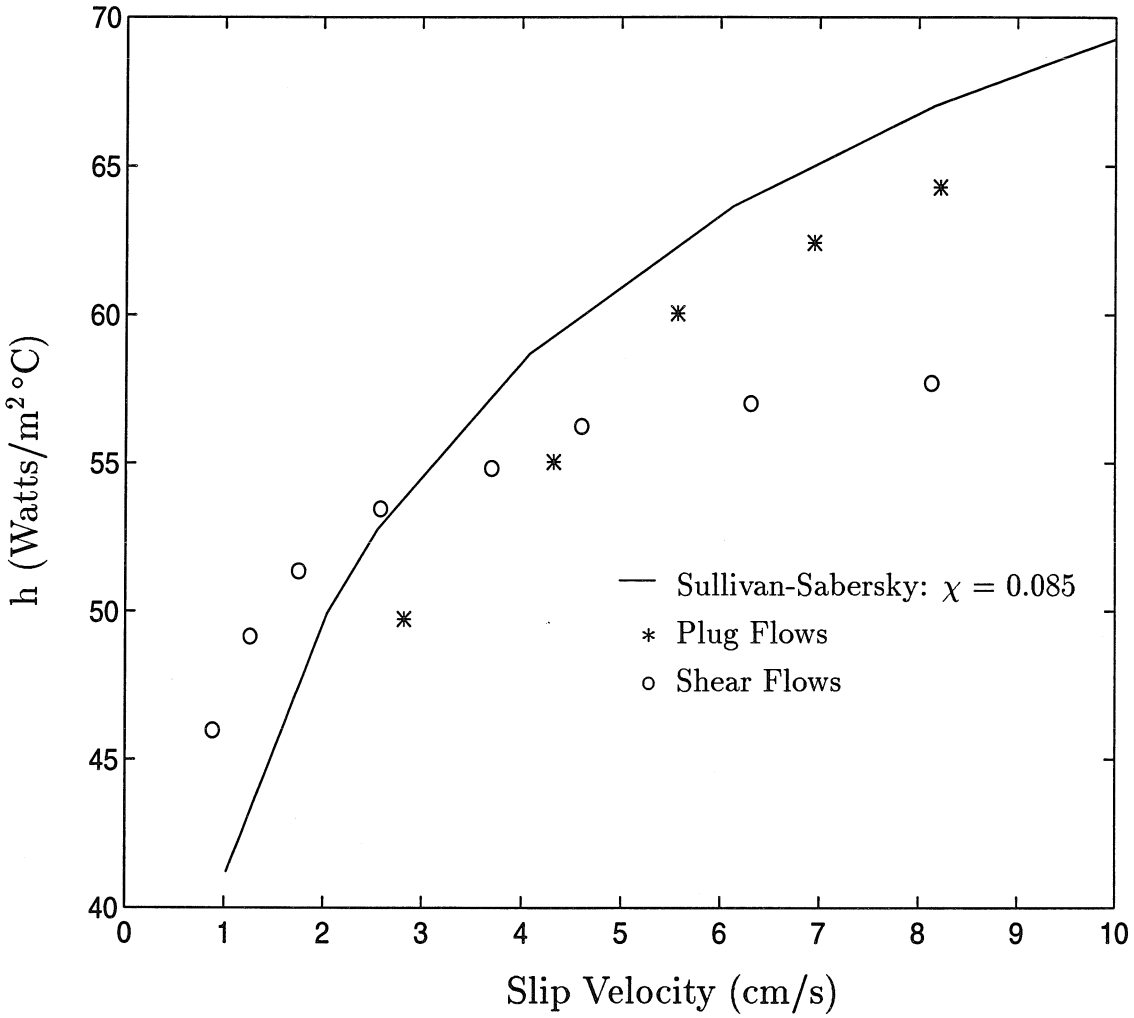


Figure 4.10: A comparison of the variation of the measured heat transfer coefficient with the flow slip velocity for the shear flow and plug flow experiments at low values of the slip velocity. Also shown is the semi-empirical result of Sullivan & Sabersky (1975).

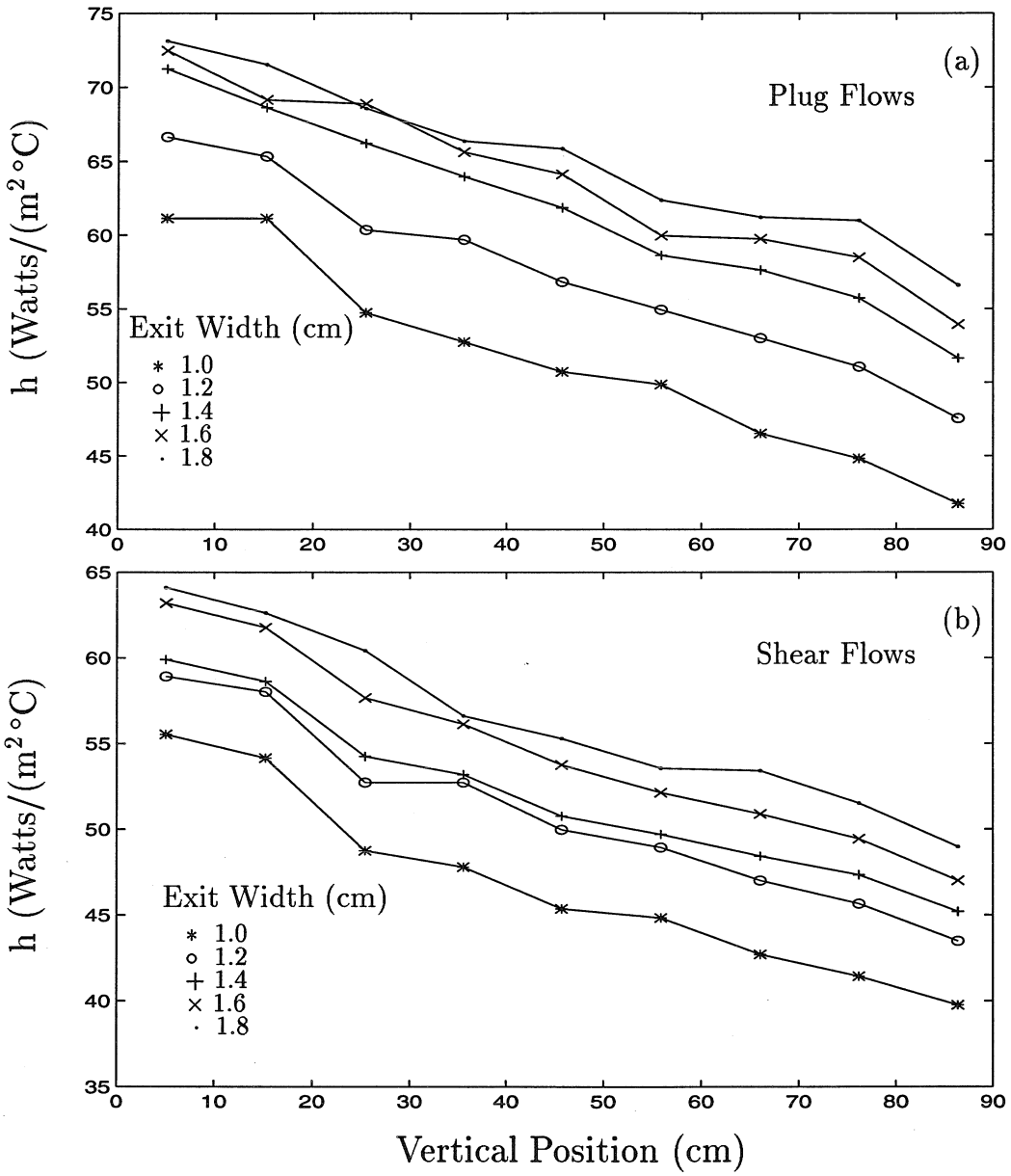


Figure 4.11: Variation of the local heat transfer coefficient with vertical position for the first five experiments with (a) plug flow and (b) shear flow.

# Chapter 5 Numerical Studies of Granular Flows in a Vertical Channel

The constitutive models for granular flows, based on dense-gas kinetic theory were discussed in Chapter 2, along with the modifications proposed by Johnson & Jackson (1987) in order to account for friction. The first part of this chapter describes the numerical solution of the momentum and fluctuation energy equations (Equations 2.7, 2.8) leading to the determination of mean and fluctuation velocity profiles for granular flows in a vertical chute. Comparisons were made with experimentally measured profiles. The second part of this chapter presents the results obtained by the numerical solution of the internal energy equation (Equation 2.35). Convective heat transfer coefficients were evaluated for a range of flow situations and compared with experimental data.

## 5.1 Solution of the Momentum and Fluctuation Energy Equations

For the numerical solutions, the flow in a vertical channel is assumed to be steady and two-dimensional, with fully developed density, velocity and fluctuation velocity profiles. For the two-dimensional flow, the Equations (2.7) and (2.8) reduce to:

$$-\left(\frac{\partial P_{xx}}{\partial x}+\frac{\partial P_{xy}}{\partial y}\right)+\rho g=0, \tag{5.1}$$

$$\left(\frac{\partial P_{yy}}{\partial y}\right)=0, \tag{5.2}$$

and

$$-P_{xy}\frac{\partial u_x}{\partial y} - \frac{\partial \Gamma_y}{\partial y} - \gamma = 0. \tag{5.3}$$

The contribution to the normal stresses from the kinetic-theory model (Equation 2.9) is given by:

$$P_{xx\mathbf{kt}} = P_{yy\mathbf{kt}} = \rho_p g_1(\nu, e_p)\mathbf{T}, \tag{5.4}$$

and the shear stresses are given by:

$$P_{xy\mathbf{kt}} = P_{yx\mathbf{kt}} = -\rho_p \sigma g_2(\nu, e_p)\mathbf{T}^{\frac{1}{2}}\frac{du_x}{dy}, \tag{5.5}$$

where the subscript **kt** refers to the contribution from collisional or translational interactions.

The flux of fluctuating energy in the direction normal to the walls is given by:

$$\Gamma_y = -\rho_p \sigma \left[ g_3(\nu, e_p)\mathbf{T}^{\frac{1}{2}}\frac{d\mathbf{T}}{dy} + g_4(\nu, e_p)\mathbf{T}^{\frac{3}{2}}\frac{d\nu}{dy} \right]. \tag{5.6}$$

An attempt was made to include the effects of frictional interactions by following Johnson & Jackson's (1987) development, as discussed in detail in section 2.1.2. The expressions in Equations (2.19) and (2.18) were used to determine the normal and planar shear stress contributions to the total stress. Hsiau (1993) showed that, for a fully developed flow, $\frac{\partial P_{xx}}{\partial x}$ is negligible for a vertical distance greater than twice the channel depth.

The non-dimensionalized momentum equations are obtained by substituting the expressions for the stresses from Equations (5.4), (5.5), (2.18) and (2.19) into Equations (5.1) and (5.2) and by substituting for the non-dimensional variables. As a result, the following expressions are obtained.

$$\frac{d}{dY}\left[ g_2(\nu, e_p)\mathbf{T}^{*\frac{1}{2}}\frac{du^*_x}{dY} + A^{\frac{1}{2}}N^*_f(\nu)\sin\phi \right] + A^{\frac{3}{2}}\nu = 0, \tag{5.7}$$

and

$$\frac{d}{dY}\left[ g_1(\nu, e_p)\mathbf{T}^* + N^*_f(\nu) \right] = 0. \tag{5.8}$$

The non-dimensionalized form of the fluctuation energy equation is given by:

$$\frac{d}{dY}\left[g_3(\nu,e_p)\mathbf{T}^{*\frac{1}{2}}\frac{d\mathbf{T}^*}{dY}+g_4(\nu,e_p)\mathbf{T}^{*\frac{3}{2}}\frac{d\nu}{dY}\right]$$

$$+Ag_2(\nu,e_p)\mathbf{T}^{*\frac{1}{2}}\left(\frac{du^*{}_x}{dY}\right)^2-A^2g_5(\nu,e_p)\mathbf{T}^{*\frac{3}{2}}=0. \tag{5.9}$$

The non-dimensional variables are given by:

$$X=\frac{x}{\sigma},$$

$$Y=\frac{y}{W},$$

$$u^*{}_x=\frac{u_x}{\sqrt{gW}},$$

$$P^*{}_{xx}=\frac{P_{xx}}{\rho_p g\sigma},$$

$$\mathbf{T}^*=\frac{\mathbf{T}}{g\sigma},$$

$$N_f^*=\frac{N_f}{\rho_p g\sigma},$$

and

$$A=\frac{W}{\sigma};$$

where $W$ is the half-width of the channel and $g$ is the acceleration due to gravity.

The nondimensionalized form of the boundary conditions (Johnson & Jackson 1987) from Equations (2.20) and (2.21) for the shear stress and the balance of fluctuation energy at the wall respectively, are given by:

$$-g_2(\nu,e_p)A^{-\frac{1}{2}}\mathbf{T}^{*\frac{1}{2}}\frac{du_x^*}{dY}+N_f^*(\nu)\sin\phi$$

$$=\frac{\phi'\sqrt{3}\pi\nu A^{\frac{1}{2}}\mathbf{T}^{*\frac{1}{2}}|u_{sl}^*|g_0(\nu)}{6\nu^*}+N_f^*(\nu)\tan\delta, \tag{5.10}$$

and

$$-\left[g_3(\nu,e_p)\frac{d\mathbf{T}^*}{dY}+g_4(\nu,e_p)\mathbf{T}^*\frac{d\nu}{dY}\right]$$

$$=-\frac{\phi'\sqrt{3}\pi\nu A^2{u_{sl}^*}^2g_0(\nu)}{6\nu^*}+\frac{\pi\nu(1-{e_w}^2)\sqrt{3}\mathbf{T}^*g_0(\nu)}{4\nu^*}. \tag{5.11}$$

An investigation of Equation (5.8) shows that given a constant particle coefficient of restitution $e_p$, the solid fraction at any point is a function of only the normalized granular temperature $\mathbf{T}^*$. Therefore, all functions of $\nu$ can be written in terms of the granular temperature in Equations (5.7) and (5.9). Consequently, a system of two coupled, ordinary second-order differential equations for the normalized flow velocity, $u_x^*$, and normalized granular temperature $\mathbf{T}^*$ has to be solved. These equations were solved using a fourth-order Runge-Kutta scheme. Given the two second-order equations, a total of four boundary conditions are required to solve the problem. Two of these conditions are obtained from Equations (5.10) and (5.11) for the shear stress and fluctuation energy balance at the wall. The other two boundary conditions are obtained by using the symmetry of the channel to set $du_x^*/dY$ and $d\mathbf{T}^*/dY$ equal to zero at the channel center-line $Y = 0$. A "shooting" method was used to solve the resultant boundary value problem. Values for $u_x^*$ and $\mathbf{T}^*$ were guessed for a particular value of solid fraction at the center-line and the equations were integrated from the center-line to the wall. The process was iterated, using a globally convergent Newton-Raphsons scheme to match the boundary conditions at the wall. Convergence was assumed to have been achieved when the difference between the left and right hand sides of Equations (5.10) and (5.11) was less than $1 \times 10^{-6}$. In some instances, in order to solve the equations for desired mass-flow rates, a third condition for the mass flow was included within the iteration routine.

It is evident from Equations (5.7) and (5.8), as well as the boundary conditions (Equations 5.10 and 5.11) that several physical parameters need to be specified. There still exists very little information, in the literature, dealing with actual measurements of most of these parameters. The coefficient of restitution for particle-particle collisions, $e_p$, was assumed to be 0.95 (Foerster et al. 1994), unless otherwise specified. A value of 0.65 was assumed for the maximum shearable solid fraction $\nu^*$ (Johnson & Jackson 1987). The internal angle of friction was assumed to be 28.5° (Johnson et

al. 1990). For the case of the rough walls, i.e. with 3 mm particles glued to them, the expression $\sin\phi = \tan\delta$ was used to determine a value of 25.5° for $\delta$, the wall angle of friction. Since no measurements of specularity coefficients $\phi'$ are available in literature, reasonable values had to be assumed arbitrarily. A value of $\phi' = 0.85$ was chosen for all the numerical calculations simulating rough walls, unless specified otherwise. This value was chosen on the basis of the comparisons between theoretical and experimental streamwise velocity profiles, and is representative of a wall that is very rough. Johnson et al. (1990) assumed values of $\phi' = 0.25$ for aluminium walls and $\phi' = 0.6$ for 160 grit sandpaper. It was anticipated that the wall with glass particles glued to it would be rougher than those examined by Johnson et al. (1990). A range of values were considered for the particle-wall coefficient of restitution $e_w$.

Following Johnson et al. (1989), the values of $p = 2$, $n = 5$, $\nu_{min} = 0.50$ and $\nu^* = 0.65$ were used in the normal frictional stress equation. However, in these calculations, the constant $Fr$ was chosen to be 0.005 kg/m$s^2$ so that $\nu = 0.60$ under the effect of a normal load equal to the weight of an overburden of a few centimeters of the particulate material. Such a value of the solid fraction is typical for particles poured into a container under the influence of gravity.

Prior to the discussion of the results of the numerical analysis, it must be reemphasised that the expressions for the frictional stresses are totally empirical, unlike the expressions for the kinetic theory analysis. As stated by Johnson et al. (1989), Equations (2.18) and (2.19) are only expected to replicate, at an extremely simplistic level, the basic qualitative behavior of a granular material under shear. These expressions encompass the reasonable assumption that for solid fractions below $\nu_{min}$, the particles no longer have long term contacts and hence frictional effects can be neglected. At the other extreme, based on some experimental observations (Scarlatt & Todd 1969), the model attempts to describe the rapid increase in the frictional stresses as $\nu$ approaches $\nu^*$, the close packed state beyond which the material cannot

be sheared and essentially behaves as a solid. The limitations of this model become apparent in the following discussions.

The first set of numerical results presented are based only on the kinetic theory model, with the frictional stress terms being set to zero. The effect of varying the wall-particle coefficient of restitution ($e_w$) is presented in Figures 5.1-5.3. While the dense-gas kinetic theory model of Lun et al. (1984) is based on the assumption that the value of $e_p$ is very close to one, there is no such stipulation for $e_w$, which appears only in the boundary conditions. Figure 5.1 shows the mean velocity profiles, for different values of the centerline solid fraction, for values of $e_w$ equal to 0.95, 0.50 and 0.20. From Figure 5.1, it is seen that for moderate or highly dense flows, there is a distinct central uniform velocity regime and a sheared regime adjacent to the walls. The granular temperature profiles, shown in Figure 5.2 increase from the center towards the walls. The solid fraction profiles in Figure 5.3 depict maximum values at the center and more dilated regions adjacent to the walls. While profiles have been presented for centerline solid fractions of 0.36 and less, it must be cautioned that these are primarily of academic interest only. At such low density values, particle interactions in the vertical chute are likely to be negligible, with each particle in a state of free fall under the influence of gravity. While the velocity profiles remain similar in shape and magnitude, comparisons of the temperature and density profiles for the three values of $e_w$ show interesting changes. A lower value of $e_w$ implies greater dissipation of random energy at the wall. Hence for the cases of $e_w = 0.50$ and $e_w = 0.20$, we see that granular temperatures decrease adjacent to the wall, accompanied by increased solid fractions in the same region. Reduced granular temperatures cause greater "clumping" of particles. Qualitatively similar behavior is observed in the experimentally measured transverse fluctuation velocity profiles in Figure 3.6. As discussed earlier, frictional interactions at the wall could also be responsible for such a lowering of fluctuation velocities close to the walls. All the above calculations were

for $\phi' = 0.85$.

Comparisons between calculated and measured mean streamwise velocity profiles are presented in Figures 5.4-5.6. The figures compare the numerical mean velocity profiles with the experimental data for experiments 1-3, for three different combinations of $e_p$ and $e_w$, all for $\phi' = 0.85$. In each case, the agreement between theoretical and experimental mean velocity profiles is very good for the sheared regimes with moderate agreement in the plug regime for the case of $e_p = e_w = 0.95$. The graphs of the numerically computed profiles of $\mathbf{T}^{\frac{1}{2}}$ versus the horizontal position are shown in Figure 5.7, along with the experimentally measured data. Note that the kinetic-theory model assumes an isotropic distribution of the fluctuation velocities. In contrast, the actual measurements (Figures 3.5 and reffig:a3) demonstrate a strongly anisotropic distribution of the fluctuation velocities. The figures also indicate that the theoretical results underpredict the root mean square fluctuation velocities significantly across most of the flow regime. However, as discussed in Section 3.2, the measurements of the streamwise fluctuation velocity are likely to include a coherent "chugging" component. Hence, it is more appropriate to compare the graphs of the numerically computed profiles of $\mathbf{T}^{\frac{1}{2}}$ with the measured profiles of the transverse fluctuation velocities, as depicted in Figure 5.8. In this case, it is seen that the numerical solutions overpredict the fluctuation velocities in the sheared regimes adjacent to the wall, but underpredict these values in the regimes away from the walls. Also, the gradients in the fluctuation velocity are much more significant in the numerical solutions. Figure 5.9 depicts the theoretical solid fraction profiles for the three cases. In each case, the solid fractions are very close to the assumed close-packed value of $\nu^* = 0.65$. While the average solid fractions measured for this set of experiments varied from 0.55 to 0.68, visual observations made it apparent that the flow densities adjacent to the walls were not close to dense packed values.

The discussion in the previous paragraph raises many questions regarding the

validity of kinetic-theory models to describe the flows studied in this experiment. While it is possible to obtain reasonable agreement between velocity profiles obtained experimentally and theoretically using fairly realistic values for various physical parameters, the predicted solid fraction values are very high. At solid fractions close to the rigid-packing limit, the basic assumptions of collisional and translational interactions, inherent to the kinetic-theory model, are no longer valid. The dynamics at such densities are determined, almost exclusively, by long term frictional interactions. Furthermore, the assumption of an isotropic radial distribution function $g_0(\nu)$ is certainly not appropriate in the current situation of wall-bounded flows. Also, at very high solid fractions, the solutions show changes of significant magnitude in the velocity fields for very small changes in solid fraction, a result that does not seem to hold much physical basis, and is certainly not apparent from the experiments.

However, the kinetic-theory model still retains significant validity in the regime of highly sheared, rapid flows with lower solid fractions. Such flows could not be studied experimentally as the measurement techniques were not capable of making reliable velocity measurements for flows with velocities greater than 30 cm/s. Also, the kinetic theory model is the only theory currently available that is capable of qualitatively predicting the features of shear induced dilation and the accompanying fluctuation velocity changes in granular flows at moderate solid fractions. These features are readily observable in Figures 5.1-5.3, especially for flows with centerline solid fractions in the range of 0.36 to 0.6. As such, these solutions serve as a good tool to investigate the convective heat transfer behavior of such flows and provide valuable insights as discussed later in this chapter.

The effect of friction, as described by the empirical Johnson et al. (1990) model is presented in Figures 5.10-5.12, with $e_p = 0.95$. All calculations are for a value of $\phi' = 0.85$. Comparisons between the two cases (with and without frictional stresses) are based on solving for both cases with identical values of the centerline solid fraction.

At values of $\nu$ closer to the value of $\nu_{min} = 0.50$ (e.g. for $\nu = 0.56$ at the centerline in the figures), the velocity, granular temperature and solid fraction profiles are essentially identical for the cases with and without friction. However, with increasing centerline solid fractions, the magnitudes of the streamwise velocities decrease (Figure 5.10) for the frictional flows. Also, at higher solid fractions (e.g. $\nu = 0.60$ at the centerline), there is enormous damping of the fluctuation energy and granular temperatures are reduced substantially due to friction. Accompanying this phenomenon is a significant increase in the solid fractions in the sheared regimes of the flow. The granular temperature and solid fraction profiles are almost uniform across the entire flow section for frictional flows at higher values of the solid fraction. Similar frictional damping and reduced diffusion coefficients were observed for particles of Type B, as described in Chapter 3.

A major drawback of the Johnson & Jackson (1987) frictional model became apparent when attempts were made to solve the momentum and fluctuation energy equations for solid fractions higher than 0.635 (for values of $e_p = e_w = 0.95$). The granular temperature values started increasing rapidly to values much higher than those obtained for the equivalent cases without friction, an obviously unphysical result. Such a result was a consequence of the fact that, at solid fraction values greater than 0.635, the frictional stresses, as defined by Equations (2.18) and (2.19), were extremely high and high values of the granular temperature were required at the wall in order to satisfy the boundary conditions in Equations (5.10) and (5.11). Furthermore, at solid fraction values greater than 0.64, the frictional stresses increased dramatically and exhibited significant variations for minute changes in solid fractions. As a result, it was impossible to attain convergence. Ironically, the model failed to work in the high-density regimes where the interactions are predominantly frictional. Consequently, it was not possible to obtain theoretical solutions incorporating friction, in order to make comparisons with the experimentally measured profiles.

The limitations of the frictional model, as discussed above, arise primarily due to the uncertainties associated with the assumptions made about the functional form of the normal stress relation in Equation (2.19). While it describes, in essence, expected behavior at the extreme limits, it has not been validated by any kind of theoretical or experimental information. It would have been possible, through suitable adjustment of the parameters $Fr, p$ or $n$, to obtain flow velocity profiles in good agreement with the profiles measured during the experiments, but it would be difficult to justify such a procedure, given the lack of sufficient knowledge about the physical basis for the exponents $p$ and $n$. However, valuable qualitative insights about the effects of frictional interactions on the velocity, granular temperature and solid fraction profiles have been gained from the used of the model, especially for centerline values of $\nu$ in the range of 0.5 to 0.6.

## 5.2 Solution of the Internal Energy Equation

The internal energy equation (Equation 2.35) was solved numerically, for the entire flow field, in order to determine the average heat transfer coefficients. For a two-dimensional, steady system, following Patankar (1980,1988), Equation (2.35) can be written in the form :

$$\frac{\partial J_x}{\partial x} + \frac{\partial J_y}{\partial y} = S, \tag{5.12}$$

where

$$J_x = \rho u_x T - \frac{k_{tot}}{c_p}\frac{\partial T}{\partial x}, \tag{5.13}$$

$$J_y = \rho u_y T - \frac{k_{tot}}{c_p}\frac{\partial T}{\partial y}, \tag{5.14}$$

and

$$\mathrm{S} = \frac{\rho_p}{\sigma} g_5(\nu, e_p)\mathbf{T}^{\frac{3}{2}} - N_f \sin\phi \frac{\partial u_x}{\partial y}. \tag{5.15}$$

Here, $J_x$ and $J_y$ are the sum of the convective and diffusive fluxes in the appropriate directions and S is the net "source" term, the sum of the energy sources arising out of the dissipation of the random fluctuation energy and the shear work done by the frictional shear stresses. In the regime immediately adjacent to the wall, where solid fractions become extremely low, the approximation $\nu\rho_p c_p + (1-\nu)\rho_{air}c_{air} \approx \rho c_p$ was replaced by the complete, unapproximated expression, to account for the increased influence of the interstitial fluid.

Assuming a grid structure and notation of the form depicted in Figure 5.13, integration of Equation (5.12) over the control volume leads to the equation

$$J_e - J_w + J_n - J_s = \mathrm{S}\Delta x\Delta y. \tag{5.16}$$

The continuity equation can be similarly integrated over the boundaries to give the equation :

$$F_e - F_w + F_n - F_s = 0, \tag{5.17}$$

where $F_e = (\rho u_x)_e \Delta y, F_w = (\rho u_x)_w \Delta y, F_n = (\rho u_y)_n \Delta x$ and $F_s = (\rho u_y)_s \Delta x$. By manipulating Equations (5.16) and (5.17), we arrive at :

$$(J_e - F_e T_P) - (J_w - F_w T_P) + (J_n - F_n T_P) - (J_s - F_s T_P) = \mathrm{S}\Delta x\Delta y, \tag{5.18}$$

with the notation as clarified in Figure 5.13. It can be shown (Patankar 1980, 1988) that one can subsequently write:

$$J_e - F_e T_P = a_E(T_P - T_E), \tag{5.19}$$

and

$$J_w - F_e T_P = a_W(T_W - T_P). \tag{5.20}$$

Similar expressions can also be written for $J_n - F_n T_P$ and $J_s - F_s T_P$. From Equations (5.18), (5.19) and (5.20), the final form of the two-dimensional discretization equation for a point within the body of the flow field is derived as:

$$a_P T_P = a_E T_E + a_W T_W + a_N T_N + a_S T_S + b \tag{5.21}$$

where

$$a_E = Z_e M(|\mathrm{Pe}_e|) + \| - F_e, 0\|, \tag{5.22}$$

$$a_W = Z_w M(|\mathrm{Pe}_w|) + \|F_w, 0\|, \tag{5.23}$$

$$a_N = Z_n M(|\mathrm{Pe}_n|) + \| - F_n, 0\|, \tag{5.24}$$

$$a_S = Z_s M(|\mathrm{Pe}_s|) + \|F_s, 0\|, \tag{5.25}$$

$$b = \mathrm{S}\Delta x \Delta y, \tag{5.26}$$

and

$$a_P = a_E + a_W + a_N + a_S. \tag{5.27}$$

In the above equations, $Z_e = \frac{(k_{tot})_e \Delta y}{\delta x_e}$, $Z_w = \frac{(k_{tot})_w \Delta y}{\delta x_w}$, $Z_n = \frac{(k_{tot})_n \Delta x}{\delta y_n}$, and $Z_s = \frac{(k_{tot})_s \Delta x}{\delta y_s}$. The Peclet numbers are given by $\mathrm{Pe}_e = \frac{F_e}{Z_e}, \mathrm{Pe}_w = \frac{F_w}{Z_w}, \mathrm{Pe}_n = \frac{F_n}{Z_n}$ and $\mathrm{Pe}_s = \frac{F_s}{Z_s}$. The function $M(|\mathrm{Pe}|)$ depends on the actual scheme used for discretizing the temperature field. Common examples of schemes used include the central difference, upwind or power-law schemes (Patankar 1980, 1988). The power-law scheme (Patankar 1980) was used in this work and assumed the form:

$$M(|\mathrm{Pe}|) = \|0, (1 - 0.1|\mathrm{Pe}|)^5\|, \tag{5.28}$$

where the symbol $\|\quad\|$ stands for the largest of the quantities contained within it. As the mean flow is in the x-direction, $F_n = F_s = \mathrm{Pe}_n = \mathrm{Pe}_s = 0$.

A similar control volume analysis for a point on the wall led to a discretization equation of the form:

$$(a_S + \frac{a_W}{2} + \frac{a_E}{2})T_P = \mathrm{S}\frac{\Delta x \Delta y}{2} + q_w \Delta y + a_s T_S + \frac{a_e}{2} T_E + \frac{a_w}{2} T_W. \tag{5.29}$$

In order to solve for the temperature field, the momentum equations were first solved to establish the mean streamwise velocity, granular temperature and solid fraction profiles. As discussed earlier, while the effect of the interstitial fluid can be neglected while investigating the dynamics of the system, it cannot be neglected in

the heat transfer problem. The interstitial fluid, especially the layer adjacent to the heated wall plays a very crucial role in the heat transfer process. For spherical particles, the solid fraction goes to zero at a flat bounding wall. However, as evident from the solid fraction profiles examined previously, the kinetic theory solutions always predict significant, non-zero solid fractions at the wall, as a result of the "continuum" assumption. Hence, in order to generate realistic solutions to the heat transfer problem, it is necessary to make assumptions about the solid fraction profile adjacent to the wall. More specifically, a profile form has to be assumed such that the solid fraction decreases from the value predicted by the kinetic-theory model at a distance of half a particle diameter from the wall, to a value of zero at the wall. Using a simple analysis, based on Figure 5.14, the solid fraction profile adjacent to the wall was assumed to be of the form:

$$\nu(y) = \nu_{\sigma/2}\left(1 - (\frac{y-(W-\sigma/2)}{\sigma/2})^2\right), \tag{5.30}$$

where $\nu_{\sigma/2}$ is the solid fraction at a distance of half a particle diameter from the wall. Also, though there is slip between the glass particles and the wall, it is realistic to expect that a no-slip condition would exist between the air and the wall. Hence, the air velocity was assumed to be linearly decreasing to zero over the distance of half a particle diameter adjacent to the wall, by adopting the profile:

$$u_x(y) = u_{x-\sigma/2}\left(1 - \frac{y-(W-\sigma/2)}{\sigma/2}\right). \tag{5.31}$$

Furthermore, in order to be consistent with the assumed solid fraction profile adjacent to the wall, the granular temperature was also assumed to go to zero at the wall. This was done to account for the fact that it is ambiguous to have a non-zero granular temperature at a position where the solid fraction is zero. Therefore, when evaluating the value of $k_{kt}$ in the regime within half a particle diameter from the wall, a linear profile was assumed for the square root of the granular temperature, of the

form:

$$\mathbf{T}^{\frac{1}{2}}(y) = \mathbf{T}^{\frac{1}{2}}_{\sigma/2}\left(1 - \frac{y-(W-\sigma/2)}{\sigma/2}\right), \tag{5.32}$$

where $\mathbf{T}_{\sigma/2}$ is the value of the granular temperature at a distance of half a particle diameter from the wall. Such an assumption is unrealistic to a certain degree, as ideally, particles impacting the wall have a non-zero translational fluctuation velocity that is constant for the whole particle. However, immediately adjacent to the wall, the continuum assumption governing the kinetic theory solutions breaks down as changes in solid fraction profiles occur over distances much less than a particle diameter. This is contrary to the stipulation of the continuum assumption that flow properties remain constant over a distance of several particle diameters. However, it is evident from the experimental data that steep gradients in the transverse fluctuation velocity profile occur over distances less than a particle diameter, in the sheared regimes adjacent to the wall.

For 3 mm particles, values of $\Delta x = \Delta y = \delta x = \delta y = 0.001$ m were chosen for the gridspacing within the bulk except for a distance of half a particle diameter from the wall. Within this region, the transverse gridspacing value was set at 0.0001 m, as large temperature gradients were anticipated within the thermal boundary layer. The values for the gridspacing used to solve for the momentum equations were half of those used to solve the energy equation. Other physical property values used in the numerical solutions are listed in Table 5.1. The temperature at the inlet section, as well as at the centerline was assumed to be 24°C. For all grid points P next to the outflow boundary, the coefficients $a_E$ were set to zero, under the assumption that the Peclet numbers in the flow direction were sufficiently large. Within the boundary layer, where Peclet numbers were small, the equivalent assumption was that the temperature gradients in the streamwise direction were much lower than the gradients in the transverse direction.

In order to make comparisons with experimental data and the Sullivan-Sabersky

model, a series of plug flow solutions were generated, using the kinetic theory model without friction, by assuming a value of 0.01 for the specularity coefficient $\phi'$. The values of the mean solid fractions for all the flows in this set of numerical solutions were in the range 0.64 to 0.65. While this regime is certainly not a rapid granular flow regime and hence cannot be described by a kinetic theory model, the purpose of the exercise was to generate a set of plug flows, with uniform velocity and solid fraction profiles, using the numerical scheme already in place. Figure 5.20 compares the variation of $Nu^*$ with $Pe^*$ for the experimental data and the Sullivan-Sabersky semi-emperical model with the calculations for the plug flows generated from kinetic-theory. Up to a value of $Pe^* \approx 600$ there is good agreement among the three different sets. However, neither the Sullivan-Sabersky model nor the calculations based on kinetic theory can replicate the measured plateau of the heat transfer coefficients at higher values of $Pe^*$. Both the Sullivan-Sabersky and kinetic-theory results are based on assumptions of constant flow density, contrary to the observations in the actual experiments.

To investigate the convective heat transfer behavior in sheared flows, three combinations of $e_p$ and $e_w$ were chosen and the momentum equations were solved for a range of centerline solid fraction values from 0.05 to 0.6495. The value of $e_p$ was kept constant at 0.95 while the values of $e_w$ were set at 0.2, 0.5 and 0.95 for the three sets. All the solutions were for a value of $\phi' = 0.85$. As discussed in detail in Chapters 2 and 4, the density of the flows, especially adjacent to the walls, plays an important role in determining the heat transfer coefficients, especially for flows that are subjected to high shear. Figure 5.15 shows the variation of the average solid fraction ($\nu_{ave}$) and $\nu_{wall}$ (or $\nu_{\sigma/2}$), with the average velocity. It is observed that for $e_w = 0.95$, the difference between the values for $\nu_{ave}$ and $\nu_{wall}$ is quite significant. However, this difference decreases with a decrease in the value of $e_w$. The variation of $\nu_{wall}$ with the slip velocity is shown in Figure 5.16. For the regime of solutions physically plausible

for flows in a vertical channel ($\nu > 0.3$), both $\nu_{ave}$ and $\nu_{wall}$ decrease with an increase in velocity, qualitatively the same behavior as that observed in experiments by Patton et al. (1986) and Ahn (1989). It is noteworthy that a change in the value of $e_w$ does not influence these curves significantly, for values of $\nu > 0.3$. Another detail is the difference between the values of $\nu_{ave}$ and $\nu_{\sigma/2}$ in a flow. As discussed in Chapter 4 with reference to Ahn's (1989) use of $\nu_{ave}$ to determine the physical properties of the flow, the properties calculated thus would not be representative of the actual parameters adjacent to the wall. Figures 5.15 and 5.16 are based on calculations made by assuming the stress tensor to be composed only of the collisional and translational components without any frictional terms. The variation of $\nu_{ave}$ with the average flow velocity, for cases including the frictional components is shown in Figure 5.17. For the sake of comparison, Figure 5.17 also includes the results calculated without any frictional components. For very high solid fractions, the value of the average velocity in the frictional case increases instead of decreasing with increasing solid fraction, and is accompanied by a rapid increase in values of the granular temperature. The reasons for such an unphysical phenomenon have been discussed previously in reference to the limitations of the frictional model. Keeping in mind the limitation of the frictional model at very high solid fractions, the numerical heat transfer results presented do not include the effect of friction, unless otherwise mentioned. The variation of the average granular temperature with the average solid fraction is presented in Figure 5.18 while Figure 5.19 depicts the corresponding values at the wall. The granular temperature decreases with an increase in solid fraction, except at extremely low solid fractions.

The results of the heat transfer calculations for the sheared flows are shown in Figure 5.21 in the form of a graph of Nu* versus Pe*. The lines depict the results obtained by suppressing the contribution of $k_{kt}$ towards the net conductivity while the symbols depict the results obtained by including $k_{kt}$. For particles of 3 mm diameter,

the kinetic contribution is negligible over the whole range of solid fractions and shear rates. A comparison of the numerical results with the experimental data for both sheared and plug flows is presented in Figure 5.22. The numerically calculated profiles for the sheared flows show a maximum value for $Nu^*$, similar to the experimental results of Spelt et al. (1982), Patton et al. (1986) and Ahn (1989). However, a comparison of the numerical profiles with the experimental data for sheared flows shows the kinetic theory underpredicting heat transfer coefficients for values of $Pe^* < 300$. Also, the theoretical results do not predict the plateau of the heat transfer coefficients observed in the experiments for higher velocities.

In order to examine the influence of particle size on the contribution of $k_{kt}$ towards the effective heat transfer, solutions were also generated for particle diameters of 1 mm and 0.5 mm (with the size of the channel scaled so that $W/\sigma$ was constant for all three cases) with $e_p = e_w = 0.95$. The length of the heated plate was set at 82.16 cm for each value of the particle diameter. The values of the average heat transfer coefficient $h$ versus the slip velocity are plotted in Figure 5.23. The influence of $k_{kt}$ increases with a decrease in the particle diameter. In the case of the smallest particle size investigated (0.5 mm), the maximum value of the heat transfer coefficient is achieved at a slip velocity three times greater in the case where the streaming component is included, than in the case where it is not. The value of the peak is also higher for the case including the effect of $k_{kt}$. Smaller particle diameters were not investigated as it was expected that at such sizes the assumption neglecting the effect of the interstitial fluid while determining the flow dynamics would no longer be valid.

All the results described previously were for a specularity of 0.85. Figures 5.24-5.27 investigate the effect of varying the value of $\phi'$. From the figures, it is apparent that the effect of lowering the value of $\phi'$ is to cause greater "clumping" of particles, increasing the solid fraction close to the walls. Consequently, as evident from Figure 5.27, the value of $Nu^*$ increases with a decrease in the value of $\phi'$ for a given value of

$Pe^*$. As elucidated by the discussion about plug flows earlier in this chapter, a lower value of the specularity coefficient leads to less shearing at the wall thereby leading to higher solid fractions.

| | |
|---|---|
| solid density | 2500 kg/m$^3$ |
| $C_p$ solid | 903.95 J/kg°C |
| $C_p$ air | 1005.70 J/kg°C |
| $k_g$ | 0.026 W/m °C |
| $k_s$ | 0.910 W/m °C |
| $k_c$ | 0.210 W/m °C |
| $\alpha_c$ | $1.5\times10^{-7}$m$^2$/s |

Table 5.1: Property values used in the numerical calculations.

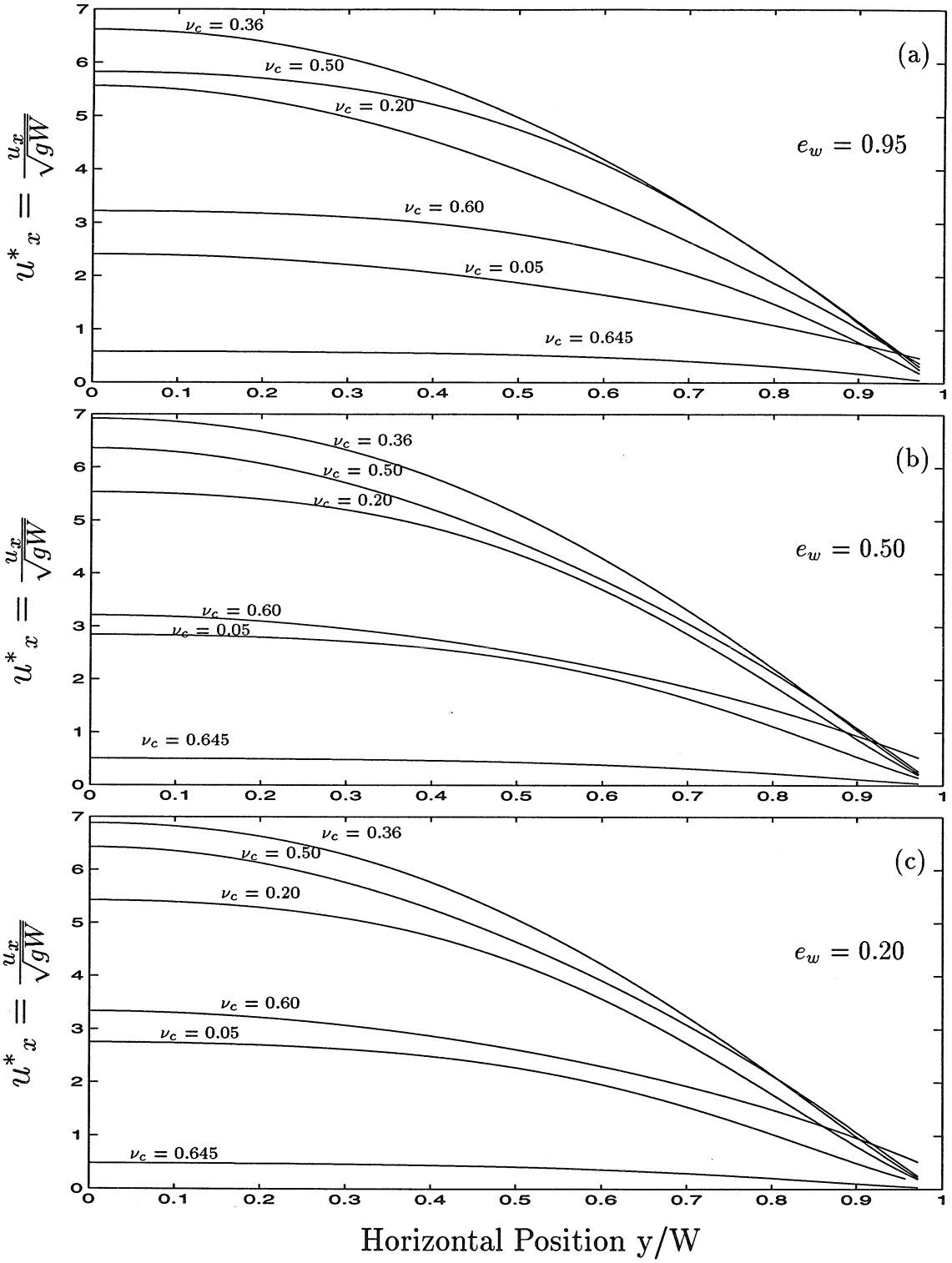


Figure 5.1: Comparison of the theoretical nondimensionalized streamwise mean velocity profiles, for values of (a) $e_w = 0.95$, (b) $e_w = 0.50$ and (c) $e_w = 0.20$. $\nu_c$ is the centerline solid fraction. $e_p = 0.95$. W=3.5 cm.

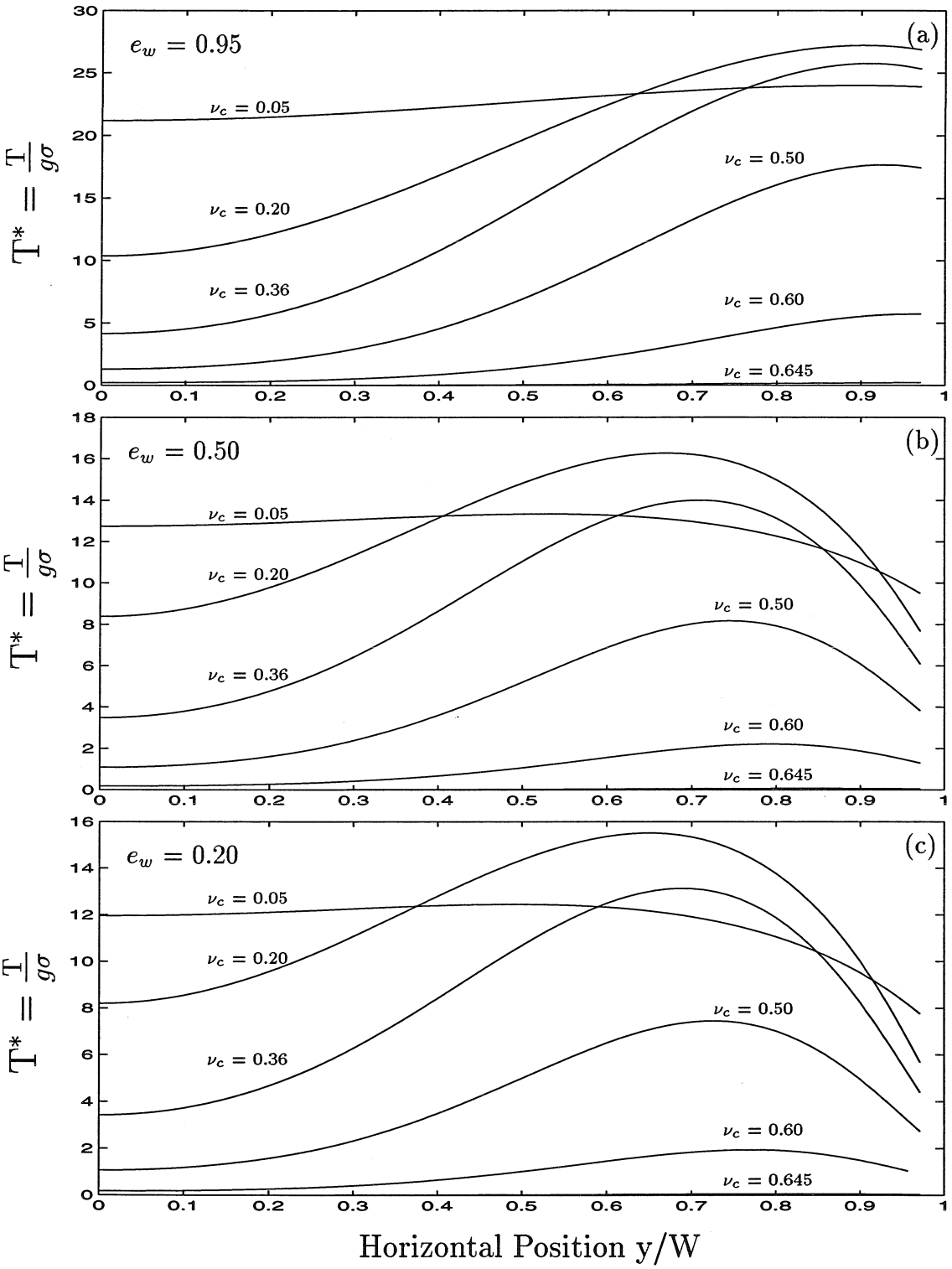


Figure 5.2: Comparison of the theoretical nondimensionalized granular temperature profiles, for values of (a) $e_w = 0.95$, (b) $e_w = 0.50$ and (c) $e_w = 0.20$. $\nu_c$ is the centerline solid fraction. $e_p = 0.95$. W=3.5 cm.

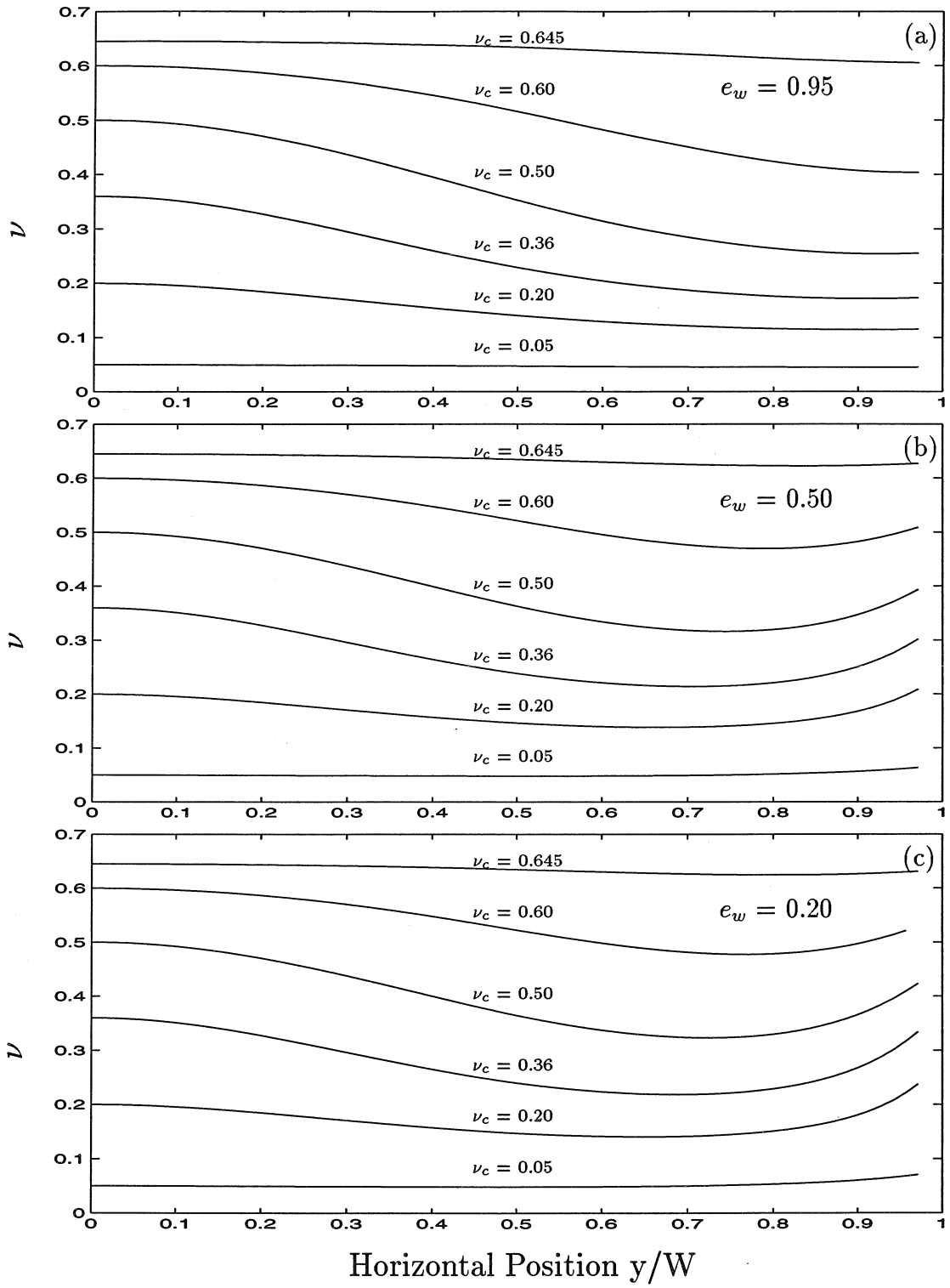


Figure 5.3: Comparison of the theoretical solid fraction profiles, for values of (a) $e_w = 0.95$, (b) $e_w = 0.50$ and (c) $e_w = 0.20$. $\nu_c$ is the centerline solid fraction. $e_p = 0.95$. W=3.5 cm.

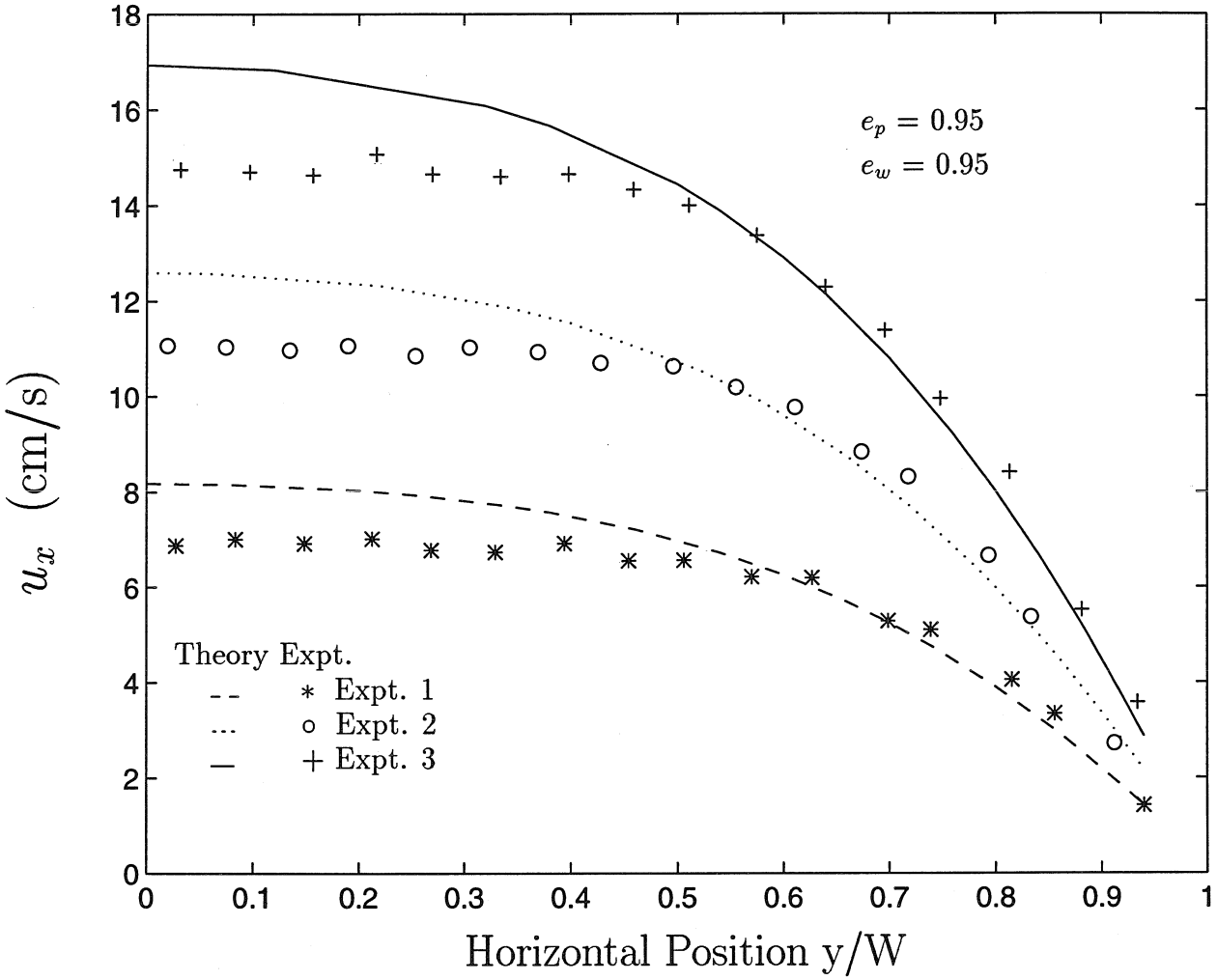


Figure 5.4: Comparison of experimental and theoretical mean streamwise velocity profiles. $e_p = 0.95$. $e_w = 0.95$. W=2.5 cm.

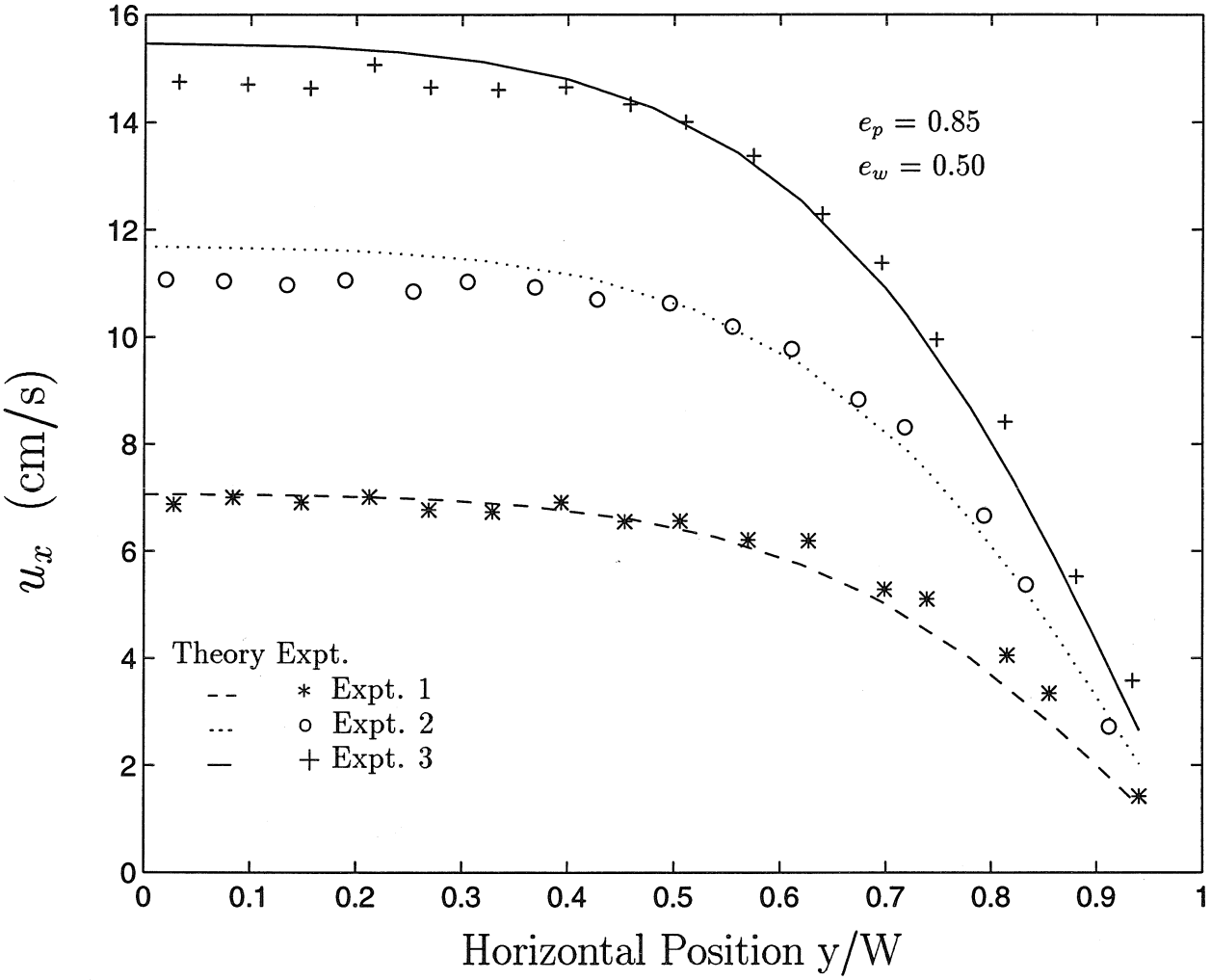


Figure 5.5: Comparison of experimental and theoretical mean streamwise velocity profiles. $e_p = 0.85$. $e_w = 0.50$. W=2.5 cm.

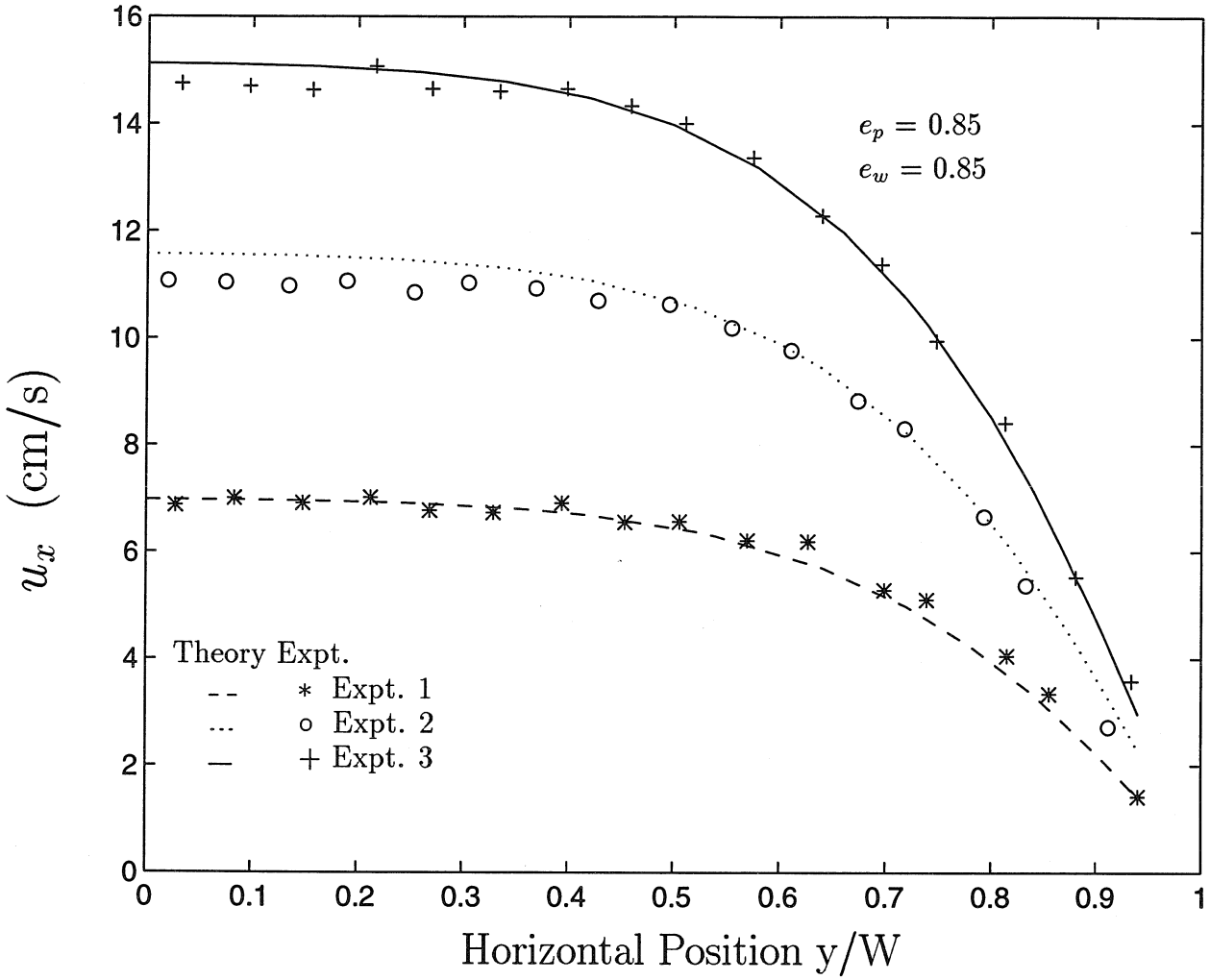


Figure 5.6: Comparison of experimental and theoretical mean streamwise velocity profiles. $e_p = 0.85$. $e_w = 0.85$. W=2.5 cm.

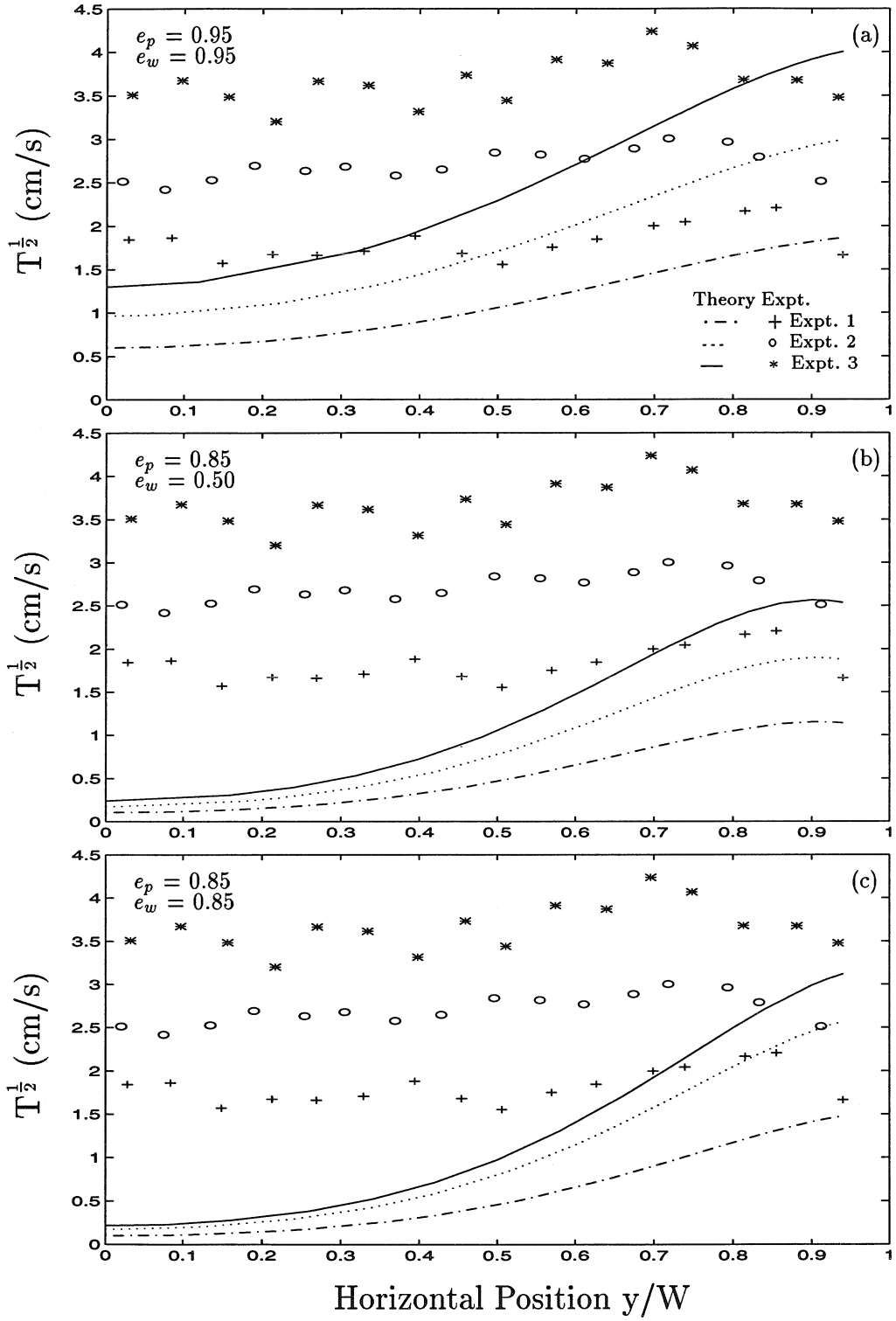


Figure 5.7: Comparison of experimental and theoretical root mean square fluctuation velocity profiles, for values of (a) $e_p = 0.95$, $e_w = 0.95$, (b) $e_p = 0.85$, $e_w = 0.50$, and (c) $e_w = 0.85$, $e_w = 0.85$. W=2.5 cm.

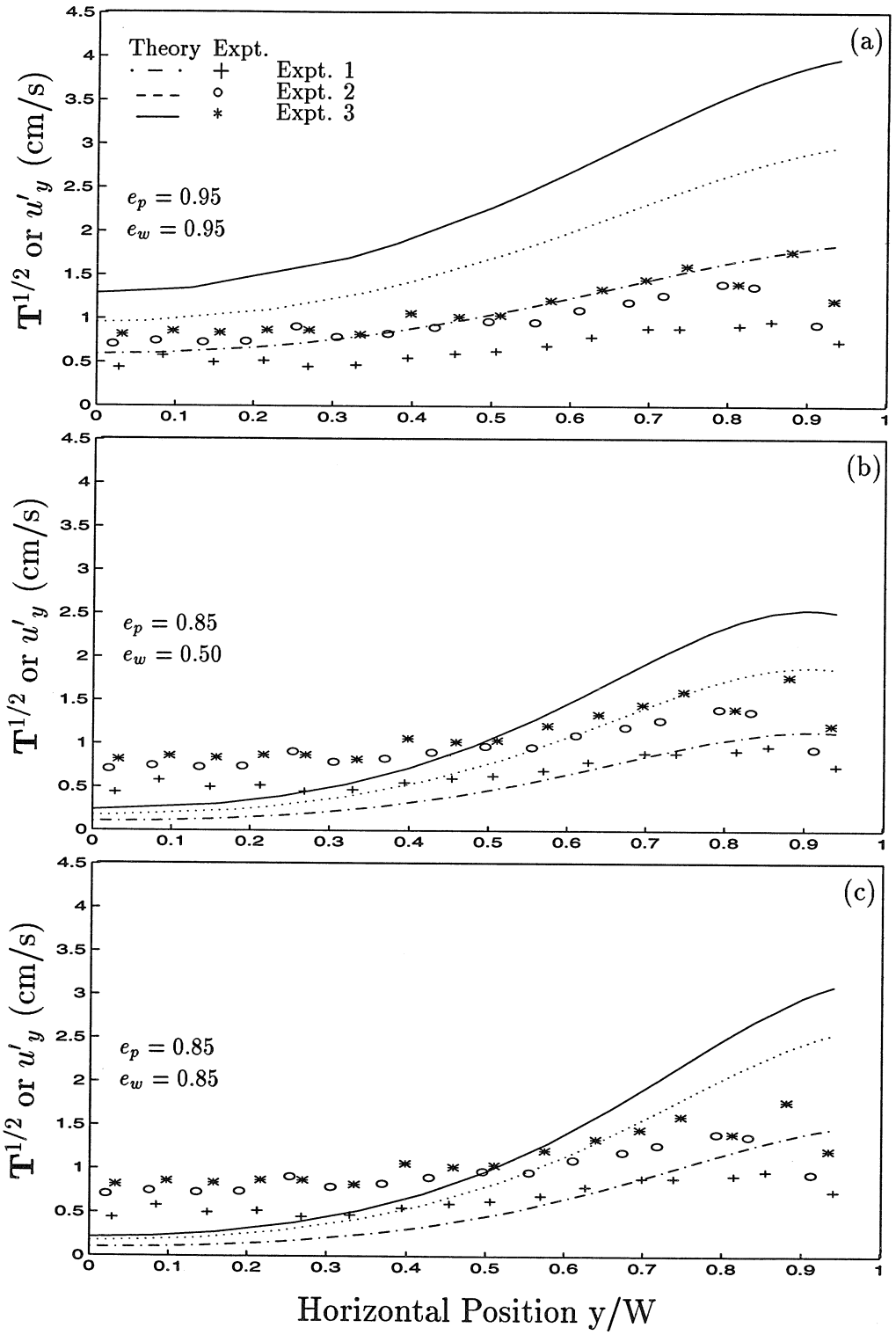


Figure 5.8: Comparison of theoretical root mean square fluctuation velocity profiles with experimental transverse fluctuation velocity profiles for values of (a) $e_p = 0.95$, $e_w = 0.95$, (b) $e_p = 0.85$, $e_w = 0.50$, and (c) $e_w = 0.85$, $e_w = 0.85$. W=2.5 cm.

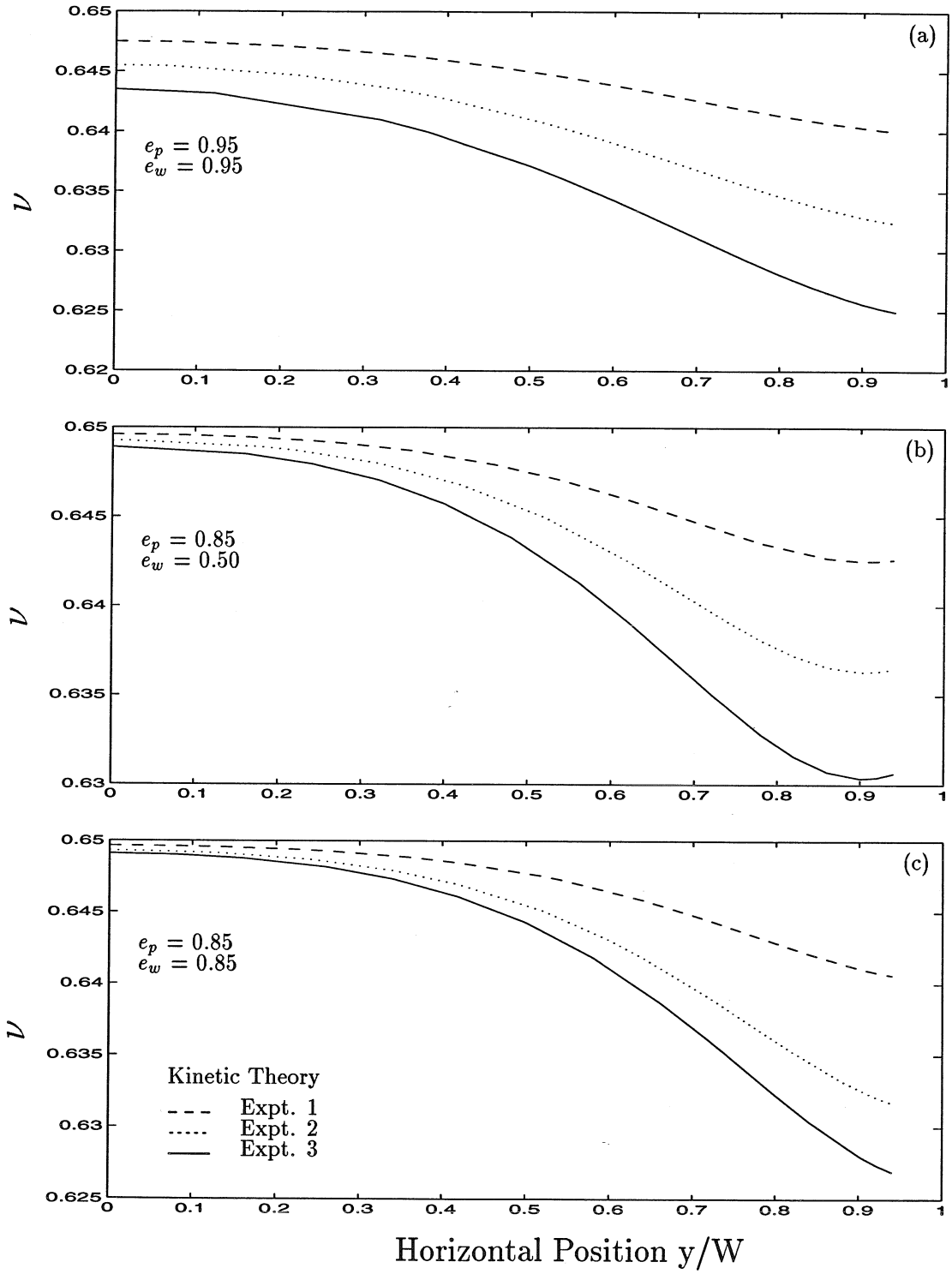


Figure 5.9: Comparison of theoretical solid fraction profiles, for values of (a) $e_p = 0.95$, $e_w = 0.95$, (b) $e_p = 0.85$, $e_w = 0.50$, and (c) $e_w = 0.85$, $e_w = 0.85$. W=2.5 cm.

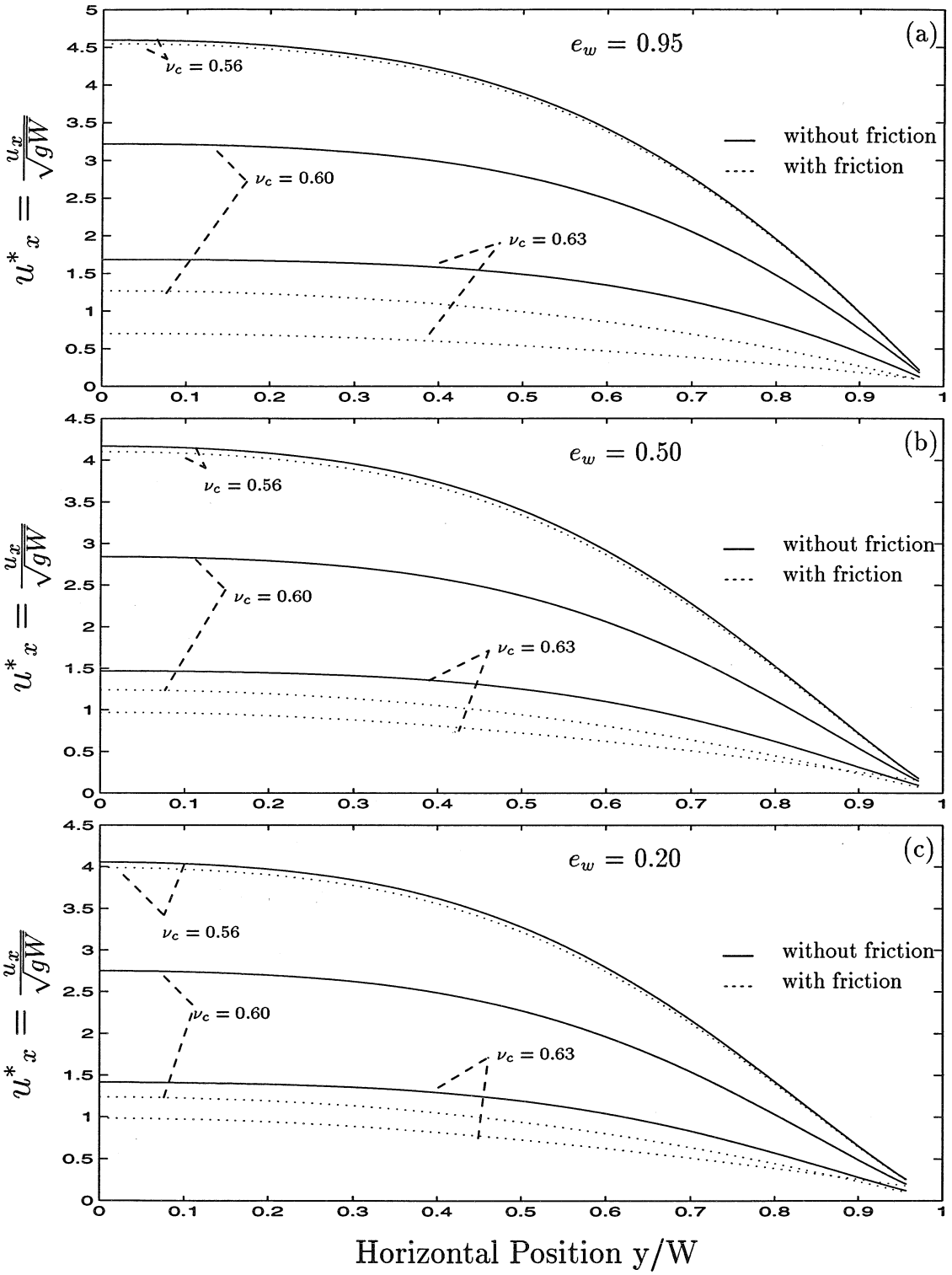


Figure 5.10: Comparison of the theoretical nondimensionalized mean streamwise velocity profiles, with and without the effect of friction, for values of (a) $e_p = 0.95$, $e_w = 0.95$, (b) $e_p = 0.95$, $e_w = 0.50$, and (c) $e_w = 0.95$, $e_w = 0.20$. $\nu_c$ is the centerline solid fraction. W=3.5 cm.

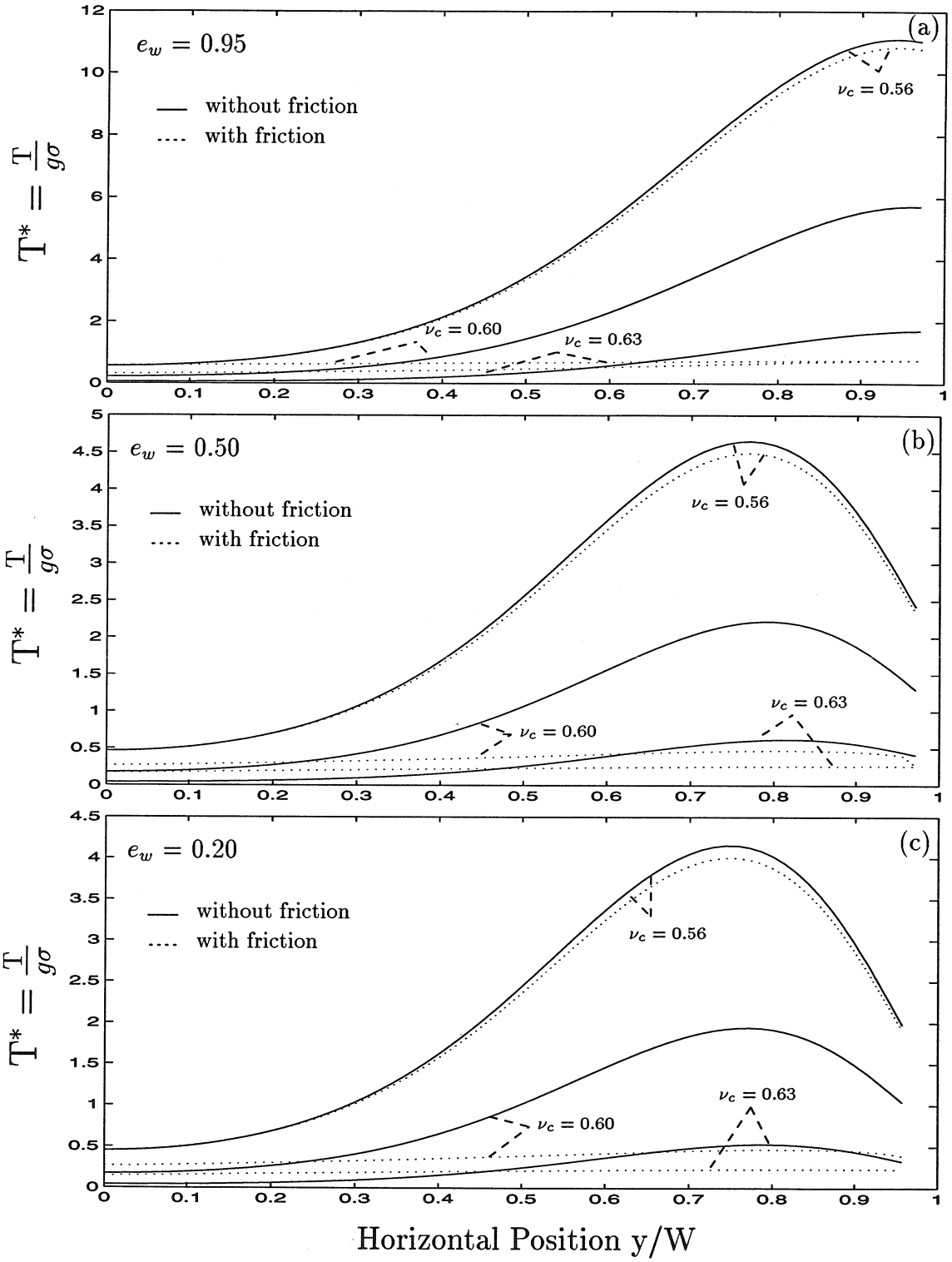


Figure 5.11: Comparison of the theoretical nondimensionalized granular temperature profiles, with and without the effect of friction, for values of (a) $e_p = 0.95$, $e_w = 0.95$, (b) $e_p = 0.95$, $e_w = 0.50$, and (c) $e_w = 0.95$, $e_w = 0.20$. $\nu_c$ is the centerline solid fraction. W=3.5 cm.

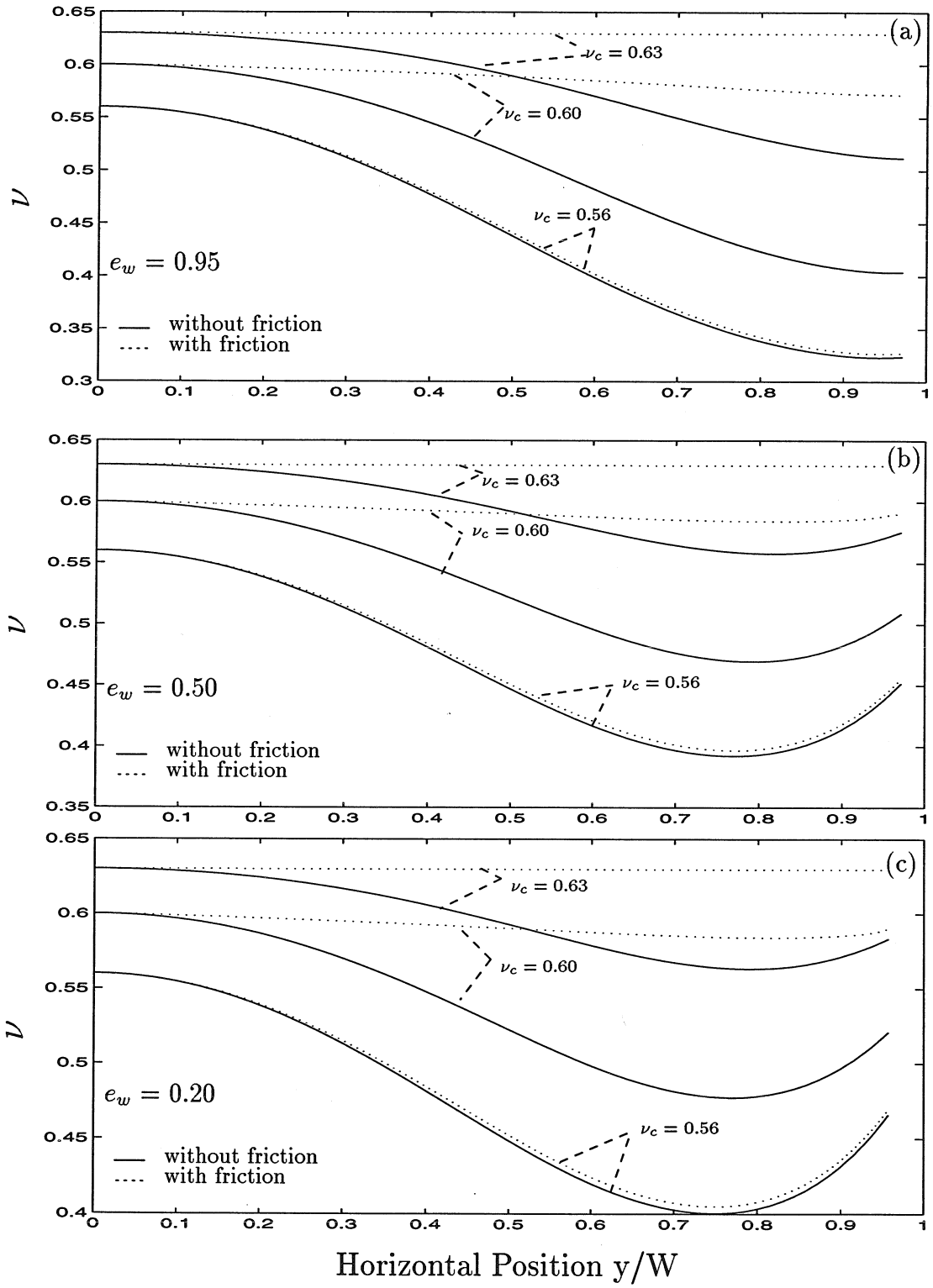


Figure 5.12: Comparison of the theoretical solid fraction profiles, with and without the effect of friction, for values of (a) $e_p = 0.95$, $e_w = 0.95$, (b) $e_p = 0.95$, $e_w = 0.50$, and (c) $e_w = 0.95$, $e_w = 0.20$. $\nu_c$ is the centerline solid fraction. W=3.5 cm.

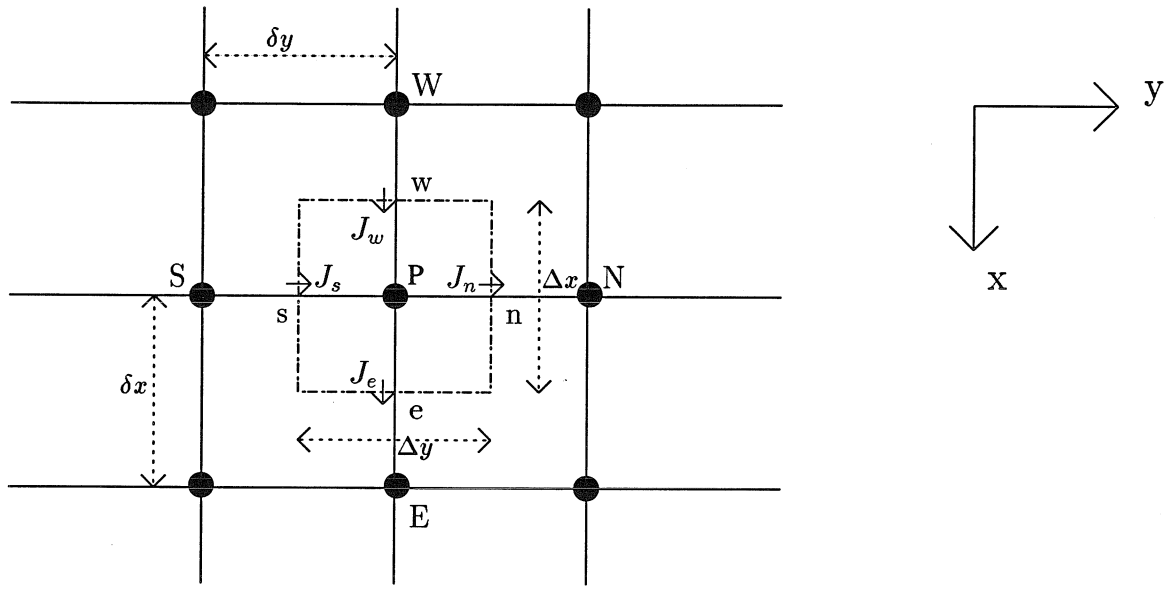


Figure 5.13: Notation for the finite-difference grid utilized to solve the energy equation.

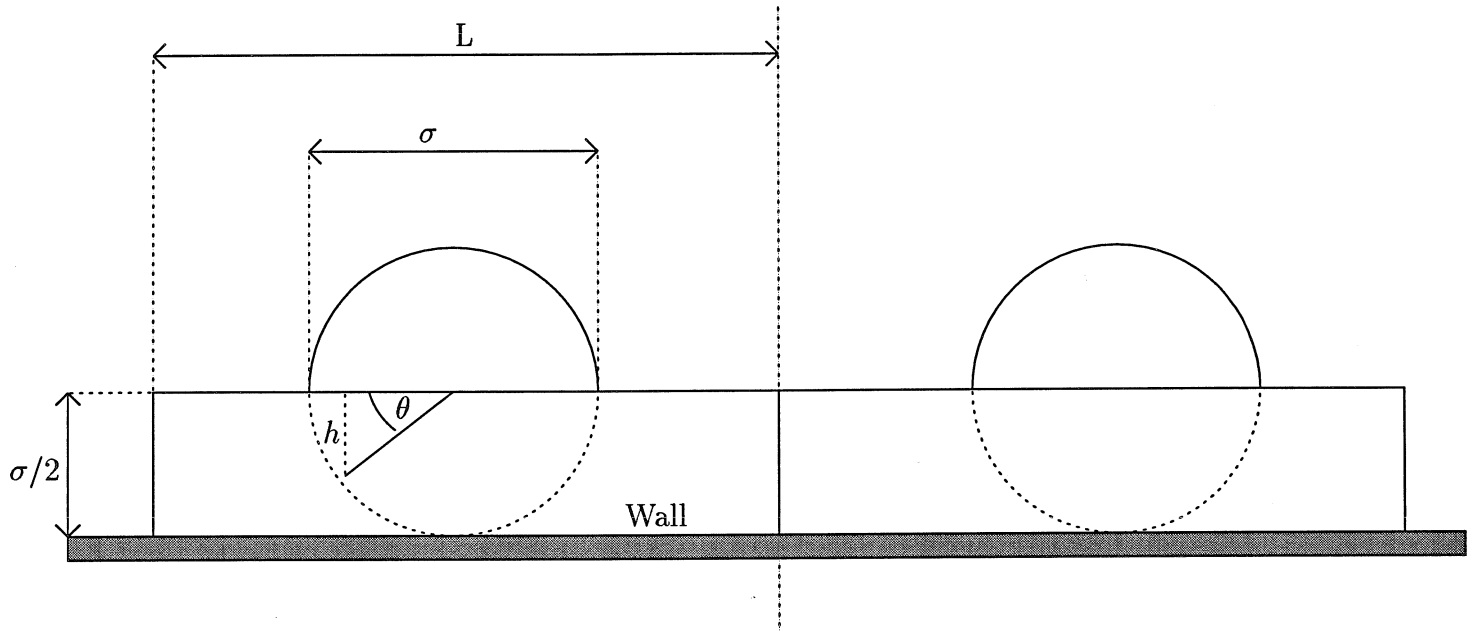


$$\nu_{\sigma/2} = \frac{\pi\sigma}{4\mathrm{L}}$$

At a distance $h$ from the particle centerline, the solid fraction is given by

$$\nu = \frac{\pi(\sigma/2)^2}{2\mathrm{L}(\sigma/2)}\cos\theta \qquad = \nu_{\sigma/2}\left(1 - \left(\frac{h}{\sigma/2}^2\right)\right)$$

Figure 5.14: Schematic for the assumed functional form of the solid fraction near the wall.

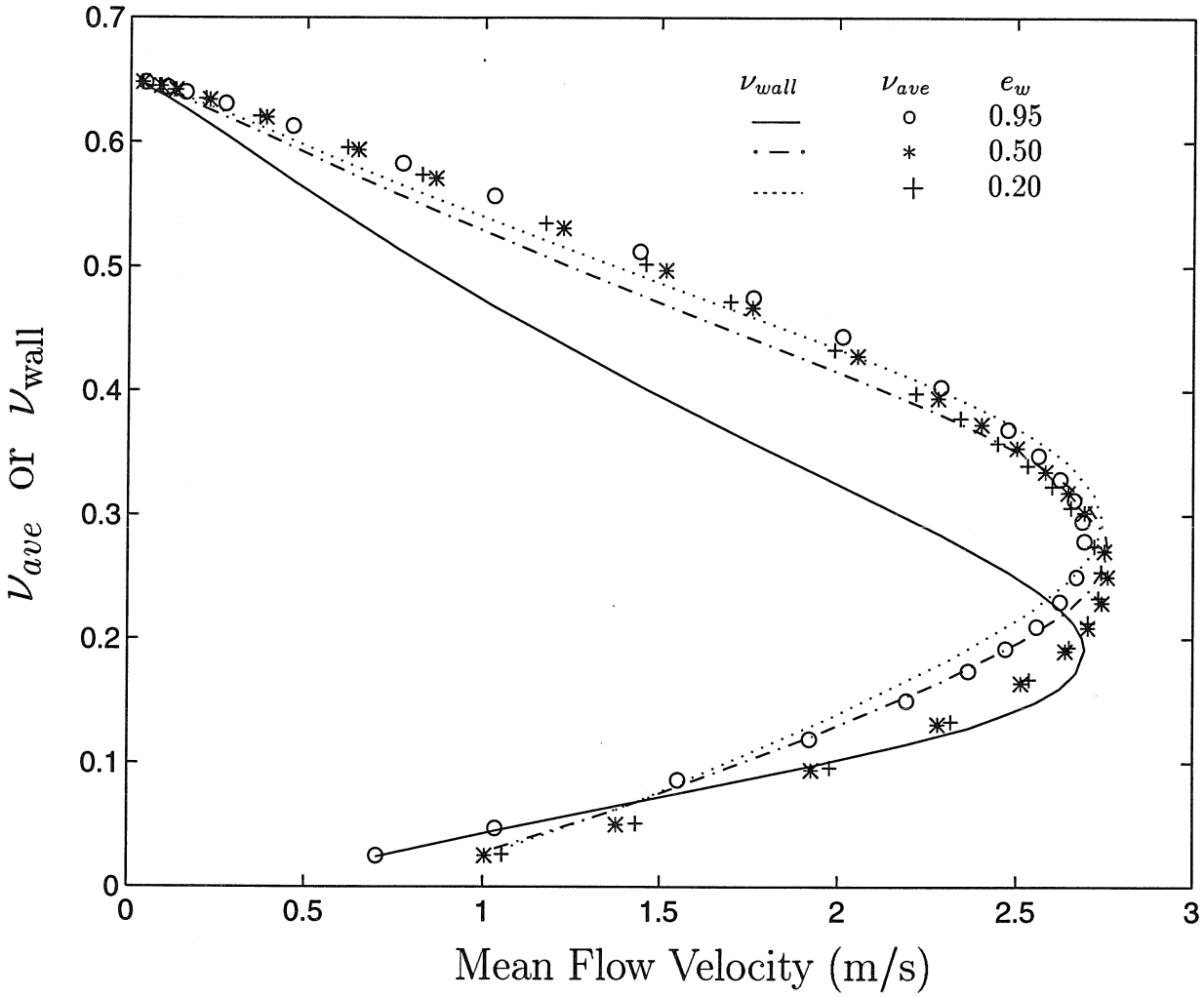


Figure 5.15: Variation of the theoretical mean solid fraction ($\nu_{ave}$) and the solid fraction at the wall ($\nu_{wall}$) with the mean flow velocity. $e_p = 0.95$. Note that both symbols and lines in the figure represent numerically calculated values and do not represent experimental data.

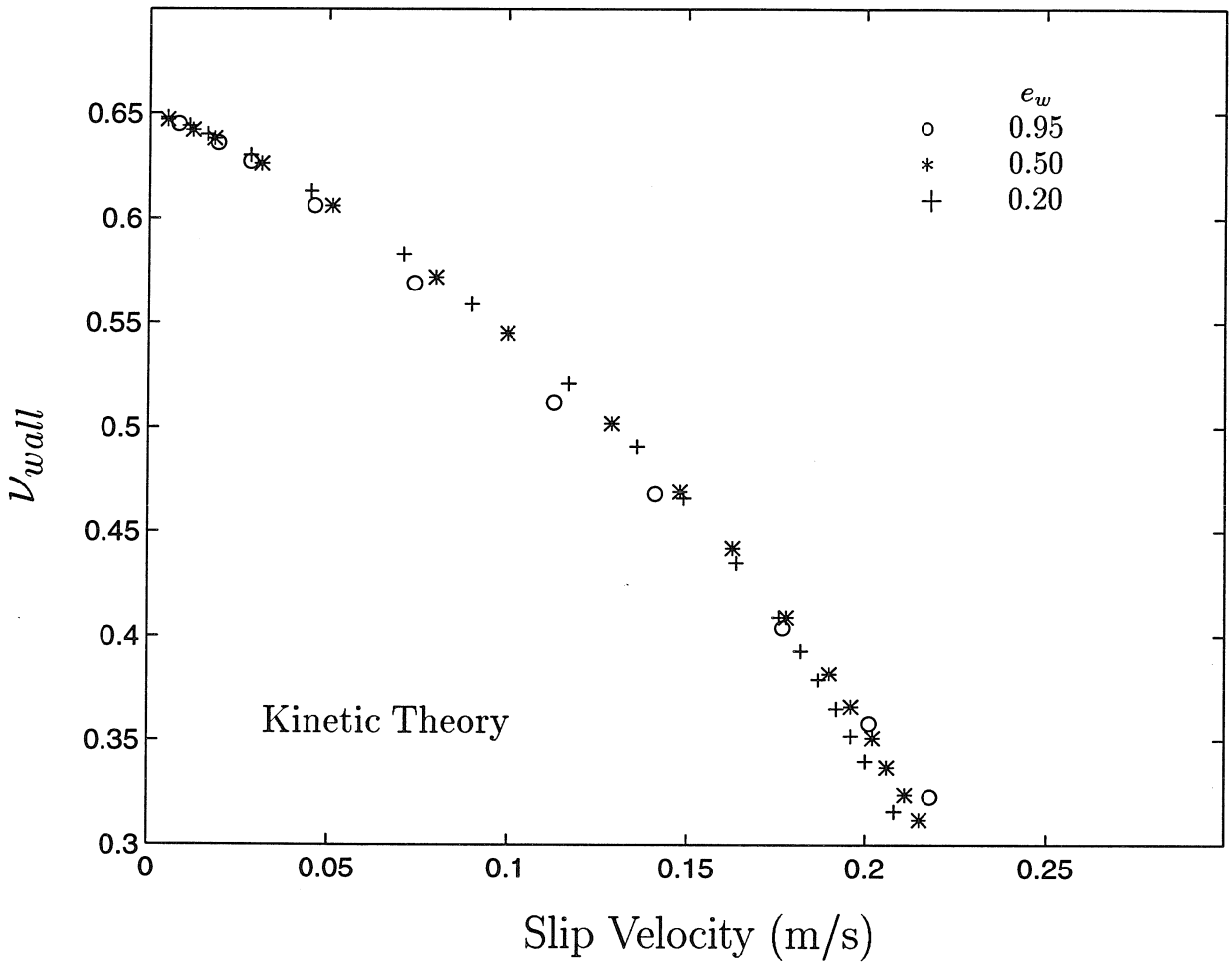


Figure 5.16: Variation of the theoretical solid fraction at the wall ($\nu_{wall}$) with the flow slip velocity. $e_p = 0.95$. Note that the symbols in the figure represent numerically calculated values and do not represent experimental data.

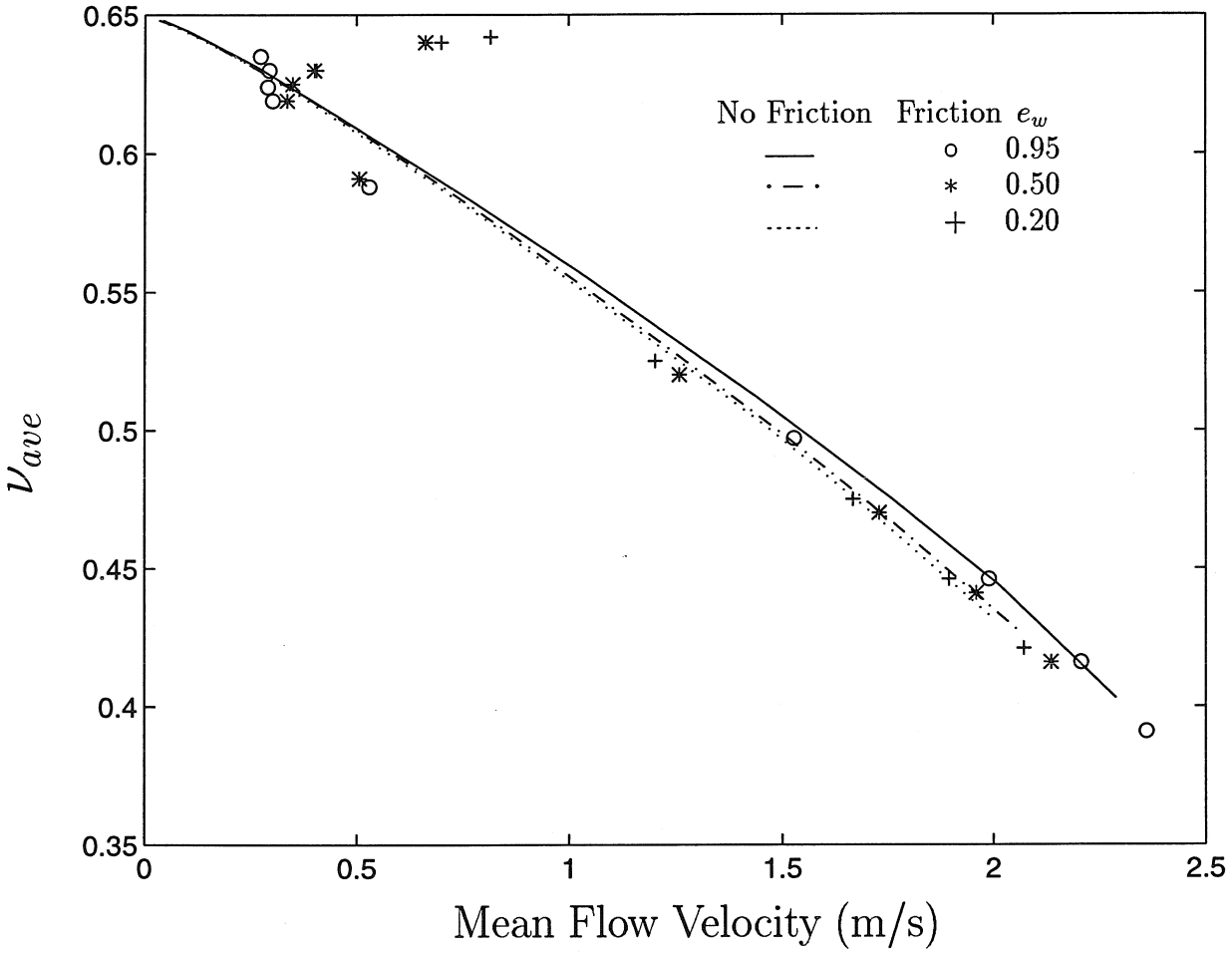


Figure 5.17: Comparison of the variation of the theoretical mean solid fraction ($\nu_{ave}$) with the mean flow velocity, with, and without, the effect of friction. $e_p = 0.95$. Note that both symbols and lines in the figure represent numerically calculated values and do not represent experimental data.

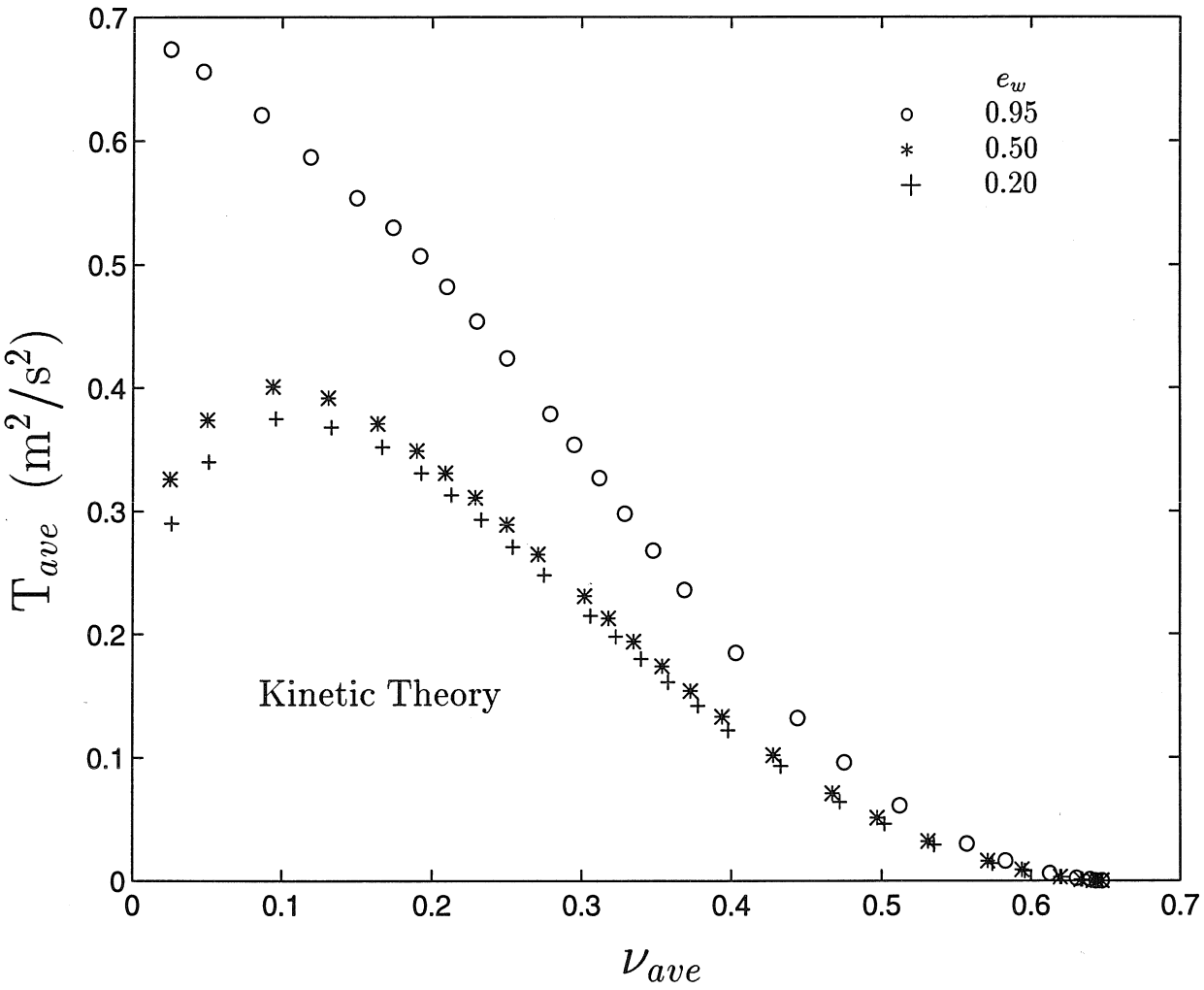


Figure 5.18: Variation of the theoretical average granular temperature with the average solid fraction ($\nu_{ave}$). $e_p = 0.95$. Note that the symbols in the figure represent numerically calculated values and do not represent experimental data.

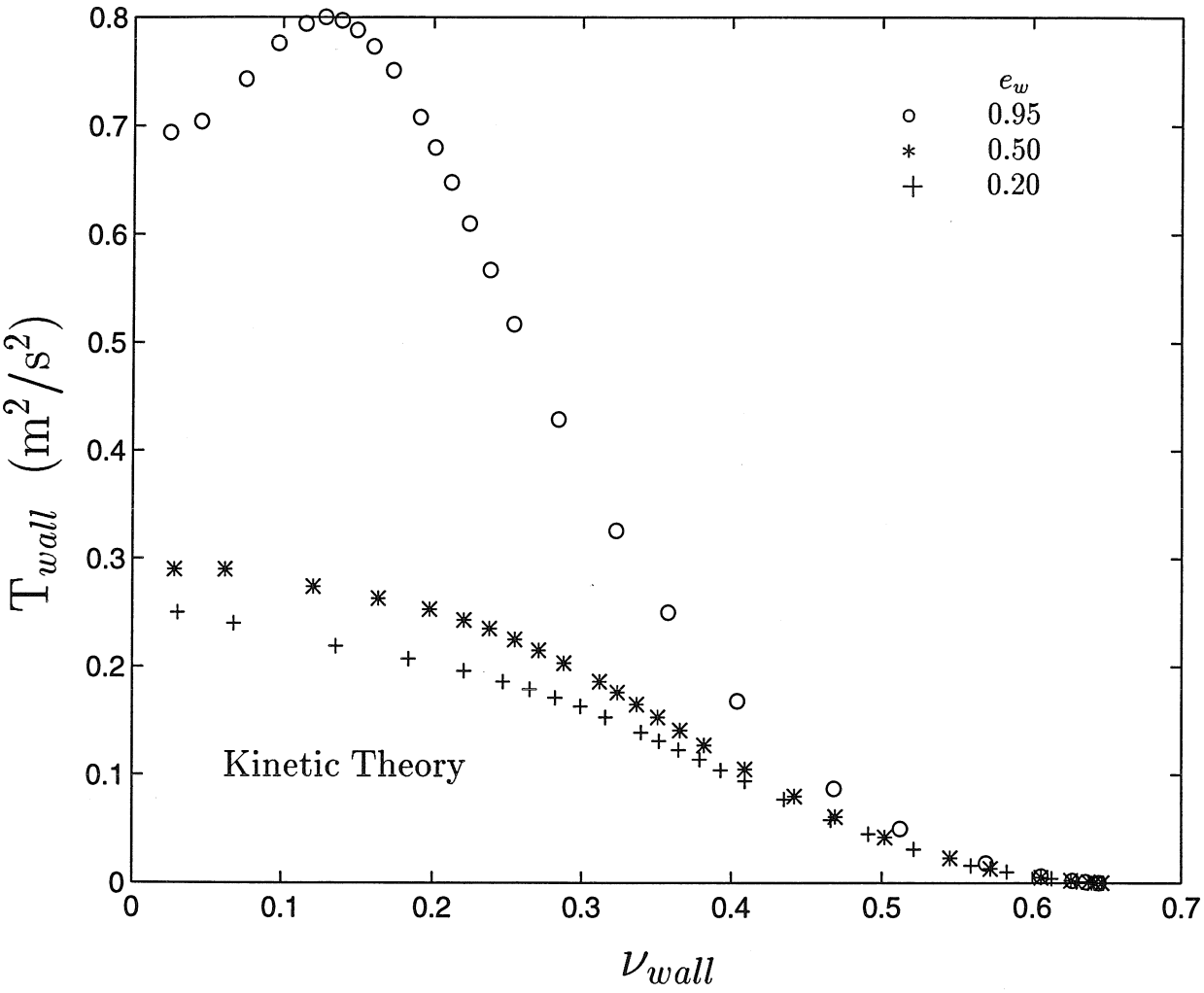


Figure 5.19: Variation of the theoretical wall granular temperature with the wall solid fraction ($\nu_{wall}$). $e_p = 0.95$. Note that the symbols in the figure represent numerically calculated values and do not represent experimental data.

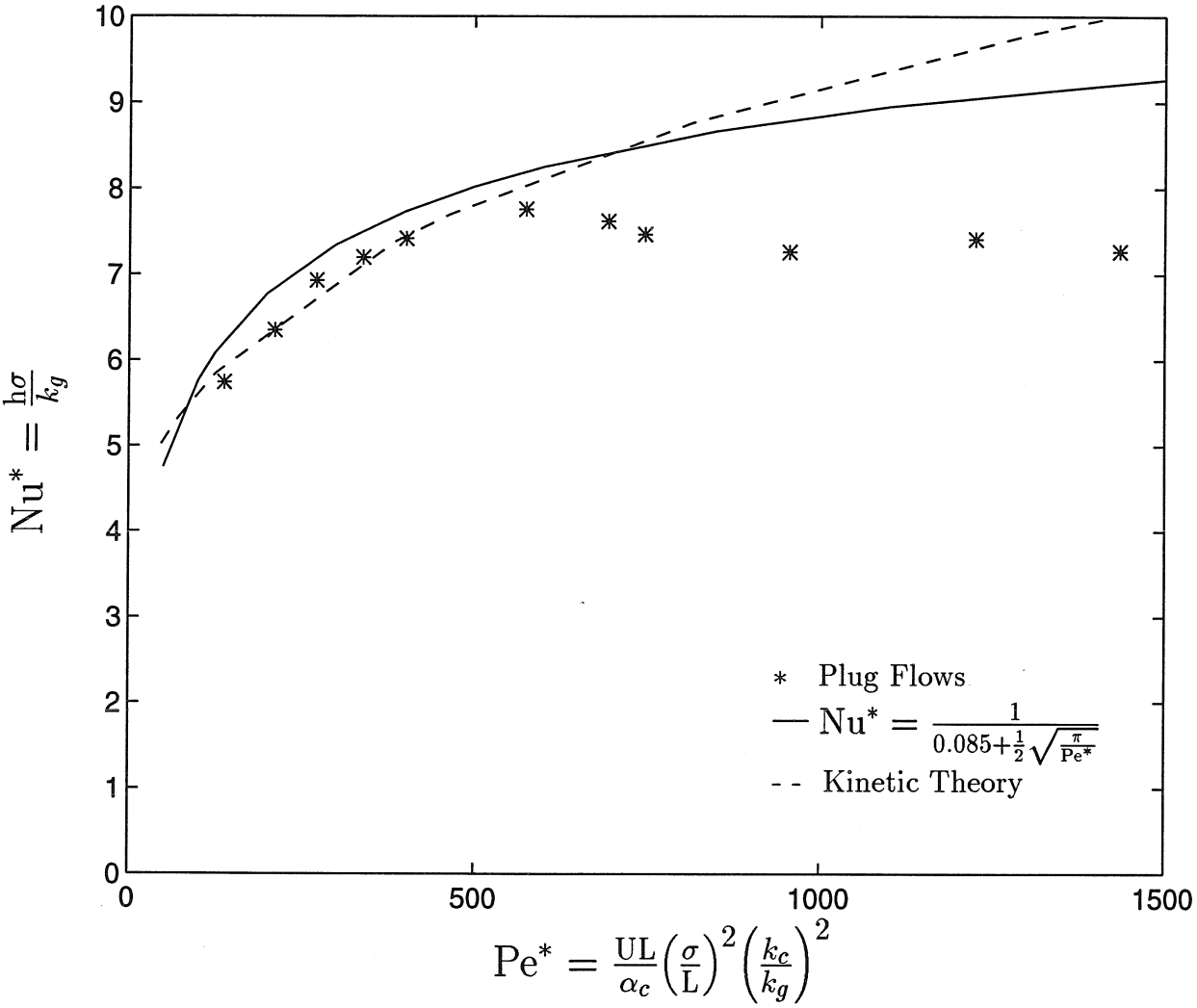


Figure 5.20: Variation of Nu* with Pe*. Comparison of the measured data for plug flows with the semi-empirical Sullivan & Sabersky relation and the numerical calculations based on kinetic theory. $\sigma = 3$ mm. $e_p = 0.95$, $e_w = 0.50$ and $\phi' = 0.025$ for the kinetic theory solution.

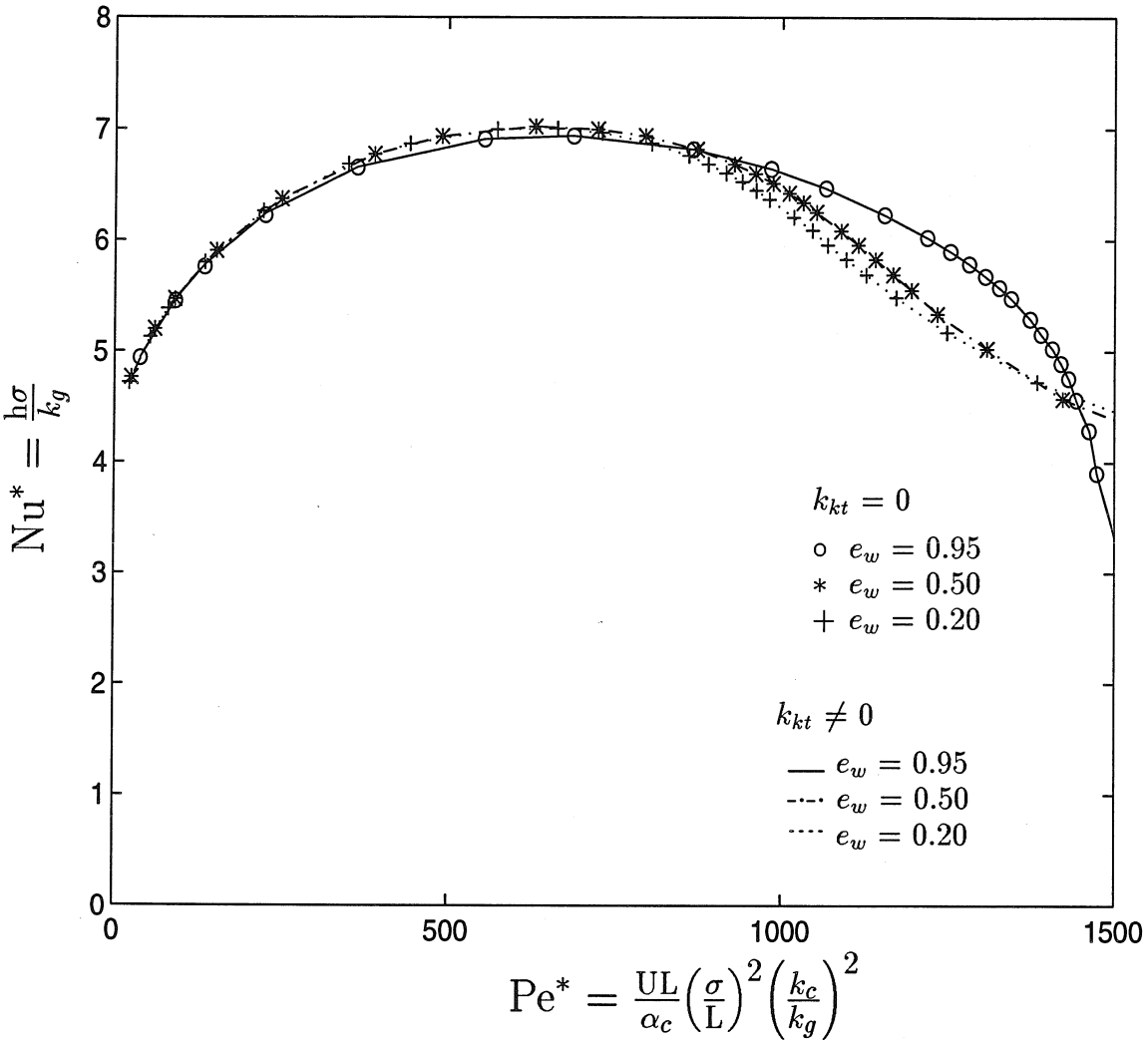


Figure 5.21: Variation of $\mathrm{Nu}^*$ with $\mathrm{Pe}^*$. Comparison of the theoretical solutions with, and without, the influence of the kinetic conductivity ($k_{kt}$) contribution. $\sigma = 3$ mm. $e_p = 0.95$. Note that both the symbols and lines in the figure represent numerically calculated results and do not represent experimental data.

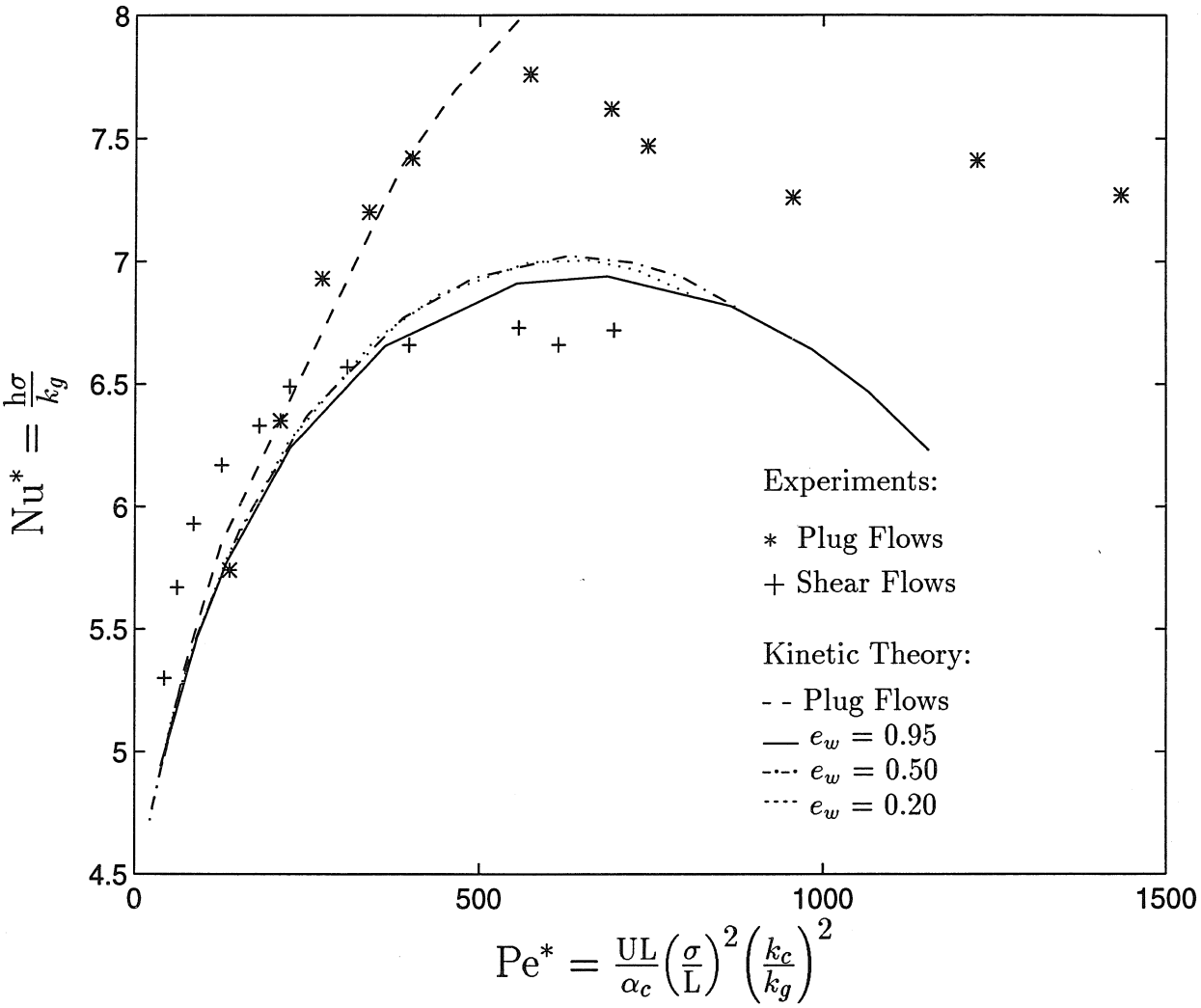


Figure 5.22: Variation of Nu* with Pe*. Comparison of the experimentally measured data for plug and shear flows with numerically calculated results. $\sigma = 3$ mm. $e_p = 0.95$.

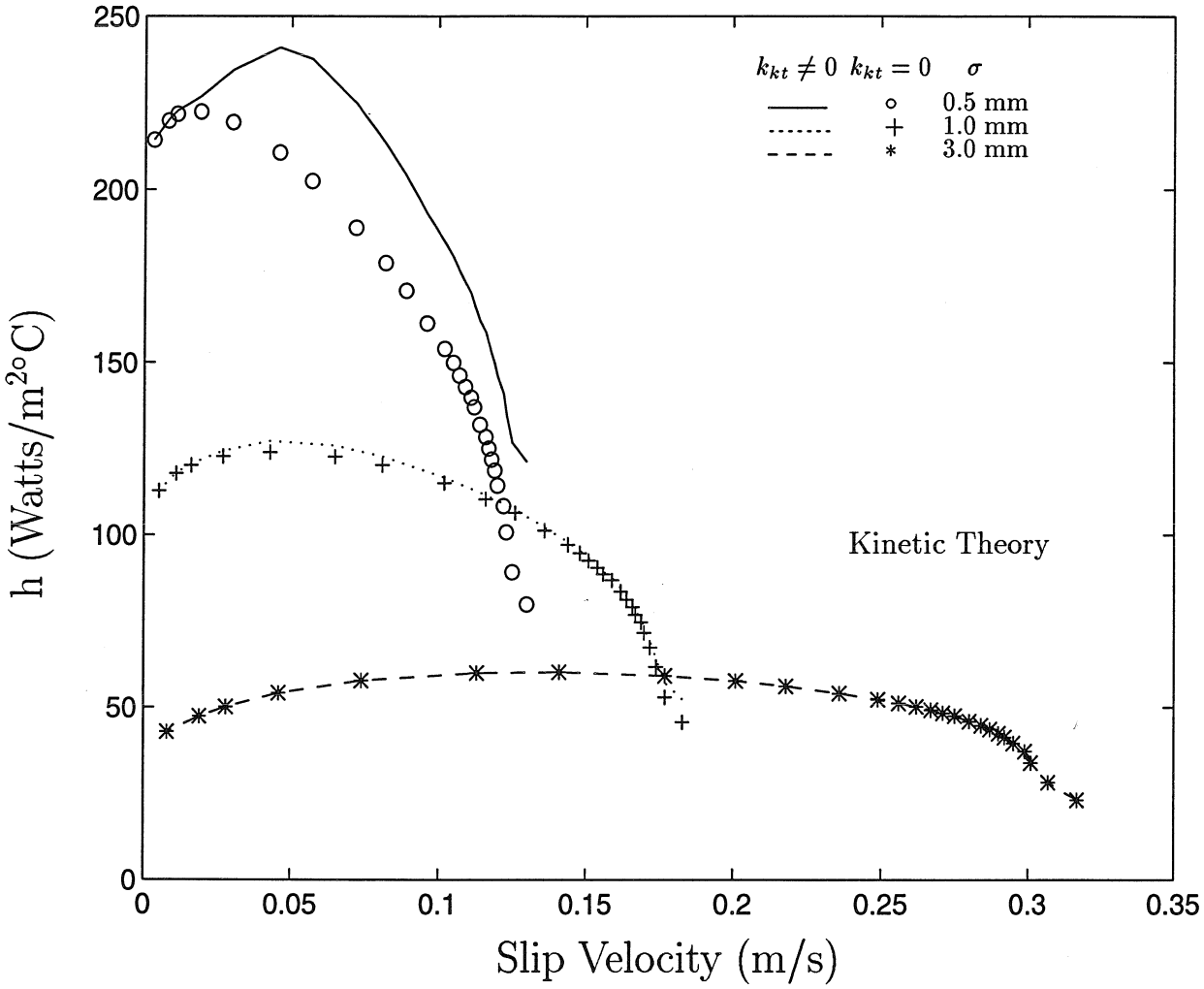


Figure 5.23: Variation of the heat transfer coefficient with flow slip velocity. Comparison of the influence of particle diameter on the heat transfer coefficient. $e_p = 0.95$. Note that both the symbols and lines in the figure represent numerically calculated results and do not represent experimental data.

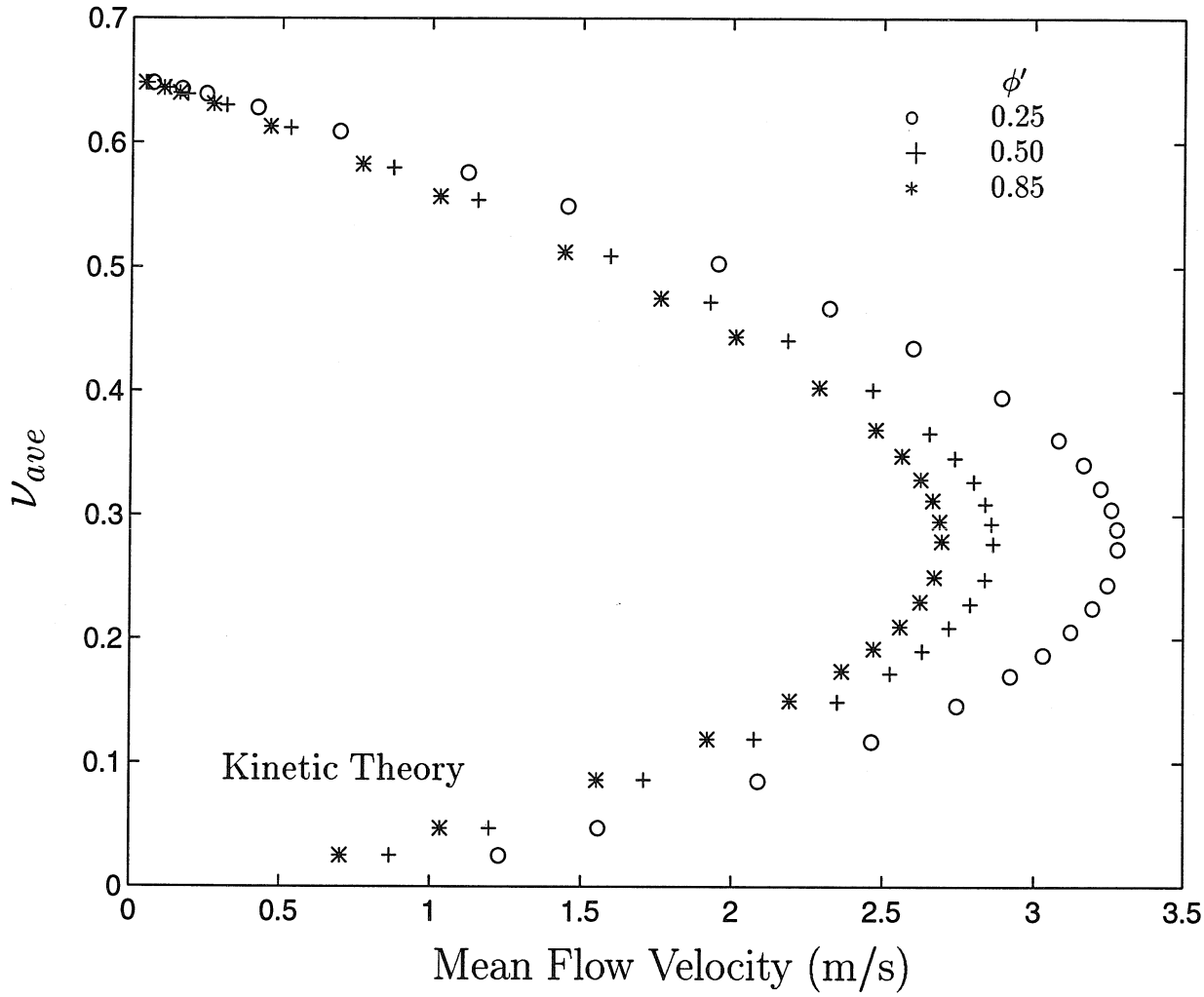


Figure 5.24: The effect of varying the value of the specularity coefficient $\phi'$ on the variation of the average solid fraction ($\nu_{ave}$) with the mean flow velocity. $e_p = 0.95$, $e_w = 0.50$. Note that the symbols in the figure represent numerically calculated results and do not represent experimental data.

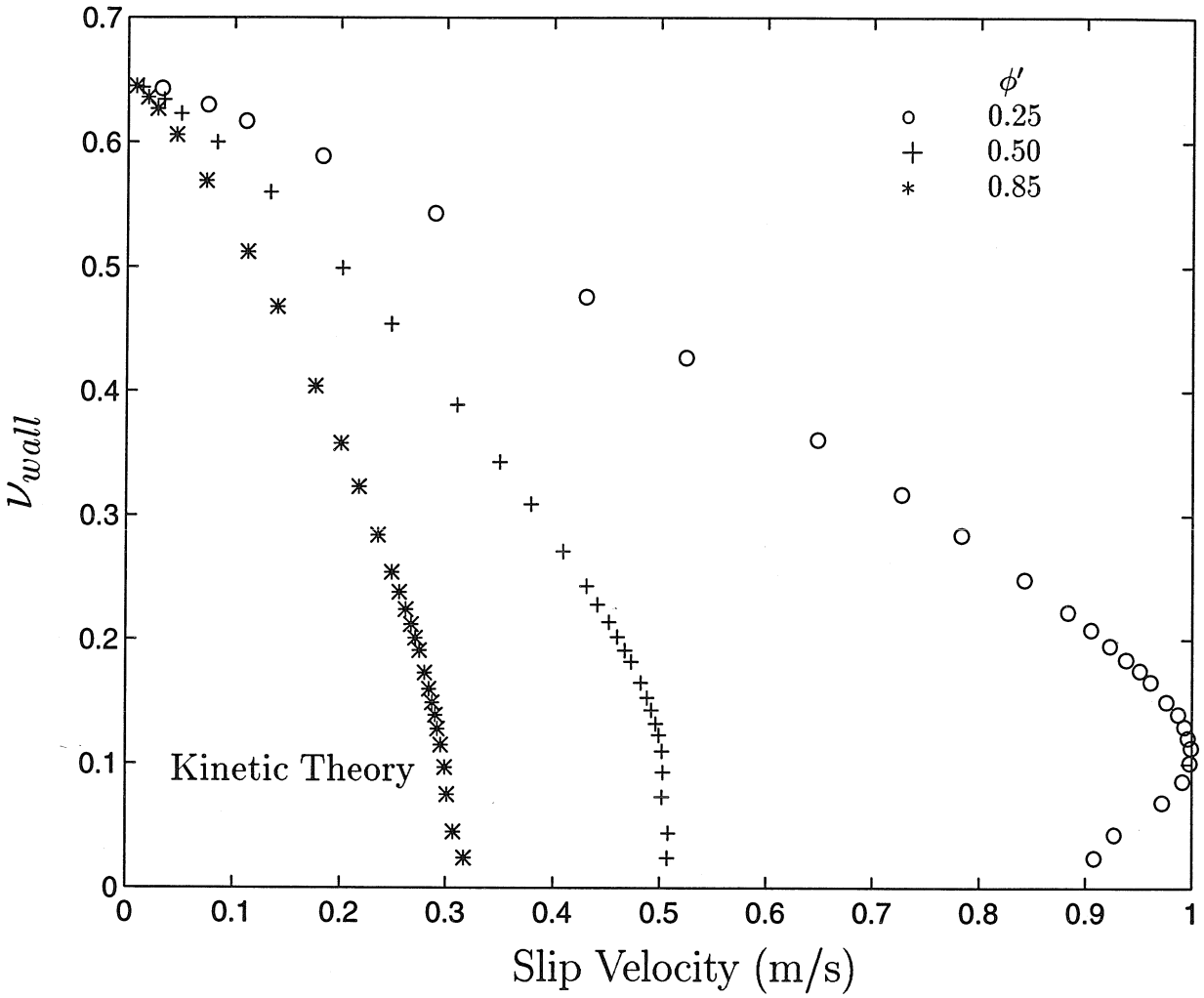


Figure 5.25: The effect of varying the value of the specularity coefficient $\phi'$ on the variation of the wall solid fraction ($\nu_{wall}$) with the flow slip velocity. $e_p = 0.95$, $e_w = 0.50$, $\sigma = 3$ mm. Note that the symbols in the figure represent numerically calculated results and do not represent experimental data.

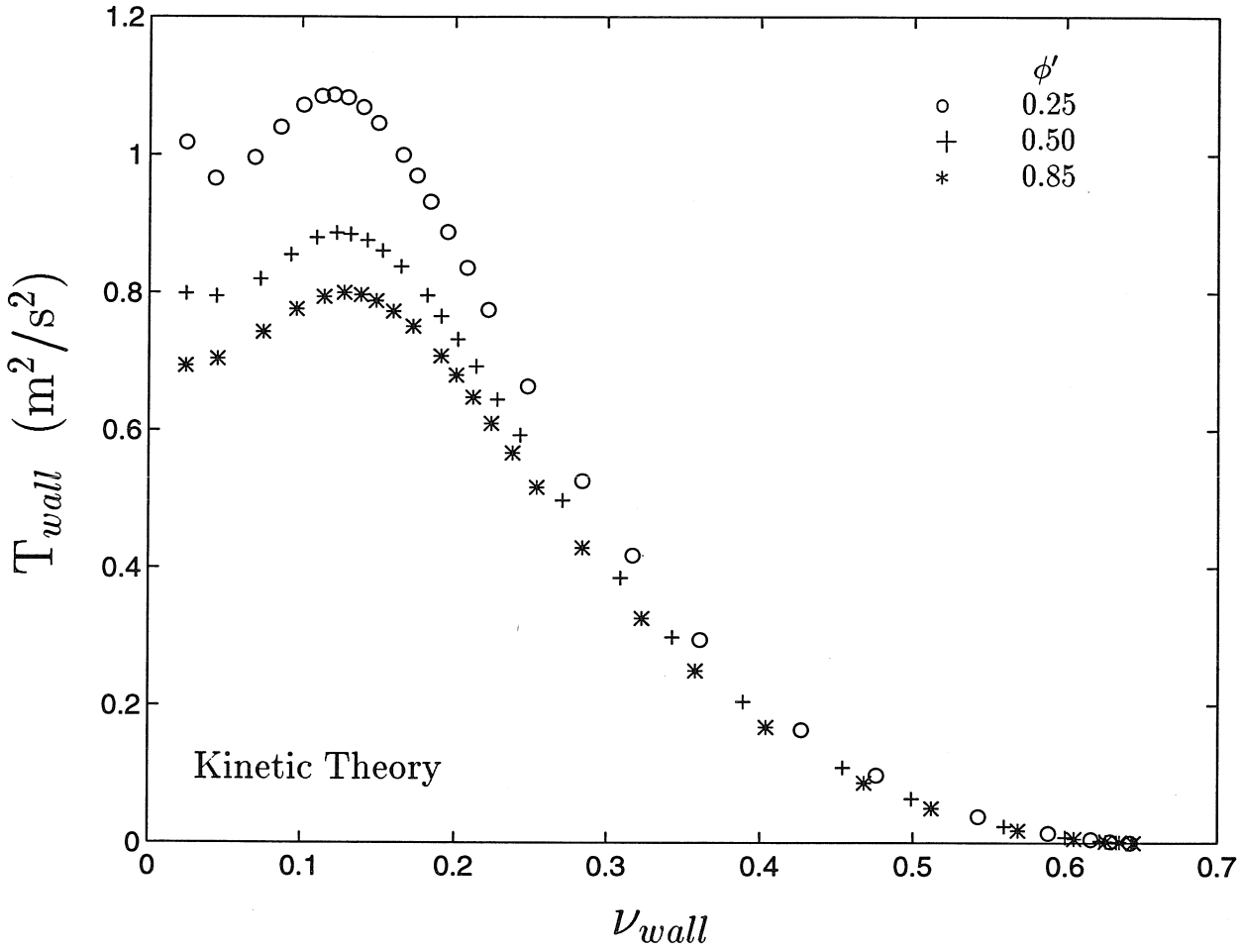


Figure 5.26: The effect of varying the value of the specularity coefficient $\phi'$ on the variation of the wall granular temperature with wall solid fraction ($\nu_{wall}$). $e_p = 0.95$, $e_w = 0.50$, $\sigma = 3$ mm. Note that the symbols in the figure represent numerically calculated results and do not represent experimental data.

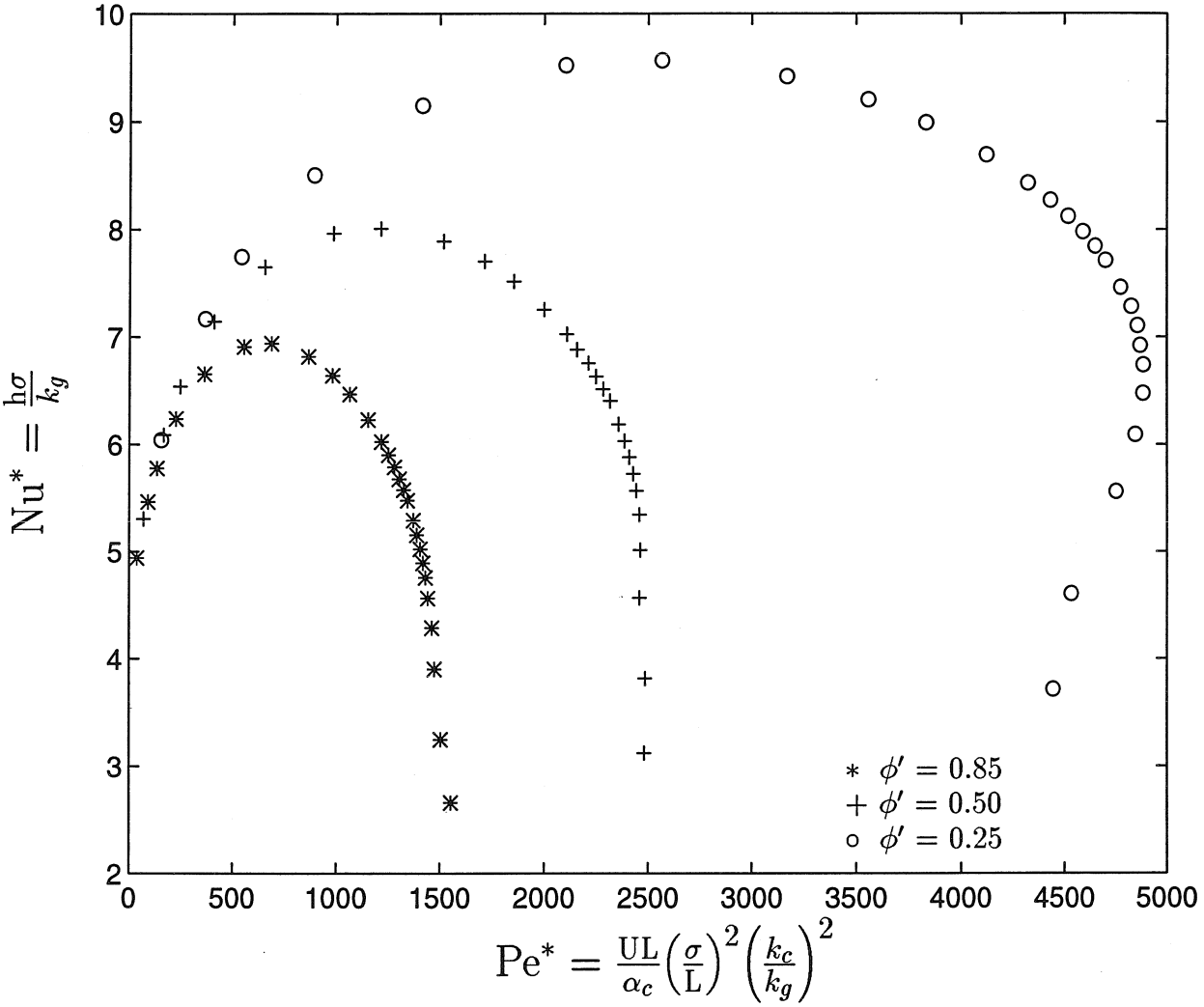


Figure 5.27: The effect of varying the value of the specularity coefficient $\phi'$ on the variation of $\mathrm{Nu}^*$ with $\mathrm{Pe}^*$. $e_p = 0.95$, $e_w = 0.50$, $\sigma = 3$ mm. Note that the symbols in the figure represent numerically calculated results and do not represent experimental data.

# Chapter 6 Conclusions

## 6.1 Summary of Results

The current work sought to make local measurements, at the level of individual particle motions, in order to determine mean and fluctuation velocity profiles as well as diffusion coefficients in granular material flows. Experiments were performed using 3 mm diameter glass particles in a vertical rectangular channel. Three different types of particles were used in order to examine the effect of particle surface properties on the velocity profiles and on diffusive behavior. The effect of the boundary surface on such flows was investigated through the use of smooth and rough walls. The smooth walls had surfaces made of highly polished glass, in the case of the self-diffusion experiments, and of aluminum in the case of the heat transfer experiments. The rough wall conditions were achieved by gluing particles of 3 mm diameter to the wall in a hexagonal close-packed pattern. Highly polished glass was used for the front and rear walls to reduce frictional interactions at these surfaces and to approximate a two-dimensional flow situation.

Image-processing methods were used to measure the mean and fluctuation velocity profiles. For the sheared flows, three mean flow rates were examined for each particle type. From the velocity profiles and the diffusive behavior, three flow regimes were identified for each sheared flow: a central uniform-flow regime, a low-shear transition regime, and an outer moderate-shear regime. In the case of the flows with smooth walls, the flow velocities and densities were essentially uniform across the entire flow section. The measurements showed that for the sheared flows, the fluctuation velocities were anisotropic with the streamwise components being about 2 to 2.5 times

the transverse components. The transverse fluctuation velocity components showed a greater dependence on the shear rates than the streamwise components. Both components of the fluctuation velocity increased with the flow rate. For comparable shear rates, the fluctuation velocities were lower in the case of rough particles, indicating a damping of the random translational fluctuation energy due to friction. In all the sheared flows, visual observations indicated that the solid fraction decreased from the center towards the walls. The magnitudes of the fluctuation velocities in the case of the flows with smooth walls were significantly lower than those in the comparable flows with rough walls.

The image-processing techniques were extended to enable the tracking of individual tracer particles for reasonable durations. The particle displacement-time histories obtained as a result, were averaged to obtain self-diffusion coefficients in both the streamwise and transverse directions. The diffusion coefficients increased with shear rate and fluctuation velocity. However, the proportionality factors depended on the shear regime. The diffusion coefficients were anisotropic, with the values in the streamwise direction being an order-of-magnitude higher. Finite fluctuation velocities and diffusive displacements were observed in the central uniform regime, in the case of the sheared flows. However, for the flows with smooth walls, the diffusion coefficients were negligibly small. Visual observations as well as the measured values indicated that the diffusive behavior depended on the solid fraction. There was a reduction in the diffusion coefficients for the case of the rough particles, because of the friction damping of the translational fluctuation energy and the associated agglomeration of the particles.

A series of experiments were performed to measure the effect of shear, and the resultant mixing of particles, on heat transfer coefficients in granular flows in a vertical channel. Two types of wall conditions were used, a smooth condition to generate uniform plug flows and a rough wall condition to generate non-uniform sheared flows.

Velocity fields were measured using image processing techniques. The results of the experiments with the smooth walls showed remarkable agreement with Sullivan & Sabersky's (1975) semi-empirical model for values of $Pe^*$ less than 600, but deviated from the model at higher values of $Pe^*$. This deviation was believed to be caused by the dilation and the accompanying decrease in bulk thermal conductivity close to the wall, at higher flow rates. For both sets of experiments, once the maximum value had been reached, the value of $Nu^*$ became essentially invariant for further increases in the flow velocity adjacent to the heated wall over the range of velocities examined. This result was contrary to the findings of Patton et al. (1986) and Ahn (1989) who observed a continued decrease in $Nu^*$ with increasing $Pe^*$, beyond the maximum. A comparison of the experimental observations for the sheared and plug flows indicated that at lower flow rates, values of the average heat transfer coefficients were higher for the sheared flows for comparable values of flow velocity close to the wall. This phenomenon was attributed to the fact that the sheared flows displayed significant particle agitation close to the walls and it was believed that this enhanced heat transfer by increasing thermal mixing within the boundary layer. However, at higher flow rates, the dilation close to the wall became a dominant factor and reduced the bulk conductivity significantly. Consequently, for higher values of $Pe^*$, values of $Nu^*$ were higher for the plug flows than for the sheared flows.

Theoretical solutions, based on a combination of the dense-gas kinetic theory and an empirical friction model, were generated to study and compare experimental and theoretical results for velocity profiles and heat transfer characteristics in granular flows in a vertical chute. Calculated mean velocity profiles were found to be in very good agreement with experimental data for three different combinations of $e_p$ and $e_w$. The theoretical solutions, in these cases, were all for solid fractions in the range of 0.64-0.65. However, in the actual experiments, there were distinct sheared regimes where the solid fractions were lower than the close-packed value. Also, the theoretical

profiles for the granular temperature showed a much stronger dependence on the shear rate than was evident in the experimental data. Furthermore, because of the assumptions of isotropy in the granular temperature, the kinetic theory results were unable to replicate the anisotropic distribution of the fluctuation velocities observed experimentally.

The effect of frictional stresses was investigated by comparing thoeretical solutions including the frictional stress components with solutions in which the frictional contributions were suppressed. It was observed that the presence of frictional interactions reduced granular temperature and increased solid fraction over most of the solid fraction range where frictional interactions were expected to exist. However, for high solid fractions, because of the limitations of the empirical frictional model, unphysical results were observed in the form of increased values for the granular temperature. Also, the extremely high frictional stresses predicted by the friction model, coupled with a high sensitivity to minute changes in the solid fraction made it difficult to obtain convergent solutions for flows with solid fraction values greater than 0.63. The theoretical studies also investigated the effect of varying the value of $e_w$. Lowering the value of $e_w$ increased the dissipation of the fluctuation energy at the wall, leading to decreased values for the granular temperature and increased solid fractions due to inelastic clumping.

The theoretical solutions were extended to the convective heat transfer problem by solving the energy equation for the entire flow field assuming the total thermal conductivity to be the simple sum of a bulk molecular component and a kinetic component arising out of the streaming motion of the particles. Solutions were generated for both plug and sheared flows. Solutions for the plug flows, obtained by assuming a value of 0.01 for $\phi'$, provided values of Nu* that were in good agreement with experimental data and the Sullivan- Sabersky model up to a value of Pe* $\approx$ 600. For higher values of Pe*, the theoretical solutions predicted values for Nu* that were higher than

those observed in the experiments.

Three combinations of $e_p$ and $e_w$ were investigated in order to examine the convective heat transfer behavior in sheared granular flows. For all three cases, the profiles of $Nu^*$ versus $Pe^*$ were found to exhibit a maximum for $Nu^*$, qualitatively similar to the experimental data of Patton et al. (1986) and Ahn (1989). However, the theoretical solutions were unable to replicate the invariance of the value of $Nu^*$ beyond the maximum, for increasing values of $Pe^*$ as observed in the experiments. Also, the theoretical solutions could not replicate the shear induced enhancement of the heat transfer coefficient observed experimentally for values of slip velocities less than 4 cm/s. It was found that the value of $e_w$ did not significantly affect the value of the heat transfer coefficients. The values of the heat transfer coefficients were found to decrease significantly with an increase in the value of the specularity coefficient $\phi'$. Rougher walls lead to reduced values of solid fraction adjacent to the heated wall, thereby increasing the effective thickness of the interstitial fluid layer adjacent to the wall.

In order to investigate the influence of the streaming conductivity component on the heat transfer coefficients, comparisons were made amongst solutions generated for three different particle sizes. The results indicated that the streaming component became more significant as the particle size decreased.

## 6.2 Comments on General Issues

The experimental and theoretical studies performed in this thesis provided significant insights about mixing phenomena in granular flows. However, during the course of this work, several constraints and limitations in the experimental and theoretical models were identified and have been discussed at different places in the text. In this section, an attempt is made to place these issues in a broader perspective pertaining

to the study of granular materials in general.

### 6.2.1 Limitations Imposed by Experimental Constraints

The nature of a granular flow imposes strong constraints on the ability to make precise and representative measurements of velocity and density profiles. Unlike the case for fluids, the finite size of the particles makes it impossible to introduce probes into the flow without disturbing the flow field in the vicinity of the probe. The expense or complexity of non-intrusive measurement techniques like Magnetic Resonance Imaging makes video imaging of the flow surfaces a preferred method for making local measurements of the mean and fluctuation velocity fields. The method followed in this work was to film the flows using a commercial video camera. Image processing methods were then used to determine the position of tracer particles in successive image frames, and velocity components in two directions were determined by dividing the particle dispacements by the time between successive frames.

Some of the major constraints in this measurement technique were those imposed by the limitations of the camera-framegrabber system. The two important factors that determine the capabilities of such a system are the camera frame-rate and the camera resolution. Ideally, a high frame rate and a high resolution (or pixels per particle diameter) are desirable in order to improve the quality of the measurements. However, in reality, there is always a trade-off between the two factors. In the current set of experiments, a frame rate of 30 fps was used. As a result, it was not possible to investigate flows at speeds greater than 30 cm/s because, at higher velocities, a tracer was not visible in more than one frame. Increasing the field of camera vision in order to obtain a tracer's image in at least two successive image frames reduced the resolution significantly. Also, higher frame rates are desirable for more rapid granular flows where the frequency of collisions is very high and higher values of the fluctuation velocity occur. Of course, to enable more accurate calculations of the

fluctuation velocities, the resolution must also be high enough to detect the small displacements that occur between successive frames.

The non-continuum nature of the granular material makes all laboratory scale experiments highly susceptible to finite-size effects. As a consequence, most flows show a strong dependence on the nature of the geometry of the boundaries as well as on the dimensions of the container. This imposes strong limitations on the ability to make quantitative comparisons between different sets of experimental results.

In experiments where velocity fields are measured at the surface, the flows have to approximate a two-dimensional flow as closely as possible so that the surface measurements are representative of actual values occurring within the bulk. In the current experiments, in order to achieve such two-dimensionality by reducing frictional interactions at the front and back walls, polished glass surfaces were used. However, as discussed in Chapter 3, due to the finite size of the particles, there is a possibility of the occurrence of "layering" parallel to these surfaces. Under such circumstances, the solid fraction distribution (Figure 3.3) in a direction normal to the front surface, becomes a strong function of the particle size. Furthermore, the extent to which such layering persists depends on the geometry of the system, especially if the flow is being sheared in planes perpedicular to the front and back walls.

Finite size effects also play a dominant role during the course of particle-boundary interactions (Campbell 1993b, 1993c). The degree of "roughness" imparted to a wall by gluing particles onto it is a very strong function of the particle spacing, particle placement pattern and the relative size of the wall particles and the flow particles. Furthermore, a comparison of two walls, one with a layer of particles glued to it and the other covered with a layer of sandpaper, might indicate comparable values for shear forces but the density distributions may be significantly different (Jenkins 1994). The sandpapered wall would encourage layering adjacent to the wall while the wall with particles glued to it would disrupt the flow structure adjacent to it. In

the context of problems involving heat transfer, such differences will certainly have a substantial influence on the effective heat transfer coefficients. Corner effects are also strongly dependent on the flow geometry.

### 6.2.2 Limitations of the Theoretical Models

While significant strides have been made in recent years in the development of models based on dense-gas kinetic theory to describe granular flows, the current set of experimental and theoretical studies exposed several severe limitations in such models' abilities, at the current level of development, to describe a large class of granular flows of considerable practical importance.

In spite of all advanced theoretical developments, the kinetic-theory models are still based on three fundamental assumptions. The first assumption is the "continuum" approximation which assumes that local properties like velocity, granular temperature and solid fraction are constant over a distance of several particle diameters. The second assumption is that all particle interactions occur by means of instantaneous collsions with no long term sliding or rolling contacts. The third assumption is that the radial distribution function $g_0(\nu)$ is isotropic.

The continuum approximation as applied to dense gases rests on the fact that the mean free path of the molecules is much larger than the size of the molecules themselves. However, in most granular flows, this is not true. Except in the limit of extremely dilute granular flows, e.g. the saltation layer in inclined chute flows, the inter-particle spacing is usually of the order of the size of the particles, if not less. In the current experiments, the mean and transverse fluctuation velocity profiles for the vertical channel displayed reasonably constant values in the central unsheared regimes, but changed significantly over distances of half a particle diameter, or less, in the sheared regimes adjacent to the walls. Paradoxically, it was in the sheared regimes where there was greater particle agitation and higher values of the transverse

fluctuation velocity were measured, that visual observations indicated a discernable extent of inter-particle collisional interactions. In the central plug regime, particle interactions were almost exclusively through long term sliding contacts.

Another anomalous result that arises as a result of the continuum assumption is that theoretical solutions always predict non-zero values for the solid fraction adjacent to a wall. For spherical particles, point contacts at a flat wall mean that the solid fraction there should be zero. Of course, for a wall with particles glued to it, i.e. the "bumpy" wall condition, defining the position of the boundary is a complex issue in itself. The validity of the continuum assumption probably increases with a decrease in particle size, but for very low particle sizes, the assumptions neglecting the effects of the interstitial fluid become invalid.

The fact that shear work at the wall serves as a significant source of random fluctuation energy that is subsequently conducted into the flow implies that regimes adjacent to the walls are likely to have higher fluctuation velocities and more agitated particles, and hence are more likely to experience the kind of collision-based interactions described by the kinetic-theory models. Again, paradoxically, it is in these very regimes, in the vicinity of the wall, that the assumption of isotropy of the radial distribution function $g_0(\nu)$ is most likely to break down given the effects of "layering" and other finite-size effects described previously. The nature of the wall surface will have a very strong influence on the distribution of flow particles in the vicinity.

The existence of long term sliding and rolling contacts necessitates the development of a model that can account for the frictional stresses that arise out of such interactions. Jenkins (1994) attempted to include frictional interactions within the framework of the instantaneous-collision based dynamics of the kinetic theory models, but such a model does not describe the long-duration interactions at all. While the Johnson & Jackson (1987) friction model studied in this work showed reasonable qualitative results, at least over certain solid fraction ranges, its overall utility was

severely hampered by the absence of any reliable experimental data, relating frictional stresses to local values of the solid fraction, that could be used to validate the functional form assumed for the frictional stresses. Furthermore, as evident in prior discussions, any such experimental data, whenever it becomes available, is likely to be highly specific to the geometry of the testing apparatus employed.

Inspite of all their limitations, the models based on kinetic theory are at present the only tools available, apart from computer simulations, for a theoretical analysis of granular flows that account for the finite nature of the medium and attempt to describe bulk flow behavior in terms of individual particle motions. The shear-induced dilation of the flow and the accompanying anomalous convective heat transfer characteristics observed experimentally, and investigated theoretically in this thesis cannot be described, even qualitatively, by any other moderately realistic theoretical construct. However, between the rapid granular flow regimes ideally described by the kinetic theory models, and the quasi-static regimes described by a variety of plasticity models, lies an entire range of intermediate flows. In these regimes, individual particle fluctuations are too low to consider collisional transfer of momentum to be a dominating mechanism, yet density and stress variations with deformation rates are high enough to invalidate the exclusive use of rate-independant plasticity models.

# References

Ahn, H. 1989, "Experimental and analytical investigations of granular materials: shear flow and convective heat transfer," Ph.D. thesis, California Institute of Technology, Pasadena.

Ahn, H., Brennen, C.E. and Sabersky, R.H. 1991, "Measurements of velocity, velocity fluctuations, density and stresses in chute flows of granular materials," *Trans. ASME* E: *J. Appl. Mech.,* Vol. 58, pp. 792-803.

Anderson, K.G. and Jackson, R. 1992, "A comparison of the solutions of some proposed equations of motion of granular materials for fully developed flow down inclined planes," *J. Fluid Mech.* Vol. 241, pp. 145-168.

Arteaga, P. and Tüzün, U. 1990, "Flow of binary mixtures of equal-density granules in hoppers: size segregation, flowing density and discharge rates," *Chem. Eng. Science,* Vol 45, No. 1, pp. 205-223.

Augestein, D.A. and Hogg. R. 1978, "An experimental study of the flow of dry powders over inclined surfaces," *Powder Technol.,* Vol. 19, pp. 205-215.

Bagnold, R.A. 1954, "Experiments on a gravity-free dispersion of large solid particles in a Newtonian fluid under shear," *Proc. R. Soc. Lond.* A, Vol. 225, pp. 49-63.

Batchelor, G.K. 1949, "Diffusion in a field of homogeneous turbulence: I. Eulerian analysis," *Australian J. Sci. Res.* Vol. 2, pp. 437-450.

Baumann, G., Jánosi, I.M. and Wolf. D.E. 1994, "Particle trajectories and segregation in a two-dimensional rotating drum," *Europhys. Lett.,* Vol. 27, No. 3, pp. 203-208.

Bossis, G. and Brady, J.F. 1987, "Self-diffusion of Brownian particles in concentrated suspensions under shear," *J. Chem. Phys.,* Vol. 87, pp. 1987

Botteril, J.S.M. and Desai, M. 1972, "Limiting factors in gas fluidized bed heat transfer," *Powder Technol.,* Vol. 6, pp. 231.

Bridgewater, J. 1980, "Self diffusion coefficents in deforming powders," *Powder Technol.,* Vol. 25, pp. 129-131.

Buggish, H. and Loffelmann, G. 1989, "Theoretical and experimental investigation into local granular mixing mechanisms," *Chem. Engng. Proc.,* Vol. 26, pp. 193-200.

Campbell, C.S. 1993a, "Self-diffusion in granular shear flows," *J. Fluid Mech.,* (submitted).

Campbell, C.S. 1993b, "Boundary interactions for two-dimensional granular flows. Part 1. Flat boundaries, asymmetric stresses and couple stresses," *J. Fluid Mech.,* Vol. 247, pp. 111-136.

Campbell, C.S. 1993c, "Boundary interactions for two-dimensional granular flows. Part 2. Roughened boundaries," *J. Fluid Mech.,* Vol. 247, pp. 137-156.

Campbell, C.S. 1990, "Rapid granular flows," *Annu. Rev. Fluid Mech.,* Vol. 22, pp. 57-92.

Campbell, C.S. 1989, "The stress tensor for simple shear flow of a granular material," *J. Fluid Mech.,* Vol. 203, pp. 449-473.

Campbell, C.S. and Brennen, C.E. 1985, "Computer simulation of granular shear flows," *J. Fluid Mech.,* Vol. 151, pp. 167-188.

Chapman, S. and Cowling, T. G. 1971, "The Mathematical theory of non-uniform gases,", 3rd edition, Cambridge University Press.

Dai, R. 1993, "Granular flow studies through kinetic theory and numerical simulation approaches,", Ph.D. thesis, McGill University, Montreal.

De Josselin de Jong, G. 1971, "The double-sliding free rotating model for granular assemblies," *Géotechnique,* Vol. 21, pp. 155-163.

Dolgunin, V.N. and Ukolov, A.A. 1995, "Segregation modeling of particle rapid gravity flow," *Powder Technol.,* Vol. 83, pp. 95-103.

Drake, T.G. 1991, "Granular flow: physical experiments and their implications for microstructural theories," *J. Fluid Mech.,* Vol. 225, pp. 121-152.

Eckstein, E.C., Bailey, D.G. and Shapiro, A.H. 1977, "Self diffusion of particles in shear flow of a suspension," *J. Fluid Mech.,* Vol. 79, pp. 191-208.

Einstein, A. 1956, In "Albert Einstein, Investigations on the theory of the Brownian movement," (ed. R.Furth), chap. 1, section 4, pp. 12-17, Dover.

Farrell, M., Lun, C.K.K., and Savage, S.B. 1986, "A simple kinetic theory for granular flow of binary mixtures of smooth, inelastic, spherical particles," *Acta Mechanica,* Vol. 63, pp. 45-60.

Foerster, S.F., Louge, M.Y., Chang, H. and Allia, K. 1994, "Measurements of the collision properties of small spheres," *Phys. Fluids,* Vol. 6, No. 3, pp. 1108-1115.

Gelperin, N.I. and Einstein, V.G. 1971, "Heat transfer in fluidized beds," *Fluidization,* (ed. J.F. Davidson and D. Harrison), Academic Press, London and New York, pp. 471-568.

Goldshtein, A. and Shapiro, M. 1995, "Mechanics of collisional motion of granular materials. Part 1. General hydrodynamic equations," *J. Fluid Mech.,* Vol. 282, pp. 75-114.

Goodman, M.A. and Cowin, S.C. 1971, "Two problems in the gravity flow of granular materials," *J. Fluid Mech.,* Vol. 45, pp. 321-339.

Haff, P.K. 1983, "Grain flow as a fluid mechanical phenomenon," *J. Fluid Mech.,* Vol. 134, pp. 401-430.

Hanes, D.M. and Inman, D.L. 1985, "Observations of rapidly flowing granular-fluid flow," *J. Fluid Mech.,* Vol. 150, pp. 357-380.

Hill, K.M. and Kakalios, J. 1994, "Reversible axial segregation of binary mixtures of granular materials," *Phys. Rev.* E, Vol. 49, No. 5, pp. 3610-3633.

Hosseiniashrafi, M.E. and Tüzün, U. 1993, "A tomographic study of voidage profiles in axially symmetrical granular flows," *Chem. Eng. Science,* Vol. 48, pp. 53-67.

Hsiau, S.S., 1993, "Shear induced transport properties of granular material flows," Ph.D. thesis, California Institute of Technology, Pasadena.

Hsiau, S.S. and Hunt, M.L. 1993a, "Shear-induced particle diffusion and longitudinal velocity fluctuations in a granular-flow mixing layer," *J. Fluid Mech.,* Vol. 251, pp. 299-313.

Hsiau, S.S. and Hunt, M.L. 1993b, "Kinetic theory analysis of flow-induced particle diffusion and thermal conduction in granular material flows," *Trans. ASME* C: *J. Heat Transfer,* Vol. 115, pp. 541-548.

Hui, K. and Haff, P.K. 1986, "Kinetic grain flow in a vertical channel," *Intl. J. Multiphase Flow,* Vol. 12, pp. 289-298.

Hui, K., Haff, P.K., Ungar, J.E. and Jackson, R. 1984, "Boundary conditions for high-shear grain flows," *J. Fluid Mech.,* Vol. 145, pp. 223-233.

Hunt, M.L., Hsiau, S.S. and Hong, K.T. 1994, "Particle mixing and volumetric expansion in a vibrated granular bed," *Trans. ASME* I: *J. Fluids Engng.,* Vol. 116, pp. 785-791.

Hwang, C.L. and Hogg, R. 1980, "Diffusive mixing in flowing powders," *Powder Technol.,* Vol. 26, pp. 93-101.

Jackson, R. 1983, in "Theory of dispersed multiphase flow," (ed. R.E. Meyer), Ch. 13, pp. 291-338, Academic Press.

Jenkins, J.T. 1994, "Rapid granular flow down inclines," *Proc. Twelfth U.S. Nat. Cong. Appl. Mech.,* pp. 240-244.

Jenkins, J.T. 1992, "Boundary conditions for rapid granular flow: Flat, frictional walls," *J. Appl. Mech.,* Vol. 59, pp. 120-127.

Jenkins, J.T. and Askari, E. 1991, "Boundary conditions for rapid granular flows: phase interfaces," *J. Fluid Mech.,* Vol. 223, pp. 497-508.

Jenkins, J.T. and McTigue, D.F. 1990, "Transport processes in concentrated suspensions: the role of particle fluctuations," in *Two Phase Flows and Waves,* (ed.

D.D. Joseph and D.G. Schaefer), Springer.

Jenkins, J.T. and Richman, M.W. 1988, "Plane simple shear of smooth inelastic circular disks: the anisotropy of the second moment in the dilute and dense limits, " Vol. 192, pp. 313-328.

Jenkins, J.T. and Richman, M.W. 1986, "Boundary conditions for plane flows of smooth, nearly elastic, circular disks," *J. Fluid Mech.,* Vol. 171, pp. 53-69.

Jenkins, J.T. and Richman, M.W. 1985, "Kinetic theory for plane flows of a dense gas of identical, rough, inelastic, circular disks," *Phys. Fluids,* Vol. 28, pp. 3485-3494.

Jenkins, J.T. and Savage, S.B. 1983, "A theory for the rapid flow of identical, smooth, nearly elastic, spherical particles, " *J. Fluid Mech.,* Vol. 130, pp. 187-202.

Johanson, J.R. 1978, "Particle segregation ... and what to do about it," *Chemical Engineering,* May 8, pp. 183-188.

Johnson, P.C., Nott. P. and Jackson, R. 1990, "Frictional-collisional equations of motion for particulate flows and their application to chutes," *J. Fluid Mech.,* Vol. 210, pp. 501-535.

Johnson, P.C. and Jackson, R. 1987, "Frictional-collisional constitutive relations for granular materials, with application to plane shearing," *J. Fluid Mech.,* Vol. 176, pp. 67-93.

Kubie, J. 1985, "Heat transfer between gas fluidized beds and immersed surfaces," *Int. J. Heat Mass Transfer,* Vol. 28, pp. 1345-1353.

Kubie, J. and Broughton, J. 1975, "A model of heat transfer in gas fluidized beds," *Int. J. Heat Mass Transfer,* Vol. 18, pp. 289-299.

Ladd, A.J.C. 1992, "Dynamical simulations of sedimenting spheres," *Phys. Fluids A.,* Vol. 5, pp. 299-310.

Langston, P.A., Tüzün, U. and Heyes, D.M. 1994, "Continuous potential discrete particle simulations of stress and velocity fields in hoppers: transition from fluid to granular flow," *Chem. Eng. Science,* Vol. 49, pp. 1259-1275.

Leighton, D. and Acrivos, A. 1987a, "Measurement of shear-induced self-diffusion in concentrated suspensions of spheres," *J. Fluid Mech.,* Vol. 177, pp. 109-131.

Leighton, D. and Acrivos, A. 1987b, "The shear-induced migration of particles in concentrated suspensions," *J. Fluid Mech.,* Vol. 181, pp. 415-439.

Liu, K.S., Kalos, M.H. and Chester, G.V. 1974, "Quantum hard spheres in a channel," *Phys. Rev.* A, Vol. 10, pp. 303-308.

Louge, M.Y. 1994, "Computer simulations of rapid granular flows of spheres interacting with a flat, frictional boundary," *Phys. Fluid.,* Vol. 6, pp. 2253-2269.

Louge, M., Yusof, J.M. and Jenkins, J.T. 1993, "Heat transfer in the pneumatic transport of massive particles," *Int. J. Heat Mass Transfer,* Vol. 36, No. 2, pp. 265-275.

Lun, C.K.K. 1991, "Kinetic theory for granular flow of dense, slightly inelastic, slightly rough spheres," *J. Fluid Mech.,* Vol. 233, pp. 539-559.

Lun, C.K.K. and Savage, S.B. 1987, "A simple kinetic theory for granular flow of rough, inelastic, spherical particles," *J. Appl. Mech.,* Vol. 54, pp. 47-53.

Lun, C.K.K. and Savage, S.B. 1986, "The effects of an impact velocity dependent coefficient of restitution on stresses developed by sheared granular materials," *Acta. Mechanica,* Vol. 63, pp. 15-44.

Lun, C.K.K., Savage, S.B., Jeffrey, D.J. and Chepurniy, N. 1984, "Kinetic theories for granular flow: inelastic particles in Couette flow and slightly inelastic particles in a general flow field," *J. Fluid Mech.,* Vol. 140, pp. 223-256.

Mandl, G. and Luque, R.F. 1970, "Fully developed plastic shear flow of granular materials," *Géotechnique,* Vol. 3, pp. 277-307.

Martin, H., 1984, "Heat transfer between gas fluidized beds of solid particles and the surfaces of immersed heat exchanger elements, Part I," *Chem. Eng. Process,* Vol. 18, pp. 157-169.

McNamara, S. and Young, W.R. 1992, "Inelastic collapse and clumping in a one-

dimensional granular medium," *Phys. Fluids* A, Vol. 4, pp. 496.

Mullier, M., Tüzün, U. and Walton, O.R. 1991, "A single-particle friction cell for measuring contact frictional properties of granular materials," *Powder Technol.,* Vol. 65, pp. 61-74.

Nakagawa, M., Altobelli, S.A., Caprihan, A., Fukushima, E. and Jeong, E.K. 1993, "Non-invasive measurements of granular flows by magnetic resonance imaging," *Experiments in Fluids,* Vol. 16, pp. 54-60.

Natarajan, V.V.R., Hunt, M.L. and Taylor, E.D. 1995, "Local measurements of velocity fluctuations and diffusion coefficients for a granular material flow," *J. Fluid Mech.,* Vol. 304, pp. 1-25.

Nedderman, R.M. and Laohakul, C. 1980, "The thickness of the shear zone of flowing granular materials," *Powder Technol.,* Vol. 25, pp. 91-100.

Nott, P.R. and Brady, J.F. 1994, "Pressure-driven flow of suspensions: simulation and theory," *J. Fluid Mech.,* Vol. 275, pp. 157-199.

Nunziato, J.W., Passman, S.L. and Thomas, J.P. 1980, "Gravitational flows of granular materials with incompressible grains," *J. Rheol.,* Vol. 24, pp. 395-420.

Ogawa, S. 1978, "Multi-temperature theory of granular materials," *Proc. U.S.-Japan Seminar on Continuum-Mechanical and Statistical Approaches in the Mechanics of Granular Materials,* pp. 208-217.

Patankar, S.V. 1988, in "Handbook of numerical heat transfer," (ed. E.M. Sparrow, W.J. Minkowycz, G.E. Schneider and R.H. Pletcher), Ch. 6, pp. 215-227, John Wiley & Sons, Inc.

Patankar, S.V. 1980, in "Numerical heat transfer and fluid flow," Ch. 5, pp. 79-109, McGraw Hill.

Patton, J.S. 1985, "Experimental study of shear flows and convective heat transfer characteristics of granular materials," Ph.D. thesis, California Institute of Technology, Pasadena.

Patton, J.S., Sabersky, R.H., and Brennen, C.E., 1986, "Convective heat transfer to rapidly flowing granular materials," *Int. J. Heat Mass Transfer,*, Vol. 29, pp. 1263-1269.

Peciar, M., Buggisch, H. and Renner, M. 1994, "Experimental investigation into the influence of the particle size distribution upon the local mixing mechanisms in a flowing bulk material," *Chem. Eng. Proc.,* Vol. 33, pp. 39-44.

Poux, M., Fayolle, P., Bertrand, J., Bridoux, D. and Bousquet, J. 1991, "Powder mixing: some practical rules applied to agitated systems," *Powder Technol.,* Vol. 68, pp. 213-234.

Richman, M.W. 1988, "Boundary conditions based upon a modified Maxwellian velocity distribution for flows of identical, smooth, nearly elastic spheres," *Acta Mechanica,* Vol. 75, pp. 227-240.

Richman, M.W. and Marciniec, R.P. 1991, "Granular chute flows," In *Recent Advances in Mechanics of Structured Continua,* AMD-Vol. 117, ASME.

Richman, M.W. and Marciniec, R.P. 1990, "Gravity-driven granular flows of smooth, inelastic spheres down bumpy inclines," *J. Appl. Mech.,* Vol. 112, pp. 1036-1043.

Richman, M.W. and Oyediran, A.A. 1992, "Grain size reduction in granular flows of spheres: the effects of critical impact energy," *J. Appl. Mech.,* Vol. 59, pp. 17-22.

Ristow, G.H. 1994, "Particle mass segregation in a two-dimensional rotating drum," *Europhys. Lett.,* Vol. 28, No. 2, pp. 97-101.

Roscoe, K.H., "The influence of strains in soil mechanics," *Géotechnique,* Vol. 20, pp. 129-170.

Savage, S.B. 1993, "Disorder, diffusion and structure formation in granular flows," In *Disorder and Granular Media,* (ed. D. Bideau and A. Hansen), North-Holland, pp. 255-286.

Savage, S.B. 1987, "Interparticle percolation and segregation in granular materi-

als: a review," In *Developments in Engineering Mechanics,* (ed. A.P.S. Selvadurai), Elsevier Science Publications, Amsterdam, pp. 347-363.

Savage, S.B. 1984, "The mechanics of rapid granular flows," *Adv. Appl. Mech.,* Vol. 24, pp. 289-366.

Savage, S.B. 1979, "Gravity flow of cohesionless granular materials in chutes and channels," *J. Fluid Mech.,* Vol. 92, pp. 53-96.

Savage, S.B. and Dai, R. 1993, "Studies of shear flows. Wall slip velocities, 'layering' and self-diffusion," *Mech. Mater.,* Vol. 16, pp. 225-238.

Savage, S.B. and Jeffrey, D.J. 1981, "The stress tensor in a granular flow at high shear rates," *J. Fluid Mech.,* Vol. 110, pp. 255-272.

Savage, S.B. and Lun, C.K.K. 1988, "Particle size segregation in inclined chute flow of dry cohesionless granular solids," *J. Fluid Mech.,* Vol. 189, pp. 311-335.

Savage, S.B. and Sayed, M. 1984, "Stresses developed by dry, cohesionless granular materials sheared in an annular shear cell," *J. Fluid Mech.,* Vol. 142, pp. 391-430.

Scarlatt, B. and Todd, A.C. 1969, "The critical porosity of free flowing solids," *Trans. ASME* B: *J. Engng. Ind.,* Vol. 91, pp. 477-488.

Schlunder, E.U. 1982, "Particle heat transfer," *Proc. Seventh Int. Heat Transfer Conf.,* Munich, Hemisphere Pub. Co.

Schofield, A.N. and Wroth, C.P. 1968, "Critical state soil mechanics," McGraw-Hill.

Scott, A.M. and Bridgewater, J. 1976, "Self-diffusion of spherical particles in a simple shear apparatus," *Powder Technol.,* Vol. 14, pp. 177-183.

Sherwood, T.K., Pigford, R.L. and Wilke, C.R. 1975, *Mass Transfer,* McGraw Hill.

Spelt, J.K., Brennen, C.E. and Sabersky, R.H. 1982, "Heat transfer to flowing granular material," *Int. J. Heat Mass Transfer,* Vol. 25, pp. 791-796.

Stephens, D.J. and Bridgewater, J. 1978, "The mixing and segregation of cohe-

sionless particulate materials. Part II: Microscopic mechanisms for particles differing in size," *Powder Technol.,* Vol. 21, pp. 29-44.

Sullivan, W.N. and Sabersky, R.H. 1975, "Heat transfer to flowing granular media," *Int. J. Heat Mass Transfer,* Vol. 18, pp. 97-107.

Sun, J. and Chen, M.M. 1988, "A theoretical analysis of heat transfer due to particle impact," *Int. J. Heat Mass Transfer,* Vol. 31, pp. 205-214.

Takahashi, H. and Yanai, H. 1973, "Flow profiles and void fraction of granular solids in a moving bed," *Powder Technol.,* Vol. 7, pp. 205-214.

Taylor, E.D. and Hunt, M.L. 1993, "Measurements of velocity fluctuations in a granular flow," In *Powders & Grains 93,* (ed. C. Thornton), Balkema.

Taylor, G.I. 1922, "Diffusion by continuous movements," *Proc. London Mathematical Society,"* Ser. 2, Vol. 20, pp. 196-212.

Taylor, G.I. 1953, "Dispersion of soluble matter in solvent flowing slowly through a tube," *Proc. R. Soc. Lond.* A, Vol. 219, pp. 186-203.

Taylor, G.I. 1954, "The dispersion of matter in turbulent flow through a pipe," *Proc. R. Soc. Lond.* A, Vol. 223, pp. 446-468.

Tüzün, U. and Arteaga, P. 1992, "A microstructural model of flowing ternary mixtures of equal-density granules in hoppers," *Chem. Eng. Science,* Vol. 47, No. 7, pp. 1619-1634.

Tüzün, U., Houlsby, G.T., Nedderman, R.M. and Savage, S.B. 1982, "The flow of granular materials-II. Velocity distributions in slow flow," *Chem. Eng. Science,* Vol. 37, pp. 1691-1709.

Walton, O.R. 1992, "Numerical simulation of inclined chute flows of monodisperse, inelastic, frictional spheres," In *Advances in Micromechanics of Granular Materials,* (ed. H.H. Shen et. al. ), Elsevier Science Publishers, Amsterdam, pp. 453-461.

Walton, O.R. and Braun, R.L. 1986, "Viscosity, granular temperature and stress calculations for shearing assemblies of inelastic, frictional disks," *J. Rheol.,* Vol. 30,

pp. 949-980.

Wang, D.G. and Campbell, C.S. 1992, "Reynolds analogy for a shearing granular material," *J. Fluid Mech.,* Vol. 244, pp. 527-546.

Wassgren, C.R. 1997, "Vibration of granular materials," Ph.D. thesis, California Institute of Technology, Pasadena.

Williams, J.C. 1976, "The segregation of particulate materials. A review," *Powder Technol.,* Vol. 15, pp. 245-251.

Yi, Z. and Campbell, C.S. 1992, "The interface between fluid-like and solid-like behavior in 2-dimensional granular flows," *J. Fluid Mech.,* Vol. 237, pp 541-568.

Zik, O. and Stavans, J. 1991, "Self-diffusion in granular flows," *Europhys. Lett.,* Vol. 16, pp. 255-258.

Zik, O., Levine, D., Lipson, S.G., Shtrikman, S. and Stavans, J. 1994, "Rotationally induced segregation of granular materials," *Phys. Rev. Lett.,* Vol. 73, No. 5, pp. 644-647.

# Appendix A Derivation of the Semi-empirical Sullivan-Sabersky Model for Convective Heat Transfer to Granular Flows.

Sullivan & Sabersky (1975) attempted to model the convective heat transfer in granular flows by considering the case of a continuum with a single thermal resistance at the wall in order to indicate the extent to which the heat transfer at the wall was influenced by the granular structure that was not adjacent to the wall. This involved the solution of the energy equation

$$\frac{\partial^2 T}{\partial y^2} = \frac{U}{\alpha}\frac{\partial T}{\partial x}$$

with the boundary conditions defined as:

$$\begin{aligned} -k\tfrac{\partial T}{\partial y}(0,x) &= K[T_w - T(0,x)], \quad && x \geq 0 \\ T(0,x) &= T_\infty, && x < 0 \\ T(\infty,x) &= T_\infty. && \forall x \end{aligned}$$

where $K$ is the conductance per unit area of the plate and $T_w$ is the constant temperature of the plate. It was shown that for a regular layered array of particles and infinitely conducting particles, $K = k/\sigma$ where $k$ is the bulk conductivity of the material. By solving for the energy equation and by averaging over the length of the heating plate, the following relation between the average Nusselt number $\mathrm{Nu}_{ave} = \frac{h_{ave}L}{k}$ and the Peclet number $\mathrm{Pe_L} = \frac{UL}{\alpha}$ was obtained.

$$\mathrm{Nu}_{ave} = \frac{1}{\frac{k}{KL} + \frac{1}{2}\sqrt{\frac{\pi}{\mathrm{Pe}_L}}}.$$

Recognizing the fact that an actual particle flow has neither a regular layered structure nor infinite particle conductivity, an attempt was made to describe the wall conductance $K$ more realistically in terms of actual physical parameters. Under the assumption that the wall conductance was due to thermal interaction between the wall and the row of particles immediately adjacent to the wall , it was conjectured that the wall conductance should be proportional to the conductivity of the interstitial gas $k_g$, provided that heat conduction through the physical contacts and thermal radiation across the voids were negligibly small. Furthermore, the wall conductance $K$ was also expected to be inversely proportional to the average thickness of the gas film between the heated plate and the particles. For geometrically similar particles with identical void ratios, this average thickness was expected to be proportional to the particle characteristic length $\sigma$, its diameter. Hence, it was expected that

$$K = \frac{1}{\chi}\frac{k_g}{\sigma},$$

where $\chi$ was a dimensionless proportionality constant independent of the thermal properties of the interstitial gas or the particles. This constant $\chi$ was interpreted as the ratio of the thickness $l$ of a uniform gas film, with a conductance $K = \frac{k_g}{l}$ to the particle characteristic length $\sigma$. For similar geometrical arrangements of particles, $\chi$ should have similar values but values would differ for different geometrical arrangements or for different particle geometries. Flows adjacent to a rough wall would have a different value of $\chi$ compared to flows adjacent to a smooth wall.

Substituting the relation for $K$ discussed above into the relationship between $\mathrm{Nu}_{ave}$ and $\mathrm{Pe_L}$ discussed previously yielded Equation (2.29)

$$\mathrm{Nu}^* = \frac{1}{(\chi + \frac{1}{2}\sqrt{\frac{\pi}{\mathrm{Pe}^*}})}.$$

According to the above equation, the heat transfer data for geometrically similar particle arrangements should lie on a single $\mathrm{Nu}^*$ versus $\mathrm{Pe}^*$ curve.